OLGA NIKOLAJEVA / OLGA NIKOLAYEVA

Fizikas maģistre / Master of Physics

# ŠTARKA SPEKTROSKOPIJA UN POLARIZĀCIJAS EFEKTI SĀRMU METĀLU DIVATOMU MOLEKULĀS

---

# STARK SPECTROSCOPY AND POLARISATION EFFECTS IN ALKALI DIMERS

Promocijas darbs / Promotion work



Latvijas Universitāte / University of Latvia

Rīga – 2000

**Promocijas darbā iekļauto publikāciju saraksts**

**A list of publications included in the promotion work**


[dis1] S. O. Adamson, A. Zaitsevskii, E. A. Pazyuk, A. V. Stolyarov, **O. Nikolayeva**, O. Docenko, I. Klincare, M. Auzinsh, M. Tamanis, R. Ferber, and R. Cimiraglia, Energy and Radiative properties of the low-lying NaRb states, *Phys. Rev. A*, submitted.

[dis2] **O. Nikolayeva**, I. Klincare, M. Auzinsh, M. Tamanis, R. Ferber, E. A. Pazyuk, A. V. Stolyarov, A. Zaitsevskii, and R Cimiraglia, Permanent electric dipoles in $B^1\Pi$ and $D^1\Pi$ states of NaRb: Experiment and theory, *J. Chem. Phys.* **113**, 2000, p. 4896-4900.

[dis3] **O. Nikolayeva**, M. Auzinsh, M. Tamanis, R. Ferber, Electric field induced alignment-orientation conversion in diatomic molecules: Analysis and observation for NaK, *J. Mol. Struct.* **480-481**, 1999, p.283-287.

[dis4] M. Tamanis, M. Auzinsh, I. Klincare, **O. Nikolayeva**, R. Ferber, A. Zaitsevski, E. A. Pazyuk, A. V. Stolyarov, Lifetimes and transition dipole moment functions of NaK low lying singlet states: empirical and *ab initio* approach, *J. Chem. Phys.* **109**, 1998, p.6725-6735.

[dis5] M. Tamanis, M. Auzinsh, I. Klincare, **O. Nikolayeva**, R. Ferber, E. A. Pazyuk, A. V. Stolyarov, A. Zaitsevski, NaK Λ-doubling and permanent electric dipoles in low lying $^1\Pi$ states: experiment and theory, *Phys. Rev. A.* **58**, 1998, 1932-1943.

[dis6] M. Tamanis, M. Auzinsh, I. Klincare, **O. Nikolayeva**, A. V. Stolyarov, R. Ferber, NaK $D^1\Pi$ electric dipole moment measurement by Stark level crossing and *e-f* mixing spectroscopy, *J. Chem. Phys.* **106**, 1997, 2195-2204.

[dis7] M. Auzinsh, I. Klincare, **O. Nikolayeva**, A. V. Stolyarov, M. Tamanis, R. Ferber, Studies of rotational level Λ-doubling by RF-optical double resonance spectroscopy: Application to NaK $D^1\Pi$, *J. Mol. Structure* **410-411**, 1997, p.55-58.

[dis8] M. Auzinsh, I. Klincare, **O. Nikolayeva**, A. V Stolyarov, M. Tamanis, R. Ferber, Stark level crossing and optical-RF double resonance in NaK $D^1\Pi$, *SPIE Proceedings*, 1997, **3090**, p.194-198

[dis9] I. Jackowska, W. Jastrzebski, R. Ferber, **O. Nikolayeva**, P. Kowalczyk, Revision of $Na_2$ $A^1\Sigma^+_u$ state molecular constants by polarisation labelling spectroscopy, *SPIE Proceedings*, 1997, **3090**, p.199-203

[dis10] I. Jackowska, W. Jastrzebski, R Ferber, **O. Nikolayeva**, P. Kowalczyk, Reanalysis of the $A^1\Sigma^+_u$ state of $Na_2$ by polarisation labelling spectroscopy, *Mol. Phys.* **88**, 1996, 1719-1724.

# Energy and radiative properties of the low-lying NaRb states

A. Zaitsevskii, S. O. Adamson, E. A. Pazyuk, and A. V. Stolyarov
*Department of Chemistry, Moscow State University, Moscow, 119899, Russia*

O. Nikolayeva, O. Docenko, I. Klincare, M. Auzinsh, M. Tamanis, and R. Ferber
*Department of Physics, University of Latvia, Riga LV-1586, Latvia*

R. Cimiraglia
*Dipartimento di Chimica, Università di Ferrara, Via Borsari 46, I-44100, Ferrara, Italy*

Many-body multipartitioning perturbation theory was applied to calculate potential energy of 11 lowest electronic states of the NaRb molecule, $A,C^1\Sigma^+ - X^1\Sigma^+$, $B,D^1\Pi - X^1\Sigma^+$, $D^1\Pi - A^1\Sigma^+$ and $D^1\Pi - B^1\Pi$ transition dipole moments, as well as non-adiabatic $L$-uncoupling matrix elements between the examined $^1\Pi$ and four lowest $^1\Sigma^+$ states for both $^{23}Na^{85}Rb$ and $^{23}Na^{87}Rb$ isotopomers. The relevant MPPT *ab initio* matrix elements and energy curves were converted by means of the approximate sum rule to radiative lifetimes and $\Lambda$-doubling constants ($q$ factors) for the particular rovibronic levels of the $B^1\Pi$ and $D^1\Pi$ states. The theoretical lifetimes agree well with their experimental counterparts for both $B^1\Pi$ and $D^1\Pi$ states. The $q$-factor estimates obtained in the singlet-singlet approximation are in good agreement with the experimental ones for the $D^1\Pi(1 \le v' \le 12; 7 \le J' \le 50)$ levels, exhibiting pronounced difference for the $B^1\Pi$ state. Considerably better agreement was achieved by accounting for the spin-orbit perturbation effect caused by the near-lying $c^3\Sigma^+$ state. Relative intensity distributions in the $D^1\Pi \rightarrow X^1\Sigma^+$ dispersed fluorescence spectra excited by fixed $Ar^+$ laser lines were measured for $v'(J') = 0(11)$, 1(104), 4(25), 6(44, 120), 10(36) and 12(50) $D^1\Pi$ levels. The experimental intensities and term values were simultaneously embedded in the nonlinear least square fitting procedure to refine the $D^1\Pi$ potential.

## I. INTRODUCTION

The heteronuclear alkali dimers are a permanent challenge to both experimental and theoretical researchers involved in collision dynamics, photoassociative spectra, laser cooled and trapped alkaline atoms due to their promising prospects for the formation of ultracold molecules [1]. As far as the NaRb molecule is concerned, in spite of a number of experimental and theoretical studies carried out in the last two decades [2–9], the knowledge of its energy and radiative properties is still rather scarce. High accuracy experimental molecular constants and corresponding RKR potentials are available only for the ground $X^1\Sigma^+$ state and, to a certain extent, for the bound part of the $a^3\Sigma^+$ state correlating to the Na(3s) + Rb(5s) atoms, as well as for the $B^1\Pi$ state correlating to the Na(3s) + Rb(5p) atoms due to systematic studies performed in the Kato group [2–5] by polarization spectroscopy and optical-optical double resonance methods. Molecular constants for the $D^1\Pi$ state, which are responsible for the strong green $D^1\Pi - X^1\Sigma^+$ absorption band first observed as early as in 1928 by Walter and Barrat [10], were only roughly estimated in [6] from the intensity distribution in the $D^1\Pi - X^1\Sigma^+$ laser-induced fluorescence (LIF). Potential energies for the ground and 27 lowest excited electronic states of NaRb have been recently calculated [7] by means of non-empirical pseudopotentials, parametrized $l$-dependent polarization potentials and full valence configuration interaction (CI) method. It should be noted that the agreement between theoretical and available experimental spectroscopic constants is not always good enough, cf., for instance, the calculated value [7] $\omega_e = 51.6$ cm$^{-1}$ for the $B^1\Pi$ state of $^{23}Na^{85}Rb$ with the experimental one 61.171 cm$^{-1}$ obtained in [2]. The existing information on radiative properties of NaRb is even poorer. Only two fragmentary measurements of collisionless radiative lifetime are reported in the literature, namely $\tau = 17.8$ ns for $B^1\Pi$ ($v' = 5$, $J' \approx 20$) [5] and $\tau = 22.1$ ns for $D^1\Pi$ ($v' = 0$, $J' = 11$) [8]. An $R$-independent estimate $\mu = 7.0$ D of the $B^1\Pi - X^1\Sigma^+$ transition dipole moment averaged within the internuclear distance region 3.73 Å $< R <$ 4.98 Å was obtained in Ref. [5] from the experimental lifetime and LIF intensity distribution. Only a very rough estimate of the relative $\mu(R)$ dependence was suggested in [6] for the $D^1\Pi - X^1\Sigma^+$ transition. No theoretical calculations of radiative properties of NaRb can be found in literature.

In our recent study on NaRb [9] the permanent electric dipole moments $d$ were measured for a number of $v', J'$ levels of the $B^1\Pi$ and $D^1\Pi$ states by combining the dc Stark effect induced $e - f$ mixing for a particular rovibronic level with the direct determination of its $\Lambda$-splitting energy $\Delta_{e,f}$ by means of the electric Radio Frequency – Optical Double Resonance (RF–ODR) method. The measured $d$-values were in good agreement with the concomitant *ab initio* calculations performed in [9] by the multipartitioning perturbation theory (MPPT) developed in [11,12]. The

MPPT method has been previously approved as an excellent tool to calculate permanent electric dipoles [13] and transition dipole moments [14] in the NaK molecule. What is more, in Ref. [15] the MPPT was adapted to calculate the electronic $L$-uncoupling matrix elements $L_{^1\Pi\Sigma}(R)$ between the sampled $^1\Pi$ and remote $^1\Sigma$ states, providing reliable estimates of the $\Lambda$-splitting energy and the $q$-factors of the $B^1\Pi$ and $D^1\Pi$ states of NaK.

The main goals of the present work are as follows. First, to apply the MPPT techniques developed and approved in [9,11,12,15] to evaluate NaRb potential energy curves $U(R)$ of the electronic states converging to the first three dissociation limits, as well as of the $E^1\Sigma^+$ state. *Second*, to calculate the transition dipole moments $\mu(R)$ for the singlet-singlet transitions, as well as the non-adiabatic $L$-uncoupling matrix elements $L_{^1\Pi\Sigma}(R)$ between the examined $^1\Pi$ state and four lowest $^1\Sigma^+$ states for both $^{23}$Na$^{85}$Rb and $^{23}$Na$^{87}$Rb isotopomers. To allow direct comparison with available experimental results, the relevant MPPT matrix elements and potential energy curves were converted to the radiative lifetimes and $\Lambda$-doubling constants ($q$-factors) for the particular rovibronic levels of the $B^1\Pi$ and $D^1\Pi$ states by using the approximate sum rule [16]. In addition, the relative intensity distributions in the $D^1\Pi \rightarrow X^1\Sigma^+$ dispersed fluorescence spectra were measured and embedded, together with the transition dipole moment function $\mu_{D^1\Pi - X^1\Sigma^+}(R)$ computed by the MPPT, the high-accurate RKR $X^1\Sigma^+$ potential [5] and experimental $D^1\Pi(v', J')$ rovibronic term values, in a nonlinear least-square fitting procedure to refine the $D^1\Pi$ potential.

## II. METHOD

### A. Experiment

In this paper we present three experimental data sets on the NaRb molecule obtained from the laser induced fluorescence measurements, namely, the $D^1\Pi$ state term values for a number of rovibronic $v', J'$ levels, and relative intensity distributions in the $D^1\Pi \rightarrow X^1\Sigma^+$ LIF progressions originating from these levels, as well as $\Lambda$-doubling constants for $v', J'$ levels of the $B^1\Pi$ and $D^1\Pi$ states. The experimental set-up has been described in more detail in our previous papers [13,14]. Let us remind here some essential points. The fixed frequency lines of Spectra Physics 171 $Ar^+$ laser, as well as of $Kr^+$ and He-Ne lasers were used to excite a particular $v', J'$ level of the $D^1\Pi$ or $B^1\Pi$ state of the NaRb molecules in a thermal cell made from the alkali-resistant glass. The cell was connected to the vacuum pump and contained the mixture of Na:Rb metals in the respective mass ratio ca. 1:1 at temperature $T \approx 550$ K.

*Term values.* The $D^1\Pi$ state rovibronic term values $T^{exp}_{v'J'}$ were obtained by adding the $D^1\Pi(v', J') \leftarrow X^1\Sigma^+(v'', J'')$ transition laser frequency to the energy of the absorbing ground state rovibronic level $v'', J''$. The assignment of the $v$, $J$ quantum numbers belonging to the particular isotopomer $^{23}$Na$^{85}$Rb or $^{23}$Na$^{87}$Rb is discussed in more detail in Ref. [9]. It is based on the careful measurements of the vibrational and rotational spacings in LIF progressions and their comparison with the spacings calculated using the high-accurate ground state molecular constants given in Ref. [25]. Vibrational numbering was supported by a comparison of the LIF relative intensity distribution with the calculated Franck-Condon factors. In addition to the $D^1\Pi$ state $v'(J')$ levels listed in Table I of Ref. [9], we have identified two more $v'(J')$ levels, namely $1(J' \approx 104)$ and $6(J' \approx 120)$, excited by the 514.5 nm $Ar^+$ laser line. However, we do not present here the term values of these states since, because of poor accuracy of ground state term values for large $J'$, the latter was only estimated, and, consequently it was impossible to assign the particular isotopomer. Nevertheless, the respective LIF progressions were involved in the relative intensity distribution analysis.

*Intensity distributions.* The $D^1\Pi \rightarrow X^1\Sigma^+$ relative intensity distributions were measured in photon counting regime by detecting LIF spectra from the $D^1\Pi(v', J')$ levels excited by single mode $Ar^+$-laser lines. The double monochromator with the slits 0.08 – 0.10 mm provided 0.3 – 0.4 Å spectral resolution. In order to avoid the temperature drift and laser excitation condition changing effects, the measurements were performed in a step-by-step regime by alternative returning to the particular fluorescence line of the same progression which served as a reference line. The spectral sensitivity of the registration system was calibrated using a standard tungsten band-lamp with the known spectral irradiance at definite temperature. To avoid the possible influence of the linear polarization of the molecular fluorescence, the polarization vector of the exciting laser beam was directed along the observation direction.

*$\Lambda$-splitting constants.* The experimental $\Lambda$-splitting energy values $\Delta_{e,f}$, measured directly by the RF–ODR method [17,18], are presented in Table I of Ref. [9]. These values have been used in the present work to extract the $\Lambda$-splitting constants, or $q$ -factors. Note that this method yields only the absolute value and not the sign of the $q$ -factor.

### B. Outline of theory

The present theoretical study of the NaRb molecule is based on the *ab initio* electronic structure calculations performed by means of the many-body multipartitioning perturbation theory (MPPT) [11,12]. The transition moments

$\mu(R)$, as well as the $L$-uncoupling matrix elements $L_{\Pi\Sigma}(R) = \langle \Pi | L^{+} | \Sigma^{+} \rangle$ between the $^1\Pi$ state under study and the remote $^1\Sigma^{\pm}$ states were determined via the perturbative spin-free one-electron transition density matrices. The scalar (spin-independent) relativistic effects have been taken into account by replacing the inner core shells with the averaged relativistic pseudopotentials [21,22], leaving 9 electrons of each atom for explicit treatment. The performed calculations employ the MPPT to incorporate effective interactions arising from the core-valence correlations and core polarization effects into the model-space CI (valence-shell full CI) problem. The completeness of the model space guarantees the size-consistency of the derived energies and matrix elements. The spin-orbit (SO) interaction effects on the electronic properties under study were neglected in the present treatment. The computational details can be found elsewhere [9,15]. The transition moment functions were obtained in the dipole-length approximation; the mass-dependent $L$-uncoupling matrix elements were computed separately for the $^{23}Na^{85}Rb$ and $^{23}Na^{87}Rb$ isotopomers. The required atomic masses of the Na and Rb isotopes were taken from Ref. [19]. For $\Pi - \Sigma$ transitions $\mu_{\Pi\Sigma}(R)$ and $L_{\Pi\Sigma}(R)$ functions relate to each other as [20]:

$$L_{\Pi\Sigma}^{^{23}Na^{87}Rb} - L_{\Pi\Sigma}^{^{23}Na^{85}Rb} = \xi \mu_{\Pi\Sigma} [U_{\Pi} - U_{\Sigma}], \tag{1}$$

where $\xi = \xi(R)$ is the shift of the center of mass and $U_{\Pi}(R) - U_{\Sigma}(R) \equiv \Delta U_{\Pi\Sigma}(R)$ is the difference of the Born-Oppenheimer potentials. Due to the small shift of the centre of mass for two isotopomers, the calculated differences of the isotopic-substituted $L$-uncoupling matrix elements are obviously expected to be very small. Nevertheless, to test self-consistency of the calculated *ab initio* $U, \mu$ and $L$ values, the relation (1) was applied to evaluate the corresponding $\mu_{\Pi\Sigma}$ moments and to compare them with their dipole-length analogues.

The splitting $\Delta_{ef}$ between $e$ and $f$ components of the initially degenerated $^1\Pi$ level is mainly determined by *regular* electronic-rotational perturbations caused by the remote singlet $^1\Sigma^{\pm}$ states [23]. Under this *singlet-singlet approximation*, strong $J$-dependence of the $\Delta_{ef}$ values is usually reduced to the so-called $q$-factors using the expression $\Delta_{ef}^{\Pi} = q_{vJ}^{\Pi} J(J+1)$ [20]. The expression for the $q$ factor is

$$q_{vJ}^{\Pi} = \frac{1}{2M^2} \sum_{\Sigma} (-1)^k \sum_{v_{\Sigma}} \frac{\left| \langle v_J^{\Pi} | L_{\Pi\Sigma} / R^2 | v_J^{\Sigma} \rangle \right|^2}{T_{vJ}^{\Pi} - T_{v'J}^{\Sigma}}, \tag{2}$$

where $M$ is the reduced molecular mass, $k = 0$ and 1 for the $\Sigma^{+}$ and $\Sigma^{-}$ states, respectively. The rovibronic term values $T_{vJ}$ and wavefunctions $|vJ\rangle$ are the eigenvalues and eigenfunctions of the respective radial Schrödinger equation.

The radiative lifetimes $\tau_{iv'J'}$ and relative $iv'J' \rightarrow jv''J''$ fluorescence intensities $I_{ij}^{v'J'v''J''}$ combine with each other through the Einstein coefficients $A_{ij}^{v'J'v''J''}$ [23]:

$$\tau_{iv'J'}^{-1} = \sum_{jv''J''} A_{ij}^{v'J'v''J''}, \qquad I_{ij}^{v'J'v''J''} = A_{ij}^{v'J'v''J''} / A_{ij}^{v'J'v''_{max}J''}, \tag{3}$$

$$A_{ij}^{v'J'v''J''} = \frac{8\pi^2}{3h\epsilon_0} (T_{iv'J'} - T_{jv''J''})^3 |\langle v'_J | \mu_{ij}(R) | v''_{J''} \rangle|^2 \frac{S_{J'J''}}{2J'+1}, \tag{4}$$

where $S_{J'J''}$ is the Hönl-London factor, $v''_{max}$ corresponds to the band with the maximum intensity within a given progression, $8\pi^2/3h\epsilon_0 = 2.026 \times 10^{-6}$, $\epsilon_0$ is the permittivity of vacuum, $\mu_{ij}$ in a.u., and $T_{ij}$ are the rovibronic term values in $cm^{-1}$.

The relevant MPPT transition dipole moments were converted into radiative lifetimes $\tau_{vJ}^{\Pi}$ for the particular rovibronic levels of the $B^1\Pi$ and $D^1\Pi$ states by applying the approximate sum rule [16], which allows one to avoid tedious summation over vibrational levels of the remote electronic states:

$$1/\tau_{vJ}^{\Pi} \approx \langle v_J^{\Pi} | A^{sum} | v_J^{\Pi} \rangle, \qquad A^{sum} = \frac{8\pi^2}{3h\epsilon_0} \sum_j \Delta U_{\Pi j}^3 \mu_{\Pi j}^2, \tag{5}$$

$\Delta U_{\Pi j} = U_{\Pi} - U_j$ being the potential difference between interacting states. Similarly, the $L$-uncoupling electronic matrix elements $L_{\Pi\Sigma}$ were converted into $q$-factors through

$$q_{vJ}^{\Pi} \approx \langle v_J^{\Pi} | Q^{sum} | v_J^{\Pi} \rangle, \qquad Q^{sum} = \sum_{j=\Sigma} Q_j = \frac{1}{2M^2} \sum_{j=\Sigma} (-1)^k \frac{L_{\Pi j}^2}{R^4 \Delta U_{\Pi j}}. \tag{6}$$

The reliability of the sum rules was confirmed numerically by performing the direct summation in Eqs. (2) and (3) for the $D^1\Pi \sim B^1\Pi$ and $B^1\Pi \sim C^1\Sigma^{+}$ pairs possessing minimum energy gap at the internuclear distances of interest.

The discrepancy between the results obtained directly and their sum rule analogues is found to be less than 0.1% for all rovibronic levels under consideration. The rovibrational wavefunctions were calculated using the empirical RKR potentials corresponding to the molecular constants from Ref. [2] for the $B^1\Pi$ state and the ones obtained in the present work for the $D^1\Pi$ state. The energy differences $\Delta U_{^1\Pi\ X^1\Sigma^+}$ were evaluated using the corresponding RKR potentials and experimental electronic energies ($T_e$), while the differences $\Delta U_{^1\Pi\ A,C,E^1\Sigma^+}$ have been calculated using the present *ab initio* potentials since the experimental molecular constants for the excited $^1\Sigma^+$ states have not been obtained yet. The infinite summation in expression (6) over all possible $^1\Sigma^+$ electronic states including those embedded into the autoionization continuum was truncated on the $E^1\Sigma^+$ state since the large potential differences and the factor $R^{-4}$ in the r.h.s. of Eq.(6) suppress significantly the contributions from the remaining remote states [15].

Relative intensity distributions in the LIF progressions are determined by the potential curves of the combining states, as well as by the $R$-dependence of the corresponding transition moment. Therefore, a knowledge of the *ab initio* $\mu_{ij}(R)$ function and experimental molecular constants for the ground state, along with relevant transition frequency measurements, provides a possibility to apply relative intensity measurements to refine a potential curve for the upper state. Since the number of the $D^1\Pi$ state term values experimentally obtained in the present work is definitely insufficient to determine a set of $D^1\Pi$ molecular constants of reasonable accuracy, both experimental term values $T^{exp}_{D^1\Pi}$ and LIF intensity distributions $I^{exp}_{D-X}$ were simultaneously embedded in the weighted nonlinear least-square fitting procedure:

$$\min \sum_{v'J'} \left[ \left( \frac{T^{exp}_{D^1\Pi} - T^{cal}_{D^1\Pi}}{\delta T^{exp}_{D^1\Pi}} \right)^2 + \sum_{v''J''} \left( \frac{I^{exp}_{D-X} - I^{cal}_{D-X}}{\delta I^{exp}_{D-X}} \right)^2 \right], \tag{7}$$

where the variation parameters are the $D^1\Pi$ state Dunham coefficients. A minimum of the functional (7) was searched by the modified Levenberg-Marquardt algorithm combined with a finite-difference approximation to the corresponding Jacobian matrix. The $A_{ij}^{v'J'v''J''}$ coefficients were evaluated basing on the present *ab initio* MPPT transition dipole moment function $\mu_{D^1\Pi\ X^1\Sigma^+}(R)$, while the rovibronic term values $T^{cal}_{D^1\Pi}$, as well as the wavefunctions $|v_J\rangle$ for the ground $X^1\Sigma^+$ and excited $D^1\Pi$ state have been obtained by a numerical solution of the radial Schrödinger equation with the RKR potentials constructed by means of the isotope-substituted Dunham molecular constants. The ground state molecular constants were taken from Ref. [5].

## III. RESULTS AND DISCUSSION

### A. Electronic structure parameters

*Energy curves.* The potential energy curves, see Fig. 1 and Table I, were calculated by the MPPT method for all singlet and triplet states of NaRb converging to the first three non-relativistic dissociation limits, as well as for the $E^1\Sigma^+$ state converging to the Na($3s$) + Rb($4d$) dissociation limit. The reliability of the derived curves can be tested by their comparison with the available experimental [2,5] and preceding *ab initio* [7,25] data. Figure 1 and Table II demonstrate that the present potentials are in satisfactory agreement with the empirical RKR curves and the corresponding experimental molecular constants for the $X^1\Sigma^+$, $a^3\Sigma^+$, $B^1\Pi$ and $D^1\Pi$ states, as well as with the recent calculations [7]. In a number of cases the present calculations are in somewhat better agreement with experimental data. For instance, for the $B^1\Pi$ state the relative difference $\delta(\omega_e)$ between the calculated and measured [2] vibrational constants is ca. 4% in the present work and ca. 16% in Ref. [7].

*Transition moment functions.* The resulting MPPT transition moments obtained in a dipole-length approximation for the most essential singlet-singlet electronic transitions are presented in Table III. The dipole moment functions for the $B^1\Pi \rightarrow X^1\Sigma^+$ and $D^1\Pi \rightarrow X^1\Sigma^+$ transitions are depicted in Fig. 2 (full symbols), along with the MPPT $\mu_{^1\Pi\Sigma^+}(R)$ functions extracted from the difference of the MPPT $L$-uncoupling matrix elements for different isotopomers according to Eq. (1) (open symbols). As can be seen, except of small $R$-region, the latter are in good agreement with their *ab initio* counterparts calculated directly in dipole-length approximation. The divergence of these two approaches in the small $R$ region seems to be attributed to the small values of the $\xi = \xi(R)$ functions in Eq. (1) which become comparable with the absolute accuracy of the difference in the isotope-substituted $L$-uncoupling matrix elements at $R < 4$ Å. As can be seen from Fig. 2, the $B^1\Pi \rightarrow X^1\Sigma^+$ transition dipole moment function $\mu_{B^1\Pi\ X^1\Sigma^+}$ does not exhibit any strong $R$-dependence in the $R$-interval under study. Such a behaviour does not contradict the estimate $\mu(R) \approx const$ at 3.73 Å $< R <$ 4.98 Å made in [5], the present absolute $\mu$-values being in consistence with the ones obtained in Ref. [5]. For the $D^1\Pi \rightarrow X^1\Sigma^+$ transition the dipole moment function $\mu_{D^1\Pi\ X^1\Sigma^+}(R)$ is steeply

growing with $R$. A rapid increasing of $\mu$ at 4.1 Å $< R <$ 4.6 Å was qualitatively predicted in Ref. [6] from the failure of the Franck-Condon approximation to describe the measured intensity distribution.

*L-uncoupling matrix elements.* The MPPT $L_{B^1\Pi\sim N^1\Sigma^+}$ and $L_{D^1\Pi\sim N^1\Sigma^+}$ electronic matrix elements for the $^{23}$Na$^{85}$Rb isotopomer, $N$ denoting $X, A, C'$ and $E$, are displayed in Fig. 3. As can be seen from Fig. 3*b*, the $L_{B^1\Pi\sim A^1\Sigma^+}(R)$ reflects, in a wide range of $R$, the VanVleck hypothesis of pure precession [26] according to which the $B^1\Pi \sim A^1\Sigma^+$ pair is considered as $\pi,\sigma$-components of the $[NaRb]^+np$ complex, leading to $L_{B^1\Pi\sim A^1\Sigma^+} = \sqrt{2}$. The behaviour of $L_{D^1\Pi\sim C^1\Sigma^+}$ reflects the generalised VanVleck hypothesis of pure precession, according to which $L_{D^1\Pi\sim C^1\Sigma^+}$ should increase from $\sqrt{2}$ to $\sqrt{6}$ as $R$ decreases, see Fig. 3*a*. The pure precession approximation fails completely for all other matrix elements at any $R$ range.

### B. Lifetime

The radiative lifetime estimates for the $B^1\Pi$ and $D^1\Pi$ states were obtained by Eq. (5) accounting for the $B^1\Pi - X^1\Sigma^+$ transition and $D^1\Pi \to X^1\Sigma^+, D^1\Pi \to A^1\Sigma^+, D^1\Pi \to B^1\Pi$ transitions, respectively. The contribution of the remaining $B^1\Pi - A^1\Sigma^+$ and $D^1\Pi - C^1\Sigma^+$ transitions, which were estimated by Eq. (1) from corresponding isotopic-substituted $L$ - uncoupling matrix elements, to the corresponding lifetimes is negligible because of small frequency and probability factors. The calculated $v'$-dependences of rovibronic lifetimes $\tau^{\Pi}_{v'J}$ for the $B^1\Pi$ and $D^1\Pi$ states are presented in Fig. 4 for $J' = 1, 50$ and 100. As can be seen, the $\tau^{\Pi}_{v'J}$ values demonstrate pronounced sensitivity to vibrational and rotational quantum numbers thus reflecting the strong $R$-dependences of the $A^{sum}(R)$ operator in Eq. (5) for both states.

To the best of our knowledge, there exist only two spontaneous lifetime $\tau_{vJ}$ measurements in the $B^1\Pi$ and $D^1\Pi$ states of the NaRb molecule, one for a particular $v, J$ level for each state. The value $\tau(v' = 5, J' \approx 20) = 17.8$ ns is reported in Ref. [5] for the $B^1\Pi$ state and $\tau(v' = 0, J' = 44) = 22.6 \pm 1.8$ ns is reported in Ref. [8] for the $D^1\Pi$ state. As can be seen from Fig. 4, the agreement between the calculated and the experimental values is quite satisfactory. It seems that the experimental $\tau_{vJ}$ value for the $B^1\Pi$ state slightly (for ca. 10%) exceeds its theoretical estimate, see Fig. 4*a*, while the measured value for the $D^1\Pi$ state is somewhat 5% smaller than the theoretical one, see Fig. 4*b*. Note however that due to the lack of experimental data it is difficult to make any definite judgement on whether the drawbacks in calculation or the experimental inaccuracies are responsible for this discrepancy, and it is clear that a more profound experimental study is needed to test the theory.

### C. Λ-doubling constants

Experimental Λ-doubling constants $q_{exp}$ are presented in Table IV for a number of rovibronic levels of the $B^1\Pi$ and $D^1\Pi$ states. Only absolute values $|q_{exp}|$ can be deduced from the RF-ODR experiment. The errors quoted for $q_{exp}$ are estimated from the statistical uncertainty in the resonance position of the RF-ODR signals. We added to our data for the $B^1\Pi$ state the $q_{exp}$ value and sign for the level $v(J) = 8(15)$, which we extracted from the high resolution spectroscopy studies reported in Ref. [5]. Note that, as follows from Ref. [5], this level is strongly locally perturbed.

*Singlet-singlet approximation.* The $q^{\Pi}_{v'J}$ values calculated in the singlet-singlet approximation, see Eqs. (2) and (6), are given in Table IV as $q^{s-s}$ for the $B^1\Pi$ and $D^1\Pi$ states. They demonstrate pronounced sensitivity to the vibrational and rotational quantum numbers involved. This reflects the strong $R$-dependences of the $Q^{sum}(R)$ operator in (6), see Fig. 5. The behaviour of $Q^{sum}(R)$ in Fig. 5 shows that the $D^1\Pi$ state obeys the unique perturber approximation [27]. Moreover, the observed crossing at $R \approx 6$(Å) between the interacting $D^1\Pi \sim E^1\Sigma^+$ states, see Fig. 1, does not affect the $q^{D}_{v'J}$-values for $v^D = 1 \ldots 12$ since the $L_{D^1\Pi\sim E^1\Sigma^+}$-uncoupling matrix element, see Fig. 3, as well as the probability densities of the corresponding vibrational wavefunctions are negligible near the crossing point. The $q$-factors for the $B^1\Pi$ state are determined by a strong competition between the lower $A^1\Sigma^+$ and upper $C^1\Sigma^+$ state contributions leading to the extremely small $q$-values. This fact explains why Λ-splitting in the $B^1\Pi$ state was not observed for the unperturbed levels in the high-resolution spectroscopy studies [2].

The $q$ factors in the $D^1\Pi$ state, being about $1 \times 10^{-5}$ cm$^{-1}$, are much larger than the ones in the $B^1\Pi$ state. As follows from Table IV, the calculated $D^1\Pi$ state $q$-factors $q^{s-s}$ are in good agreement with the experimental ones in a wide range of $v'(J')$ levels except of the level $v'(J') = 10(36)$, in which $q_{exp}$ exceeds the calculated value by a factor of almost two. The comparison of $q^{s-s}$ and $q_{exp}$ values for the $B^1\Pi$ state shows less consistency, which can be probably attributed to the effect of local perturbations.

*Singlet-triplet perturbation effect.* The spin-orbit (SO) interaction $B^1\Pi \sim c^3\Sigma^+$ mixes the $B^1\Pi(S = 0, \Omega = \Lambda = \pm 1)$ state with the $^3\Sigma^+_1(S = 1, \Omega = \Sigma = \pm 1)$ components of the crossing $c^3\Sigma^+$ state, see Fig. 1. In the framework of the simplest two-level model, the $e$-parity levels of the perturbed $B^1\Pi$ state interact with the $^3\Sigma^+_0(S = 1, \Omega = \Sigma = 0)$

component of the $c^3\Sigma^+$ state due to the $S$-uncoupling matrix element $C^{s-t}\sqrt{J(J+1)}/MR^2$, where $C^{s-t}$ is the mixing coefficient corresponding to a fraction of the $c^3\Sigma^+$ state in the perturbed $B^1\Pi$ state wavefunction [23]. Then, assuming the regularity of the spin-rotational perturbation, the contribution $q^{s-t}$ of the singlet-triplet $B^1\Pi \sim c^3\Sigma^+$ interaction into the $q$-factors of the $B^1\Pi$ state is roughly reduced by the sum rule (6) to the form:

$$q^{s-t} = \frac{1}{M^2}\langle v_J^{\Pi}|\frac{1}{\lambda R^4}\left(\frac{1-\Delta U_{B-c}/\lambda}{1+\Delta U_{B-c}/\lambda}\right)|v_J^{\Pi}\rangle, \tag{8}$$

where $\lambda(R) = \sqrt{\Delta U_{B-c}^2 + 4V_{so}^2}$ and $V_{so}(R)$ is the $B^1\Pi \sim c^3\Sigma^+$ SO matrix element. The required $V_{so}^{NaRb}(R)$ function was estimated from the corresponding *ab initio* $V_{so}^{NaK}(R)$ function for the NaK molecule [28] which was scaled by the ratio of the experimental SO constants of Rb and K atoms [29]: $V_{so}^{NaRb}(R) = V_{so}^{NaK}(R)\varsigma_{so}^{Rb}/\varsigma_{so}^{K}$, where $\varsigma_{so}^{Rb} = 158$ cm$^{-1}$, $\varsigma_{so}^{K} = 38$ cm$^{-1}$. In spite of the crude model used, the resulting $q$-factors $q^{sum} = q^{s-s} + q^{s-t}$ presented in Table IV are in reasonable agreement with their experimental analogues, especially taking into account the small values of the $B^1\Pi$ state $q$-factors. The possible SO $B^1\Pi \sim b^3\Pi$ perturbation effect on the $q$-factors of the $B^1\Pi$ state is expected to be much less pronounced than the $B^1\Pi \sim c^3\Sigma^+$ one since its influence appears only in the third order of the nondegenerate perturbation theory. Moreover, Fig.1 induces one to assume that the overlap integrals between vibrational wavefunctions of the $B^1\Pi$ and $b^3\Pi$ states are negligible for the low $v_B$-levels, thus, assignment of a number of local $B^1\Pi$ state perturbations to a direct $B^1\Pi \sim b^3\Pi$ SO interaction [3] seems to be questionable. It should be also added that in Hund's case (c) coupling representation the difference in perturbation effects caused by the $^3\Pi_1$ and $^3\Sigma_1$ components becomes indistinguishable.

Although an admixture of the triplet $d^3\Pi$ and $c^3\Sigma^+$electronic wave functions to the $D^1\Pi$ state wave function seems to be of lesser importance than for the $B^1\Pi$ state because of much smaller SO effects in the $Na(3p)$ atom as compared to $Rb(5p)$, the local singlet-triplet interaction could be responsible for the relatively small irregular changes of the measured $q_{v'J}^{\Pi}$ factor, see Table IV.

### D. Refinement of the $D^1\Pi$ potential

The relative intensity distributions in the $D^1\Pi \rightarrow X^1\Sigma^+$ LIF progressions resulting from the fixed $D^1\Pi$ state vibrational-rotational levels $v'(J')$ measured in the present work, namely 0(44), 1(104), 4(25), 6(44), 6(120), 10(36) and 12(50) are presented in Fig. 6 (open bars), along with the $v'(J')$ equal to 0(44), 5(62), 6(44) from Ref. [6] (striped bars). Table V contains the experimentally determined term values $T_{v'J'}^{exp}$ obtained by adding the wavenumbers of $Ar^+$ laser lines causing $D^1\Pi(v',J') \leftarrow X^1\Sigma^+(v'',J'')$ transitions to the corresponding $X^1\Sigma^+(v'',J'')$ energies, which were calculated by means of Dunham constants from Ref. [5]. Term values with $J' \geq 100$ are not presented in Table V since their accuracy is insufficient due to still unknown centrifugal-distortion constants of the $X^1\Sigma^+$ state, hence, the $J'$ assignment is not unambigious for large $J'$ values.

The measured intensity distributions and term values were involved in the simultaneous non-linear fitting procedure, see Eq. (7), to produce the refined molecular constant set for the $D^1\Pi$ state of the $^{23}Na^{85}Rb$ molecule. Three different initial sets of the $D^1\Pi$ state molecular constants were used, namely, the constants given in Ref. [6], as well as the constants estimated from the present and preceding [7] *ab initio* potentials. The independence of the final set of the molecular constants of the choice of the initial sets guarantees the achievement of the global minimum of the functional (7). The refined $D^1\Pi$ state molecular constants are given in Table II, while the corresponding RKR potential is depicted in Fig. 1 (solid bold line). The calculated relative intensity distributions are displayed in Fig. 6 (full bars). As follows from Fig. 6, the present experimental and theoretical intensities are in satisfactory agreement, especially for high vibrational levels $v'$. They agree with the preceding intensity distributions measured by the Kato group [6], which are also depicted in Fig. 6 (striped bars) when available. The $D^1\Pi$ state rovibronic term values $T_{v'J'}$ calculated with the refined molecular constants from the Table II reproduce their experimental counterparts much better than the calculations based on the previous constants from Ref. [6], cf. the differences $\Delta_{v'J'}$ between the observed and calculated $T_{v'J'}$ values in Table V. The maximum deviation between the theoretical and experimental term values has been obtained for the level $v' = 10, J' = 36$, which seems to be locally perturbed by the near-lying $d^3\Pi$ and/or $c^3\Sigma^+$ state, see Fig.1. Note that it is just this level possessing the largest deviation between the observed and calculated $q$-factor, see Table IV.

It is worth mentioning that the refinement of the $D^1\Pi$ state molecular constants is achieved mainly through the improvement of the rotational constants. Indeed, the changes in $B_i$ are ca. 1%, while $\omega_i$ was changed only by ca. 0.3%, see Table II. This can be clearly understood from the fact that the Franck-Condon factors are more sensitive to the variation of the rotational constants than of the vibrational ones.

## IV. CONCLUDING REMARKS

The MPPT calculation method previously used to estimate the NaRb permanent electric dipoles [9] has been successfully applied to evaluate the energy and radiative properties of the NaRb molecule. Further improvement of the theoretical treatment apparently demands an explicit consideration of overall singlet-triplet interactions based on relativistic calculations of the spin-orbit matrix elements [28]. The *ab initio* calculations required are currently in progress.

The paper demonstrates that in the case when only few experimental term values of the upper state are available, an improvement of the molecular constant set can be achieved by including the relative LIF intensities into the simultaneous fitting routine. The required accurate transition dipole moment functions can be obtained as the *ab initio* MPPT estimates.

The calculated transition moments $\mu(R)$ and $L$-uncoupling matrix elements of NaRb are very close to the corresponding $\mu(R)$ and $L(R)$ functions of the NaK molecule [14,15]. The minor changes of $\tau_{v'J'}$ and $q_{v'J'}$ in passing from NaK to NaRb can be attributed to the mass dependence, small relative position changes of the interacting electronic states, as well as to the more pronounced SO effects.

## V. ACKNOWLEDGMENTS

Financial support by the Russian Fund of Fundamental Research under Grants No.00-03-32978 and No. 00-03-33004 is gratefully acknowledged by Moscow group. Riga group is appreciating the financial support from the Latvian Science Council under Grant No. 96.0323. O.N. is grateful for the support from the Latvian Science Council Doctoral Studies Grant No. 44. R.C. gratefully acknowledges support from the Italian MURST (Grant 9803246-003). The authors are grateful to Prof. W. C. Stwalley for useful discussions.

---

[1] H. Wang and W. C. Stwalley, J. Chem. Phys. **108**, 5767 (1998).
[2] Y. C. Wang, M. Kajitani, S. Kasahara, M. Baba, K. Ishikawa, and H. Kato, J. Chem. Phys. **95**, 6229 (1991).
[3] Y. C. Wang, K. Matsubara, and H. Kato, J. Chem. Phys. **97**, 811 (1992).
[4] K. Matsubara, Y.-C. Wang, K. Ishikawa, M. Baba, A. J. McCaffery, and H. Katô, J. Chem. Phys. **99**, 5036 (1993).
[5] S. Kasahara, T. Ebi, M. Tanimura, H. Ikoma, K. Matsubara, M. Baba, and H. Katô, J. Chem. Phys. **105**, 1341 (1996).
[6] N. Takahashi and H. Katô, J. Chem. Phys. **75**, 4350 (1981).
[7] M. Korek, A. R. Allouche, M. Kobeissi, A. Chaalan, M. Dagher, K. Fakherddin, and M. Aubert-Frecon , Chem. Phys. **256**, 1 (2000).
[8] M. Jansons, J. Klavins, Z. Kharcheva, and M. Tamanis, Physica Scripta **45**, 328 (1992).
[9] O. Nikolayeva, I. Klincare, M. Auzinsh, M. Tamanis, R. Ferber, E. A. Pazyuk, A. V. Stolyarov, A. Zaitsevski, and R. Cimiraglia, J. Chem. Phys. **113**, 4896 (2000).
[10] J. M. Walter and S. Barrat, Proc. R. Soc. London Sec. A **119**, 257 (1928).
[11] A. Zaitsevskii and J. P. Malrieu, Theor. Chem. Acc. **96**, 269 (1997).
[12] A. Zaitsevskii and R. Cimiraglia, Int. J. Quantum Chem. **73**, 395 (1999).
[13] M. Tamanis, M. Auzinsh, I. Klincare, O. Nikolayeva, R. Ferber, E. A. Pazyuk, A. V. Stolyarov, and A. Zaitsevskii, Phys. Rev. A. **58**, 1932 (1998).
[14] M. Tamanis, M. Auzinsh, I. Klincare, O. Nikolayeva, R. Ferber, A. Zaitsevskii, E. A. Pazyuk, and A. V. Stolyarov, J. Chem. Phys. **109**, 6725 (1998).
[15] S. O. Adamson, A. Zaitsevskii, E. A. Pazyuk, A. V. Stolyarov, M. Tamanis, R. Ferber, and R. Cimiraglia, J. Chem. Phys. **113** (2000), in press.
[16] A. V. Stolyarov and V. I. Pupyshev, Phys. Rev. A **49**, 1693 (1994).
[17] S. J. Silvers, T. H. Bergeman, and W. Klemperer, J. Chem. Phys. **52**, 4385 (1970).
[18] R. W. Field and T. H. Bergeman, J. Chem. Phys. **54**, 2936 (1971).
[19] G. Audi and A. M. Wapstra, Nuclear Physics, **A595**, 409 (1995).
[20] M. Mizushima, *Theory of Rotating Diatomic Molecules* (J.Wiley and Sons, New York, 1975).
[21] L. F. Pacios and P. A. Christiansen, J. Chem. Phys. **82**, 2664 (1985).
[22] L. A. LaJohn, P. A. Christiansen, R. B. Ross, T. Atashroo, and W. C. Ermler, J. Chem. Phys. **87**, 2812 (1987).
[23] H. Lefebvre-Brion and R. W. Field, *Perturbations in the Spectra of Diatomic Molecules* (Academic, New York, 1986).

[24] E. A. Pazyuk, A. V. Stolyarov, and V. I. Pupyshev, Chem. Phys. Lett. **228**, 219 (1994).
[25] G. Igel-Mann, U. Wedig, P. Fuentealta, and H. Stoll, J. Chem. Phys. **84**, 5007 (1986).
[26] J. H. van Vleck, Phys. Rev. **33**, 467 (1929).
[27] R. N. Zare, A. L. Schmeltekopf, W. J. Harrop, and D. L. Albritton, J. Mol. Spectrosc. **46**, 37 (1973).
[28] R. Ferber, E. A. Pazyuk, A. V. Stolyarov, A. Zaitsevskii, P. Kowalczyk, Hongmin Chen, He Wang, and W. C. Stwalley, J. Chem. Phys. **112**, 5740 (2000).
[29] W. L. Wiese, M. W. Smith, and B. M. Miles, *Atomic Transition Probabilities* **2**, Nat. Stand. Ref. data Ser., NBS Circ. 22, U.S.G.P.O. Washington, D.C. 1969.

## Captions to figures

Figure 1. The MPPT potential energy curves for the low-lying singlet (solid lines) and triplet (dashed lines) states of NaRb. The empirical RKR potentials for the $X^1\Sigma^+$ [5], $a^3\Sigma^+$ [5], $B^1\Pi$ [2] and $D^1\Pi$ (present) states are depicted by bold solid lines.

Figure 2. The MPPT transition dipole moments $\mu_{B^1\Pi-X^1\Sigma^+}$ and $\mu_{D^1\Pi-X^1\Sigma^+}$ calculated in the dipole-length approximation (full symbols), extracted from the isotopic-substituted $L$-uncoupling matrix elements (open symbols). The empirical estimates from Refs. [5,6] are shown by bold solid lines.

Figure 3. The $R$-dependence of the MPPT $L$-uncoupling electronic matrix elements between the $^1\Pi$ state and the first four $^1\Sigma^+$ states for the $^{23}Na^{85}Rb$ isotopomer. (a) $D^1\Pi$ state. (b) $B^1\Pi$ state.

Figure 4. The calculated radiative lifetimes of $^{23}Na^{85}Rb$ versus vibrational quantum number $v'$ for three different rotational quantum numbers $J'$. (a) $B^1\Pi$ state. (b) $D^1\Pi$ state. Full circles denote the experimental lifetimes of the $B^1\Pi(v'=5, J'\approx 20)$ [5] and $D^1\Pi(v'=0, J'=44)$ [8] levels.

Figure 5. The calculated according to Eq. 6 partial ($Q_J$) and summary ($Q^{sum}$, bold) contributions of the first four $^1\Sigma^+$ states into the $q$-values of the $D^1\Pi$ state (a) and $B^1\Pi$ state (b) of $^{23}Na^{85}Rb$.

Figure 6. Comparison of the preceding [6] and present measured relative intensity distributions in the $D^1\Pi(v', J') \rightarrow X^1\Sigma^+$ LIF progressions with their theoretical analogues. Both measured and calculated probabilities for each progression were normalized to 1 for the band having maximum intensity. (*) — intensity could not be determined due to overlapping with other lines.

TABLE I. MPPT potential curves of the NaRb molecule (in $cm^{-1}$).

| R(a.u.) | $X^1\Sigma^+$ | $A^1\Sigma^+$ | $B^1\Pi$ | $C^1\Sigma^+$ | $D^1\Pi$ | $E^1\Sigma^+$ |
|---|---|---|---|---|---|---|
| 5.4 | 2664 | 17926 | 20772 | 23482 | 24117 | 26698 |
| 5.9 | 998 | 15426 | 18721 | 21130 | 22149 | 24380 |
| 6.4 | 192 | 13716 | 17451 | 19506 | 20807 | 22937 |
| 6.9 | 2 | 12655 | 16769 | 18177 | 19997 | 22162 |
| 7.4 | 237 | 12015 | 16457 | 17839 | 19545 | 21829 |
| 7.9 | 734 | 11763 | 16429 | 17557 | 19429 | 21823 |
| 8.4 | 1340 | 11708 | 16506 | 17456 | 19483 | 21719 |
| 8.9 | 1980 | 11812 | 16660 | 17512 | 19691 | 21520 |
| 9.4 | 2603 | 12025 | 16831 | 17678 | 19998 | 21397 |
| 9.9 | 3186 | 12322 | 16974 | 17939 | 20321 | 21336 |
| 10.4 | 3673 | 12660 | 17107 | 18237 | 20629 | 21268 |
| 10.9 | 4082 | 13043 | 17228 | 18586 | 20920 | 21221 |
| 11.5 | 4469 | 13543 | 17362 | 19037 | 21209 | 21156 |
| 12.1 | 4751 | 14066 | 17463 | 19479 | 21421 | 21093 |
| 12.65 | 4942 | 14557 | 17542 | 19867 | 21561 | 21043 |
| 13.25 | 5091 | 15078 | 17612 | 20235 | 21651 | 21011 |
| R(a.u.) | $a^3\Sigma^+$ | $b^3\Pi$ | $c^3\Sigma^+$ | $d^3\Pi$ | $e^3\Sigma^+$ | |
| 5.4 | 11531 | 13115 | 22890 | 24032 | 24769 | |
| 5.9 | 9306 | 11923 | 19979 | 21991 | 22530 | |
| 6.4 | 7759 | 11210 | 17934 | 20631 | 21114 | |
| 6.9 | 6739 | 11060 | 16655 | 19836 | 20394 | |
| 7.4 | 6030 | 11302 | 15867 | 19396 | 20058 | |
| 7.9 | 5629 | 11804 | 15518 | 19260 | 20074 | |
| 8.4 | 5353 | 12436 | 15386 | 19261 | 20273 | |
| 8.9 | 5204 | 13147 | 15427 | 19378 | 20603 | |
| 9.4 | 5128 | 13870 | 15571 | 19573 | 20981 | |
| 9.9 | 5115 | 14574 | 15777 | 19765 | 21331 | |
| 10.4 | 5110 | 15217 | 15991 | 19984 | 21643 | |
| 10.9 | 5130 | 15789 | 16212 | 20225 | 21826 | |

| | | | | | |
|---|---|---|---|---|---|
| 11.5 | 5169 | 16364 | 16463 | 20535 | 21907 |
| 12.1 | 5207 | 16798 | 16690 | 20837 | 21905 |
| 12.65 | 5245 | 17099 | 16875 | 21091 | 21875 |
| 13.25 | 5282 | 17330 | 17050 | 21319 | 21849 |

TABLE II. Comparision of the experimental and *ab initio* molecular constants for the $X^1\Sigma^+$, $a^3\Sigma^+$, $B^1\Pi$ and $D^1\Pi$ states of $^{23}Na^{85}Rb$. (Energies in $cm^{-1}$, $R_e$ in Å).

| | | Experimental | *Ab initio* | | |
|---|---|---|---|---|---|
| | | Ref. [2,5] | present | Ref. [7] | Ref. [25] |
| $X^1\Sigma^+$ | $R_e$ | 3.6435 | 3.62 | 3.71 | 3.63 |
| | $\omega_e$ | 106.86 | 107.3 | 103.9 | 106.0 |
| $a^3\Sigma^+$ | $T_e$ | 4847.75 | 5110 | 4363 | |
| | $R_e$ | 5.75 | 5.46 | 5.94 | |
| | $\omega_e$ | 18.8 | 21.7 | 15.3 | |
| $B^1\Pi$ | $T_e$ | 16527.79 | 16420 | 16321 | |
| | $R_e$ | 4.1767 | 4.08 | 4.34 | |
| | $\omega_e$ | 61.17 | 58.8 | 51.6 | |

| | | Experimental | | *Ab initio* | |
|---|---|---|---|---|---|
| | | Ref. [6] | present | present | Ref. [7] |
| $D^1\Pi$ | $T_e$ | 19695 | 19692.06 | 19475 | 19529 |
| | $R_e$ | 4.139 | 4.2155 | 4.22 | 4.31 |
| | $\omega_e$ | 73.5 | 73.26 | 70.3 | 71.9 |
| | $\omega_e x_e$ | 0.459 | 0.4744 | | |
| | $\omega_e y_e$ | | $0.8297\times10^{-2}$ | | |
| | $B_e$ | 0.0544 | 0.05244 | | |
| | $\alpha_e$ | $0.36\times10^{-3}$ | $0.3311\times10^{-3}$ | | |
| | $\gamma_e$ | | $0.9350\times10^{-6}$ | | |

TABLE III. MPPT transition dipole moment functions.

| R, a.u. | $\mu(R)$, a.u. | | | | | |
|---|---|---|---|---|---|---|
| | $A-X$ | $B-X$ | $C-X$ | $D-X$ | $D-A$ | $D-B$ |
| 5.4 | 3.589 | 3.176 | 0.918 | 0.792 | 1.588 | 1.977 |
| 5.9 | 3.694 | 3.111 | 0.914 | 0.950 | 1.698 | 2.218 |
| 6.4 | 3.814 | 3.111 | 0.911 | 1.094 | 1.735 | 2.402 |
| 6.9 | 3.939 | 3.078 | 0.997 | 1.252 | 1.694 | 2.403 |
| 7.4 | 4.076 | 3.035 | 1.083 | 1.447 | 1.584 | 2.252 |
| 7.9 | 4.197 | 2.974 | 1.191 | 1.662 | 1.434 | 1.968 |
| 8.4 | 4.304 | 2.897 | 1.321 | 1.892 | 1.258 | 1.581 |
| 8.9 | 4.377 | 2.812 | 1.461 | 2.107 | 1.079 | 1.175 |
| 9.4 | 4.408 | 2.739 | 1.605 | 2.288 | 0.913 | 0.803 |
| 9.9 | 4.394 | 2.663 | 1.739 | 2.458 | 0.756 | 0.477 |
| 10.4 | 4.332 | 2.620 | 1.859 | 2.577 | 0.620 | 0.245 |
| 10.9 | 4.229 | 2.596 | 1.966 | 2.667 | 0.196 | 0.072 |
| 11.5 | 4.071 | 2.590 | 2.072 | 2.740 | 0.368 | -0.063 |
| 12.1 | 3.901 | 2.599 | 2.171 | 2.784 | 0.255 | -0.151 |
| 12.65 | 3.753 | 2.612 | 2.268 | 2.810 | 0.165 | -0.201 |
| 13.25 | 3.617 | 2.637 | 2.381 | 2.820 | 0.073 | -0.227 |

TABLE IV. The calculated ($q^{s\ s}, q^{sum}$) and experimental ($q_{exp}$) Λ-doubling constants (in $10^{-5}$ cm$^{-1}$) for the $B^1\Pi$ and $D^1\Pi$ states. The $q^{s\ s}$ values are obtained in the singlet-singlet approximation, while $q^{sum}$ takes into account the spin-orbit $B^1\Pi \sim c^3\Sigma^+$ interaction.

| Isotopomer | $v'(J')$ | $\lvert q_{exp}\rvert$ | $q^{s\ s}$ | $q^{sum}$ |
|---|---|---|---|---|
| | | $B^1\Pi$ state | | |
| $^{23}Na^{85}Rb$ | 4(98) | $0.023 \pm 0.001$ | -0.04 | -0.02 |
| $^{23}Na^{85}Rb$ | 5(116) | $0.054 \pm 0.001$ | -0.04 | -0.03 |
| $^{23}Na^{87}Rb$ | 6(24) | $0.29 \pm 0.03$ | -0.01 | +0.2 |
| $^{23}Na^{85}Rb$ | 8(15) | 0.5[a] | -0.01 | +0.4 |
| | | $D^1\Pi$ state | | |
| $^{23}Na^{85}Rb$ | 0(44) | $0.971 \pm 0.003$ | +1.20 | |
| $^{23}Na^{85}Rb$ | 1(7) | $1.19 \pm 0.12$ | +1.22 | |
| $^{23}Na^{85}Rb$ | 4(25) | $1.08 \pm 0.03$ | +1.17 | |
| $^{23}Na^{85}Rb$ | 4(41) | $1.087 \pm 0.002$ | +1.16 | |
| $^{23}Na^{87}Rb$ | 6(44) | $1.130 \pm 0.003$ | +1.13 | |
| $^{23}Na^{87}Rb$ | 10(36) | $1.818 \pm 0.003$ | +1.10 | |
| $^{23}Na^{85}Rb$ | 12(50) | $1.091 \pm 0.001$ | +1.06 | |

[a] $q$ value was obtained with "+" sign from the high-resolution spectroscopy data [5].

TABLE V. Experimental $D^1\Pi$ state term values $T_{v'J'}$. $\lambda_{exc}$ is the exciting laser wavelength (in nm) and $\Delta_{v-c}$ is the difference between the observed term values and the term values calculated using either the present constant set ($\Delta_{v-c}^{present}$) or the constants given in Ref. [6] ($\Delta_{v-c}^{Ref.\ [6]}$). $T_{v'J'}$ and $\Delta_{v-c}$ are in cm$^{-1}$.

| Isotopomer | $v',J' \leftarrow v'',J''$ | $\lambda_{exc}$ | $T_{v'J'}^{exp}$ | $\Delta_{v-c}^{present}$ | $\Delta_{v-c}^{Ref.\ [6]}$ |
|---|---|---|---|---|---|
| $^{23}Na^{85}Rb$ | 0,11←2,11 | 511.5 | 19831.53 | 0.07 | 9.53 |
| $^{23}Na^{85}Rb$ | 1,7←3,8 | 514.5 | 19804.03 | -0.21 | 13.80 |
| $^{23}Na^{85}Rb$ | 4,25←5,24 | 514.5 | 20042.02 | -0.91 | 13.13 |
| $^{23}Na^{85}Rb$ | 4,41←0,41 | 501.7 | 20099.61 | 0.68 | 9.27 |
| $^{23}Na^{87}Rb$ | 6,44←6,45 | 514.5 | 20248.61 | 1.72 | 8.53 |
| $^{23}Na^{87}Rb$ | 10,36←2,35 | 496.5 | 20472.87 | -4.24 | 21.40 |
| $^{23}Na^{85}Rb$ | 12,50←3,49 | 496.5 | 20673.00 | -0.19 | 20.21 |

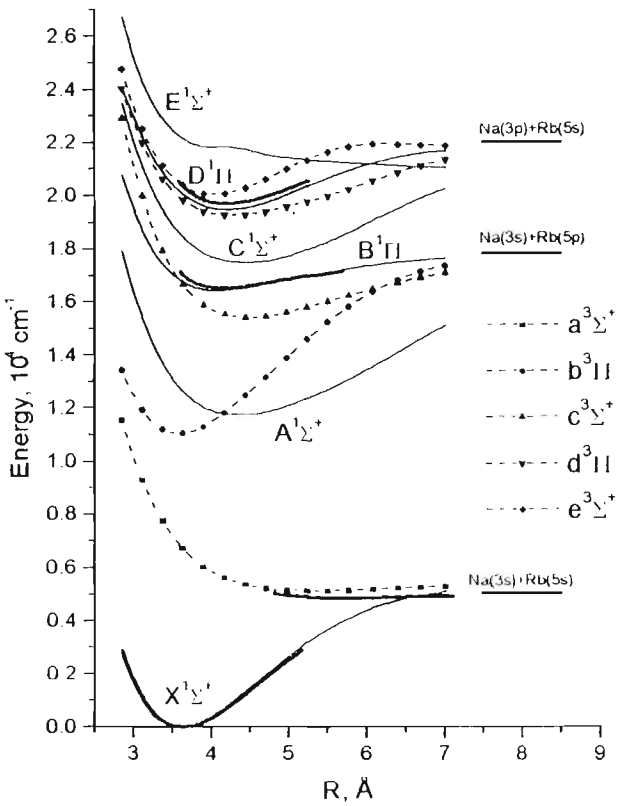


Fig. 1.

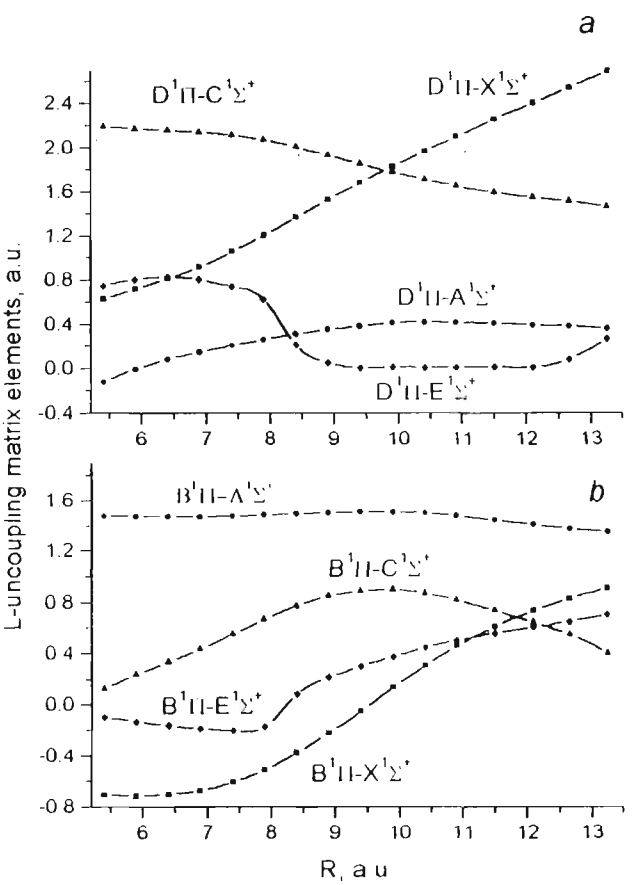


Fig. 3.

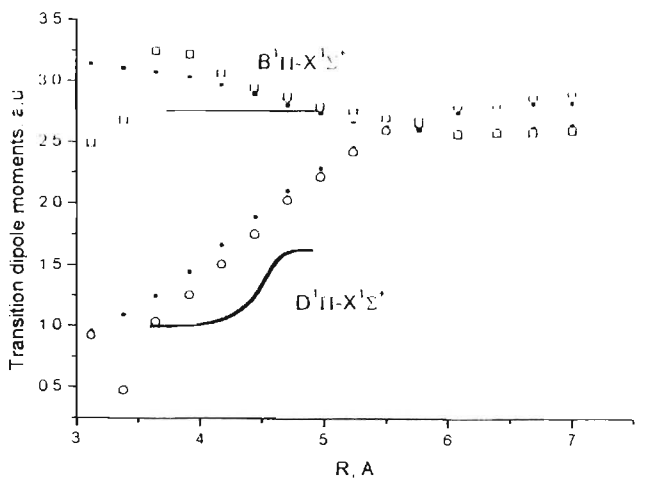


Fig. 2.

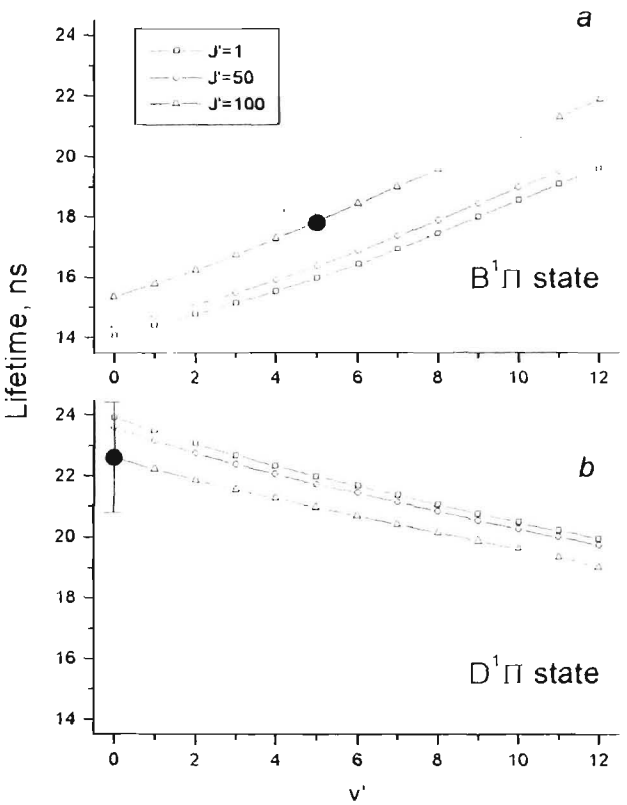
a
J'=1
J'=50
J'=100
B¹Π state
b
D¹Π state
Lifetime, ns
v'

Fig. 4.

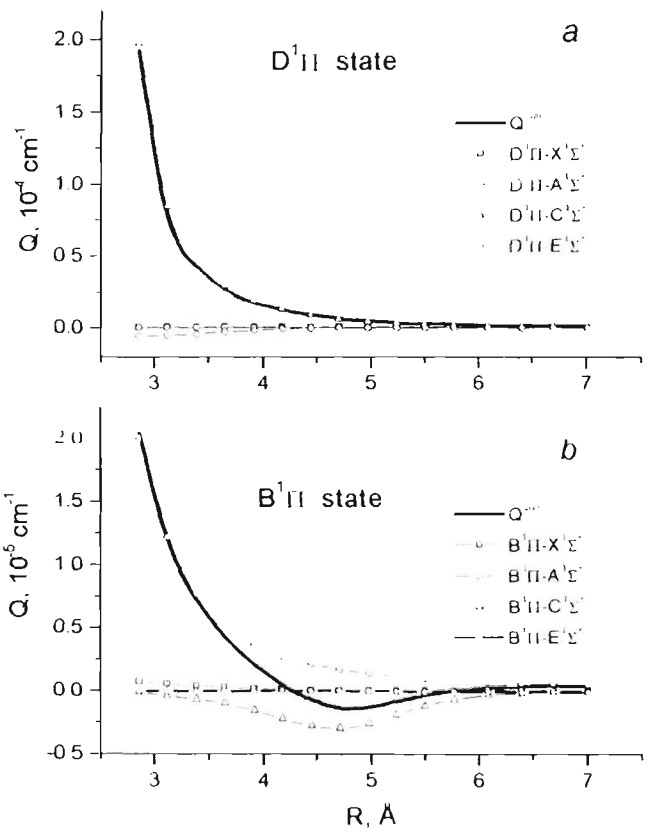
a
D¹Π state
Q, 10⁻⁴ cm⁻¹
D¹Π-X¹Σ⁺
D¹Π-A¹Σ⁺
D¹Π-C¹Σ⁺
D¹Π-E¹Σ⁺
b
B¹Π state
Q, 10⁻⁵ cm⁻¹
B¹Π-X¹Σ⁺
B¹Π-A¹Σ⁺
B¹Π-C¹Σ⁺
B¹Π-E¹Σ⁺
R, Å

Fig. 5.

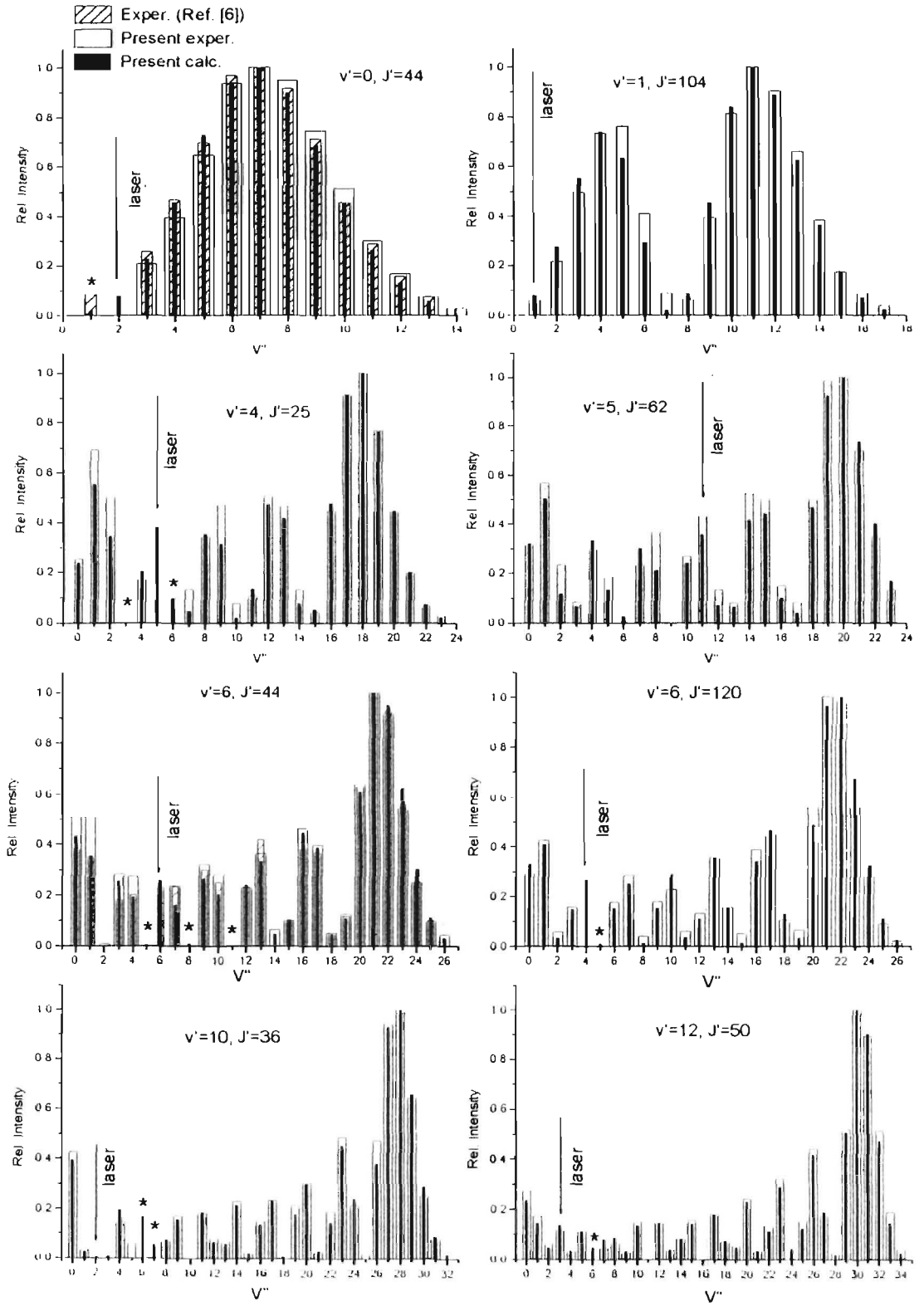
Exper. (Ref. [6])
Present exper.
Present calc.
v'=0, J'=44
v'=1, J'=104
v'=4, J'=25
v'=5, J'=62
v'=6, J'=44
v'=6, J'=120
v'=10, J'=36
v'=12, J'=50
laser
Rel Intensity
V''

Fig. 6.

JOURNAL OF CHEMICAL PHYSICS VOLUME 113, NUMBER 12 22 SEPTEMBER 2000

# Permanent electric dipoles in $B^1\Pi$ and $D^1\Pi$ states of NaRb: Experiment and theory

O. Nikolayeva, I. Klincare, M. Auzinsh, M. Tamanis, and R. Ferber
*Department of Physics, University of Latvia, Riga LV-1586, Latvia*

E. A. Pazyuk, A. V. Stolyarov, and A. Zaitsevskii
*Department of Chemistry, Moscow State University, Moscow 119899, Russia*

R. Cimiraglia
*Dipartimento di Chimica, Università di Ferrara, Via Borsari 46, I-44100, Ferrara, Italy*

(Received 26 April 2000; accepted 27 June 2000)

The paper presents experimentally obtained permanent electric dipole moment values ($\mu$) in electronically excited $B\,^1\Pi$ and $D\,^1\Pi$ states of $^{23}Na^{85}Rb$ and $^{23}Na^{87}Rb$ isotopomer molecules for a number of vibrational and rotational levels ($v',J'$). The method is based on measuring relative intensities of "forbidden" fluorescence lines appearing due to dc Stark effect induced $e/f$ parity mixing for a particular ($v',J'$)-level, combined with electric radio frequency optical double resonance measurement of $\Lambda$-splitting energy $\Delta_{e,f}$. The measured $D\,^1\Pi$ state $\mu$ values are close to 6 D, representing minor changes with the vibrational level $v'$ varying from 0 to 12 and $J'$ in the region between 7 and 50, while the measured $B\,^1\Pi$ state $\mu$ values are about 3 D for $v' = 4$, 5 and 6. The $X\,^1\Sigma^+$, $B\,^1\Pi$, and $D\,^1\Pi$ dipole moment functions $\mu(R)$ are calculated *ab initio* using the many body multipartitioning perturbation theory for explicit treatment of core-valence correlations. The theoretical and experimental dipole moment estimates are in a perfect agreement for the ground state and the $D\,^1\Pi$ state, differing by 15%–25% for the $B\,^1\Pi$ state. © *2000 American Institute of Physics*. [S0021-9606(00)00336-6]

## I. INTRODUCTION

The permanent electric dipole moment of an electronically excited molecular state carries valuable information on its electronic structure as well as on energy transfer properties. As has been demonstrated by our recent studies[1,2] on the NaK molecule, which is up to now the best-understood heteronuclear alkali dimer, it is possible to obtain reliable permanent electric dipole moment values for given $v'$ and $J'$ levels belonging to the excited $^1\Pi$ states by measuring dc Stark effect induced changes in laser induced fluorescence (LIF) spectra combined with the direct determination of $e/f$ $\Lambda$-splitting frequency ($\Delta_{e,f}$) of the ($v',J'$)-level under study by applying the electric Radio Frequency Optical Double Resonance (RF–ODR) method. On the other hand, the *ab initio* calculation based on the multipartitioning perturbation theory (MPPT) demonstrated excellent agreement with experimentally obtained permanent dipole values of the $D\,^1\Pi$ state.[1] The NaK data on permanent electric dipoles are the only ones existing for electronically excited heteronuclear alkali dimers, the objects that are now of increased interest because of studies of collision dynamics and photoassociative spectra, laser cooled and trapped alkaline atoms. As follows from the present state of research, mixed alkali diatomics, such as NaK, NaRb, and KRb seem to be promising for the formation of ultracold molecules.[3,4]

The main purpose of the present work is to use the methods of measurement and *ab initio* calculations of permanent electric dipole moments, developed and approved for NaK in Ref. 1 and 2, to study the NaRb molecule. The NaRb molecule has been recently intensively studied spectroscopically by the Kató group.[5–9] However, the existing spectroscopic information on NaRb is much scarcer than for NaK. Only the $X\,^1\Sigma^+$ and $B\,^1\Pi$ electronic states have been studied systematically by high resolution methods of polarization spectroscopy and optical-optical double resonance spectroscopy.[6–9] The dense perturbation pattern discovered in the $B\,^1\Pi$ state was ascribed to interaction with perturbing $b\,^3\Pi$ and $c\,^1\Sigma^+$ triplet states correlating to the same atomic limit Na ($3s$) + Rb ($5p$). As far as molecular terms correlating to the Na ($3p$) + Rb ($5s$) atoms are concerned, only the $D\,^1\Pi$ state has been studied[5] using LIF methods, namely, by exciting selectively the $D\,^1\Pi$ ($v',J'$)-levels with the fixed frequency $Ar^+$-laser lines and analyzing spectrally resolved $D\,^1\Pi(v',J') \rightarrow X\,^1\Sigma^+(v'',J'')$ LIF progressions. The difficulties in working on NaRb arise from the presence of two isotopomer mixture $^{23}Na^{85}Rb$ and $^{23}Na^{87}Rb$ and more dense rotational pattern than in NaK, as well as from the stronger spin-orbit interaction leading to more pronounced perturbations due to the role of Rb atom.[10]

We report the first experimental data on permanent electric dipole moments for a number of ($v',J'$)-levels belonging to the $B\,^1\Pi$ and $D\,^1\Pi$ states of $^{23}Na^{85}Rb$ and $^{23}Na^{87}Rb$ molecules, as well as the corresponding results of *ab initio* MPPT calculations. The employed computational procedure is based on direct perturbative construction of one-electron density matrix avoiding somewhat burdensome finite-field technique of Ref. 1. Neither experimental nor theoretical data on the NaRb excited states permanent dipoles can be found in literature. The only measurement was performed for the ground $X\,^1\Sigma^+$ state by molecular beam deflection method yielding electric dipole moment value $3.1 \pm 0.3$ D.[11]

 

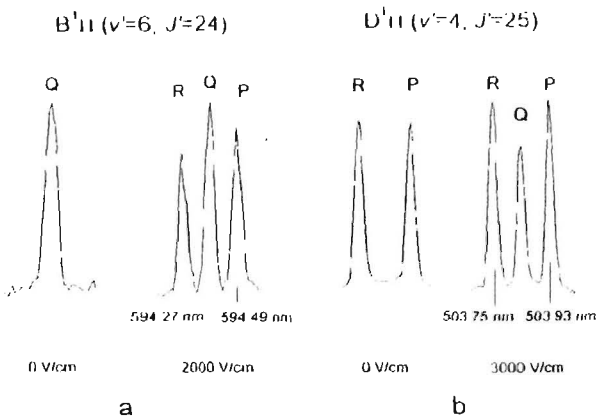


FIG. 1. Fragments of NaRb LIF spectra demonstrating appearance of extra lines induced by dc Stark effect in the $B\,^1\Pi(6,24) \rightarrow X\,^1\Sigma^+(0,24)$ transition following $Q$-type excitation (a) and in the $D\,^1\Pi(4,25) \rightarrow X\,^1\Sigma^+(1,24$ and 26) transitions following $R$ type excitation (b).

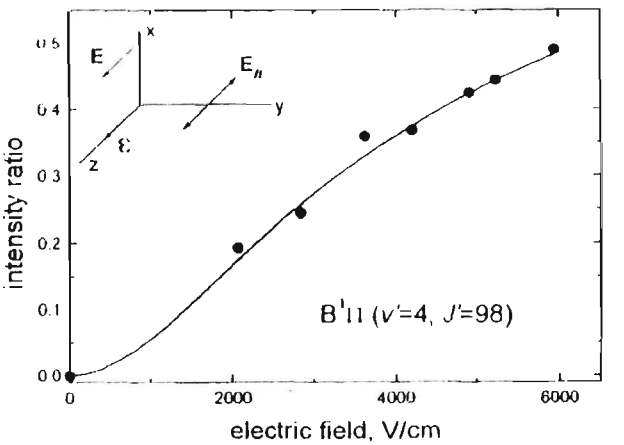


FIG. 2. Experimentally obtained intensity ratios $I_f/I_a$ for LIF originating from $^{23}Na^{85}Rb$ $B\,^1\Pi(4,98)$ level versus applied dc electric field $\mathcal{E}$. $\mathbf{E},\mathbf{E}_{fl}$ denote exciting light and fluorescence light vectors, respectively. Fitting procedure yields $\Delta_{e,f}/\mu = 6.06\times10^{-4}$ cm$^{-1}$/D.

## II. EXPERIMENT

### A. Method

The procedure of experimental determining of the permanent electric dipole moment values $\mu$ for the $^1\Pi$-state $(v',J')$-levels, which is described in more details in Ref. 1, consists of two steps.

First, after selecting and identifying a definite LIF $^1\Pi \rightarrow X\,^1\Sigma^+$ progression consisting of either singlets (following the $Q$-excitation) or doublets (following the $P$- or $R$-excitation), a dc electric field $\mathcal{E}$ is applied to achieve $e-f$ parity mixing between the $\Lambda$-doublet components of the $^1\Pi$ state. As a result, extra lines appear in the LIF spectrum, namely $P$- and $R$ lines following $Q$-excitation or $Q$-lines following $P$- or $R$-excitation, when the Stark energy $W_{e,f} = -\mu\mathcal{E}$ becomes comparable to $\Lambda$-splitting $\Delta_{e,f}$.[12] Thus, the LIF spectra are transformed from $Q$-singlets or $(P,R)$-doublets to the $(P,Q,R)$-triplets, see Fig. 1. The ratio $I_f/I_a$ of extra ("forbidden") line intensity $I_f$ over the "allowed" line intensity $I_a$ is governed by the absolute value of parameter $\mu\mathcal{E}/\Delta_{e,f}$, thus, fitting the $I_f/I_a$ as dependent on $\mathcal{E}$, see Fig. 2, will yield an absolute value of the $\mu/\Delta_{e,f}$ ratio. Some details on simulation of $\mathcal{E}$-dependence of $I_f/I_a$ and fitting routine used to obtain the $\mu/\Delta_{e,f}$ ratio, including the treatment for different polarization and geometry, as well as discussion of possible sources of errors, can be found in Refs. 1 and 2.

At the second step the absolute value of the $\Lambda$ splitting energy $\Delta_{e,f}$ is measured directly by the electric RF ODR method, the essence of which is the following.[13–15] Position of a "forbidden" line of the LIF progression under study is singled out with the monochromator in the presence of a dc external electric field, see Fig. 1. Then, instead of the dc electric field, the frequency scanned RF electric field is applied to the Stark plates. When frequency $f$ hits the resonance condition $hf = \Delta_{e,f}$, forbidden line $I_f$ is observed at its maximum intensity. The resonance signal $I_f(f)$, see Fig. 3, in the simplest case is of the Lorentzian shape.[14] Knowing the $\Lambda$-splitting value $\Delta_{e,f}$, one may pass from the $\mu/\Delta_{e,f}$ ratio to the absolute value of the permanent electric dipole moment $\mu$ for a particular $v',J'$ level belonging to the $^1\Pi$ electronic state.

### B. Experimental setup

The experimental setup and equipment used is similar to that employed in our previous NaK studies.[1,2,15] Briefly, the $^{23}Na^{85}Rb$ and $^{23}Na^{87}Rb$ molecules were formed from a mixture of rubidium and sodium metal, approximately 4:1 (by weight), in an alkali-resistant glass cell at the temperature $T \approx 550$ K. The natural abundance of $^{85}Rb$ and $^{87}Rb$ isotopes is about 72.2% and 27.8%, respectively. The cell contained Stark plates made of carefully polished stainless steel $\sim 6.5$ mm in diameter with the spacing about 1.0 mm measured with $\sim 3\%$ accuracy. The exciting laser beam was directed through the gap between the Stark plates. The fluorescence zone was imaged onto the entrance slit of a double-monochromator with two 1200 groves/mm gratings provid-

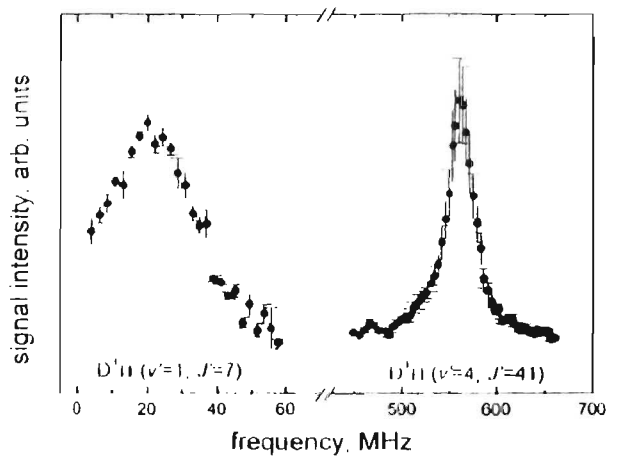


FIG. 3. Examples of experimentally obtained RF ODR signals for $D\,^1\Pi$ state of $^{23}Na^{85}Rb$.

TABLE I. Exciting laser wavelengths ($\lambda_{exc}$), measured $e$–$f$ splittings ($|\Delta_{e,f}|$), and permanent electric dipole moments obtained from the experiment ($|\mu_{exp}|$) and calculated by MPPT ($\mu_{calc}$). Positive $\mu$-values correspond to Na$^+$Rb$^-$ polarity.

| Isotopomer | $(v'',J'')$–$(v',J')$ | $\lambda_{exc}$ (nm) | $\lvert\Delta_{e,f}\rvert$ (MHz) | $\lvert\mu_{exp}\rvert$ (D) | $\mu_{calc}$ (D) |
|---|---|---|---|---|---|
| | | $B\,^1\Pi$ state | | | |
| $^{23}Na^{85}Rb$ | (11,97–4,98) | 647.1 | 68±3 | 3.5±0.3 | −2.7 |
| $^{23}Na^{85}Rb$ | (7,115–5,116) | 632.8 | 220±5 | 3.1±0.2 | −2.6 |
| $^{23}Na^{87}Rb$ | (10,24–6,24) | 632.8 | 52±5 | 3.0±0.4 | −2.6 |
| | | $D\,^1\Pi$ state | | | |
| $^{23}Na^{85}Rb$ | (2,44–0,44) | 514.5 | 576.5±2 | 6.0±0.4 | +6.2 |
| $^{23}Na^{85}Rb$ | (3,8–1,7) | 514.5 | 20±2 | 6.7±1.0 | +6.1 |
| $^{23}Na^{85}Rb$ | (5,24–4,25) | 514.5 | 210±5 | 6.2±0.5 | +6.1 |
| $^{23}Na^{85}Rb$ | (0,41–4,41) | 501.7 | 561±1 | 5.6±0.4 | +6.1 |
| $^{23}Na^{87}Rb$ | (6,45–6,44) | 514.5 | 671±2 | 6.2±0.4 | +6.1 |
| *$^{23}Na^{87}Rb$* | *(2,35–10,36)* | *496.5* | *726±1* | *6.1±0.4* | *+6.0* |
| $^{23}Na^{85}Rb$ | (3,49–12,50) | 496.5 | 834.5±1 | 5.8±0.5 | +5.9 |

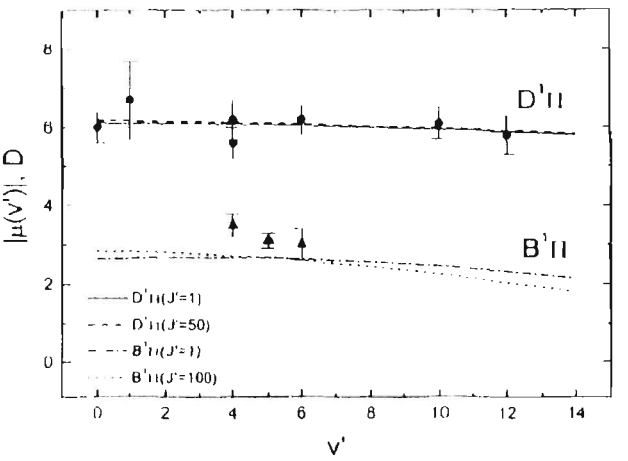


FIG. 4. Absolute values of electric dipole moments $|\mu(v')|$ for the $D\,^1\Pi$ (circles) and $B\,^1\Pi$ (triangles) states of NaRb as functions of vibrational quantum number $v'$. The respective $J'$ values can be found in Table I. The smooth lines represent $|\mu(v')|$ obtained from *ab initio* MPPT calculations for $J'=1$ and 100 ($B\,^1\Pi$ state), as well as for $J'=1$ and 50 ($D\,^1\Pi$ state).

ing reciprocal dispersion of 5 Å/mm and spectral resolution of ≈0.2 Å. Calibration of LIF spectra by neon and argon discharge lines allowed to achieve an absolute spectral accuracy of about 0.1 Å. We used fixed frequency lines from Spectra Physics 171 $Ar^+$ laser, as well as from $Kr^+$ and He–Ne lasers, see Table I, to excite a particular $(v',J')$-level belonging to the $D\,^1\Pi$ and $B\,^1\Pi$ states of NaRb. To maintain the conditions of simultaneous excitation of $e$ and $f$ parity components, we preferred to employ the multi-mode laser operation, with typical laser line contour widths ≈10 GHz for $Ar^+$ or $Kr^+$ lasers and ≈1.2 GHz for the He–Ne laser. In some cases we were forced to employ the single-mode regime to simplify the LIF spectra. The RF field for the RF–ODR measurements was produced by Mini-circuit voltage controlled oscillators covering the frequency region 5–900 MHz followed by an amplifier Mini-circuit ZHL-2-12 to obtain RF field amplitude value up to 5 V, as well as by Wavetek generator covering the 1–60 MHz region.

## III. EXPERIMENTAL RESULTS

Examples of Stark effect induced changes in LIF spectra and corresponding fits of the $I_f/I_a$ signal are shown in Figs. 1 and 2, while some typical electric RF–ODR signals are presented in Fig. 3. Experimental values of the $\Delta_{e,f}$ splitting are presented in Table I. The permanent electric dipole moments $\mu(v',J')$, which are obtained by combining $\Delta_{e,f}$ values with the $\Delta_{e,f}/\mu$ ratios resulted from the fitting of signals as given in Fig. 2, are depicted in Fig. 4 and presented in Table I for all studied $(v',J')$-levels of the $B\,^1\Pi$ and $D\,^1\Pi$ states. The permanent electric dipole moment error in Table I accounts for the inaccuracies in $\Delta_{e,f}$ values and in determining the gap between the Stark plates, as well as for the discrepancies of $\mu$-values obtained in different experiments.

A few notes ought to be made concerning the $v',J'$ assignment. Unambiguous vibrational assignment has been achieved from the vibrational spacings in LIF progressions and by comparision of the experimental LIF intensity distribution with the simulated Franck–Condon factors.

As it appeared, rotational and isotope assignments of the LIF spectra progressions were neither easy, nor unambiguous. As a tentative guide we used the data given in Table II of Ref. 5, where a number of $(v',J')$-levels of $B\,^1\Pi$ and $D\,^1\Pi$ states excited by $Kr^+$, He–Ne, and $Ar^+$ laser lines is presented. However, the $J'$ values are not always given there and the particular isotopomer is not defined. Besides, we have observed several progressions not mentioned in Ref. 5. To identify the LIF progressions originating from a definite $B\,^1\Pi$ state $(v',J')$-level, we used spectroscopic constants for the $B\,^1\Pi$ state from Refs. 6 and 7 and for the $X\,^1\Sigma^+$ state from Refs. 6 and 9. As far as the $B\,^1\Pi$ state level with $v'=6$ excited by a $Q$-transition is concerned, we managed to assign unambiguously the value $J'=24$ for the $^{23}Na^{87}Rb$ isotopomer, see Table I, by the following routine. First, we measured the rotational spacing between $P$, $Q$, and $R$ lines in presence of an external dc electric field, which yielded $J'=23\pm1$. The least deviation of 0.002 $cm^{-1}$ between the $B\,^1\Pi(v'=6,J')\rightarrow X\,^1\Sigma^+(v''=10,J'')$ transition frequencies calculated using molecular constants from Refs. 6 and 9 and the exciting laser frequency was obtained for $J'=22$ of $^{23}Na^{85}Rb$ and for $J'=24$ of $^{23}Na^{87}Rb$. In order to decide between these possibilities, we checked the deviation $\Delta\nu$ between the measured ($\nu_{exp}$) and calculated ($\nu_{calc}$) line positions for the LIF $v''$-progression $B\,^1\Pi(v'=6,J')\rightarrow X\,^1\Sigma^+(v'',J'')$. As it revealed, only in the case of $J'=24$ for the $^{23}Na^{87}Rb$ isotopomer the deviation is within limits of the experimental errors. The high $J'$–100 values of the $B\,^1\Pi$ state given in Table I are less reliable because of less accuracy of the molecular constants in Refs. 6 and 9 for high $J'$. It also means that the isotopomer is not determined unambiguously for these transitions since the respective procedures are mutually interrelated. Similar situation takes place in the $D\,^1\Pi$ state, see Table I, in which we suppose that the data for smaller $J'$ values are more reliable, the possible inaccuracy of $J'$ not exceeding ±1. It has to be noted that the set of $D\,^1\Pi$ state molecular constants in Ref. 5

is rather scarce; it does not allow to reproduce the term energies accurately enough, leading up to several wave numbers deviation from the excitation energy. However, the possible inaccuracy in $J'$ values practically does not affect the dipole moment values presented in Table I.

## IV. *Ab initio* DIPOLE MOMENT CALCULATIONS

The *ab initio* electronic structure calculations of NaRb were performed by means of the many-body multipartitioning perturbation theory (MPPT). This approach implies the perturbative construction of a state-selective effective Hamiltonian $\tilde{H}$ within the model space spanned by an appropriate set of Slater determinants $\{|J\rangle\}$, using several quasi-one-*electron zero-order Hamiltonians simultaneously*.[16,17] The second-order MPPT expression for the Hermitian effective Hamiltonian matrix resembles the one which is appearing in the conventional quasidegenerate perturbation theory,[18]

$$\langle J|\tilde{H}|J'\rangle=\langle J|H|J'\rangle+\frac{1}{2}\sum_{K}\sum_{|K\rangle\notin I_{\mu}}\langle J|H|K\rangle \times\left(\frac{1}{\Delta(J'\to K)}+\frac{1}{\Delta(J\to K)}\right)\langle K|H|J'\rangle, \quad (1)$$

where $\tilde{H}$ is the total many-electron Hamiltonian and the energy denominators $\Delta(J\to K)$ are given by the formula

$$\Delta(J\to K)=\sum_{i}{}'\sum_{\Lambda_i^J}(N_i^J-N_i^K)\epsilon_i^{(0)} \sum_{i}{}'\sum_{\Lambda_i^K-\Lambda_i^J}(N_i^K-N_i^J)\epsilon_i^{(0)}. \quad (2)$$

Here $N_i^J$ and $N_i^K$ denote the occupancy of the $i$th spatial orbital in the model space determinant $|J\rangle$ and the outer space determinant $|K\rangle$, respectively. The entities $\epsilon_i^{(0)}$, $\epsilon_i^{(0)}$ are the nonrelaxed orbital ionization potentials and electron affinities with opposite signs, defined with respect to the model-space approximation for the target states. Diagonalization of $\tilde{H}$ provides energy estimates and model wave functions $|\tilde{\psi}_m\rangle$ for all the target states simultaneously.

To extend the MPPT scheme to one-electron property calculations, one can proceed via the evaluation of the (transition) density matrix (cf. Ref. 19). The first-order approximation for the spin-free $m\to n$ transition density matrix ${}^{mn}\rho$ compatible with the use of the second-order effective Hamiltonian (1) is given by

$${}^{mn}\rho_{rs}\equiv\langle\tilde{\psi}_m|E_{rs}|\tilde{\psi}_n\rangle+\sum_{J,J'}{}'\langle\tilde{\psi}_m|J\rangle \times\langle J'|\tilde{\psi}_n\rangle\sum_{K}{}'\left(\frac{\langle J|E_{rs}|K\rangle\langle K|H|J'\rangle}{\Delta(J'\to K)}+\frac{\langle J|H|K\rangle\langle K|E_{rs}|J'\rangle}{\Delta(J\to K)}\right), \quad (3)$$

where $E_{rs}$ is the conventional spin-free one-electron excitation operator (unitary group generator) which can be expressed in terms of the spin–orbital creation/annihilation operators as $E_{rs}=a_{r\alpha}^{\dagger}a_{s\alpha}+a_{r\beta}^{\dagger}a_{s\beta}$. The required dipole moment estimates are immediately obtained as $\Sigma_{rs}{}^{mn}\rho_{rs}D_{sr}$, where $\|D_{sr}\|$ is the electric dipole matrix in the orbital basis. It is worth noting that the procedure described above is strictly equivalent to the MPPT computation of the first-order effective electric dipole operator with subsequent evaluation of its diagonal matrix element for the $m$th model wave function $|\tilde{\psi}_m\rangle$.

Since summation over the outer space determinants ($|K\rangle$) in Eq. (3) is in fact restricted to single excitations of the model space configurations, the direct perturbative construction of ${}^{mn}\rho_{rs}$ is not expensive and, therefore, offers an attractive alternative to the accurate but rather cumbersome *finite field technique* successfully used in our previous studies.[1,15]

The procedure of MPPT correlation treatment employed in the present work was generally similar to that used in Refs. 15 and 20. In order to incorporate the scalar (spin-independent) relativistic effects into our calculations, we replaced the inner core shells by averaged relativistic pseudopotentials,[21,22] leaving 9 electrons of each atom for explicit treatment. The atomic Gaussian basis sets $(7s7p5d2f)/[6s6p4d2f]$ Rb, $(8s8p5d1f)/[7s6p4d1f]$ Na were composed of the outer-core and valence pseudopotential-adapted $(sp)$ bases,[21,22] diffuse parts of the "all-electron" bases for electric property calculations,[23] and additional diffuse and polarization functions. The determinants were constructed from the solutions of the state-average SCF problem for two lowest ${}^2\Sigma^+$ electronic states of $NaRb^+$. The model space for the MPPT calculations was a full valence CI space, i.e., it comprised all the possible distributions of two valence electrons among the valence and virtual orbitals; therefore, the perturbative corrections corresponded to the core–valence correlation and residual core polarization effects. The completeness of the model space and the separability of energy denominators (2) guaranteed the size consistency of energy and dipole moment estimates.

The *ab initio* permanent electric dipole moment functions $\mu(R)$ for the $X\,{}^1\Sigma^+$, $B\,{}^1\Pi$, and $D\,{}^1\Pi$ states of NaRb are presented in Table II. These functions were converted to the relevant theoretical $\mu_{v,v'}(v',J')$ values (Table I, Fig. 4) by means of vibrational wave functions corresponding to the RKR potential curves. The $B\,{}^1\Pi$ curve has been derived from the molecular constants given in Ref. 6, while for the $D\,{}^1\Pi$ state we used the data from Ref. 5. The ground state $\mu$ value with $v''=0$, calculated with the RKR potential from Ref. 6, is 3.3 D, which agrees with the experimental value $3.1\pm0.3$ D.[11]

## V. DISCUSSION

The measured absolute values of permanent electric dipoles for the $D\,{}^1\Pi$ state of NaRb for vibrational levels varying from $v'=0$ to $v'=12$ are close to 6 D, demonstrating minor changes with $v',J'$ (see Table I and Fig. 4). The experimental $\mu$ values for the NaRb $B\,{}^1\Pi$ state are approximately two times smaller, being close to 3 D. As follows from the results presented in Table I, the experimental data

TABLE II. *Ab initio* permanent electric dipole moment values $\mu$ for the $X\,^1\Sigma^+$, $B\,^1\Pi$, and $D\,^1\Pi$ states of NaRb as functions of the internuclear distance $R$. Positive $\mu$-values correspond to $Na^+Rb^-$ polarity.

| | $d(R)$ (D) | | |
|---|---|---|---|
| $R$ (a.u.) | $X\,^1\Sigma^+$ | $B\,^1\Pi$ | $D\,^1\Pi$ |
| 5.4 | 2.949 | 0.469 | 1.060 |
| 5.9 | 3.063 | −0.134 | 0.349 |
| 6.4 | 3.204 | −0.781 | 1.821 |
| 6.885[a] | 3.337 | −1.419 | 3.289 |
| 7.4 | 3.448 | −2.076 | 4.734 |
| 7.8928[b] | 3.501 | −2.615 | 5.938 |
| 8.4 | 3.463 | −2.962 | 6.786 |
| 8.9 | 3.329 | −3.053 | 7.148 |
| 9.4 | 3.086 | −2.878 | 7.077 |
| 9.9 | 2.750 | −2.554 | 6.644 |
| 10.4 | 2.349 | −2.174 | 5.874 |
| 10.9 | 1.928 | −1.787 | 4.973 |
| 11.5 | 1.458 | −1.389 | 3.903 |
| 12.1 | 1.058 | −1.059 | 2.955 |
| 12.65 | 0.768 | −0.816 | 2.214 |
| 13.25 | 0.542 | −0.629 | 1.631 |

[a,b]Correspond to $R_e$ values experimentally obtained in Ref. 6 for $X\,^1\Sigma^+$ and $B\,^1\Pi$ states, respectively.

for the $D\,^1\Pi$ state agree with their calculated counterparts within error bars, whereas the experimental data for the $B\,^1\Pi$ state are somewhat 15%–25% larger. The observed discrepancy exceeding the experimental error might be attributed to strong local spin-orbit coupling of the studied $B\,^1\Pi$ levels with near-lying rovibronic levels of the $b\,^3\Pi$ and $c\,^3\Sigma^+$ triplet states, see Fig. 3 of Ref. 7. An admixture of triplet electronic wave functions for the $B\,^1\Pi$ state is expected to be more pronounced than for the $D\,^1\Pi$ state because of much larger spin–orbit effects in the excited Rb($5p$) atom as compared to the Na($3p$) atom. Experimental data confirm the theoretical prediction of weak dipole moment dependence on rotational and vibrational quantum numbers, see Fig. 4.

It makes sense to mention that permanent electric dipole moments for the $B\,^1\Pi$ and $D\,^1\Pi$ states of NaRb are very close to the corresponding $\mu(R)$-functions and $\mu(v')$-values of the NaK molecule. Indeed, the experimental $\mu(v')$-values of the nonperturbed $D\,^1\Pi$ levels of the NaK molecule vary from 5.9 D to 6.6 D for $v'=1-14$, see Table I of Ref. 1. Results of the most reliable *ab initio* finite-field MPPT $\mu(R)$ calculations for the NaK $B\,^1\Pi$ and $D\,^1\Pi$ states[1] are almost the same as in NaRb in the vicinity of the corresponding equilibrium distances.

It should be noted that any quantitative interpretation of the measured $\Lambda$-splittings is not possible at the present stage because of the lack of information about the relevant perturbing states of NaRb. The *ab initio* calculation of the required potential curves and nonadiabatic matrix elements responsible for $\Lambda$-splitting of the $^1\Pi$ states is currently in progress.

## ACKNOWLEDGMENTS

The Riga group participants have been supported by the Latvian Science Council (Grant No. 96.0323). O.N. is grateful for the support from Latvian Science Council Doctoral Studies Grant No. 44. The Moscow group participants have been supported by the Russian Fund of Basic Research under Grants No. 00-03-33004 and No. 00-03-32978. The authors would like to thank Dr. Monique Aubert-Frecon for placing the unpublished information on NaRb potentials to our disposal. The assistance of Olga Hrabrova in assigning the rovibronic levels, as well as of Janis Alnis and Arvids Zalcmanis in fixing the experimental setup is gratefully acknowledged. We want to thank Dr. Janis Abolinsh for his efforts to improve the English style of the manuscript.

[1] M. Tamanis, M. Auzinsh, I. Klincare, O. Nikolayeva, R. Ferber, E. A. Pazyuk, A. V. Stolyarov, and A. Zaitsevskii, Phys. Rev. A **58**, 1932 (1998).
[2] M. Tamanis, M. Auzinsh, I. Klincare, O. Nikolayeva, A. V. Stolyarov, and R. Ferber, J. Chem. Phys. **106**, 2195 (1997).
[3] H. Wang and W. C. Stwalley, J. Chem. Phys. **108**, 5767 (1998).
[4] H. Wang, P. L. Gould, and W. C. Stwalley, Z. Phys. D: At., Mol. Clusters **36**, 317 (1996).
[5] N. Takahashi and H. Katô, J. Chem. Phys. **75**, 4350 (1981).
[6] Y.-C. Wang, M. Kajitani, S. Kasahara, M. Baba, K. Ishikawa, and H. Katô, J. Chem. Phys. **95**, 6229 (1991).
[7] Y. C. Wang, K. Matsubara, and H. Katô, J. Chem. Phys. **97**, 811 (1992).
[8] K. Matsubara, Y.-C. Wang, K. Ishikawa, M. Baba, A. J. McCaffery, and H. Katô, J. Chem. Phys. **99**, 5036 (1993).
[9] S. Kasahara, T. Ebi, M. Tanimura, H. Ikoma, K. Matsubara, M. Baba, and H. Katô, J. Chem. Phys. **105**, 1341 (1996).
[10] C. Amiot, O. Dulieu, and J. Vergès, Phys. Rev. A **83**, 2316 (1999).
[11] P. J. Dagdigian and L. Wharton, J. Chem. Phys. **57**, 1487 (1972).
[12] H. Lefebvre Brion and R. W. Field, *Perturbations in the Spectra of Diatomic Molecules* (Academic, New York, 1986).
[13] S. J. Silvers, T. H. Bergeman, and W. Klemperer, J. Chem. Phys. **52**, 4385 (1970).
[14] R. W. Field and T. H. Bergeman, J. Chem. Phys. **54**, 2936 (1971).
[15] M. Tamanis, M. Auzinsh, I. Klincare, O. Nikolayeva, R. Ferber, A. Zaitsevskii, E. A. Pazyuk, and A. V. Stolyarov, J. Chem. Phys. **109**, 6725 (1998).
[16] A. Zaitsevskii and J. P. Malrieu, Theor. Chem. Acc. **96**, 269 (1997).
[17] A. Zaitsevskii and R. Cimiraglia, Int. J. Quantum Chem. **73**, 395 (1999).
[18] V. Kvasnicka, Int. J. Quantum Chem. **24**, 335 (1983).
[19] C. Angeli, R. Cimiraglia, and M. Persico, Theor. Chem. Acc. **100**, 324 (1998).
[20] E. A. Pazyuk, A. V. Stolyarov, A. Zaitsevskii, R. Ferber, P. Kowalczyk, and C. Teichteil, Mol. Phys. **96**, 955 (1999).
[21] H. F. Pacios and P. A. Christiansen, J. Chem. Phys. **82**, 2664 (1985).
[22] L. A. LaJohn, P. A. Christiansen, R. B. Ross, T. Atashroo, and W. C. Ermler, J. Chem. Phys. **87**, 2812 (1987).
[23] A. J. Sadlej and M. Urban, J. Mol. Struct.: THEOCHEM **234**, 147 (1991).

Reprinted from

Journal of MOLECULAR STRUCTURE

Journal of Molecular Structure 480–481 (1999) 283–287

# Electric field induced alignment-orientation conversion in diatomic molecules: analysis and observation for NaK

O. Nikolayeva*, M. Auzinsh, M. Tamanis, R. Ferber

*Institute of Atomic Physics and Spectroscopy, Department of Physics, University of Latvia, 19 Rainis blvd., LV-1586, Riga, Latvia*

ELSEVIER

# JOURNAL OF MOLECULAR STRUCTURE

URL MOLSTRUC HomePage: http://www.elsevier.nl/locate/molstruc

The *Journal of Molecular Structure* is dedicated to the publication of full-length articles, review articles, and short communications, providing important new structural information on all types of chemical species, including: stable and unstable molecules in any environment (vapour, molecular beam, liquid, solution, liquid crystal, solid state, matrix-isolated, surface-adsorbed, etc.); chemical intermediates; molecules in excited states; biochemicals; polymers.

The methods used may include any combination of spectroscopic and non-spectroscopic techniques, for example: infrared spectroscopy (mid, far, near); Raman spectroscopy and non-linear Raman methods (CARS, etc.); force constant and molecular mechanics calculations; electronic absorption spectroscopy; optical rotatory dispersion and circular dichroism; fluorescence and phosphorescence techniques; electron spectroscopies (PES, XPS), EXAFS, etc.; microwave spectroscopy; electron diffraction; NMR and ESR spectroscopies; Mössbauer spectroscopy; X-ray crystallography.

Papers describing routine studies of little structural significance (e.g. straightforward X-ray crystal structure determinations) are not encouraged.

Publications combining experimental and theoretical approaches to a problem are particularly welcomed. However, purely theoretical (semiempirical or ab initio) studies should be submitted to the *Journal of Molecular Structure (Theochem)*.

## Editors



**USA mailing notice:** *Journal of Molecular Structure* (ISSN 0022-2860) is published monthly by Elsevier Science BV (P.O. Box 211, 1000 AE Amsterdam, The Netherlands). Annual subscriptions price in the USA US$ 4863 (valid in North, Central and South America), including air speed delivery. Application to mail at periodical postage rate is pending at Jamaica, NY 11431.

**USA POSTMASTER:** Send address changes to *Journal of Molecular Structure*, Publications Expediting Inc., 200 Meacham Avenue, Elmont, NY 11003.

**AIRFREIGHT AND MAILING** in the USA by Publications Expediting Inc., 200 Meacham Avenue, Elmont, NY 11003.

**Publication information.** *Journal of Molecular Structure* (ISSN 0022-2860). For 1999 volumes 470–486 are scheduled for publication. Subscription prices are available upon request from the Publisher or from the Regional Sales Office nearest you or from this journal's website (http://www.elsevier.nl/locate/molstruc). Further information is available on this journal and other Elsevier Science products through Elsevier's website: (http://www.elsevier.nl). Subscriptions are accepted on a prepaid basis only and are entered on a calendar year basis. Issues are sent by standard mail (surface within Europe, air delivery outside Europe). Priority rates are available upon request. Claims for missing issues must be made within six months of the date of dispatch.

**Advertising information.** Advertising orders and enquiries can be sent to: **USA, Canada and South America**: Mr Tino de Carlo, The Advertising Department, Elsevier Science Inc., 655 Avenue of the Americas, New York, NY 10010-5107, USA; phone: (+1) (212) 633 3815; fax: (+1) (212) 633 3820; e-mail: t.decarlo@elsevier.com. **Japan**: The Advertising Department, Elsevier Science K.K., 9-15 Higashi-Azabu 1-chome, Minato-ku, Tokyo 106-0044, Japan; phone: (+81) (3) 5561 5033; fax: (+81) (3) 5561 5047. **Europe and ROW**: Rachel Gresle-Farthing, The Advertising Department, Elsevier Science Ltd., The Boulevard, Langford Lane, Kidlington, Oxford OX5 1GB, UK; phone: (+44) (1865) 843565; fax: (+44) (1865) 843976; e-mail: r.gresle-farthing@elsevier.co.uk

**Orders, claims and product enquiries**: please contact the Customer Support Department at the Regional Sales Office nearest you:

**New York**: Elsevier Science, PO Box 945, New York, NY 10159-0945, USA; phone: (+1) (212) 633 3730 [toll free number for North American customers: 1-888-4ES-INFO (437-4636)]; fax: (+1) (212) 633 3680; e-mail usinfo-f@elsevier.com

**Amsterdam**: Elsevier Science, PO Box 211, 1000 AE Amsterdam, The Netherlands; phone: (+31) 20 4853757; fax: (+31) 20 4853432; e-mail: nlinfo-f@elsevier.nl

**Tokyo**: Elsevier Science, 9–15 Higashi-Azabu 1-chome, Minato-ku, Tokyo 106-0044, Japan; phone: (+81) (3) 5561 5033; fax: (+81) (3) 5561 5047; e-mail: info@elsevier.co.jp

**Singapore**: Elsevier Science, No. 1 Temasek Avenue, #17-01 Millenia Tower, Singapore 039192; phone: (+65) 434 3727; fax: (+65) 337 2230; e-mail: asiainfo@elsevier.com.sg

**Rio de Janeiro**: Elsevier Science, Rua Sete de Setembro 111/16 Andar, 20050-002 Centro, Rio de Janeiro - RJ, Brazil; phone: (+55) (21) 509 5340; fax: (+55) (21) 507 1991; e-mail: elsevier@campus.com.br [Note (Latin America): for orders, claims and help desk information, please contact the Regional Sales Office in New York as listed above].

⊗ The paper used in this publication meets the requirements of ANSI/NISO Z39.48-1992 (Permanence of Paper)
Printed in The Netherlands

ELSEVIER

Journal of Molecular Structure 480–481 (1999) 283–287

Journal of
MOLECULAR
STRUCTURE

# Electric field induced alignment-orientation conversion in diatomic molecules: analysis and observation for NaK

O. Nikolayeva*, M. Auzinsh, M. Tamanis, R. Ferber

*Institute of Atomic Physics and Spectroscopy, Department of Physics, University of Latvia, 19 Rainis blvd., LV-1586, Riga, Latvia*

Received 24 August 1998

**Abstract**

This article reports the observation of the molecular fluorescence circularity under irradiation with linearly polarised light. This alignment-orientation conversion phenomenon arises as a result of partial transformation from alignment of the ensemble of $^1\Pi$ state molecular angular momenta into their orientation under the effect of non-linear dc Stark effect. Circularity rate up to 0.12 was observed in $D\,^1\Pi \rightarrow X\,^1\Sigma$ fluorescence of $^{23}Na^{39}K$ molecules in agreement with the theoretically predicted value.


*Keywords:* Alignment-orientation conversion; NaK

## 1. Introduction

As is well known, excitation by linearly polarised light **E**, caused by symmetry considerations, is capable to create alignment of the angular momenta which results in linear polarisation of observed fluorescence, and is not capable to create orientation which would result in circular polarisation of fluorescence. For a considerable time there has been major interest in analysing the conditions under which these strict symmetry rules may be broken, thus leading to alignment-orientation conversion (**AOC**) see [1] and references therein. The required conditions may be caused by an external perturbation, in particular, external field, producing such magnetic sublevels splitting ${}_J\omega_{MM'} = (W_M - W_{M'})/\hbar$ which satisfies ${}_J\omega_{MM\pm1} \neq {}_J\omega_{-M\mp1-M}$ [1]. This condition is obeyed when non-linear dependence of the energy shift $W_M$ on external magnetic or electric field strength takes place. The appearance of magnetic field induced **AOC** in diatomic molecules was observed earlier [2], while Stark effect induced **AOC** was considered only theoretically [1,3].

In present article the electric field **F** induced **AOC** has been observed in $D\,^1\Pi$ state of NaK molecule, where the non-linear Stark energies lead to the condition for $\omega_{MM'}$ mentioned above already in the first approximation. The **AOC** signals have been registered in $D\,^1\Pi \rightarrow X\,^1\Sigma$ transition ($R$- and $P$-emission) from $v'(J') = 7(23)$ and 12(7) rovibronic levels as emergence of the degree of circularity

$$C = (I_r - I_l)/(I_r + I_l), \tag{1}$$

using the appropriate geometry of linearly polarised excitation, observation and electric field **F** direction, $I_{r,l}$ being right- and left-handed circularly polarised fluorescence intensities. The presented calculation of the expected **AOC** signals has been based on the $^1\Pi$ state Stark effect studies performed earlier in Refs. [4,6].

* Corresponding author.

0022-2860/99/$ - see front matter 
PII: S0022-2860(98)00700-5

## 2. Theoretical description

The main peculiarity of $^1\Pi$ state consists in the fact that each rotational energy level $J$ is splitted in two different parity components usually denoted as $e$ and $f$. This effect is called $\Lambda$-splitting leading to the energy splitting $\Delta_{ef}^J = qJ(J+1)$, $q$ being $\Lambda$-doubling constant. Let us consider the interaction of diatomic molecules with cw broad band (with respect to $\Delta_{ef}^J$) laser light causing $^1\Pi(v', J') \leftarrow {}^1\Sigma(v'', J'')$ transition which creates the excited state density matrix ${}^{kl}f_{MM'}$, where $k$ and $l$ denote either $e$ or $f$. In the density matrix formalism the intensity of the fluorescence light possessing polarisation vector $\hat{\mathbf{E}}_f$ and originating from the $^1\Pi$ state in the $J' \rightarrow J''_1$ transition can be expressed as [3]:

$$I\left(\hat{\mathbf{E}}_f\right) = I_0 \sum_{MM'\mu} \sum_{kl} \left\langle M'^1\Pi k \middle| \hat{\mathbf{E}}_f^* \hat{\mathbf{D}} \middle| \mu^1\Sigma \right\rangle \times \left\langle M'^1\Pi l \middle| \hat{\mathbf{E}}_f^* \hat{\mathbf{D}} \middle| \mu^1\Sigma \right\rangle^* {}^{kl}f_{M'M}, \quad (2)$$

where $I_0$ is proportionality coefficient and $\hat{\mathbf{D}}$ is the transition dipole moment unit vector. The excited state density matrix elements ${}^{kl}f_{MM'}$ may be written as [3]

$${}^{kl}f_{MM'} = \frac{\tilde{\Gamma}_p}{\Gamma + i^{kl}\omega_{MM'}} \sum_{\mu} \left\langle M'^1\Pi k \middle| \hat{\mathbf{E}}^* \hat{\mathbf{D}} \middle| \mu^1\Sigma \right\rangle \times \left\langle M'^1\Pi l \middle| \hat{\mathbf{E}}^* \hat{\mathbf{D}} \middle| \mu^1\Sigma \right\rangle^*. \quad (3)$$

Here $\mu$ are magnetic sublevels of the ground $^1\Sigma$ state with rotational quantum number $J''$ while $M$, $M'$ are magnetic sublevels of the excited state with rotational quantum number $J'$ belonging to the $\Lambda$-doublet components $k$, $l$. The unit vector $\hat{\mathbf{E}}$ describes exciting light polarisation, $\tilde{\Gamma}_p$ is the reduced absorption rate, $\Gamma$ is the excited state effective relaxation rate, ${}^{kl}\omega_{MM'}$ is the energy splitting between, $M$, $M'$ sublevels belonging either to the same ($l = k$) or to the different ($l \neq k$) $\Lambda$-doublet components, thus accounting both for $\Lambda$-doubling and Stark effect level shifts. In such formalism density matrix diagonal elements reflect population of the respective magnetic sublevels, while the nondiagonal matrix elements reflect coherences between the respective substate wavefunctions (WF). The structure of Eq. (2) allows one to notice that the terms entering the sums are formed as the excited state density matrix elements ${}^{kl}f_{MM'}$ multiplied by the observation density matrix elements.

Note, that the WF's in Eqs. (2) and (3) are not the usual $|JM\rangle$ WF's owing to the fact that, though electric field destroys the spherical symmetry, it does not change the axial symmetry, therefore $\mathbf{J}$ is not a good quantum number any more, while $M$ is still conserved. The WF's included in Eqs. (2) and (3) are obtained in a coupled-basis set as an expansion over the non-perturbed states with different $J'_i (i = e,f)$ values, as well as different $J''$ values, which are mixed by the static external electric field $\mathbf{F}$. For $^1\Pi$ excited state we have

$$\left| M^1\Pi k \right\rangle = \sum_{J'=1}^{\infty} \sum_{i=e,f} C_{\Pi i}^k (J', M) |J'M\rangle, \quad (4)$$

thus obtaining, as it is usually done, a new WF for each $k = 1$ and 2 constructed as the linear combination of $e$ and $f$ substates with the mixing coefficients $C_{\Pi e,f}^k(J', M)$. Similarly, for the ground $^1\Sigma$ state the $J''$ mixing can be taken into account using

$$\left| \mu^1\Sigma \right\rangle = \sum_{J'=0}^{\infty} C_\Sigma (J'', \mu) |J'', \mu\rangle\rangle. \quad (5)$$

Coefficients $C_{\Pi i}$ and $C_\Sigma$ have to be calculated from the diagonalisation of the Hamiltonian accounting both for molecular rotation and Stark effect.

The explicit form of the dipole transition matrix elements with $|JM\rangle$ WF's can be found [1,3] by applying the definition of scalar multiplication in cyclic coordinates along with the Wigner–Eckart theorem and expressing cyclic components of vector $\hat{\mathbf{E}}$ via spherical angles $\theta$ and $\varphi$ ($z$ axis coincide with the direction of external field). After performing these transformations one must use Eqs. (4) and (5) to pass to the WF's entering Eqs. (2) and (3). As a result, one arrives at the expressions for the intensities $I_r$, $I_l$ and for the difference $I_r - I_l$ which is responsible for appearance of circularity:

$$I_r - I_l = \frac{sin2\theta}{2} K\left(J', J'', J''_1, \varphi, {}^{kl}\omega_{MM'}\right). \quad (6)$$

Here the function $K(J', J'', J''_1, \varphi, {}^{kl}\omega_{MM'})$, which is

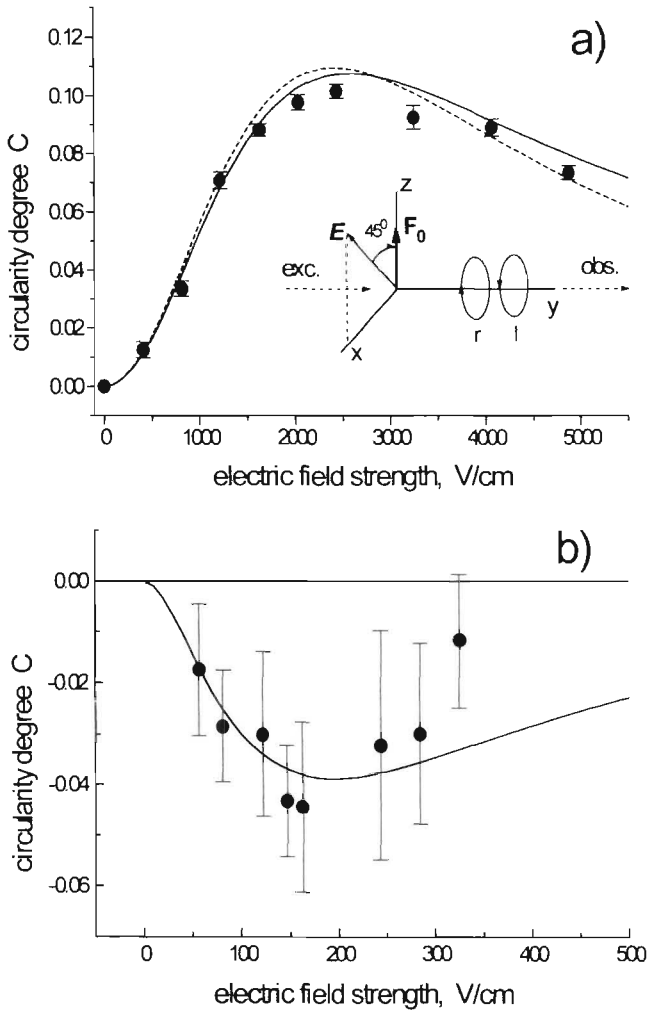


Fig. 1. Experimentally obtained (full circles) and calculated fluorescence circularity degree $C$ as dependent on electric field strength $F$. (a) — for $\nu'(J') = 7(23)$, (b) — for $\nu'(J') = 12(7)$. Dashed line represents the first order ${}^{(1)}W_M^{el}$ approximation.

independent of $\theta$, appears as a result of summation over all indices in Eqs. (2)–(5) and represents a rather cumbersome expression. As it immediately follows from Eq. (6), the maximal circularity degree appears at $\theta = 45°$, while for $\theta = 0°$ and $\theta = 90°$ the circularity degree is zero. The expression for $I_r + I_l$ necessary to calculate $C$ can also be found from Eqs. (2)–(5). Note that $K\left(J', J'', J_1'', \varphi, {}^{kl}\omega_{MM'}\right)$ is determined for a particular transition $J'' \rightarrow J' \rightarrow J_1''$ and definite spherical angle $\varphi$ of linear polarised excitation if the Stark energy pattern $W_M^{el}$ is known. In the first approximation ${}^{(1)}W_M^{el}$ may be obtained in a simple analytical form:

$$ {}^{(1)}W_M^{el} = \frac{1}{2}\Delta_{ef}^J \pm \sqrt{\left(\Delta_{ef}^J\right)^2/4 + d_p^2 F^2 M^2/[J'(J'+1)]^2}, \tag{7} $$

where the energy of ${}^1\Pi\nu'(J')$ state $f$ sublevel is considered to be zero at $F = 0$.

It is easy to see that, as $F$ increases leading to $d_p FM/[J'(J'+1)] \gg \Delta_{ef}^J/2$, the Stark energy shifts exhibit linear asymptotic behaviour with respect to $F$. To account for the interaction between $J'$ and

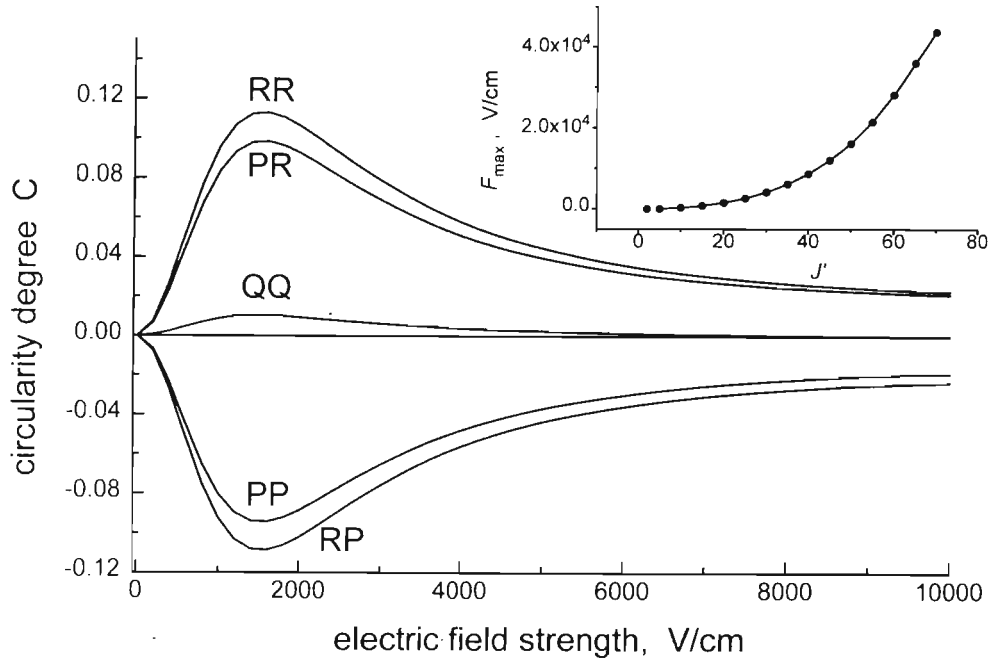


Fig. 2. Circularity degree dependence on electric field strength for all allowed fluorescence transitions, $J' = 20$, $d = 6.4$ D, $q = 1.51 \times 10^{-5}$ cm$^{-1}$, $\Gamma = 6 \times 10^7$ s$^{-1}$. Inset of the picture shows $J'$-dependence of electric field strength in maximum.

$J' \pm 1$ excited state levels it is necessary to pass to the second order approximation $^{(2)}W_M^{el}$, when analytical expression is still possible [5]. However, strictly speaking, for large enough $F$ values the second-order perturbation treatment becomes incorrect as well, and one has to solve the secular equation system for the relevant Hamiltonian matrix. The manifestation of second and higher order corrections in Stark effect induced fluorescence intensity changes was studied previously [6].

As a result of the above mentioned routine, it becomes possible to calculate $^1\Pi$ state fluorescence circularity degree under linearly polarised excitation caused by external dc electric field. The simulation of expected $C(F)$ dependencies will be presented in Section 4.

## 3. Experimental

The experimental set-up has been described in more detail in Ref. [6], hence we will dwell on it only briefly. $^{23}Na^{39}K$ molecules have been formed in thermal cells made from alkali-resistant glass and attached to a vacuum system via a dry valve. Characteristic working temperatures of the metal containing reservoir (weight ratio Na : K $\approx$ 1:3) were T $\approx$ 525 $\div$ 575 K. A number of visible blue-green Spectra-Physics 171 $Ar^+$-laser lines have been used to excite $D\ ^1\Pi\ \nu(J) \leftarrow X\ ^1\Sigma^+\ \nu''(J'')$ transitions. Visible LIF lines originating from the ca. 1 mm diameter laser excitation region was imaged onto the entrance slit of a double-monochromator and resolved by two 1200 lines/mm gratings blazed in the first order, providing an overall spectral resolution of ca. 0.03 nm. The dc electric field was applied to the carefully polished stainless steel Stark plates, ca. 0.8 cm in diameter, separated by a 1.2 mm gap. The excitation-observation geometry is schematically depicted in Fig. 1. A polariser and polarisation plane rotator were used to realise the $\theta = \left(\widehat{\boldsymbol{EF}}\right) = \pm 45°$ excitation geometry. The LIF was observed along the exciting laser beam. The $I_r$ and $I_l$ circularly polarised components were singled out by means of $\lambda/4$ plate followed by a linear polariser with its axis either parallel or perpendicular to **F**. The $D\ ^1\Pi\ \nu'(J')$

state selection has been maintained by finding in the overall LIF spectrum the particular LIF progressions mentioned in Ref. [7] and originating from the chosen $\nu'(J')$ level under study. The signal from a photomultiplier was registered using the photon counting technique. The experimentally obtained circularity degree was multiplied by a factor 1.25 which takes into account depolarisation in registration system and was determined by careful calibration of the registration channels with two orthogonal polarisers using the source of light with well-known degree of circularity.

## 4. Results and discussion

Fig. 2 presents the circularity degree for NaK $D\ ^1\Pi$ $J' = 20$ state calculated for all allowed $J', J'', J''_1$ combinations in different transition types. The $q$ and $d$ values were taken from Ref. [8]. An inset in Fig. 2 demonstrates the $J$-dependence of the electric field strength $F_{max}$ corresponding to maximal circularity degree. To illustrate the non-negligible contribution of higher than the first order terms in Stark energy expansion, the circularity for $J' = 23$ was calculated both in first order energy approximation (dashed line in Fig. 1a) and accounting up to third order terms in Stark energy expansion (solid line in Fig. 1a).

Examples of the experimentally observed $F$-dependence of the circularity degree are presented in Fig. 1a, b for $D\ ^1\Pi$ state 7(23) and 12(7) rovibrational levels, respectively. The fitting (see solid curves in Fig. 1) has been performed using an approach which involves diagonalisation of the Hamiltonian accounting for dc Stark mixing between all $J \pm \Delta J$ levels with $\Delta J \leq 3$ in the initial, excited and final rovibronic states of a LIF transition, see Ref. [6] for details. We used the values of excited state $\Lambda$-doubling constant $q$ and permanent electric dipole moment $d$ which were previously measured in Ref. [8], namely $d = 6.4$ **D**, $q = 1.51 \times 10^{-5}\,\mathrm{cm}^{-1}$ for 7(23) and $d = 5.1$ **D**, $q = 1.03 \times 10^{-5}\,\mathrm{cm}^{-1}$ for 12(7). The excited state relaxation rate $\Gamma = \tau^{-1}$ value was taken as $\Gamma = 8 \times 10^7\,\mathrm{s}^{-1}$ for both states to perform the best fitting of experimental values. This value exceeds the $\tau^{-1}$ measured in Ref. [9] by a factor which is over than the expected increase of excited state $\Gamma$ values because of collisions between NaK molecules and atoms. Fig. 1a,b demonstrates satisfactory agreement between theory and experiment. The results for 12(7) state in Fig. 1b are not so accurate because of large relative errors because of ca. 10 times smaller fluorescence intensities.

## Acknowledgements

This work was supported by the Latvian Science Council (Grant No. 96.0323). One of us (O.N.) is grateful for support from Latvian Science Council fellowship Grant No. 970. The authors are expressing their gratitude to Dr. Ilze Klincare and Janis Alnis for considerable help in experiments. We are heartily indebted to Dr. Andrey Stolyarov and Dr. Elena Pazyuk for multiple helpful discussions.

## References

[1] M.P. Auzinsh, R.S. Ferber, J. Chem. Phys. 99 (1993) 5742.
[2] I.P. Klincare, M.Ya. Tamanis, A.V. Stolyarov, M.P. Auzinsh, R.S. Ferber, J. Chem. Phys. 99 (1993) 5748.
[3] M. Auzinsh, R. Ferber, Optical Polarization of Molecules, Cambridge University Press, Cambridge, 1995.
[4] M. Auzinsh, I. Klincare, A.V. Stolyarov, O. Nikolayeva, M. Tamanis, R. Ferber, J. Mol. Struct. 410-411 (1997) 55.
[5] M. Mizushima, Theory of Rotating Diatomic Molecules, Wiley, New York, 1975.
[6] M. Tamanis, M. Auzinsh, I. Klincare, O. Nikolayeva, A.V. Stolyarov, R. Feber, J. Chem. Phys. 106 (1997) 2195.
[7] M.M. Hessel, S. Giraud-Cotton, NaK revisited: The ground $^1\Sigma$ and $D\ ^1\Pi$ states, unpublished preprint.
[8] M. Tamanis, M. Auzinsh, I. Klincare, O. Nikolayeva, R. Ferber, A. Zaitsevskii, E.A. Pazyuk, A.V. Stolyarov, J. Chem. Phys., 109 (1998).
[9] M. Tamanis, M. Auzinsh, I. Klincare, O. Nikolayeva, R. Ferber, E.A. Pazyuk, A.V. Stolyarov, A. Zaitsevskii, Phys. Rev. A, 58 (1998) 1932.

INFORMATION FOR AUTHORS

# JOURNAL OF MOLECULAR STRUCTURE

## Scope

The *Journal of Molecular Structure* is dedicated to the publication of full-length articles, review articles, and short communications, providing important new structural information on all types of chemical species, including:

- stable and unstable molecules in any environment (vapour, molecular beam, liquid, solution, liquid crystal, solid state, matrix-isolated, surface-adsorbed, etc.)
- chemical intermediates
- molecules in excited states
- biochemicals
- polymers

The methods used may include any combination of spectroscopic and non-spectroscopic techniques, for example:

- infrared spectroscopy (mid, far, near)
- Raman spectroscopy and non-linear Raman methods (CARS, etc.)
- force constant and molecular mechanics calculations
- electronic absorption spectroscopy
- optical rotatory dispersion and circular dichroism
- fluorescence and phosphorescence techniques
- electron spectroscopies (PES, XPS), EXAFS, etc.
- microwave spectroscopy
- electron diffraction
- NMR and ESR spectroscopies
- Mössbauer spectroscopy
- X-ray crystallography

Papers describing routine studies of little structural significance (e.g. straightforward X-ray crystal structure determinations) are not encouraged.

Publications combining experimental and theoretical approaches to a problem are particularly welcomed. However, purely theoretical (semiempirical or ab initio) studies should be submitted to the *Journal of Molecular Structure (Theochem)*.

## Submission of manuscripts

Authors are requested to send three good copies of their manuscript to one of the following editors.

- Dr Austin Barnes, Department of Chemistry and Applied Chemistry, University of Salford, Salford, M5 4WT, UK. Tel: (+44) 161 295 5698, Fax: (+44) 1204 656 958; e-mail: a.j.barnes@chemistry.salford.ac.uk
- Professor Jaan Laane, Department of Chemistry, Texas A&M University, College Station, TX 77843-3255, USA. Tel: (+1) 409 845 3352, Fax: (+1) 409 845 3154; e-mail: laane@chemvx.tamu.edu

Submission of an article is understood to imply that the article is original and is not being considered for publication elsewhere. Those intending to write a review should first contact an Editor. Letters to the Editor, book reviews and meeting/course announcements are also welcome. There are no page charges.

## Language

Please use good, explicit English. Consult a native speaker and/or dictionary where necessary.

## Manuscript preparation

The manuscript should be double spaced with wide margins. The content should be ordered as follows: Title, author(s) name(s), affiliations and addresses, abstract, up to five keywords for indexing. Illustrations must be original drawings or sharp black and white prints. Notations and details must be legible after reduction. Please number consecutively and refer to in the text.

## Reference style

[1] J.R. Durig, G.A. Guirgis, I. Badejo and J.F. Davis, J. Mol. Struct., 354 (1995) 15.

## Electronic manuscripts

Contributions on disk are encouraged. Upon acceptance of the article, the disk and three exactly matching printouts should be submitted together. Instructions for disk preparation are available from the Editors on request.

## Colour

Colour illustrations can be reproduced at the author's expense. The author should contact the Publisher for details (Fax: (+353) 61 472144).

## Refereeing

All articles submitted will be refereed. The Editors reserve the right to reject articles and to edit manuscripts when necessary. Authors are encouraged to suggest the names of 2 to 3 prospective referees.

## Reprints

50 Reprints will be supplied free of charge.

*Journal of Molecular Structure*, Homepage
www.elsevier.nl/locate/molstruc
www.elsevier.com/locate/molstruc
For full Instructions to Authors and other journal information

JOURNAL OF CHEMICAL PHYSICS VOLUME 109, NUMBER 16 22 OCTOBER 1998

# Lifetimes and transition dipole moment functions of NaK low lying singlet states: Empirical and *ab initio* approach

M. Tamanis, M. Auzinsh, I. Klincare, O. Nikolayeva, and R. Ferber
*Department of Physics, University of Latvia, Riga LV-1586, Latvia*

A. Zaitsevskii, E. A. Pazyuk, and A. V. Stolyarov
*Department of Chemistry, Moscow M. Lomonosov State University, Moscow 119899, Russia*

(Received 22 January 1998; accepted 16 July 1998)

The paper presents experimental $D\,^1\Pi$ state lifetime $\tau_{v'J'}$ data and develops empirical and *ab initio* approaches concerning $D\,^1\Pi$ and $B\,^1\Pi$ lifetimes, as well as $D\,^1\Pi-X\,^1\Sigma^+$, $B\,^1\Pi-X\,^1\Sigma^+$ and $D\,^1\Pi-A\,^1\Sigma^+$ transition dipole moment functions $\mu(R)$ of the NaK molecule. Experimental $D\,^1\Pi(v',J')$ state $\tau_{v'J'}$ values for $v'$ varying from 1 to 22 have been obtained from experimentally measured electric radio frequency optical double resonance (rf ODR) signal contours. The rf ODR signals have been produced by $D\,^1\Pi-X\,^1\Sigma^+$ laser induced optical transition and rf field (1–900 MHz) induced $e-f$ transition within the $D\,^1\Pi(v',J')$ level. The possibility to determine empirical absolute $\mu(R)$ function in a wide $R$ range from experimental $\tau_{v'J'}$ dependence on $v'$ and $J'$ has been demonstrated; such an approach has been applied to obtain $\mu(R)$ for the $B\,^1\Pi-X\,^1\Sigma^+$ transition on which relative intensity data are absent. The empirical $D\,^1\Pi-X\,^1\Sigma^+\,\mu(R)$ function has been considerably improved by simultaneous fitting of relative intensity and lifetime data implicitly accounting for the $J'$ dependence of measured lifetime values. The finite-field technique combined with the many-body multipartitioning perturbation theory was used for *ab initio* all-electron transition moment calculations. This approach appeared to be adequate to compute reliable $\mu(R)$ functions due to a proper description of core-valence correlations. As a result, excellent agreement between *ab initio* and empirical $B\,^1\Pi-X\,^1\Sigma^+$ and $D\,^1\Pi-X\,^1\Sigma^+$ transition dipole moment functions has been achieved. © *1998 American Institute of Physics*. [S0021-9606(98)02139-4]

## I. INTRODUCTION

It is well known that for such test diatomics as alkali dimers the calculated potential energies agree well enough with the experimental ones (see Ref. 1, and references therein). However, *ab initio* calculations are still less effective in reproducing intensities in molecular spectra arising from excited electronic states. At the same time, such radiative quantities as transition dipole moments $\mu(R)$, the corresponding lifetimes $\tau$ and intensity data represent, along with permanent electric dipole moments, a different and, in many cases, an extremely useful test of the validity of calculation methods and of the accuracy of molecular constant sets. This situation reflects the fact that one may expect considerable electron charge redistribution within particular molecular configurations without any substantial impact on the energy of the system.[2] First results obtained in the pioneering papers on homonuclear alkali dimer $Na_2$ appeared to be quite promising since a very good agreement between empirical[3,4] and calculated[5] $\mu(R)$ has been achieved. It was, however, not the case with the transition dipole moment function $\mu(R)$ for a heteronuclear diatomic molecule NaK. Indeed, a considerable (though not large) discrepancy comes to light if one compares the absolute values of empirical transition dipole moments reported for $D\,^1\Pi-X\,^1\Sigma^+$ transition in the NaK molecule by Pfaff, Stock and Zevgolis (PSZ) in Ref. 6, as well as by Katô and Noda (KN) in Ref. 7, with *ab initio* pseudopotential calculations of the same quantities performed by Ratcliff, Konowalow and Stevens (RKS).[2] Experimental lifetimes of a lower lying NaK $B\,^1\Pi$ state presented by Derouard, Debontride, Nguyen and Sadeghi (DDNS) in Ref. 8 are also significantly different from their theoretical counterparts calculated by exploiting the *ab initio* $B\,^1\Pi-X\,^1\Sigma^+$ transition dipole moment $\mu(R)$ given by RKS. At the same time, the $\mu(R)$ behavior for low lying singlet states of NaK is of general interest because of the much more pronounced $R$ dependence due to the partially ionic character of charge distribution.

It was not easy to judge whether the measured empirical (PSZ, KN, DDNS) or the calculated (RKS) $\mu$ and $\tau$ values are responsible for such a discrepancy. This circumstance stimulated us to undertake in the present work an attempt to obtain more accurate empirical $\mu(R)$ data, as well as to carry out *ab initio* all-electron calculations using many-body multipartitioning perturbation theory (MPPT),[9] which seems to be more adequate for the description of core-valence correlations than previously used pseudopotential schemes.[2] To obtain more reliable absolute values of the empirical $\mu_{D\,X}(R)$ function for $D\,^1\Pi-X\,^1\Sigma^+$ transition, we have performed lifetime $\tau_{v'J'}$ measurements in a wide range of NaK $D\,^1\Pi$ state vibrational levels $v'$ varying from 1 to 22. These data, along with somewhat corrected $D\,^1\Pi-X\,^1\Sigma^+$ transition relative intensities taken from Ref. 6, have been processed simultaneously in order to gain the empirical $\mu_{D\,X}(R)$ function. An improved method to invert the experimental lifetimes into the $\mu(R)$ function has been applied in order to get the empirical $B\,^1\Pi-X\,^1\Sigma^+$ transition dipole moment. In ad-

 

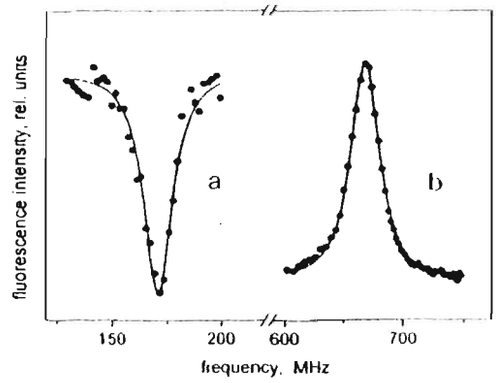


FIG. 1. Experimental NaK $D\,^1\Pi$ state rf-ODR signal contours (a) $v'=4$, $J'=19$, allowed $Q$-line, fitting parameters $f_0=171.4$ MHz, $\Delta_{1/2}=14.95$ MHz; (b) $v'=11$, $J'=46$, forbidden $Q$-line, fitting parameters $f_0=673.7$ MHz, $\Delta_{1/2}=26.48$ MHz. The solid line is a Lorentzian fit, see Eq. (1).

dition, we have undertaken a detailed theoretical study of the transition moment functions at the *ab initio* all-electrons level with accurate treatment of core-valence electron effects.

## II. EXPERIMENTAL RESULTS

The most straightforward and well-developed method to measure excited state lifetimes is, of course, to record directly the fluorescence decay kinetics after pulsed laser excitation. It is however also possible, after careful examination of distorting factors, to gain $^1\Pi$ state lifetime data from the electric radio frequency—optical double resonance (rf-ODR) signal contours. The idea of such a method is very simple and goes back to Refs. 10–12. Since each rotational level $J''$ in the ground $X\,^1\Sigma^+$ state has a definite parity, due to parity selection rule the laser induced transition $D\,^1\Pi(v',J')$ $X\,^1\Sigma^+(v'',J'')$ excites only one ($e$ or $f$) component of the $^1\Pi$ state $\Lambda$ doublet. This is why only the ($P$,$R$)-doublet lines are emitted at $P$- or $R$- type excitation, while, on the contrary, only the $Q$-singlet lines can be found in the laser induced fluorescence (LIF) spectrum after $Q$-type excitation. If the external ac electric field frequency is swept in the vicinity of $\Lambda$-splitting energy $\Delta_{ef}$, due to electric dipole $e\leftrightarrow f$ transitions one can observe either the resonant appearance of a "forbidden" line in the LIF spectrum, or the resonant diminution of "allowed" line intensity, thus giving rise to the respective rf-ODR signals, see Fig. 1, centered at the resonance frequency $f_0=\Delta_{ef}/h$.

To obtain NaK $D\,^1\Pi$ state $\tau_{v'J'}$ values, we have exploited the same rf-ODR setup used previously[13,14] for the purpose of $\Lambda$-splitting energy determination. Briefly, $Ar^+$-laser lines (Table I) have been used to excite a number of $D\,^1\Pi(v',J')$ levels of NaK molecules formed in thermal cells at temperatures $T=525$–$575$ K. The identification of $D\,^1\Pi(v',J')$ states in $D\,^1\Pi(v',J')\rightarrow X\,^1\Sigma(v'',J'')$ LIF progression has been based upon the data reported in Ref. 15. rf electric field voltage (usually up to 5 V) was applied to round polished Stark electrodes placed inside the cell with the spacing $\sim$1 mm and swept over the 5–900 MHz range. A monochromator with spectral resolution $\sim$0.03 nm was used to single out the wavelength corresponding to either "forbidden" or "allowed" line position in LIF spectra. The rf voltage supply scheme was carefully adjusted to avoid parasitic noise and to achieve constant rf electric field amplitude over the frequency sweeping region across the resonance position.

TABLE I. Excitation laser wavelength ($\lambda_{exc}$), NaK $D\,^1\Pi$ state $v'$, $J'$ values, rf-ODR resonance FWHM's ($\Delta_{1/2}$) and lifetimes ($\tau_{v'J'}$) obtained in the present work from rf-ODR experiments.

| $\lambda_{exc}$ (nm) | $v'$ | $J'$ | $\Delta_{1/2}$ (MHz) | $\tau$ (ns) |
|---|---|---|---|---|
| 496.5 | 1 | 27 | 14.7 ± 1.1 | 22.4 ± 1.7 |
| 514.4 | 1 | 67 | ... | 18.6 ± 0.3[b] |
| 501.7 | 3 | 23 | 17.7 ± 2.9 | 18.5 ± 3.0 |
| 496.5 | 3 | 43 | 17.1 ± 1.4 | 19.2 ± 1.5 |
| 496.5 | 4 | 19 | 14.0 ± 0.4 | 23.6 ± 0.7 |
| 496.5 | 7 | 8 | 16.8 ± 2.7 | 19.5 ± 3.0[a] |
| 488.0 | 7 | 20 | 16.5 ± 1.3 | 19.9 ± 1.5[a] |
| 488.0 | 7 | 23 | 16.5 ± 0.9 | 19.9 ± 0.1 |
| 488.0 | 7 | 23 | ... | 20.0 ± 0.3[b] |
| 488.0 | 10 | 102 | ... | 17.9 ± 0.3[b] |
| 496.5 | 11 | 46 | 24.3 ± 1.1 | 13.4 ± 0.6[c] |
| 476.5 | 12 | 7 | 25.5 ± 2.0 | 12.7 ± 1.0[c] |
| 476.5 | 14 | 19 | 17.7 ± 2.0 | 18.5 ± 2.0 |
| 476.5 | 17 | 94 | ... | 16.1 ± 0.3[b] |
| 488.0 | 22 | 35 | 20.0 ± 1.0 | 16.3 ± 0.8 |

[a]$^{23}Na^{41}K$ isotope.
[b]Reported by Pfaff, Stock, and Zevgolis (PSZ) (Ref. 6).
[c]Levels perturbed by the $d\,^3\Pi$ state.

The rf-ODR signal shape $I(f)$ has been analyzed by Field and Bergeman.[11] In the most simple case of a weak rf field one would arrive at the Lorentz shape contour

$$I(f)=\frac{I_0}{(\Gamma/2\pi)^2+(f-f_0)^2}, \tag{1}$$

where the full width at half maximum (FWHM) of the rf resonance is $\Gamma/\pi$, thus accounting for two natural widths originating from the two $\Lambda$ components contribution of $\Gamma/2\pi$ each. In Eq. (1) we neglect power broadening due to ac Stark effect. The estimations based on the approach given in Ref. 13 show that a small enough rf voltage is yet able to cause electric dipole transitions between the $\Lambda$-doublet components. Both evaluations and test measurements carried out with different rf field amplitudes allowed us to assume that one can neglect the power broadening effects in the particular experimental conditions. In particular, special experiments which included the diminishing of rf field amplitude from 5 to 1 V did not reveal any changes in signal width, thus confirming for us that one can neglect the power broadening effects.

A typical experimentally obtained fixed optical frequency, a rf swept rf-ODR signal recorded at the "allowed" $Q$-line originating from the $D\,^1\Pi$ state level $v'(J')=4(19)$ is presented in Fig. 1(a), while the analogous signal for the "forbidden" line originating from $11(46)$ is presented in Fig. 1(b). Experimental rf-ODR signals have been processed by Lorentz contour, Eq. (1), thus yielding the FWHM values $\Delta_{1/2}$. The FWHM values averaged over a number of measurements in different fluorescent cells are given in Table I. The errors in Table I reflect the discrepancy of the results obtained in different experiments.

As it has been shown in our treatment of the hyperfine (HF) interaction performed in Ref. 14, one can expect some small HF broadening effect upon the resonance signal. Owing to the $\Delta F=0$ selection rule, the HF broadening of the rf signals can be caused only by the difference in the HFS splitting of $e$ and $f$ components. The main cause of such effect for nonperturbed $D\,^1\Pi$ state levels is due to the presence of nonzero off-diagonal (transversal) matrix elements of the electric quadrupole HF interaction operator. Preliminary estimations[14] of HF structure constants performed by an internally contracted configuration-interaction method have shown that the HF broadening effect on the rf-ODR signals is rather small, being of the order of ~0.5 MHz. This broadening effect has been taken into account by a subsequent correction of experimentally measured $\Delta_{1/2}$ values. The corrected $\Delta_{1/2}$ values have been used to pass to the lifetimes $\tau_{v'J'}=\Gamma^{-1}$. The $\tau_{v'J'}$ values thus obtained are listed in Table I, which also contains the lifetimes presented by PSZ[6] for four $D\,^1\Pi(v',J')$ levels of the NaK molecule. Surprisingly good agreement of the $v'(J')=7(23)$ lifetime $\tau_{v'J'}=19.9\pm1.1$ ns obtained by us from the rf-ODR signal FWHM with $\tau_{v'J'}=20.0\pm0.3$ ns obtained by PSZ from fluorescence decay kinetics, see Table I, encouraged us to believe that our experimental rf-ODR contours can be used to get reliable lifetime values. It has, however, to be noted that, as pointed out in Ref. 14, although the isolated NaK $D\,^1\Pi$ state levels should exhibit only negligible HF broadening of rf-ODR signals, the latter may not be true for the levels which are perturbed by the adjacent $d\,^3\Pi$ state. For such levels one may expect an additional HF broadening caused by the HF nuclear spin–electron spin dipole interaction which is different for $e$ and $f$ components. Another cause for rf signal broadening by the $d\,^3\Pi$–$D\,^1\Pi$ mixing may appear in cases when the adiabatic lifetimes of triplet levels are shorter than the ones of the $D\,^1\Pi$ state. To exclude the influence of singlet–triplet interaction effects on empirical determination of $D$–$X$ transition moment functions, the experimental data for the perturbed $v(J)$ levels 11(46) and 12(7) were excluded from the data processing routine.

## III. EMPIRICAL DETERMINATION OF TRANSITION DIPOLE MOMENT FUNCTIONS

### A. Method

It is well known that both radiative lifetimes ($\tau_{v'J'}$) and relative $v'J'\to v''J''$ fluorescence intensities ($I_{ij}^{v'J'v''J''}$) can be used for the empirical determination of $R$ dependence of the transition moment $\mu_{ij}(R)$:[16]

$$\tau_{v'J'}^{-1}=\frac{8\pi^2}{3h\epsilon_0}\sum_{jv''J''}(\nu_{ij}^{v'J'v''J''})^3(\mu_{ij}^{v'J'v''J''})^2\frac{S_{J'J''}}{2J'+1}, \tag{2}$$

$$\frac{I_{ij}^{v'J'v''J''}}{I_{ij}^{v'J'v''_{\max}J''}}=\left(\frac{\nu_{ij}^{v'J'v''J''}}{\nu_{ij}^{v'J'v''_{\max}J''}}\right)^n\left(\frac{\mu_{ij}^{v'J'v''J''}}{\mu_{ij}^{v'J'v''_{\max}J''}}\right)^2, \tag{3}$$

where $8\pi^2/3h\epsilon_0=2.026\times10^{-6}$, $\epsilon_0$ is the permittivity of vacuum, $\tau$ is in s, $\mu_{ij}$ in a.u., and $\nu_{ij}$ is the rovibronic transition wave number in reciprocal centimeters. Here $n=3$ under photon counting and $n=4$ under intensity measurements in energy units, $S_{J'J''}$ is the Hönl–London factor, $v''_{\max}$ corresponds to the band with maximal intensity within a given progression, and $\mu_{ij}^{v'J'v''J''}$ is treated as[17]

$$\begin{aligned}\mu_{ij}^{v'J'v''J''}&=\langle v'_{J'}|\mu_{ij}(R)|v''_{J''}\rangle\\&=\sum_{k=0}^{N}a_k\langle v'_{J'}|R^k|v''_{J''}\rangle\\&=\langle v'_{J'}|v''_{J''}\rangle\sum_{k=0}^{N}a_k\frac{\langle v'_{J'}|R^k|v''_{J''}\rangle}{\langle v'_{J'}|v''_{J''}\rangle},\end{aligned} \tag{4}$$

where $a_k$ are the desired fitting parameters, while the wave functions (WFs) $|v_J\rangle=\chi_{vJ}(R)$ are the eigenfunctions of the radial Schrödinger equation:

$$\left[-\frac{1}{2m}\frac{d^2}{dr^2}+U^J(R)\right]\chi_{vJ}(R)=E_{vJ}\chi_{vJ}(R). \tag{5}$$

Here $m$ is the reduced molecular mass, $U^J(R)=U_{\rm BO}(R)+[J(J+1)-\Lambda^2]/2mR^2$ is the effective (centrifugally distorted) internuclear potential function, and $U_{\rm BO}(R)$ is the rotationless potential based on the Born–Oppenheimer (BO) separation. The BO potentials can be obtained from direct *ab initio* calculations, as well as from experimental rovibronic level positions either by the semiclassical Rydberg–Klein–Rees (RKR) inversion procedure, or in the framework of a full quantum-mechanical inverted perturbation approach (IPA).[18] In most practical cases the empirical RKR and IPA potentials are essentially more accurate than their *ab initio* counterparts. For this reason, only the empirical potentials have been exploited in the present study since the conventional spectroscopic information (Dunham molecular constants) required for their construction is available for all electronic states under consideration. To solve Eq. (5) numerically, we implemented the iterative renormalized Numerov algorithm[19] combined with the Richardson extrapolation.[20] An efficient phase-matching method was employed to find the eigenvalues.[21] This construction allows one to reduce the absolute errors in rovibrational WFs and in the corresponding overlap integral matrix elements to $10^{-5}$–$10^{-6}$. The accuracy of the overlap integrals was estimated by calculating the so-called "noise factors:" $s_{ij}=|\langle v_i|v_j\rangle|$, where $i\neq j$ and $|v_i\rangle$, $|v_j\rangle$ are vibrational WFs of a given electronic state. The deviation of $s_{ij}$ values from zero is a measure of the nonorthogonality of the calculated WFs.

It is obviously enough to record only one fluorescence progression in order to determine the relative $R$ dependence of the transition dipole moment, whereas $\tau$ values for a number of rovibronic $v'$, $J'$ levels are required for the same purpose in case lifetimes are used. At the same time, relative intensities do not allow one to gain the absolute values of the transition moment. From these considerations, the following procedure is usually exploited to determine the $\mu_{ij}(R)$ function. First, by using relative intensities of HF progression originating from the particular upper rovibronic level, the relative transition moment function is determined, which is subsequently normalized with respect to the experimental lifetime of the $v'$, $J'$ level.[22] Besides, the $\mu_{ij}(R)$ function is

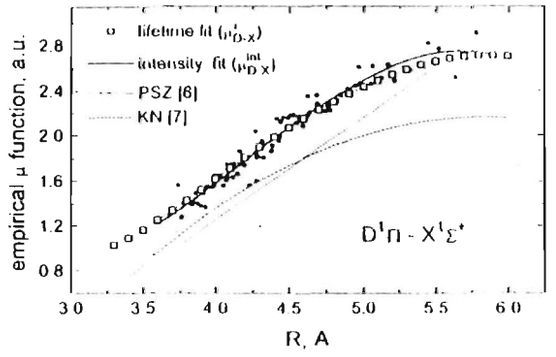


FIG. 2. Empirical $D\,^1\Pi$–$X\,^1\Sigma^+$ transition dipole moment functions extracted in the present work: (i) $\mu^{t}_{D-X}$ exploiting lifetimes given in Table I; (ii) $\mu^{int}_{D-X}$ exploiting relative intensities taken from Ref. 6. $\mu(R)$ functions obtained previously by PSZ (Ref. 6) and KN (Ref. 7) are also presented. Closed circles correspond to normalized $\mu^{int}_{D-X}(R)$ values obtained from corrected PSZ relative intensities data in the framework of the $R$-centroid approximation (6).

usually expanded in a power series of $R$ [see Eq. (4)], which can be transformed into one parametric function $\mu_{ij}(R^k)$ using the so called $R$ centroid approximation.[4,7]

$$R^k_{v'J'v''J''}=\frac{\langle v'_{J'}|R^k|v''_{J''}\rangle}{\langle v'_{J'}|v''_{J''}\rangle}\approx\left(\frac{\langle v'_{J'}|R|v''_{J''}\rangle}{\langle v'_{J'}|v''_{J''}\rangle}\right)^k=(R'_{v'J'v''J''})^k. \tag{6}$$

It is this method which has been used by PSZ[6] in order to determine the normalized absolute transition moment function for the $D$–$X$ transition in NaK as $\mu_{D-X}(R)=-6.0+2.3R$ ($\mu$ in debyes, $R$ in angstroms), see the dependence in Fig. 2 labeled as PSZ. It is also worth mentioning that the PSZ $\mu_{D-X}$ function was later modified by Katô and Noda[7] as $\mu_{D-X}(R)=-6.0+2.8R-0.24R^2$ (the dependence KN in Fig. 2) in order to describe their relative intensities measured for a single LIF progression which originates from the perturbed $v'=12, J'=7$ $D\,^1\Pi$ state level.

A modified approach has been exploited in the present paper to gain $\mu_{ij}(R)$ from experimental lifetimes and relative intensity data. The essence of the method we are offering here involves the two following steps.

(1) Replacement of exact equation (2) by the approximate expression

$$\tau^{-1}_{v'J'}\approx\frac{8\pi^3}{3h\epsilon_0}\sum_j\langle v'_{J'}|\Delta U^3_{ij}(R)\mu^2_{ij}(R)|v'_{J'}\rangle, \tag{7}$$

where $\Delta U_{ij}(R)=U_i(R)-U_j(R)$ is the difference potential between $i$ and $j$ electronic states.[25–27] Approximation (7) is based on the additional assumption that the difference potential is independent of $J$, and $|v'_{J'}\rangle\approx|v'_{J'\pm1}\rangle$, thus allowing one to perform separate summation over $v''$ and $J''$ in Eq. (2). As a result, the sum of Hönl–London factors yields $2J'+1$, and the rotational factor in Eq. (7) vanishes.

(2) The simultaneous employment of relative intensities for a number of LIF progressions and lifetime data for the overall set of rovibronic levels in a weighted nonlinear least-squares method (LSM) fitting by means of Eqs. (3) and (7).

Let us stress that the use of the approximate expression (7) practically does not cause any additional inaccuracy in the $\mu_{ij}(R)$ determination since, as was shown by a direct numerical comparison of Eq. (7) with the exact Eq. (2),[27] the relative error of the values obtained by Eq. (7) does not exceed 0.002% for all levels under consideration. Thus, formula (7) can be, in some sense, considered as an "exact" one since the accuracy of both lifetime measurements and *ab initio* transition dipole moment calculations are still essentially lower than the accuracy of approximation (7).

The present approach has the following advantages in comparison with the conventional one: (i) Formula (7) avoids the necessity of solving a complete eigenvalue and eigenfunction problem for lower states, being most efficient for distant states and nondiagonal systems. (ii) Formula (7) is much simpler than the exact sum given by Eq. (2), thus allowing one to apply the more stable linear LSM for empirical $\mu_{ij}(R)$ determination from the experimental lifetime values instead of the tedious nonlinear fitting procedure required for the direct application of Eq. (2). (iii) The present approach goes beyond the frame of the $R$ centroid approximation (6) which, as is known, may cause considerable errors in $\mu_{ij}(R)$ determination, especially when a weak fluorescence band (that is, with small FCF values) is exploited.[24,27]

Since the inversed lifetime (2) is the sum of probabilities of transitions into all lower levels, the individual dipole moment for a transition into a particular state may be obtained explicitly only in two cases: (a) the sum is reduced to a single term, i.e., only a transition into the ground state is possible; (b) the sum is dominated by one strong term, which is likely to occur in cases of comparatively high transition frequency $\nu_{ij}$ (since $\tau^{-1}_{v'J'}$ is proportional to $\nu^3_{ij}$), or in cases when all transitions but one are "forbidden," i.e., they have very small transition probabilities. Thus, strictly speaking, one may use lifetime measurements to normalize the available relative intensity data only if all relative probabilities (branching coefficients) contributing to the sum (2) are known.[28] It is also worth mentioning that experimental lifetimes and relative intensities exploited for determination of the empirical transition dipole moment must correspond to unperturbed levels, otherwise the deperturbation analysis is certainly required before any fitting procedure.[16]

### B. $B\,^1\Pi$–$X\,^1\Sigma^+$ transition

The $B\,^1\Pi$–$X\,^1\Sigma^+$ transition in NaK is a typical example of the present spectroscopic situation when systematic lifetime measurements have been carried out in a wide range of vibrational quantum numbers for the upper state ($1\leq v'_B\leq14$, see Fig. 3),[8] while experimental relative intensity data are absent. In this case the empirical $\mu^{em}_{B-X}(R)$ function can be, in principle, obtained from the lifetime $v'_B$ dependence $\tau(v')$ only. In doing so, we have implemented the approximate relation (7). The required difference potential $\Delta U_{B-X}(R)=U_{B\,^1\Pi}(R)-U_{X\,^1\Sigma^+}(R)$ has been computed from RKR potentials for $B\,^1\Pi$ and $X\,^1\Sigma^+$ states using the respective molecular constants given in Refs. 29 and 30. Since the experimental $B\,^1\Pi$ state lifetimes correspond to compara-

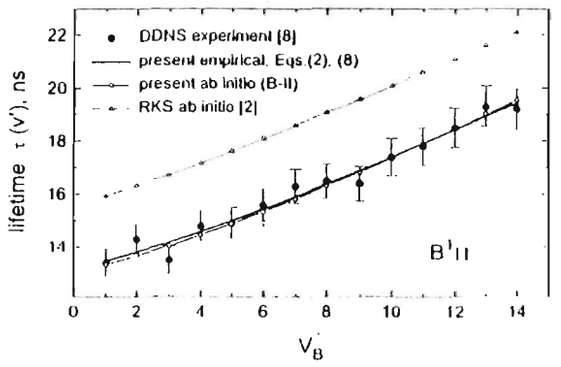


FIG. 3. $B\,^1\Pi$ state lifetimes $\tau(v')$ derived in present work from empirical and *ab initio* $\mu(R)$ functions calculated with larger basis (B II) set in comparison with experimental data given by DDNS (Ref. 8) for averaged $J'<40$, and with *ab initio* calculations given by RKS (Ref. 2).

tively low $J'$ levels ($J'<40$),[8] most of the lifetimes being averaged over several rotational levels, we have evaluated the expectation values of $\Delta U_{ij}^3(R)R^k$ operators using vibrational WFs corresponding to $J'=30$. Then, the experimental lifetimes given in Ref. 8, along with obtained rovibronic matrix elements, have been processed by a linear LSM procedure in order to obtain the fitting parameters $a_k$. The singular value decomposition (SVD) of the plan matrix was used to control the linear dependence of the normal equations arising in LSM.[31] The resulting empirical $\mu_{B\,X}^{\rm em}(R)$ function (the bold solid line in Fig. 4) takes the form

$$\mu_{B\,X}^{\rm em}(R) = -4.4428 + 5.3071R - 1.2145R^2 + 0.0871R^3, \tag{8}$$

with $\mu$ in a.u. and $R$ in Å. Equation (8) is valid within the range $3.4 \le R(\text{Å}) \le 5.8$, which actually corresponds to the interval between the outermost and innermost classical turning points of the highest vibrational $B\,^1\Pi$ state level to be fitted, namely $v'_B=14$. To prove the correctness of the applied inversion procedure, we have recalculated radiative $B\,^1\Pi$ state lifetimes by putting the obtained empirical $\mu_{B\,X}^{\rm em}$ function (8) into the exact equation (2). The result is shown in Fig. 3 (the bold solid line). Note that, although there is one more formally allowed electronic transition from $B\,^1\Pi$ to the lower

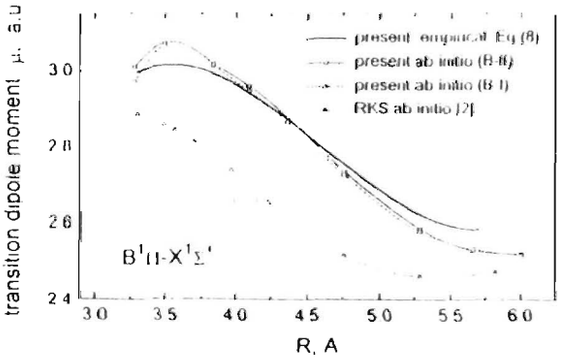


FIG. 4. Empirical $B\,^1\Pi$–$X\,^1\Sigma^+$ transition dipole moment functions $\mu_{B\,X}(R)$ and then *ab initio* calculations with smaller basis (B I) and larger basis (B II) accomplished in the present work in comparison with *ab initio* calculations performed by RKS (Ref. 2).

lying $A\,^1\Sigma^+$ state, its contribution into the $B\,^1\Pi$ state lifetime values is negligible due to both frequency and probability factors, since $\nu_{B\text{-}A}^3 \ll \nu_{B\text{-}X}^3$ and $\mu_{B\text{-}A}^2 \ll \mu_{B\,X}^2$.[2]

### C. $D^1\Pi$–$X^1\Sigma^+$ transition

The following distinctions between $D\,^1\Pi - X\,^1\Sigma^+$ and $B\,^1\Pi - X\,^1\Sigma^+$ systems should be pointed out concerning the empirical determination of transition dipole moments.

(1) In addition to lifetime measurements, the experimental relative intensities in the $D\,^1\Pi \to X\,^1\Sigma^+$ LIF spectrum originating from a particular $D\,^1\Pi v',J'$ level are available from PSZ data.[6]

(2) Lifetime and relative intensity measurements have been carried out for a number of $v',J'$ levels, without any averaging over $J'$, including very high $J'$ values ($J'\sim 100$, see Table I) for which it is necessary to take into account the effect of rotation on vibrational WFs and corresponding matrix elements.

(3) Some levels under study can be locally perturbed by the close lying $d\,^3\Pi$ state due to intramolecular spin–orbit interaction,[14,32] which means that the corresponding experimental lifetimes and relative intensities can differ from the "true" ones. Indeed, as was shown in Ref. 14, the $v'=11, J'=46$ and $v'=12, J'=7$ levels are certainly perturbed and experimentally measured lifetimes for these levels have therefore been excluded from the fitting. It has to be added, however, that, in obtaining empirical $D$–$X$ transition dipole moment functions, we have completely ignored the branching ratio coefficients, that is the ratios of singlet bound–bound $D\,^1\Pi \to X\,^1\Sigma^+$ and triplet bound–free $d\,^3\Pi \to a\,^3\Sigma^+$ transitions for the $D\,^1\Pi$ state levels $v'=1, J'=67$; $v'=7, J'=23$ and $v'=10, J'=102$, see Table III from Ref. 6. PSZ[6] supposed that the above levels are considerably mixed with the $d\,^3\Pi$ state levels. To clarify this point, we have estimated the mixing coefficients for these levels using experimental deperturbed molecular constants of the perturbing $d\,^3\Pi$ state and corresponding nondiagonal spin–orbit electronic matrix elements given in Ref. 32. These calculations confirmed for us that the $D\,^1\Pi$ state $v',J'$ levels under discussion are practically not perturbed by the $d\,^3\Pi$ state in contrast to the $v'=11, J'=46$ and $v'=12, J'=7$ levels mentioned above. Therefore, the transition probabilities into the triplet continuum given in Table III of Ref. 6 seem to have to be attributed to the bound–free LIF spectrum arising from other strongly perturbed $D\,^1\Pi$ levels excited by the same laser line (see Tables II and VII in Ref. 15).

(4) The $D\,^1\Pi \to A\,^1\Sigma^+$ transition can, in general, contribute to $D\,^1\Pi$ lifetime values. This contribution has been estimated by exploiting Eq. (7) and the *ab initio* $\mu_{D\,A}(R)$ function (see Table II; the calculations will be described in detail in Sec. IV). The difference $\Delta U_{D\,A}(R) = U_{D\,^1\Pi}(R) - U_{A\,^1\Sigma^+}(R)$ has been obtained using the $D\,^1\Pi$ state IPA potential represented in Table VIII of Ref. 15 and the $A\,^1\Sigma^+$ state RKR potential derived from the molecular constants given in Ref. 33. The obtained $D$–$A$ transition probabilities $A_{D\,A}$ (Table III) make a small but non-negligible contribution in the $D\,^1\Pi$ state lifetimes. This contribution should therefore be subtracted from the inversed experimental life-

TABLE II. *Ab initio* finite-field MPPT transition dipole moment functions obtained with the two atomic basis sets (B-I and B-II).

| | $\mu(R)$ (a.u.) | | | | | |
|---|---|---|---|---|---|---|
| | $D\,^1\Pi - X\,^1\Sigma^+$ | | $B\,^1\Pi - X\,^1\Sigma^+$ | | $D\,^1\Pi$ $A\,^1\Sigma^+$ | |
| R(Å) | B-I | B-II | B-I | B-II | B-I | B-II |
| 3.281 | 1.275 | 1.214 | 2.971 | 3.009 | 1.574 | 1.652 |
| 3.498 | 1.220 | 1.227 | 3.065 | 3.072 | 1.597 | 1.597 |
| 3.837 | 1.470 | 1.464 | 3.014 | 3.019 | 1.417 | 1.456 |
| 4.101 | 1.696 | 1.680 | 2.949 | 2.961 | 1.285 | 1.317 |
| 4.366 | 1.929 | 1.910 | 2.865 | 2.880 | 1.127 | 1.163 |
| 4.763 | 2.247 | 2.242 | 2.728 | 2.738 | 0.897 | 0.942 |
| 5.292 | 2.565 | 2.561 | 2.579 | 2.588 | 0.620 | 0.659 |
| 5.662 | 2.699 | 2.701 | 2.535 | 2.530 | 0.483 | 0.516 |
| 6.006 | 2.772 | 2.771 | 2.515 | 2.522 | 0.353 | 0.375 |

times gained from Table I in order to get, by means of the fitting procedure, the empirical $\mu_{D\text{-}X}(R)$ function corresponding to the $D$-$X$ transition only. The remaining allowed $D\,^1\Pi \rightarrow B\,^1\Pi$ and $D\,^1\Pi \rightarrow C\,^1\Sigma^+$ transitions contribute practically nothing in $D\,^1\Pi\,\tau(v',J')$ values owing to very small frequency and electronic probability factors, since $\nu^4_{D\,C} \ll \nu^4_{D\,B} \ll \nu^4_{D\,X}$ and $\mu^2_{D\,C} \ll \mu^2_{D\,B} \ll \mu^2_{D\,X}$.[2]

To check the self-consistency of experimental lifetime and relative intensity data we have exploited them independently of each other in order to obtain, in two different ways, the empirical $\mu(R)$ functions for the same $D-X$ transition. First, the $D\,^1\Pi(v',J')$ state lifetime with values measured in the present work from rf-ODR contours (the open squares in Fig. 5), along with the PSZ[6] lifetimes measured from fluorescence decay kinetics (the closed circles in Fig. 5), have been processed by the weighted linear LSM making use of Eq. (7). The resulting empirical function $\mu^{\tau}_{D\,X}(R)$ is depicted in Fig. 2 (open squares). Second, the relative intensities of the $D\,^1\Pi(v',J') \rightarrow X\,^1\Sigma^+(v'',J'')$ LIF spectrum presented in

TABLE III. Radiative NaK $D\,^1\Pi(v',J')$ state lifetimes (in ns) calculated by Eq. (7) with empirical potential curves using the following $D\,^1\Pi - X\,^1\Sigma^+$ transition dipole moment functions: (a) empirical, obtained in the present work ($\tau^{\text{present}}_{\text{em}}$) or given by PSZ. Ref. 6 ($\tau^{\text{PSZ}}_{\text{em}}$) and KN. Ref. 7 ($\tau^{\text{KN}}_{\text{em}}$), (b) *ab initio* calculated in the present work (FF MPPT, $\tau^{\text{present}}_{\text{ab}}$) or given by RKS Ref. 2 (pseudopotential, $\tau^{\text{RKS}}_{\text{ab}}$). The *ab initio* FF-MPPT $D\,^1\Pi - A\,^1\Sigma^+$ transition probabilities $A_{D\text{-}A}$ (in $10^6\ s^{-1}$) calculated in the present work are also presented.

| $v'$ | $J'$ | $\tau^{\text{present}}_{\text{em}}$ | $\tau^{\text{present}}_{\text{ab}}$ | $\tau^{\text{PSZ}}_{\text{em}}$ | $\tau^{\text{KN}}_{\text{em}}$ | $\tau^{\text{RKS}}_{\text{ab}}$ | $A_{D\text{-}A}$ |
|---|---|---|---|---|---|---|---|
| 1 | 27 | 22.5 | 23.0 | 34.5 | 31.2 | 15.1 | 1.631 |
| 1 | 67 | 21.8 | 22.3 | 33.2 | 30.3 | 14.9 | 1.572 |
| 3 | 23 | 21.8 | 22.2 | 32.9 | 30.7 | 14.9 | 1.574 |
| 3 | 43 | 21.6 | 22.0 | 32.4 | 30.4 | 14.9 | 1.553 |
| 4 | 19 | 21.5 | 21.8 | 32.1 | 30.4 | 14.9 | 1.546 |
| 7 | 8 | 20.5 | 20.8 | 29.7 | 29.6 | 14.7 | 1.458 |
| 7 | 20 | 20.4 | 20.8 | 29.6 | 29.5 | 14.6 | 1.453 |
| 7 | 23 | 20.4 | 20.8 | 29.5 | 29.5 | 14.6 | 1.450 |
| 10 | 102 | 17.8 | 18.4 | 23.8 | 26.7 | 13.9 | 1.184 |
| 11 | 46 | 18.8 | 19.3 | 25.7 | 28.1 | 14.2 | 1.294 |
| 12 | 7 | 18.8 | 19.3 | 25.6 | 28.2 | 14.3 | 1.296 |
| 11 | 19 | 18.1 | 18.6 | 23.9 | 27.6 | 14.1 | 1.222 |
| 17 | 94 | 16.0 | 16.6 | 18.4 | 25.2 | 13.1 | 0.948 |
| 22 | 35 | 15.8 | 16.3 | 17.1 | 25.5 | 13.3 | 0.904 |

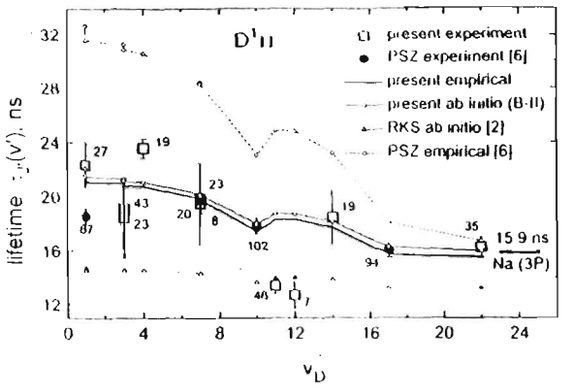


FIG. 5. Experimentally measured NaK $D\,^1\Pi$ state rovibrational lifetimes $\tau_{v'}(v')$, their calculated empirical values obtained using empirical $\mu^{\text{em}}_{D\text{-}X}(R)$ functions given in present work (present empirical) and in Ref. 6 (PSZ empirical). The *ab initio* lifetime calculations obtained in present work with basis II (present *ab initio*) and given in Ref. 2 (RKS *ab initio*) are also depicted. Numbers denote $J'$ values of the levels under study.

Tables I and II of Ref. 6 have been fitted in accordance with Eq. (3) by linear LSM in order to determine the relative transition dipole moment function $\mu^{\text{int}}_{D\,X}(R)$. The required rovibrational WFs for $D\,^1\Pi$ and $X\,^1\Sigma^+$ states have been obtained by the numerical solution of Eq. (5) with the corresponding effective potentials. Note that, as distinct from PSZ,[6] in the course of exploiting their data we have used the correct *cubic* relative intensity dependence on transition frequency $\nu$, that is, taking $n=3$ in Eq. (3) instead of $n=4$. This correction is based upon the fact that intensity measurements in Ref. 6 have been performed by detecting the *numbers of photon counts* using the photon counting regime. Besides, we have exploited the $X\,^1\Sigma^+$ state RKR potential based upon essentially improved molecular constants,[30] which is of particular importance for large $v',J'$ and $v'',J''$ values. The relative $\mu^{\text{int}}_{D\,X}(R)$ function has been scaled to the absolute $\mu^{\tau}_{D\,X}(R)$ function discussed above. It is easy to see from Fig. 2 that the normalized $\mu^{\text{int}}_{D\,X}(R)$ function (the solid line) is in good agreement with its lifetime counterpart $\mu^{\tau}_{D\,X}(R)$. As it also follows clearly from Fig. 2, both functions go steeply toward the value of the transition dipole moment between $3P$ and $3S$ states of the Na atom (2.52 $\pm$0.04 a.u.[34]), which is exactly what should be expected if one remembers that the interacting $D\,^1\Pi$ and $X\,^1\Sigma^+$ states dissociate into $(3P)\text{Na}+(4S)\text{K}$ and $(3S)\text{Na}+(4S)\text{K}$ atomic limits, respectively. At the same time, the present functions are significantly different from the PSZ[6] and KN[7] empirical functions. The above discussion allows us to suppose that the present empirical $\mu^{\text{int}}_{D\,X}(R)$ and $\mu^{\tau}_{D\,X}(R)$ functions are more reliable than the dependencies presented by PSZ[6] and KN.[7] Finally, the relative intensities for four progressions given by PSZ,[6] along with lifetimes data for the overall set of rovibronic levels given in Table I, have been processed simultaneously by a weighted nonlinear LSM fitting procedure exploiting Eqs. (3) and (7), yielding the following unified empirical $D\,^1\Pi - X\,^1\Sigma^+$ transition dipole moment function ($\mu^{\text{em}}_{D\,X}$ in a.u., $R$ in Å):

$$\mu^{\text{em}}_{D\,X}(R) = 4.1610 - 3.6822R + 1.1280R^2 - 0.0919R^3, \tag{9}$$

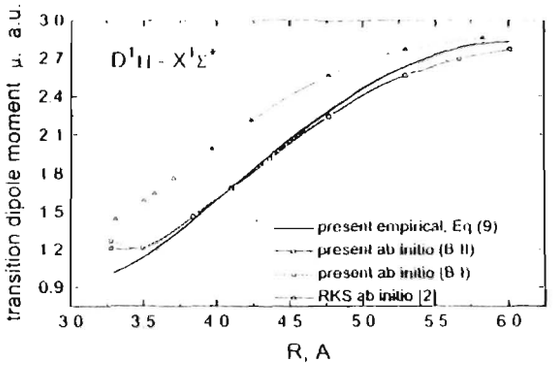


FIG. 6. Empirical and *ab initio* $D\,^1\Pi$ $X\,^1\Sigma^+$ transition dipole moment functions $\mu_{D\text{-}X}(R)$.

which is reliable within the range $3.3 < R(\text{Å}) < 6.0$ (the bold solid line in Fig. 6).

## IV. *AB INITIO* CALCULATIONS

The transition dipole moment functions have been computed using the finite-field (FF) technique[35–37] which is known as an efficient tool for *ab initio* studies of electric properties of molecules in pure electronic states. The generalization of the FF technique for transition property calculations is rather straightforward and can be briefly presented as follows. A molecule placed in external uniform electric field with intensity $F$ is described by the Hamiltonian

$$H = H(F) = H(0) \quad \mu F, \tag{10}$$

where $H(0)$ denotes the Hamiltonian of the free molecule and $\mu = -(\partial H/\partial F)$ is the conventional electric dipole operator. Exact $F$ dependent eigenfunctions $\Psi_i$, $\Psi_j$ and eigenvalues $E_i$, $E_j$ of $H$ should satisfy the off-diagonal Hellmann–Feynman relation:

$$\langle \Psi_i | \mu | \Psi_j \rangle = (E_i - E_j) \left\langle \Psi_i \left| \frac{\partial \Psi_j}{\partial F} \right. \right\rangle. \tag{11}$$

The central two-point finite-difference approximation for the derivative on the right-hand side of Eq. (11) at $F=0$ provides the following working formula of the FF method for the transition moment in a free molecule:

$$(\mu_{ij}^{\text{FF}})_\eta \approx (E_i - E_j)\langle \Psi_i(F_\eta = -\Delta/2) | \Psi_j(F_\eta = \Delta/2) \rangle / \Delta,$$
$$\eta = x, y, z, \tag{12}$$

where $\Delta$ is a numerical differentiation step size. Since Eq. (11) generally does not hold for approximate wave functions (WFs) resulting from practical *ab initio* calculations, the estimate (12) can differ from the corresponding off-diagonal electric dipole matrix element (dipole length form of the transition moment) computed with the same approximate electronic WFs. As has been demonstrated recently,[38] the FF results are normally more stable with respect to the level of electronic correlation treatment than their dipole-length analogs. This advantage of the FF technique seems to overcome its evident drawbacks which consist of limited numerical accuracy because of rounding errors for small $\Delta$ and significant nonlinear contributions when $\Delta$ is large, as well as the necessity to perform at least two series of calculations with different $F$ values. One should also realize that the external field can lower the symmetry of the system under study, thus giving rise to additional computational work. For instance, the FF calculations on the $\Sigma-\Pi$ transition moments in NaK should be performed in $C_s$ symmetry, and the states involved in the transitions have the same symmetry ($A'$) in the presence of an external field.

A quantitative *ab initio* description of excited electronic states of NaK requires an adequate reproduction of complicated valence configuration mixing strongly affected by the core-valence correlations. At the all-electron level of the theory, this implies the necessity to correlate a rather large number of electrons (including at least outer core shells of both atoms) within an inherently multiconfigurational (i.e., multireference) approach. In the present study the calculations of the WFs in the finite field were carried out by the many-body multipartitioning perturbation theory (MPPT).[9] With an appropriate choice of model (reference) space, this approach may take advantage of the physically grounded separation of electron correlation effects into valence and core-valence correlations, properly taking into account their interplay. Offering the possibilities to maintain strict size consistency and to treat vast model spaces without any risk of instabilities caused by intruder states, the second-order MPPT appears to be ideally suited to our task.

We used a recently developed MPPT code[39] interfaced to the MOLCAS suite of programs for electronic structure calculations.[40] Two basis sets were employed in our study. The smaller one, $(14s10p4d1f)/[7s5p3d1f]$[Na, $(15s13p4d1f)/[9s7p3d1f]$[K (hereafter referred as B-I) was obtained from the standard basis for electric property calculations[41] by decontracting the outermost $d$ functions and adding the $f$ functions with exponential parameters 0.06(Na) and 0.04(K). The larger one, referred as B-II, comprised additional single sets of diffuse $s$, $p$ and $d$ functions (exponential parameters 0.0033, 0.0019, 0.016 and 0.0025, 0.0013, 0.007 for Na and K, respectively), however the original contraction of the $d$ shell proposed in Ref. 41 was restored. Orthogonal molecular orbitals were generated by solving the state-average self-consistent field (SCF) problem for the two lowest $^2\Sigma^+$ states of NaK$^+$. The model space for MPPT calculations with B-I basis was the full valence configuration-interaction space, or, in other words, it comprised the configurations with doubly occupied core molecular orbitals and all possible arrangements of two valence electrons among the valence and virtual orbitals. When the larger basis (B-II) was used, we had to restrict the model space size to ~500, omitting the valence configurations with negligible contributions to the WFs of interest. This choice of model spaces guarantees a strict (B-I) or a very good approximate (B-II) size consistency of results. Within the model space, we have constructed a state-selective Hermitian effective Hamiltonian[9,42] with five $^1A'$ target states which corresponded to the three lowest $\Sigma$ and two $\Pi$ singlet states of the free molecule. The effective Hamiltonian incorporated the core-valence correlation and core polarization effects at the second order in MPPT. At the perturbation step the in-

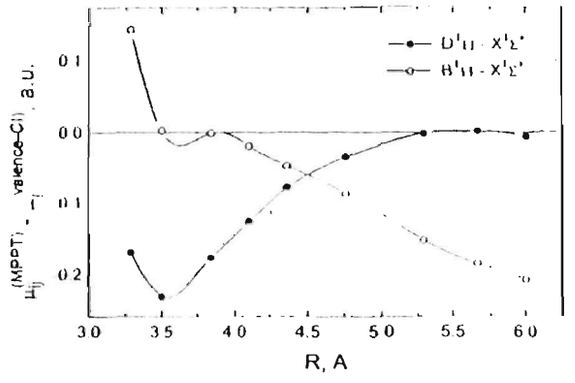


FIG. 7. Core-valence correlation effects upon calculated transition dipole moments.

nermost core orbitals $1s$(Na), $1s2s2p$(K) were frozen, i.e., 18 electrons were explicitly correlated.

The external electric field intensities corresponded to the step size $\Delta = 10^{-4}$ a.u.; additional calculations with $\Delta$ values in the range $10^{-5} \leq \Delta \leq 2\times 10^{-4}$ a.u. provided the $\mu_{ij}^{FF}$ estimates which were stable within $10^{-3}$ a.u. The overlap integrals entering the FF formula (12) for transition dipole moments have been evaluated with the valence eigenfunctions obtained by diagonalizing the effective Hamiltonian. Although the direct contributions to these integrals from core-excited configurations were thus ignored, the use of the FF scheme allowed us to incorporate implicitly the corresponding contributions into transition moment estimates (see the Appendix). Moreover, owing to the "perturb-then-diagonalize" strategy realized in our approach, the influence of core-valence correlations on $\mu_{ij}^{FF}$ values via correlation interference effects[43,44] was fully taken into account. The importance of core-valence correlation effects are demonstrated by the comparison of MPPT transition moments with the full valence CI ones in Fig. 7. Notice that the popular polarization pseudopotential technique[1,2,45] gives a less adequate description of these effects since: (1) the two-particle effective interactions of valence electrons arising from core-valence correlations cannot be properly fitted by any one-particle pseudopotential; (2) the direct contributions from core-excited configurations to any property other than the energy are completely ignored; (3) the spurious contributions to transition moments arising from nonorthogonality of valence pseudo-WFs to the core, in contradistinction with similar contributions to the total energy, are not automatically countervailed. The high accuracy of the transition moments for free non-valence electron atoms computed by the pseudopotential method[2] imply that the two latter factors should not be of crucial importance. In contrast, the effective two-particle interactions in the valence shell can affect the valence part of the WFs and therefore the characteristics of valence transitions.

The resulting $B\,^1\Pi - X\,^1\Sigma^+$ and $D\,^1\Pi - X\,^1\Sigma^+$ transition dipole moment functions are presented in Table II and plotted in Figs. 4 and 6, respectively. Let us first note that the $\mu_{ij}$ estimates obtained with two different bases (B-I and B-II) are almost identical. The discrepancy exceeds 1% only for the $D-X$ transition at very short internuclear distance ($R$ $\approx$3.5 Å). The $\mu_{B\,X}$ and $\mu_{D\,X}$ *ab initio* data closely fit the corresponding empirical transition moment functions obtained in Sec. III. Unfortunately, the accuracy of the computed $D\,^1\Pi - A\,^1\Sigma$ transition moment (Table II) cannot be directly estimated from the available experimental data since intensity measurements of the $D\,^1\Pi - A\,^1\Sigma$ transition are absent and the contribution of the $D\,^1\Pi - A\,^1\Sigma$ channel to the radiative decay of the $D\,^1\Pi(v',J')$ levels is rather small (Table III). It is worth noting the qualitative agreement of our transition moment functions with the RKS data; quantitative differences can be explained by the simplified treatment of core-valence correlations and the use of rather restricted valence basis sets in the pseudopotential calculations.[2] The relative strengths of the remaining allowed transitions $D\,^1\Pi - B\,^1\Pi$, $D\,^1\Pi - C\,^1\Sigma^+$ and $B\,^1\Pi - A\,^1\Sigma^+$ have also been obtained in the course of the present *ab initio* calculations in order to estimate their contributions to radiative lifetimes of $D\,^1\Pi$ and $B\,^1\Pi$ states, respectively.

## V. LIFETIME CALCULATIONS

The present empirical and MPPT *ab initio* $\mu_{D\,X}(R)$ functions, as well as those from pseudopotential *ab initio* calculations of RKS[2] and empirical functions given by PSZ[6] and KN[7] have been exploited to calculate $D\,^1\Pi$ state lifetimes by using Eq. (7) and empirical potentials. The results are presented in Table III. The corresponding $\tau_{v'J'}$ values corrected by accounting for the $D-A$ transition contribution (see Table III) are plotted in Fig. 5. One can see that both FF MPPT and empirical function $\mu_{D\,X}(R)$ (9) allow one to reproduce the experimental lifetimes significantly better than the RKS[2] and the empirical PSZ[6] and KN[7] $\mu(R)$ functions. The $B\,^1\Pi(v')$ state radiative lifetimes $\tau_{v'}$ derived from the present *ab initio* transition dipole moments and empirical potential curves quantitatively reproduce the experimental values as well (Fig. 3). It should be emphasized that an improvement over the results of RKS[2] pseudopotential calculations was gained for the lifetimes of both electronic states under study.

As it was already shown, the introduction of a centrifugal distortion term into the effective potential $U^J(R)$ in Eq. (5) is definitely required to properly take into account the rotation effect on vibrational WFs for high $J'$ levels, since the rotation effect can dramatically change the magnitude of small rovibronic matrix elements (4) corresponding to small Franck–Condon factors $|\langle v'_{J'}|v''_{J''}\rangle|^2$.[17] Obviously, the rotation effect has to cause lifetime variation with rotational quantum number $J'$. Indeed, under the simplest harmonic approximation, the lifetime $J'$ dependence for a given vibrational level $v'$ can be expressed by means of Eq. (7) in the following analytical form:

$$\tau_{v'J'} = \tau_{v'}(1 - \gamma_{v'}[J'(J'+1) - \Lambda^2]), \tag{13}$$

$$\gamma_{v'} = \left(\frac{2B_{e'}}{\omega_{e'}}\right)^2 R_{e'}\left[\sum_j \frac{2\mu'_{1j}(R_{e'})}{\mu_{1j}(R_{e'})} - \frac{m\omega_{e'}^2}{11.238}\sum_j \frac{R_{e'} - R_{ej}}{T_{e'} - T_{ej}}\right], \tag{14}$$

where the reduced mass $m$ is in Aston units,[46] equilibrium distances $R_{e'}, R_{ej}$ are in Å, while electronic energies

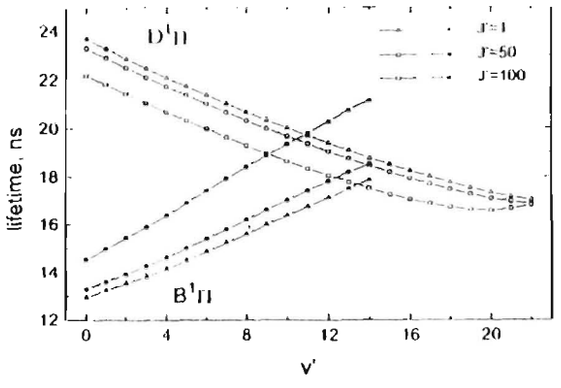


FIG. 8. Rotational effect on radiative lifetimes of $B\,^1\Pi$ and $D\,^1\Pi$ states

$T_{ei}, T_{ej}$, rotational ($B_{ei}$) and vibrational ($\omega_{ei}$) molecular constants are in cm$^{-1}$. The $\mu'_{ij}(R_{ei}) \equiv d\mu_{ij}/dR$ denotes the first derivative of the dipole moment function $\mu_{ij}(R)$ with respect to internuclear distance $R$. Relations (13) and (14) demonstrate that the lifetime $J$ dependence should be most pronounced for long living states corresponding to small $\nu_{ij} = T_{ei} - T_{ej}$ and small $\mu_{ij}$ factors, as well as for the non-diagonal systems (with large $\Delta R_e = R_{ei} - R_{ej}$ values) possessing pronounced $R$ dependence of the dipole moment function (large $d\mu_{ij}/dR$).

To estimate the rotation effect upon the lifetimes of the $B\,^1\Pi$ and $D\,^1\Pi$ states, we have evaluated the corresponding $\gamma_i$ parameters in Eq. (14) by using respective molecular constants and empirical $B-X$ and $D-X$ transition dipole moment functions. The $\gamma$ values obtained ($\gamma_{B\,^1\Pi} = -8.3 \times 10^{-6}$, $\gamma_{D\,^1\Pi} = 7.2 \times 10^{-6}$) mean that $\tau(B\,^1\Pi)$ has to increase as $J'$ increases, while $\tau(D\,^1\Pi)$ has to decrease as $J'$ increases. Indeed, for the $D\,^1\Pi$ state an "unexpected" minimum can be distinguished in Fig. 5 upon the relatively smooth $v'$ dependence of both experimental and calculated lifetime values. This minimum corresponds to a rovibronic level with maximal $J'$ value under study, namely $J' = 102$. Hence, we can suppose that it is the rotation effect which is responsible for the lifetime decrease. To check this point, we have calculated $\tau(D\,^1\Pi)$ and $\tau(B\,^1\Pi)$ for lowest ($J' = 1$), medium ($J' = 50$) and high ($J' = 100$) $J'$ values. The results obtained are represented in Fig. 8 and completely confirm the above statements. Moreover, a linear fit of the calculated $\tau(v', J')$ values for the lowest $v'$ values yields $\gamma_i$ parameters $\gamma_{B\,^1\Pi} = -12.1 \times 10^{-6}$ and $\gamma_{D\,^1\Pi} = 6.6 \times 10^{-6}$, being in good agreement with those obtained above within the harmonic approximations (13) and (14). The obtained $\gamma_{D\,^1\Pi}$ values allow one to explain the diminution of the experimental $D\,^1\Pi$ lifetimes for high $J$ levels, namely $\tau_{v'=10}(J' = 102) = 17.9$ ns and $\tau_{v'=17}(J' = 94) = 16.1$ ns, see Table I. Indeed, at $J' = 1$ our lifetime calculations for these levels performed with semiempirical transition moments yielded larger values, namely $\tau_{v'=10}(J' = 1) = 19.3$ ns and $\tau_{v'=17}(J' = 1) = 17.1$ ns. At the same time, Eq. (13) with $\gamma_{D\,^1\Pi} = 6.6 \times 10^{-6}$ gives the values $\tau_{v'=10}(J' = 102) = 18.0$ ns and $\tau_{v'=17}(J' = 94) = 16.2$ ns which agree with the experimental results. Thus, the rotation effect leads to a noticeable (≈1.5–2.0 ns) contribution to the lifetimes of high $J'$ levels for both states under study. As is well known, the probability densities of rovibrational WFs shift smoothly to the right along the $R$ axis as $v'$ and $J'$ increase. This leads to a situation when $\chi^2_{v'J'}(R)$ functions for two different rovibronic levels $(v'_1, J'_1)$ and $(v'_2, J'_2)$, belonging to the same electronic state, can be localized predominantly in the same relatively narrow $R$ region if the following conditions are fulfilled simultaneously: $v'_2 > v'_1 \gg 1$ and $J'_2 \ll J'_1$. This means that the integrand functions $\Delta U^3_{ij}(R)\mu^2_{ij}(R)\chi^2_{vJ}(R)$ for these levels, along with the corresponding lifetime values, should be close to each other in case of any smooth dipole moment function $\mu_{ij}(R)$. This is the reason why, for instance, $\tau_{J'=102}(v' = 10) \approx \tau_{J'=0}(v' = 14)$ and $\tau_{J'=94}(v' = 17) \approx \tau_{J'=15}(v' = 22)$ for the $D\,^1\Pi$ state (Table III).

## VI. CONCLUSIONS

Excellent agreement between *ab initio* and empirical $B\,^1\Pi - X\,^1\Sigma^+$ and $D\,^1\Pi - X\,^1\Sigma^+$ transition dipole moment functions obtained in the framework of the present approaches has been achieved.

A possibility has been demonstrated allowing one to determine the absolute transition dipole moment function $\mu(R)$, in wide $R$ range, by means of the approximate relation (7) and the experimental data on lifetime variations with vibrational and rotational quantum numbers. The approach was employed successfully to describe the $B\,^1\Pi - X\,^1\Sigma^+$ transition in which relative intensity data are absent. Satisfactory agreement between the results obtained applying Eq. (7) and the ones gained from the relative intensities by applying Eq. (3) with $n = 3$ has been achieved in the case of $D\,^1\Pi - X\,^1\Sigma^+$ transition.

The empirical $D\,^1\Pi - X\,^1\Sigma^+$ transition dipole moment function $\mu(R)$ has been improved considerably by means of: (a) extension of the $(v', J')$ range of the experimental lifetime data; (b) corrected description of relative intensities measured by the photon-counting regime [$n = 3$ in Eq. (3)]; (c) simultaneous fitting of lifetime and relative intensity data; (d) taking into account implicitly the $J'$ dependence of experimental lifetime values in fitting procedures.

The combination of the finite-field (FF) technique and many-body multipartitioning perturbation theory (MPPT) has been shown to be adequate for obtaining reliable transition dipole moment values owing to a proper description of the core-valence correlation contributions into transition moment estimates.

## ACKNOWLEDGMENTS

Financial support for this work by the Russian Foundation of Basic Research under Grant Nos. 97-03-32215a and 97-03-33714a is gratefully acknowledged by three of us (I.P., A.S., and A.Z.). A.Z. thanks Professor Björn O. Roos for supplying him with the MOLCAS 3 package. This work was supported by the European Commission in the frame of PECO Human Capital and Mobility (Network) LAMDA program, Contract No. ERBCIPDCT940633, and we are especially indebted to Dr. Henrik Rudolph and Dr. Henk Dijkerman for their constant efforts to help us in carrying out the project. The Riga group participants have been supported by the Latvian Science Council (Grant No. 96.0323). Support

by the research group "Interaction of Oriented Molecules" of the Center for Interdisciplinary Research (ZiF) at the University of Bielefeld is gratefully acknowledged by one of us (M.A.). We are especially grateful to graduate student Janis Alnis for his considerable help in fixing the setup and participation in measurements.

## APPENDIX

Let us assume that the basis configuration state functions do not depend on the field intensity $F$. In the present study this is ensured by the use of nonrelaxed molecular orbitals of the free ($F=0$) $NaK^+$ ion in the calculations on NaK for any field intensity. Denoting the model-space and outer-space basis functions by $|m\rangle,|n\rangle\ldots$ and $|a\rangle,|b\rangle\ldots$, respectively, and introducing the model-space projector $P=\Sigma_m|m\rangle\langle m|$ which is also independent of $F$, we can write down the $F$-dependent second-order Hermitian effective Hamiltonian in the form:

$$H_{\rm eff}^{[2]}(F)=PH(F)P+\frac{1}{2}\sum_{mn}\sum_{a}|m\rangle H_{ma}(F)\times\left(\frac{1}{D_{ma}}+\frac{1}{D_{na}}\right)H_{an}(F)\langle n|. \tag{A1}$$

Here $D_{ma}$, $D_{na}$ are the energy denominators defined by the MPPT manifold of zero-order Hamiltonians (see Ref. 9 for explicit formulas). For the sake of simplicity, we shall suppose that these entities are $F$ independent, i.e., that MPPT zero-order Hamiltonians constructed for $F=0$ are further used in the second-order calculations for nonzero field intensities. If calculations for different $F$ values are performed separately, neglecting the $F$ dependence of the energy denominators is a reasonable approximation. Substituting the expression for the field-dependent total Hamiltonian (10) into Eq. (A1) and regrouping the terms according to their powers in $F$, one gets:

$$H_{\rm eff}^{[2]}(F)=H_{\rm eff}^{[2]}(0)-FM+O(F^2), \tag{A2}$$

where

$$M=P\mu P+\frac{1}{2}\sum_{mn}\sum_{a}|m\rangle(H_{ma}(0)\mu_{an}+\mu_{ma}H_{an}(0))\times\left(\frac{1}{D_{ma}}+\frac{1}{D_{na}}\right)\langle n|. \tag{A3}$$

Obviously,

$$M=-\left.\frac{\partial H_{\rm eff}^{[2]}}{\partial F}\right|_{F=0}. \tag{A4}$$

One easily notices that Eq. (A3) resembles the expression for the first-order effective electric dipole operator:[47,48]

$$\mu_{\rm eff}^{[1]}=P\mu P+\sum_{mn}\sum_{a}|m\rangle\times\left(\frac{H_{ma}(0)\mu_{an}}{D_{ma}}+\frac{\mu_{ma}H_{an}(0)}{D_{na}}\right)\langle n|. \tag{A5}$$

Provided that $|D_{ma}-D_{na}|\ll|D_{ma}|$ (this requirement is normally satisfied at least for model space configurations $|m\rangle$, $|n\rangle$ with large weights in the target vector expansions), the $M$ matrix elements between the target states should approach the corresponding $\mu_{\rm eff}^{[1]}$ matrix elements:

$$\langle\Psi_i|M|\Psi_j\rangle\cong\langle\Psi_i|\mu_{\rm eff}^{[1]}|\Psi_j\rangle. \tag{A6}$$

Since $\mu_{\rm eff}^{[1]}$ is Hermitian, its eigenfunctions $\Psi_i$, $\Psi_j$, $i\neq j$ satisfy

$$\langle\Psi_i|\Psi_j\rangle=0,\ \langle\Psi_i|H_{\rm eff}^{[2]}|\Psi_j\rangle=0. \tag{A7}$$

Differentiating Eq. (A7) with respect to field intensity and taking into account Eq. (A4), one readily arrives at a Hellmann–Feynman-like relation

$$(E_i-E_j)\left\langle\Psi_i\left|\frac{\partial\Psi_j}{\partial F}\right\rangle\right|_{F=0}=\langle\Psi_i|M|\Psi_j\rangle\cong\langle\Psi_i|\mu_{\rm eff}^{[1]}|\Psi_j\rangle. \tag{A8}$$

Although the functions $\Psi_i,\Psi_j$ are restricted to the model space and do not comprise any contributions from outer-space (core-excited) configurations, Eq. (A8) clearly indicates that FF transition dipole moment estimates computed with these functions implicitly incorporate the bulk of such contributions entering the first-order effective electric dipole operator (A5). To achieve a similar level of accuracy with the dipole-length formula, one should explicitly construct the first-order effective operator (A5) or, equivalently, evaluate the outer-space part of the WFs using first-order wave operator.[9,47,48]

[1] S. Magnier and Ph. Millie, Phys. Rev. A **54**, 204 (1996).
[2] I. B. Ratcliff, D. D. Konowalow, and W. J. Stevens, J. Mol. Spectrosc. **110**, 242 (1985).
[3] M. M. Hessel, E. W. Smith, and R. F. Drullinger, Phys. Rev. Lett. **33**, 1251 (1974).
[4] W. Demtröder, W. Stetzenbach, M. Stock, and J. Witt, J. Mol. Spectrosc. **61**, 382 (1976).
[5] W. J. Stevens, M. M. Hessel, P. J. Bertoncini, and A. C. Wahl, J. Chem. Phys. **66**, 1477 (1977).
[6] J. Pfaff, M. Stock, and D. Zevgolis, Chem. Phys. Lett. **65**, 310 (1979).
[7] H. Katô and C. Noda, J. Chem. Phys. **73**, 4940 (1980).
[8] J. Derouard, H. Debontride, T. D. Nguyen, and N. Sadeghi, J. Chem. Phys. **90**, 5936 (1989).
[9] A. Zaitsevskii and J. P. Malrieu, Theor. Chim. Acta **96**, 269 (1997), and references therein.
[10] S. J. Silvers, T. H. Bergeman, and W. Klemperer, J. Chem. Phys. **52**, 4385 (1970).
[11] R. W. Field and T. H. Bergeman, J. Chem. Phys. **54**, 2936 (1971).
[12] R. F. Drullinger, M. M. Hessel, and E. W. Smith, in *Laser Spectroscopy*, edited by S. Haroche *et al.* (Springer, Berlin, 1975), p. 91.
[13] M. Tamanis, M. Auzinsh, I. Klincare, O. Nikolayeva, A. V. Stolyarov, and R. Ferber, J. Chem. Phys. **106**, 2195 (1997).
[14] M. Tamanis, M. Auzinsh, I. Klincare, O. Nikolayeva, R. Ferber, I. A. Pazyuk, A. V. Stolyarov, and A. Zaitsevskii, Phys. Rev. A **58**, 1932 (1998).
[15] M. M. Hessel and S. Girard Cotton (unpublished).
[16] H. Lefebvre-Brion and R. W. Field, *Perturbations in the Spectra of Diatomic Molecules* (Academic, New York, 1986).
[17] Ya. A. Haya, R. S. Ferber, N. E. Kuz'menko, O. A. Shmit, and A. V. Stolyarov, J. Mol. Spectrosc. **125**, 1 (1987).
[18] W. M. Kosman and J. Hinze, J. Mol. Spectrosc. **56**, 93 (1975); C. R. Vidal and H. Scheingraber, *ibid.* **65**, 46 (1977).
[19] B. R. Johnson, J. Chem. Phys. **67**, 4086 (1977).
[20] J. F. Richardson, Philos. Trans. R. Soc. London, Ser. A **226**, 299 (1927).
[21] A. V. Abarenov and A. V. Stolyarov, J. Phys. B **23**, 2419 (1990).

[22] A. V. Stolyarov, N. E. Kuz'menko, Ya. A. Harya, and R. S. Ferber, J. Mol. Spectrosc. **137**, 251 (1989).
[23] P. A. Fraser, Can. J. Phys. **32**, 515 (1954).
[24] C. Noda and R. N. Zare, J. Mol. Spectrosc. **95**, 254 (1982); N. E. Kuz'menko and A. V. Stolyarov, J. Quant. Spectrosc. Radiat. Transf. **35**, 415 (1986).
[25] J. Tellinghuisen, Chem. Phys. Lett. **105**, 241 (1984).
[26] A. V. Stolyarov and V. I. Pupyshev, Phys. Rev. A **49**, 1693 (1994).
[27] E. A. Pazyuk, A. V. Stolyarov, and V. I. Pupyshev, Chem. Phys. Lett. **228**, 219 (1994).
[28] R. S. Ferber, Ya. A. Harya, and A. V. Stolyarov, J. Quant. Spectrosc. Radiat. Transf. **47**, 143 (1992).
[29] R. F. Barrow, R. M. Clements, J. Derouard, N. Sadeghi, C. Effantin, J. d'Incan, and A. J. Ross, Can. J. Phys. **65**, 1154 (1987).
[30] A. J. Ross, C. Effantin, J. d'Incan, and R. F. Barrow, Mol. Phys. **56**, 903 (1985).
[31] L. Lawson and R. J. Hanson, *Solving Least Squares Problems* (Prentice-Hall, Englewood Cliffs, NJ, 1974).
[32] P. Kowalczyk, J. Mol. Spectrosc. **136**, 1 (1989).
[33] A. J. Ross, R. M. Clements, and R. F. Barrow, J. Mol. Spectrosc. **127**, 546 (1988).
[34] W. L. Wiese, M. W. Smith, and B. M. Miles, *Atomic Transition Probabilities*, Natl.Stand.Ref.Data Ser., NBS Circ. No. 22 (USGPO, Washington, D.C. 1969), Vol. 2.
[35] J. A. Pople, J. W. McIver, and N. S. Ostlund, J. Chem. Phys. **49**, 2965 (1968).
[36] A. J. Sadlej, J. Chem. Phys. **75**, 320 (1981); G. H. F. Diercksen and A. J. Sadlej, *ibid.* **75**, 1253 (1981), and references therein.
[37] P. M. Kozlowski and E. R. Davidson, Int. J. Quantum Chem. **53**, 149 (1995).
[38] S. O. Adamson, A. Zaitsevskii and N. F. Stepanov (unpublished).
[39] R. Cimiraglia and A. Zaitsevskii (unpublished).
[40] K. Andersson, M. R. A. Blomberg, M. P. Fülscher, G. Karlström, V. Kellö, R. Lindh, P.-A. Malmqvist, J. Noga, J. Olsen, B. O. Roos, A. J. Sadlej, P. E. M. Siegbahn, M. Urban, P.-O. Widmark, MOLCAS 3, University of Lund, Sweden, 1995.
[41] A. J. Sadlej and M. Urban, J. Mol. Struct.: THEOCHEM **234**, 147 (1991).
[42] A. Zaitsevskii and J. P. Malrieu, Chem. Phys. Lett. **250**, 366 (1996).
[43] J. P. Malrieu, J.-L. Heully, and A. Zaitsevskii, Theor. Chim. Acta **90**, 167 (1995).
[44] J. P. Malrieu, in *Recent Progress in Many-body Theories*, edited by E. Schachinger, H. Mitter, and H. Sormann (Plenum, New York, 1995), Vol. 4, p. 109.
[45] W. J. Stevens, D. D. Konowalow, and L. B. Ratcliff, J. Chem. Phys. **80**, 1215 (1984).
[46] K. P. Huber and G. Herzberg, *Molecular Spectra and Molecular Structure. IV. Constants of Diatomic Molecules* (van Nostrand, New York, 1979).
[47] F. J. Ellis and E. Osnes, Rev. Mod. Phys. **49**, 777 (1977).
[48] H. Sun and K. F. Freed, J. Chem. Phys. **88**, 2659 (1988); V. Hurtubise and K. F. Freed, Adv. Chem. Phys. **83**, 465 (1993).

PHYSICAL REVIEW A VOLUME 58, NUMBER 3 SEPTEMBER 1998

# NaK Λ doubling and permanent electric dipoles in low-lying $^1\Pi$ states: Experiment and theory

M. Tamanis, M. Auzinsh, I. Klincare, O. Nikolayeva, and R. Ferber
*Department of Physics, University of Latvia, Riga LV-1586, Latvia*

E. A. Pazyuk, A. V. Stolyarov, and A. Zaitsevskii
*Department of Chemistry, Moscow M. Lomonosov State University, Moscow 119899, Russia*

(Received 23 December 1997)

The paper presents Λ splittings and $q$ factors in the NaK $D\,^1\Pi$ state, directly measured from the electric radio-frequency-optical double resonance (RF-ODR) in laser-induced fluorescence (LIF) for a number of vibrational states $v=1$–22 with definite rotational levels $J$ between 7 and 46. Permanent electric dipole moment values ($d$) have been obtained by measuring in LIF spectra the relative intensities of "forbidden" lines caused by dc Stark effect induced $e/f$ mixing in the $^1\Pi$ state, with their subsequent processing, which allowed us to obtain the $q/d$ ratio. A possible influence of the hyperfine structure on the RF-ODR signal and relative intensities has been calculated, showing that this influence can be neglected. The $q(v)$ values exhibited a decrease from $q(1)=-5.29\times10^{-3}$ cm$^{-1}$ to $q(22)=-1.71\times10^{-3}$ cm$^{-1}$, which has been explained by an increase of the difference potential between $D\,^1\Pi$ and $C\,^1\Sigma^+$ states with internuclear distance ($R$), the respective $L$-uncoupling matrix element was evaluated as 1.81. It was shown, both by semiempirical treatment and population analysis of *ab initio* molecular wave functions, that considerable $\pi d$ and $\sigma d$ configuration admixtures are present in the $D\,^1\Pi$ and the $C\,^1\Sigma^+$ states. For the $B\,^1\Pi$ state, it was demonstrated that Λ doubling is caused by two competing perturbers ($A\,^1\Sigma^+$ and $C\,^1\Sigma^+$), yielding $q$ factors of $+2\cdot10^{-6}$ cm$^{-1}$, in agreement with high resolution spectroscopy data given in the literature; single configuration approximation is valid for interacting $B\,^1\Pi(\sigma^3s_{Na},\pi^4p_K)$ – $A\,^1\Sigma^+(\sigma^3s_{Na},\sigma^4p_K)$ states. The measured $d(v)$ values, which varied from 6.6 to 4.6 D, have been used to obtain the empirical $D\,^1\Pi$ state $d(R)$ function for $R=6$–12 a.u. by means of an improved instability-free inversion procedure exploiting a special functional form. Two independent series of *ab initio* all electron calculations of $d(R)$ and $d(v)$ have been performed for the $D\,^1\Pi$ and $B\,^1\Pi$ states of NaK. First, $d$ values were computed as expectation values of the electric dipole operator with conventional multireference configuration interaction wave functions. Second, the finite field (FF) technique, combined with a multipartitioning perturbation theory (MPPT) treatment of electronic eigenstates, was applied for the calculation of $d(R)$ functions. The FF-MPPT calculations showed excellent agreement with experimental $D\,^1\Pi$ $d(v)$ values obtained in the present work, as well as the proximity to experimental $B\,^1\Pi$ $d(v)$ values given in the literature, thus showing that, as distinct from the ground state, it is important to account correctly for effective interactions of valence electrons arising from core-valence correlations, *which could not be done properly with previously used pseudopotential techniques*. The experimental $d$ and $q$ values dropping out from a smooth $v$ dependence have been considered as perturbed by $D\,^1\Pi$ – $d\,^1\Pi$ interaction and exploited to evaluate respective $d_1$ and $c_1$ values for the perturbing $d\,^1\Pi$ state. [S1050-2947(98)11309-4]

PACS number(s): 33.15.–e, 31.15.–p

## I. INTRODUCTION

Experimental determination of the permanent electric dipole moment (PEDM) in diatomic molecules is of great interest for the following reasons. First, the dipole moment gives direct information about charge distribution in the particular molecular state, as well as about the type of binding. Besides, the PEDM value enters the expressions describing the intensities of microwave transitions between the levels belonging to the same electronic molecular states. Next, the PEDM is extremely sensitive to the details of the electronic wave function (WF), hence an accurate experimental knowledge of this quantity is very useful as a test allowing us to judge to what extent the *ab initio* calculations of WF's are reliable.

Though there exists considerably rich information on experimentally measured electronic $^1\Sigma^+$ ground-state electric dipole moments of small molecules, see, e.g., [1], the situation is different for electronically excited states. Speaking about the heteronuclear alkali-metal diatomic molecules, one has to admit that even for NaK, which is the most closely studied molecule of this class, there still exist more questions than answers. The first results have been reported on NaK PEDM measurements in the $B\,^1\Pi$ [2] and $D\,^1\Pi$ [3] electronic states, while their *ab initio* pseudopotential calculations are presented in [4]. In particular, in our previous paper [3] the PEDM $d^{\rm expt}(D\,^1\Pi)$ values have been determined for two rovibronic levels $v(J)$ as 5.9–6.4 D for 7(23) and 4.5–4.8 D for 12(7). From another point, theoretical methods that would permit us to calculate, with sufficiently high accuracy, the excited state PEDM are still questionable. The ground $X\,^1\Sigma^+$ state PEDM's calculated in the vicinity of the minimum of the potential curve using the effective core potential (or pseudopotential) methods by Müller and Meyer [5] as 2.735 D, by Stevens and co-authors [4] as 2.95 D, and by Magnier and Millié [6] as 2.758 D, are in excellent agree-

 

ment with the experimental value $d^{\rm expt}(X\,^1\Sigma^+)=2.73$ D [7]. Yet, it is still not clear enough whether the above approaches allow us to obtain reliable results to describe excited state dipole moments. The authors of Ref. [2] have found large discrepancies between their measured $d^{\rm expt}(B\,^1\Pi)=(2.4-2.1)$ D values for $v$ ranging from 1 to 14, and the PEDM's calculated in Ref. [4] as (4.5–2.8) D. Calculations [4] for NaK $D\,^1\Pi$ also exhibit some tendency to exceed the above experimental $d^{\rm expt}(D\,^1\Pi)$ evaluations [3]. It is probably worth mentioning that an attempt has been made [8] to study the PEDM of NaK by the *ab initio* internally contracted configuration-interaction (CI) method using the MOLPRO package [9]. While for the *ab initio* calculated value for NaK $X\,^1\Sigma^+$ $d(R_e)=2.79$ D is quite good, the $-9$ D value obtained for the NaK $D\,^1\Pi$ state is much above the experimental value of $-5.6$ D [3]. For a definite conclusion, more experimental data are needed, in particular, those allowing us to obtain the experimental $d(R)$ dependence within a somewhat considerable $R$ range.

A peculiarity of spectroscopic investigations of $^1\Pi$ states is that such states possess Λ splitting into two $e,f$ components within each vibronic level $v(J)$. In the simplest case Λ splitting $\Delta_{ef}$ is characterized by a so-called $q$ factor [10,11]

$$\Delta_{ef}=E_e-E_f=qJ(J+1). \tag{1}$$

It is quite obvious that, especially for large $J$ values, highly accurate $q_{vJ}$ values are necessary to have a reliable set of molecular constants: without such data it is hopeless to reproduce the $^1\Pi(v,J)$ state energy. On the other hand, the $q$ values reflect directly the measure of intramolecular $^1\Pi$ $^1\Sigma$ interaction, yielding an essentially novel insight into the structure not only of an isolated $^1\Pi$ state, but of a $^1\Pi$ $\sim$ $^1\Sigma$ complex and, to some extent, of a $^1\Pi$ $\sim$ $^1\Pi$ complex as well. The existing information about Λ doubling in alkali-metal dimers is far from sufficient also for the NaK molecule, which has been the subject of intensive spectroscopic studies [2,3,12–15]. In particular, some contradictions have been revealed for the NaK $B\,^1\Pi$ state between the $q$ values measured from line positions in optical spectra [15] and from Stark effect based methods [2]. For the NaK $D\,^1\Pi$ state under study in the present paper, there is also a discrepancy between the average $q$ value of the order of $1.16\times10^{-5}$ cm$^{-1}$, as obtained from conventional spectroscopic analysis for high $J>70$ [12] and the value $1.42\times10^{-5}$ cm$^{-1}$ measured in Ref. [3] for $v(J)=7(23)$. In the case of the NaK molecule, it can be expected that the comparison between experimental and theoretical $q$ values might allow us to judge to what extent the simple single configurational $4s_{\rm K}+3p_{\rm Na}$ approximation of the $D\,^1\Pi$ state is correct.

The purpose of the present work is to elaborate the methods developed in [3] and to apply them to get more accurate experimental $d$ and $q$ values within a wide range of NaK $D\,^1\Pi$ state vibrational levels, as well as to perform high accuracy *ab initio* $d(R)$ calculations, and to check their reliability by comparison with experimentally obtained data.

The rest of this paper runs as follows. In the next section we describe briefly the basis of the method, experimental details, and the signal processing routine. Section III contains the obtained experimental data. The polynomial approximation of the $q$ factor data, as well as their semiempirical estimations, are presented in Sec. IV. Section V contains the description of the inversion procedure allowing to pass from experimentally obtained $d(v,J)$ values to $d(R)$ functions for the $D\,^1\Pi$ and $B\,^1\Pi$ states of the NaK molecule. The *ab initio* PEDM calculation is described in Sec. VI, followed by a discussion on the influence of $d\,^1\Pi\sim D\,^1\Pi$ mixing upon dipole moments and $q$ factors in Sec. VII, and concluding remarks in Sec. VIII.

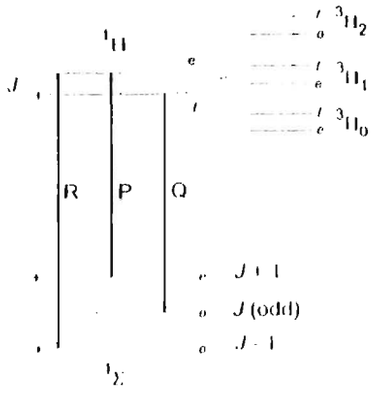


FIG. 1. Λ doubling scheme and selection rules for optical transitions.

## II. METHOD

### A. Basic considerations

The idea of the method is very simple; see Fig. 1, cf. [2,3,16–18]. Focusing on diatomics in $^1\Pi$ singlet states, one faces the necessity of distinguishing between the two Λ-doublet states of a rotating molecule. The electronic rotational WF $|\Lambda JM\epsilon\rangle$ can be expressed as a linear combination over rotational $|\Lambda JM\rangle$ parts [10,19,20]:

$$|\Lambda JM\epsilon\rangle=\frac{1}{\sqrt{2}}\left(|\Lambda\rangle|\Lambda JM\rangle+\epsilon(-1)^{J-\Lambda}|-\Lambda\rangle|-\Lambda JM\rangle\right), \tag{2}$$

$\epsilon=+1$ being the "parity index" distinguishing between the two Λ doublet states possessing total parity $+(-1)^J$ for $\epsilon=+1$ (labeled as $e$), and $-(-1)^J$ for $\epsilon=-1$ (labeled as $f$), $\Lambda=|\Lambda|$. The two Λ-doublet states are degenerate in the first order with respect to their energy. Thus, the energy splitting $\Delta_{ef}$ in Eq. (1) appears as a perturbation of a $^1\Pi$ state. Most frequently the dominating perturbation is caused by the fact that the rotationally induced $^1\Pi$ state interaction with a $^1\Sigma$ state can take place only for one of the $\epsilon=\pm1$ components. In most cases one member of a Λ-doublet pair ($e$ or $f$) has a preferred population both in optical excitation [due to the $(+1)\leftrightarrow(-)$ total parity selection rules [10,21]; see Fig. 1], as well as in chemical reactions and inelastic collisions. Owing to the same selection rule, the $^1\Pi-{}^1\Sigma$ fluorescence spectrum consists either of singlets following $Q$ excitation or of doublets following $P,R$ excitation; see Fig. 1. In the presence of a dc electric field, $e$ and $f$ levels are mixed via the Stark interaction operator $\mathbf{d}\mathcal{E}$, $\mathcal{E}$ being the dc electric field strength. This leads to the appearance of "forbidden" lines in the fluorescence spectra, in which one can now observe the whole $P,Q,R$ triplet. The intensity of the "forbidden" line ($I_f$) is "borrowed" from the "allowed" lines, and the $\mathcal{E}$

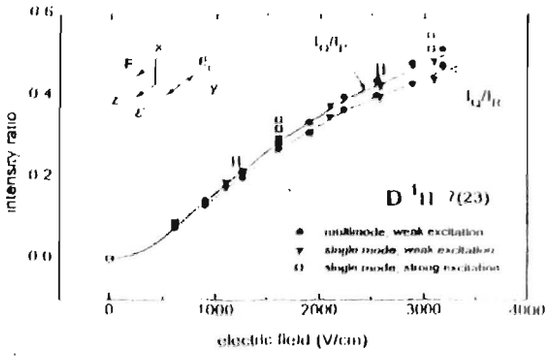


FIG. 2. Experimentally obtained $I_f/I_p$ intensity ratios for LIF progression originating from NaK $D\ ^1\Pi\ v(J)=7(23)$ level. E,E$_f$ denote exciting light and LIF electric vectors, $\mathcal{E}$ being external electric field.

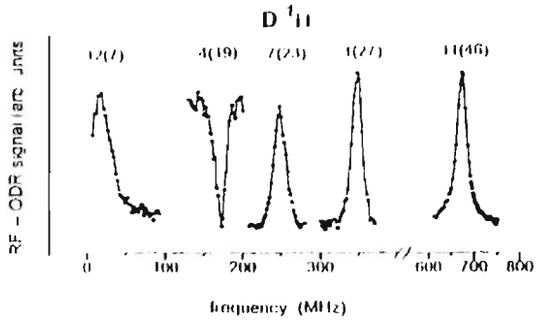


FIG. 3. Experimentally obtained RF-ODR signals for various $v(J)$ $D\ ^1\Pi$ levels.

dependence of the ratio $I_f/I_p$, see Fig. 2, $I_p$ being the "parent" line intensity, allows us, by proper fitting described in detail in Ref. [3], to obtain the ratio $\Delta_{ef}/d$.

In the case when a radio-frequency (RF) electric field is applied, in resonance with $e,f$ splitting $\Delta_{ef}$, the appearance of a "forbidden" line is also expected in the laser induced fluorescence (LIF) spectrum. This means that, if the spectral apparatus is tuned to the "forbidden" line position, one will be able to detect, against zero background, even the slightest appearance of the missing line in a situation when the scanned RF electric field frequency equals $\Delta_{ef}/h$; see Fig. 3. This permits us to measure $\Delta_{ef}$ directly and to pass to the $q$ factors; see Eq. (1). On the other hand, it is also possible to use the resonant diminution of the allowed transition intensity $I_p$ (Fig. 3) for the same purpose. Thus, by combining the electric RF–optical double resonance (RF-ODR) method [22] yielding $\Delta_{ef}$ with the dc Stark effect induced $e$ $f$ mixing yielding $\Delta_{ef}/d$, one obtains the $d$ values desired.

### B. Experimental details

The experimental setup has been described in more detail in [3], hence we dwell on it only briefly. NaK molecules have been formed in thermal cells made from special alkali-metal-resistant glass and attached to a vacuum system via a dry valve. Characteristic working temperatures of the metal containing reservoir (weight ratio Na:K≈1:3) were $T\approx 525-575$ K. A number of visible blue-green Spectra Physics 171 $Ar^+$-laser lines (see Table I) have been used to excite $D\ ^1\Pi v(J)$ $X\ ^1\Sigma^+ v''(J'')$ transitions. Visible LIF lines, originating from the ~1 mm diam laser excitation region, have been viewed at right angles to the exciting laser beam, imaged onto the entrance slit of a double-monochromator and resolved by a 1200 lines/mm grating blazed in the first order, providing an overall spectral resolution of ~0.03 nm. Polarizers were used to realize all possible linear polarization options in rectangular excitation-observation geometry. $D\ ^1\Pi v(J)$ state selection has been maintained by finding in the overall LIF spectrum the particular LIF progressions mentioned in [12] and originating from the chosen $v(J)$ level under study. The signal from a photomultiplier was recorded using the photon counting technique.

The electric field, either dc or RF, was applied to the carefully polished stainless steel Stark plates, ~0.8 cm in diameter, separated by a 1.2 mm gap. The RF field 5–900 MHz, usually possessing an amplitude of ~5 V, required to induce resonant Λ-doublet mixing, was produced either by a

TABLE I. Exciting laser wavelengths ($\lambda_{exc}$), experimentally obtained values of electric RF-ODR resonance frequencies ($f_0$), Λ-doubling factors ($q$), and PEDM values ($d$) for NaK ($D\ ^1\Pi$) $v,J$ states.

| $\lambda_{exc}$ (nm) | $v$ | $J$ | $f_0$ (MHz) | $q$ ($10^{-5}$ cm$^{-1}$) | $d$ (D) |
|---|---|---|---|---|---|
| 496.5 | 1 | 27 | 346±2 | 1.526±0.006 | 5.9±0.2 |
| 501.7 | 3 | 23 | 242±3 | 1.461±0.010 | 6.4±0.2 |
| 496.5 | 3 | 43 | 853±3 | 1.503±0.004 | |
| 496.5 | 4 | 19 | 172±2 | 1.509±0.010 | 6.6±0.2 |
| 496.5 | 7 | 8 | 30±2 | (1.389±0.070)[a] | |
| | | | | (1.437±0.070)[b] | |
| 488.0 | 7 | 20 | 172±2 | (1.365±0.010)[a] | 6.2±0.3 |
| | | | | (1.416±0.010)[b] | |
| 488.0 | 7 | 23 | 249±2 | 1.504±0.008 | 6.4±0.2 |
| 496.5 | 11 | 46 | 673±3 | 1.038±0.003 | 5.1±0.2 |
| 476.5 | 12 | 1 | 17±1.5 | 1.012±0.080 | 4.7±0.6 |
| 476.5 | 14 | 19 | 162±3 | 1.421±0.020 | 5.9±0.3 |
| 488.0 | 22 | 35 | 448±2 | 1.185±0.004 | 4.6±0.2 |

[a]For isotope $^{23}Na\ ^{41}K$.

[b]Values transformed from $^{23}Na\ ^{41}K$ to $^{23}Na\ ^{39}K$.

Wavetek RF generator (1–300 MHz), or by Mini-circuit voltage controlled oscillators (20–900 MHz), followed by a high power amplifier (Mini-circuit ZHL-2-12). The RF field frequency $f$ was swept repeatedly, with a 1–2 MHz step within the expected double resonance region by means of a computer-driven dc power supply. The typical signal storage time was 20–90 min, with overall averaging during 20–60 s for each RF value.

It was noticed that specific features could arise, under particular conditions, in the resonance region, leading in some cases to the trend to exhibit some parasitic peaks in the resonance signal. At the beginning, we were inclined to ascribe these peaks to the influence of some hyperfine structure (HFS). Careful testing convinced us, however, that these peaks were artifacts since their position and shape have been fully determined by a particular arrangement of the RF loop. The parasitic peaks disappeared after carefully matching the connecting line parameters.

### C. Signal processing

Typical examples of the experimentally observed $\mathcal{E}$ dependence of the intensity ratio $I_f/I_p$ are given in Fig. 2. The fitting (see the solid curve in Fig. 2) has been performed using an approach that involves diagonalization of the Hamiltonian, accounting for dc Stark mixing between all $J \pm \Delta J$ levels with $\Delta J \leq 2$ in the initial, excited, and final rovibronic states of a LIF transition, see Ref. [3] for details. As tested in [3], the fitting yields, with satisfying accuracy, the desired $\Delta_{ef}/d$ value, provided that the upper level relaxation rate $\Gamma$ is known at least within ~30% accuracy. At first we used $\Gamma$ values based on the NaK $D\ ^1\Pi\ v(J)=7(23)$ lifetime measured in [23] as $\tau=\Gamma^{-1}=20$ ns. However, it appeared also possible to obtain $\Gamma$ directly from the RF-ODR signal contour (see Fig. 3), yielding lifetimes within 13–23 ns for various $v(J)$ levels under study [24]. The approach [3] implies broad line excitation under conditions when ground-state optical pumping effects [25] can be neglected. To check the possible influence of the above effects, the $\mathcal{E}$ dependencies of $I_f/I_p$ ratios have been recorded at various exciting laser regimes; see Fig. 2. We have also checked that the dependences obtained at different excitation-observation geometries and polarizations of the exciting light ($\mathbf{E}$) and fluorescence light ($\mathbf{E}_f$) vectors yielded the same $\Delta_{ef}/d$ ratio.

Some of the experimental RF-ODR signals obtained are presented in Fig. 3. Resonance frequencies $f_0$ (see Table I) have been obtained from Lorentz shape contour fitting. It was proved experimentally that the $f_0$ values remain the same at different RF electric field amplitudes.

### D. Hyperfine structure

Let us now consider the possible influence on the $\mathcal{E}$ dependencies of $I_f/I_p$ and on the RF-ODR signals of the hyperfine (HF) interaction in the NaK $D\ ^1\Pi$ state. We will first focus on RF-ODR signals. It is clear that, owing to the $\Delta F=0$ selection rule [26], one has to examine the difference in the HFS patterns of $e$ and $f$ components. The origin of different HF splitting is related to the geometrical properties of the WF, since the WF with $\epsilon=+1$ ($\epsilon=-1$) in Eq. (2) is symmetric (antisymmetric) with respect to reflection in the plane of molecular rotation, the respective molecular orbitals lying in the rotational plane and at right angles to it [27]. From the well known expression for the magnetic HFS interaction operator $\langle {}^1\Pi_{ef}|\hat{\mathbf{H}}_{\mathrm{mg}}|{}^1\Pi_{ef}\rangle$ [26], the magnetic HF energy terms are the same for the $e$ and $f$ components, being dependent on $\Lambda^2$, thus having no influence on the RF resonance signal. Nevertheless, in the next approximation one has to account for the existence of the nonzero magnetic HFS operator matrix element $\langle {}^1\Sigma^+|\hat{\mathbf{H}}_{\mathrm{mg}}|{}^1\Pi_e\rangle$, which leads to a HF shift of the $e$ component only, $\Delta E_e^{mg}=c_f\mathbf{IJ}$ [26]. The estimated $c_f$ value is proportional to the ratio of the $^1\Pi$ state $q$ factor and the rotational constant $B_v$, namely $c_f \approx aq_v/B_v$, $a$ being the magnetic HFS constant

$$a=\frac{2\mu_0\mu}{I}\overline{r^{-3}}, \tag{3}$$

where $\mu$ is the nuclear magnetic moment, $\mu_0$ is the Bohr magneton, and the averaging includes only the electrons giving nonzero contribution to the electronic orbital momentum $\mathbf{L}$.

Electric quadrupole HF interaction may also cause a different energy shift for $e,f$ levels. The respective Hamiltonian $\hat{\mathbf{H}}_Q$ can be written, in standard multipole form, as $\hat{\mathbf{H}}_Q=\sum_{q=-2}^{2}(-1)^q V_q^{(2)}Q_{-q}^{(2)}$. Here the nuclear quadrupole moment $Q$ operator $Q_q^{(2)}$ acts on the nuclear coordinates only while the electric field gradient operator $V_q^{(2)}$ acts upon the electron coordinates. The electric quadrupole interaction constant $b_{\Lambda\Lambda'}$ can be written as [28]

$$\begin{aligned} b_{\Lambda\Lambda'} &= eQq_{\Lambda\Lambda'} \\ &= 2eQN(-1)^{\Lambda}\langle -\Lambda|\mu\|eC_{\mu}^{(2)}(\delta,\phi)\overline{r^{-3}}\|-\Lambda\rangle, \end{aligned} \tag{4}$$

where $C_{\mu}^{(2)}(\delta,\phi)$ is proportional to a spherical function [29], $N$ denotes the number of electrons, and the $\overline{r^{-3}}$ value is averaged over all electrons. As already pointed out in [26], the matrix elements in Eq. (4) with $\Delta\Lambda=\pm 2$ can differ from zero; see also [30]. To consider the contribution of these matrix elements to the $^1\Pi$ state HFS, one has to apply the respective quadrupole interaction operator $H_Q$, which is a second rank tensor, to our WF given by Eq. (2), thus arriving at the energy shift of the $e,f$ components:

$$\Delta E_{ef}^{Q}=\Delta E_{\pm}^{Q}=eQq_{11}X_1 \pm eQq_{1-1}X_2, \tag{5}$$

where $X_1$ and $X_2$ depend only on $J$, $I$, and $F$. Here the diagonal (longitudinal) matrix element $b_{11}=eQq_{11}$ gives the usual HF energy for symmetric top molecules [26,31], in which $K$ plays the same role as $\Lambda$ for the diatomics, while the nonzero off diagonal (transversal) matrix elements $b_{1-1}=eQq_{1-1}$ are responsible for different HF energies in $e$ and $f$ $\Lambda$ doubling components, which is specific for the $^1\Pi$ state.

It is not an easy matter to estimate the magnetic HFS constant $a$ and field gradient values $q_{\Lambda,\Lambda'}$ since these quantities include the value of $\overline{r^{-3}}$ averaged over the electrons; see Eqs. (3) and (4). For this purpose a preliminary attempt has been made to perform *ab initio* calculations [8] by the internally contracted CI method [9]. The estimated values are (in MHz) $a^{\mathrm{Na}}=4.1$, $a^{\mathrm{K}}=0.08$, $b_{11}^{\mathrm{Na}}=0.1$, $b_{11}^{\mathrm{K}}=-0.8$,

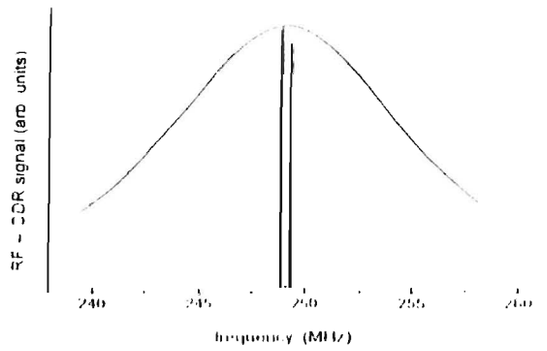


FIG. 4. Expected HF components position of RF-ODR signal for $D\ ^1\Pi$, $J=23$.

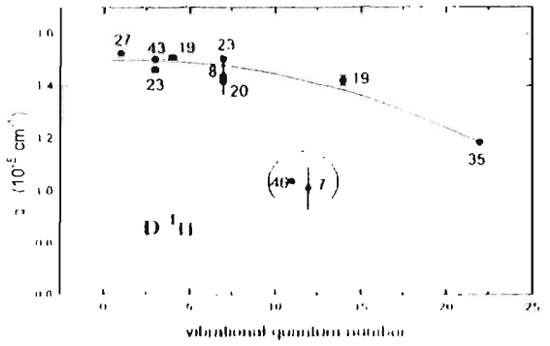


FIG. 5. NaK $D\ ^1\Pi$ state $q(v)$ values for various $J$ obtained from RF-ODR measurements.

$b_{1,1}^{Na}=-0.8$, and $b_{1,1}^{K}=+0.06$. The calculated positions of HF $e$-$f$ transitions are presented in Fig. 4. Similar and somewhat smaller HFS parameters have been obtained using the GAMESS program package [32]. It should be noted that all HFS parameters were estimated without accounting for local spin-orbit $D\ ^1\Pi$–$d\ ^3\Pi$ perturbations. As can be seen from the figure, the scale of HF splitting is ~0.5 MHz, the RF-ODR signal width being typically ~15–25 MHz; see Fig. 3. This allows us to suggest that the HFS influence on the position of the resonance signal, and, hence, on $q$ values is negligible. The same data about HFS coefficients have been used to check the possible HFS influence on the $\mathcal{E}$ dependencies of intensity ratios $I_f/I_p$. The respective HFS energy levels and transition matrix elements have been calculated by $H$-matrix diagonalization in an external dc electric field. Calculation was performed for the $v(J)=12(7)$ state, with the smallest $J$, because of the greatest expected HFS influence. The results obtained, using $\Gamma$, $q$, and $d$ values from Ref. [3], showed that relative changes in $\mathcal{E}$ dependencies of $I_Q/I_{P,R}$ did not exceed 3% for the smallest $\mathcal{E}$ ~10 V/cm value used in our experiments, falling asymptotically to zero with increasing $\mathcal{E}$. The above simulations permitted us to conclude that, if our HFS constants are not too underestimated, the inaccuracy in experimentally obtained $q$ and $\Delta_{ef}/d$ values due to HFS influence is negligible.

## III. RESULTS

The resonance frequencies $f_0$ for various $v(J)$ levels, averaged over the series of measurements, are presented in Table I. These values allowed us to determine the NaK $D\ ^1\Pi$ state $q$ factor values defined by Eq. (1); see Table I. The errors given in the table reflect the divergence of the results in various experiments. The two levels, namely 7(8) and 7(20), belong to the $^{23}Na\ ^{41}K$ isotope molecule [12], and their $q$ values have been transformed into the ones expected for $^{23}Na\ ^{39}K$ as $q^{39}\approx q^{41}(\mu^{41}/\mu^{39})^2$, where $\mu^{41}$ and $\mu^{39}$ are the respective reduced molecular masses. Since the $J$ values are not too large, we have depicted, in Fig. 5, the $q$ values from Table I as dependent on $v$, and approximated them by a parabolic function (dashed line). As is clear at first glance, all $q$ values, except for the ones for 11(46) and 12(7), do not contradict too much the quadratic $q(v)$ dependence, when the $J$ dependence is ignored. The $q$ values for 11(46) and 12(7) drop out completely from the general picture, which inclines one to think of local perturbations caused by the $D\ ^1\Pi$–$d\ ^3\Pi$ spin-orbit interaction; see Sec. VII.

The experimental $q$ values from Table I, together with $\Delta_{ef}/d$ ratios obtained as a single fitting parameter from $I_f/I_p$ $\mathcal{E}$ dependencies, permitted us to pass to electric dipole moments $d$, which are also listed in Table I. In two cases, namely for the 3(43) and 7(8) states, we found it impossible to get reliable $\Delta_{ef}/d$ ratios, and, thus, $d$ values are not presented for these states. The $d$ value errors in Table I reflect mainly the variations of $\Delta_{ef}/d$ in different experiments, as well as the inaccuracy in measuring the gap between the Stark plates. $D\ ^1\Pi$ state $d$ values are depicted in Fig. 6 as dependent on $v$. Again, $d$ values for perturbed 11(46) and 12(7) levels fall out markedly from the $d(v)$ dependence.

## IV. Λ-DOUBLING CONSTANTS

### A. $q(v,J)$ fitting

The $q(v,J)$ values measured in the present work, see Table I, have been processed together with the $q(v,J)$ data, which have been extracted by us from the traditional high resolution spectroscopy data given in [12]. The latter have been obtained from the differences between experimental rovibrational term values for $PR$ and $Q$ branches originating from the same rotational state $J$. Since the absolute accuracy of term value measurements in [12] was not better than 0.05 $cm^{-1}$, the only way to evaluate $q$ values was averaging over a group of closely situated $J$ levels with sufficiently high $J$ >60. The results are presented in Table II. The overall experimental $q(v,J)$ set from Table II was treated by the

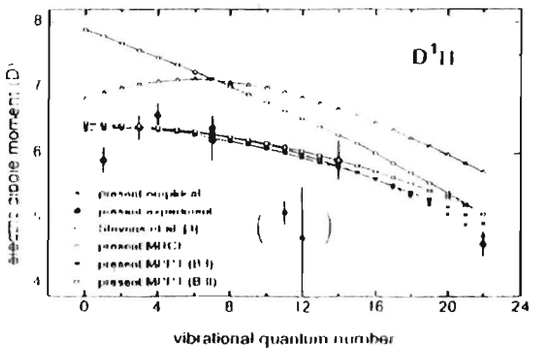


FIG. 6. $D\ ^1\Pi$ state $d(v)$ values.

TABLE II. Λ-doubling constants (in $10^{-5}$ cm$^{-1}$): $q^{\exp}$, measured in the present work or obtained by processing Ref. [12] data; $q^{\mathrm{fit}}$, obtained by fitting according to Eq. (6); and $q^{\mathrm{se}}$, obtained by semiempirical estimation with $L^{\mathrm{el}}=1.87$. The fitting parameters $q_i$ (cm$^{-1}$), see Eq. (6), are $q_e=1.570(-05)$, $q_{v1}=-5.15(-08)$, $q_{v2}=-4.665(-09)$, and $q_J=-3.069(-10)$.

| $v(J)$ | $q^{\exp}$ | $q^{\mathrm{fit}}$ | $q^{\mathrm{se}}$ |
|---|---|---|---|
| | Present data | | |
| 1(27) | 1.526(6) | 1.538 | 1.427 |
| 3(23) | 1.461(10) | 1.528 | 1.432 |
| 3(43) | 1.503(4) | 1.487 | 1.396 |
| 4(19) | 1.509(10) | 1.524 | 1.419 |
| 7(8) | 1.437(70) | 1.501 | 1.419 |
| 7(20) | 1.416(10) | 1.490 | 1.420 |
| 7(23) | 1.504(8) | 1.486 | 1.420 |
| 11(46) | 1.038(3) | 1.379 | 1.326 |
| 12(7) | 1.012(80) | 1.427 | 1.380 |
| 14(19) | 1.421(20) | 1.381 | 1.341 |
| 22(35) | 1.185(4) | 1.174 | 1.154 |
| | Data based on Ref. [12] | | |
| 1(66) | 1.51(20) | 1.425 | 1.365 |
| 1(95) | 1.20(13) | 1.281 | 1.255 |
| 5(105) | 0.98(11) | 1.184 | 1.209 |
| 6(75) | 1.39(35) | 1.340 | 1.302 |
| 10(101) | 1.15(22) | 1.145 | 1.170 |
| 17(93) | 1.15(20) | 1.063 | 1.068 |

weighted least-squares method (LSM) in the framework of the following Dunham like model:

$$q(v,J)=q_e+q_{v1}(v+1/2)+q_{v2}(v+1/2)^2+q_JJ(J+1). \tag{6}$$

The fitted $q(v,J)$ values for $D\,^1\Pi$ $v,J$ states under study are presented in Table II, along with fitting parameters $q_i$ entering Eq. (6). As may be seen, $q$ is diminishing, as $v$ and $J$ are increasing. It is worth mentioning that the authors of Ref. [12] have presented the only parameter $q_0=1.16(0.07)\times10^{-5}$ cm$^{-1}$ obtained from simultaneous fitting of all rovibrational levels of both $D\,^1\Pi$ and $X\,^1\Sigma^+$ electronic states, since the accuracy of their measurements was not sufficient for determining the $v,J$ dependence of $q$ values. At first glance, the $q_0$ value given in [12] may seem smaller than the respective value in the present work, since $q_e=1.57\times10^{-5}$ cm$^{-1}$. If, however, one takes into account that $q_0$ in [12] is related to $J$ from 60 to 106, and $v$ from 1 to 22, it is easy to arrive from Eq. (6) at $q(\bar v=11,\bar J=83)=1.24\times10^{-5}$ cm$^{-1}$, which is much closer to the $q_0$ value given in Ref. [12].

### B. Semiempirical interpretation

#### $D\,^1\Pi$ state

In order to clarify the reason for a decline in $q$ values with $v$ and $J$, we have performed $q(v,J)$ calculations within a wide $v$ and $J$ range, namely $0<v<25$ and $1<J<100$, based on the $D\,^1\Pi\sim C\,^1\Sigma^+$ interaction:

$$q_{\Pi}(v,J)\approx 2\sum_{v_\Sigma}\frac{(v_\Pi^J|L^{\mathrm{el}}(R)\hbar/(2\mu R^2)|v_\Sigma^J)^2}{E^{\Pi}_{v_\Pi J}-E^{\Sigma}_{v_\Sigma J}}\cdot|L^{\mathrm{el}}|^2S(v,J), \tag{7}$$

where

$$S(v,J)=2\sum_{v_\Sigma}\frac{|(v_\Pi^J|\hbar/2\mu R^2|v_\Sigma^J)|^2}{E^{\Pi}_{v_\Pi J}-E^{\Sigma}_{v_\Sigma J}},\qquad L^{\mathrm{el}}(R)=L^{\mathrm{el}}=\mathrm{const}, \tag{8}$$

and the vibrational WF's $|v^J\rangle=\chi_{vJ}(R)$ are eigenfunctions of the radial Schrödinger equation:

$$\left|\frac{1}{2\mu}\frac{d^2}{dR^2}+U_J(R)\right|\chi_{vJ}(R)=E_{vJ}\chi_{vJ}(R). \tag{9}$$

Here $\mu$ is the reduced molecular mass, $U_J(R)=U(R)+[J(J+1)-\Lambda^2]\hbar^2/(2\mu R^2)$ is the effective (centrifugally distorted) internuclear potential function, and $U(R)$ is the rotationless potential based on the Born-Oppenheimer (BO) separation. In the present work we used for the NaK $D\,^1\Pi$ state the BO potential calculated in Ref. [12] with high accuracy by the inverted perturbation approach (IPA) [33,34], while for the $C\,^1\Sigma^+$ state the Rydberg Klein Rees (RKR) potential has been constructed using Dunham molecular constants from Ref. [35]. To solve numerically the Schrödinger equation (9), we implemented the iterative renormalized Numerov algorithm [36], combined with the Richardson extrapolation [37]. An efficient phase matching method [38] was employed to find the eigenvalues. This construction allowed us to reduce the relative errors in $S(v,J)$ values to $10^{-5}$–$10^{-6}$.

It turned out that the $S(v,J)$ values calculated according to Eq. (8) exhibit a monotonous decrease with increasing $v$ and $J$. Further, using the $S(v,J)$ values thus obtained we transformed experimental $q(v,J)$ values into electronic $L$-uncoupling matrix elements $L^{\mathrm{el}}\approx\sqrt{q_{\exp}(v,J)/S(v,J)}$. The $L^{\mathrm{el}}$ values thus obtained appeared to be equal to 1.87, the spread not exceeding 10%. This shows that, first, the decrease of $q(v,J)$ with an increase in $v$ and $J$ is determined mainly by the increase with $R$ in potential difference $U_{D\,^1\Pi}(R)-U_{C\,^1\Sigma^+}(R)$ and, second, that the $L^{\mathrm{el}}=\mathrm{const}$ assumption holds with quite a good approximation, which is perfectly understandable, since, as can be seen from Eq. (7), the $R$ dependence of $q(v,J)$ within the narrow $R$ range is mainly determined by the $1/R^2$ factor. The semiempirical values $q^{\mathrm{se}}$ calculated according to Eqs. (7) and (8) with $L^{\mathrm{el}}=1.87$ are presented in Table II. It is interesting that the electronic matrix element of electron-rotation interaction exceeds considerably the value $l(l+1)=\sqrt{2}$. This can be expected from a pure precession approximation [10,39] under the simplest single configuration model for the perturbed $D\,^1\Pi(\sigma4s_{\mathrm{K}},\pi3p_{\mathrm{Na}})$ and the perturbing $C\,^1\Sigma^+(\sigma4s_{\mathrm{K}},\sigma3p_{\mathrm{Na}})$ electronic states. This fact can probably be explained by a considerable admixture of corresponding $\pi d$ and $\sigma d$ atomic electronic configurations in molecular electronic WF's. Indeed, assuming, for the sake of simplicity, the equal contribution of $\pi d$ and $\sigma d$ configurations to the respective $D\,^1\Pi$ and $C\,^1\Sigma^+$ states, that is, $|\pi(D\,^1\Pi)\rangle\approx C_1|\pi p\rangle+C_2|\pi d\rangle$ and $|\sigma(C\,^1\Sigma^+)\rangle\approx C_1|\sigma p\rangle+C_2|\sigma d\rangle$, where $C_1^2+C_2^2=1$, one easily arrives at

$$\langle D\,^1\Pi|\hat{\mathbf{L}}_+|C\,^1\Sigma^+\rangle \approx C_1^2\sqrt{2} + C_2^2\sqrt{6} \approx \sqrt{2} + C_2^2(\sqrt{6}-\sqrt{2}) \approx 1.87, \tag{10}$$

which allows us to conclude that the contribution of the $\pi d$ and $\sigma d$ configurations is ~44% each. Of course, it is a very gross approximation to assume the same $p\text{-}d$ mixing for $\sigma$ and $\pi$ orbitals. The difference, however, is not too large ($\lesssim$20%) at small internuclear distance where the $L$-uncoupling matrix elements are most important.

Indeed, the population analysis of multireference configuration-interaction (MRCI) wave functions, see Sec. VI for details, has shown that the $\pi d$ configuration contributes to the $D\,^1\Pi$ state from ~25% at $R=8$ a.u., up to ~40% at $R=5$ a.u., and to the $C\,^1\Sigma^+$ state from ~20% up to ~35%, respectively. Similar estimates performed for the lower $A\,^1\Sigma^+$ and the higher (4) $E\,^1\Sigma^+$ states revealed negligible $\sigma d$ contribution as compared to the one in the $C\,^1\Sigma^+$ state for the same $R$ region. Besides, the $S(v,J)$ factors in Eq. (8) calculated for $A\,^1\Sigma^+$ and (4) $E\,^1\Sigma^+$ states revealed to be 2–3 times smaller than the respective factors for the $C\,^1\Sigma^+$ state, due to energy considerations. It is obvious that the $S(v,J)$ factors for (4) $E\,^1\Sigma^+$ and $A\,^1\Sigma^+$ states possess different signs, which practically compensate their contributions to the $D\,^1\Pi$ state $\Lambda$ doubling constants.

We may thus formulate the following conclusions regarding the behavior of $q$ values for the NaK $D\,^1\Pi$ state: (i) the unique perturber $D\,^1\Pi \sim C\,^1\Sigma^+$ approximation [10] is quite valid for the $D\,^1\Pi$ state $\Lambda$ doubling due to the fact that the contributions of upper (4) $E\,^1\Sigma^+$ and lower $A\,^1\Sigma^+$ states are, first, small with respect to the $C\,^1\Sigma^+$ contribution and, second, practically compensate each other; (ii) the fact that the pure precession approximation [39] (with $l=1$ for a single $np$ configuration) does not hold, along with relatively large $q$ values, stems from the considerable contribution of $nd$ configurations to the electronic WF's of interacting $D\,^1\Pi \sim C\,^1\Sigma^+$ states at small $R$; (iii) a decrease of $q$ values with increasing $v$ and $J$ has nothing to do with the decrease in the $L$ uncoupling matrix element, but is mainly connected with the increase with $R$ in the difference potential between $D\,^1\Pi$ and $C\,^1\Sigma^+$ states.

### $B\,^1\Pi$ state

Let us now estimate, by means of Eq. (7), contributions of the $A\,^1\Sigma^+$ and $C\,^1\Sigma^+$ states to the $q_{vJ}$ values of the NaK $B\,^1\Pi$ state. It is interesting to mention that the unique perturber approximation breaks down in this case [2,15] since the lower-lying $A\,^1\Sigma^+$ state and the higher lying $C\,^1\Sigma^+$ state produce comparable contributions, with opposite signs, to the $B\,^1\Pi$ state $q$ values. This leads to a noticeable decrease in $q$ values, which are smaller by almost an order of magnitude than those of the $D\,^1\Pi$ state. Unlike the $D\,^1\Pi$ and $C\,^1\Sigma^+$ states, the single configuration approximation is valid for the interacting $B\,^1\Pi(\sigma 3s_{\mathrm{Na}}, \pi 4p_{\mathrm{K}})$ and $A\,^1\Sigma^+(\sigma 3s_{\mathrm{Na}}, \sigma 4p_{\mathrm{K}})$ states; we thus get $\langle B\,^1\Pi|\hat{\mathbf{L}}_+|A\,^1\Sigma^+\rangle = \sqrt{2}$. In order to estimate $\langle B\,^1\Pi|\hat{\mathbf{L}}_+|C\,^1\Sigma^+\rangle$, let us recall that the $C\,^1\Sigma^+$ state is built up by the $\sigma p$ molecular orbital only to the extent of 56%, which, in the simplest case, can be assumed as a primitive linear combination of atomic orbitals (LCAO), $|\sigma p\rangle = 2^{-1/2}[|\sigma 3p_{\mathrm{Na}}\rangle + |\sigma 4p_{\mathrm{K}}\rangle]$, yielding

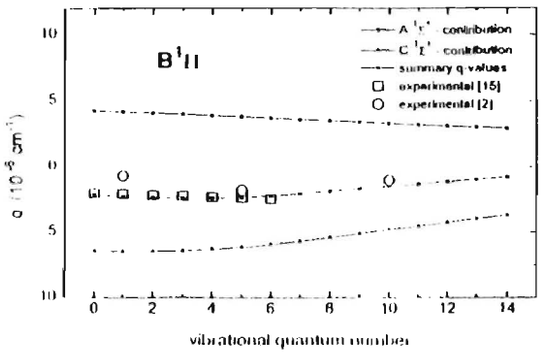


FIG. 7. $B\,^1\Pi$ state $q$ factors

$\langle B\,^1\Pi|\hat{\mathbf{L}}_+|C\,^1\Sigma^+\rangle \approx 0.75$. The $S(v,J)$ factors, see Eq. (8), were calculated using RKR potentials. The resulting $A\,^1\Sigma^+$ and $C\,^1\Sigma^+$ contributions to the $B\,^1\Pi$ state $q$ factors thus calculated are presented in Fig. 7. The total $q(v,J)$, as may be seen from the figure, are in satisfactory agreement (within 10%) with the high accuracy experimental data from Ref. [15] obtained by Doppler-free laser polarization spectroscopy. The discrepancy with $q$ values measured indirectly in [2] by the dc Stark effect can be, most likely, connected with the drawbacks of the experimental method applied. In particular, the $\Lambda$ doubling constants presented in Ref. [2] for $v=1$, 5, and 10 were obtained from the $\mathcal{E}$ dependencies of the ratio of forbidden to allowed intensities for a number of $J$ levels varying from $J=4$ up to $J=24$ for each $v$. For these levels $\Delta_{cl}$ is smaller than the natural linewidth and, hence, the $e$ / $f$ Stark mixing measurements may not be sensitive enough to the value of $q$ factor.

Since the molecular $\hat{\mathbf{L}}_+^{\mathrm{mol}}$ operator is defined with respect to the center of mass of the molecule, while the exploited atomic orbitals are centered at the nucleus of the respective atom, the present estimates of the $L_+$ matrix elements should be, in general, corrected in accordance with the coordinate origin shift effect pointed out by Colbourn and Wayne [40]. The molecular $\hat{\mathbf{L}}_+^{\mathrm{mol}}$ operator is connected with its atomic counterpart as

$$\hat{\mathbf{L}}_+^{\mathrm{mol}} = \hat{\mathbf{L}}_+^{A} - \frac{m_B R}{m_A + m_B}\hat{\mathbf{P}}_+, \tag{11}$$

where $\hat{\mathbf{L}}_+^{A}$ is the angular momentum operator with respect to the nucleus $A$, $\hat{\mathbf{P}}$ is the momentum of the electrons, and $m_A$ and $m_B$ are the atomic masses. From the well-known commutation relation $\hat{\mathbf{P}} = i(m_e/\hbar)[\hat{\mathbf{H}}^{\mathrm{el}}, \hat{\mathbf{d}}]$, where $m_e$ is the electron mass, $\hat{\mathbf{H}}^{\mathrm{el}}$ is the electronic Hamiltonian, and $\hat{\mathbf{d}}$ is the electric dipole moment operator, one gets from Eq. (11)

$$\langle n|\hat{\mathbf{L}}_+^{\mathrm{mol}} - \hat{\mathbf{L}}_+^{A}|m\rangle = \frac{m_e m_B R}{\hbar(m_A + m_B)}(E_n^{\mathrm{el}} - E_m^{\mathrm{el}})\langle n|\hat{\mathbf{d}}_+|m\rangle, \tag{12}$$

where $E_n^{\mathrm{el}} - E_m^{\mathrm{el}} = \Delta U(R)$ is the difference potential and $\langle n|\hat{\mathbf{d}}_+|m\rangle$ is the matrix element of the transition dipole moment. The application of Eq. (12) to the matrix elements $L_+$ between the states under consideration shows that, within the internuclear distance between 4 and 10 a.u., the maximum corrections for $\langle D\,^1\Pi|\hat{\mathbf{L}}_+|C\,^1\Sigma\rangle$, $\langle B\,^1\Pi|\hat{\mathbf{L}}_+|C\,^1\Sigma\rangle$, and

$\langle B\ ^1\Pi|\hat{L}_+|A\ ^1\Sigma\rangle$ matrix elements are 0.3%, 2.1%, and 15.5%, respectively. The correction values were calculated using the RKR potential curves of the interacting states and the corresponding *ab initio* transition dipole moment functions given in Ref. [41]. It is worth mentioning that the above corrections for the states under consideration appeared to be rather small as compared to those of the ground states owing to the fact that these states have a significant Rydberg character at relatively small internuclear distances.

## V. INVERSION PROCEDURE FOR DIPOLE MOMENT FUNCTION

The PEDM $d(v,J)$ for a particular vibrational-rotational level means the expectation value of the PEDM $R$ function $d(R)$, namely $d(v,J) = \langle v'|d(R)|v'\rangle$, where $d(R)$ is, in its turn, the electric dipole moment operator expectation value over the respective electronic state WF's. In order to deduce $d(R)$ from the experimentally measured $d(v,J)$, the realistic functional $d(R)$ form is of critical importance. Most conveniently, $d(R)$ can be represented as a linear superposition of some basis functions $f_i(R)$: $d(R) = \Sigma_i a_i f_i(R)$, where the coefficients $a_i$ are given by a system of linear equations:

$$d(v,J) = \sum_{i=0}^{N} a_i \langle v'|f_i(R)|v'\rangle, \tag{13}$$

which is generally overdetermined and can be solved by the standard LSM [42] routine. Usually the simplest $R$-function forms such as $R^i$, $(R - R_e)^i$ or $(R/R_e - 1)^i$ are used as basis functions $f_i(R)$, $R_e$ being the equilibrium internuclear distance for a particular electronic state. Employment of these functions leads, however, to an unphysical asymptotic behavior of $d(R)$, both at small ($R \to 0$) and large ($R \to \infty$) internuclear distances, often accompanied by noticeable $d(R)$ oscillations that increase with the power $i$. Besides, such a functional form leads to an increase in linear dependence in the equation system (13), in particular when the number of basis functions is growing, thus producing solution instability, which, in its turn, produces large errors in the determination of coefficients $a_i$. To overcome these difficulties we used the functional form, which has been successfully exploited before in the IPA method [34] only, namely

$$f_i(R) = P_i(x)\exp(-x^{2n}), \tag{14}$$

where $P_i(x)$ are Legendre polynomials of order $i$, $x$ is a smooth function of $R$, while $n$ is typically 2 or 3. It is obvious that the Gaussian part of Eq. (14) provides a smooth cutoff, avoiding any unphysical oscillations of the moment, while Legendre polynomials form an orthogonal basis set that leads to fast convergence of expansion (14) and helps to minimize the linear dependence in Eq. (13).

For the $R$ dependence of $x$ we used, following Ref. [34], the nonlinear interpolation $x = (R - R_e)(R_{max} - R_{min})/[(R_{min} + R_{max})(R_e + R) - 2R_{min}R_{max} - 2RR_e]$, where $R_{max}$ and $R_{min}$ were chosen as the outermost and innermost classical turning points of the internuclear potential, which correspond to the highest vibrational level to be fitted. For the $D\ ^1\Pi$ state it is the level $v = 22$, thus $R_{max} = 5.97$ Å and $R_{min} = 3.31$ Å, while for the $B\ ^1\Pi$ state it is the level $v = 14$, thus $R_{max} = 5.85$ Å and $R_{min} = 3.37$ Å. Such an interpolation procedure treats the inner and outer turning points with comparable weights and reduces markedly the number of necessary Legendre polynomials in Eq. (14). The $d(R)$ functions for the $D\ ^1\Pi$ and $B\ ^1\Pi$ states were approximated by Eq. (14) with the number $N$ of the basis functions varying from 3 to 5, depending on the model. The $a_i$ parameters were determined, using the weighted LSM with singular value decomposition of the plan matrix to control the linear dependence of normal equations arisen in LSM [42].

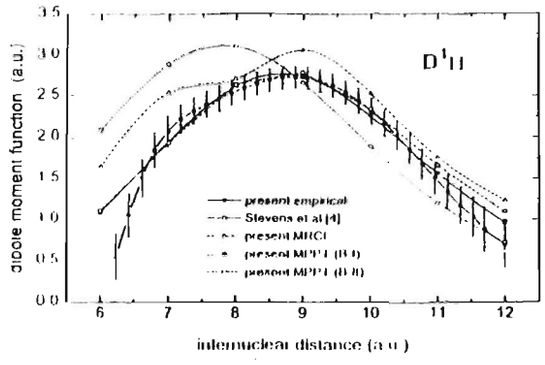


FIG. 8. $D\ ^1\Pi$ state $d(R)$ functions.

For the NaK $D\ ^1\Pi$ state the experimental $d(v,J)$ values obtained in the present work (Table I, Fig. 6) have been used as the basis data. In doing so, we have excluded $d$ values for the perturbed $v(J)$ levels 11(46) and 12(7), see Sec. VII for details. The resulting empirical function $d(R)$ is reproduced in Fig. 8 (solid circles). To prove the adequacy of the dependence thus obtained, we have exploited it to solve a direct problem, that is, to calculate $D\ ^1\Pi$ state $d$ values at $J = 1$ for $v$ ranging from 0 to 22 (small solid circles in Fig. 6).

To demonstrate the viability of the method suggested, we have determined the empirical dipole moment function $d(R)$ also for the $B\ ^1\Pi$ state of NaK using $d(v,J)$ measurements for four levels $v = 1$, 5, 10, and 14, carried out in Ref. [2] (see the solid circles in Fig. 9). The resulting $d(R)$ function is presented in Fig. 10 (small solid circles), while the corresponding PEDM's $d(v)$ are presented in Fig. 9 (small solid circles). It has to be mentioned that the determination of the $B\ ^1\Pi$ state $d(v)$ for $v = 1$, 5, and 10 from the measured $q/d$ ratios in Ref. [2] has been based upon $q_v$ evaluations that, for $v = 1$ and 5, appeared to be considerably smaller than the $q_v$ values obtained later by the authors of Ref. [15] from Doppler-free polarization spectroscopy measurements. If we

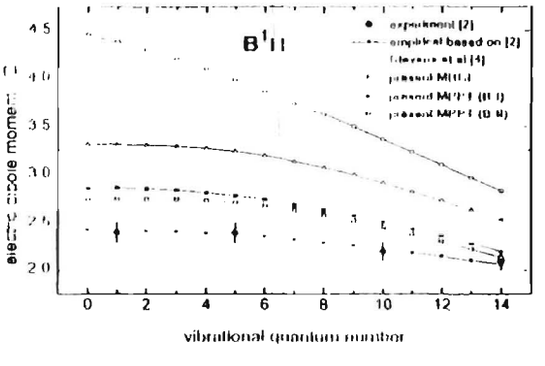


FIG. 9. $B\ ^1\Pi$ state $d(v)$ functions.

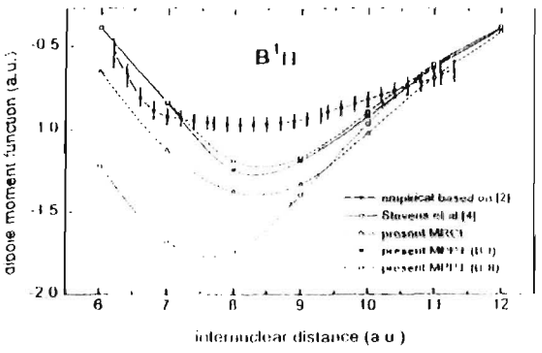


FIG. 10. $B\ ^1\Pi$ state $d(R)$ functions.

believe that the $q/d$ ratios measured in Ref. [2] from the dc Stark effect induced forbidden/allowed LIF line intensity ratios are correct, it is not excluded that the respective dipole moment values are larger than the ones presented in Ref. [2]. For instance, if one takes $q_{v''=5}=2.36\times10^{-6}$ cm$^{-1}$ [15] instead of $q_{v''=5}=1.77\times10^{-6}$ cm$^{-1}$ [2], the $d$ value with $v=5$ becomes 3.2 D instead of 2.4 D.

## VI. *AB INITIO* DIPOLE MOMENT CALCULATIONS

We have performed two independent series of *ab initio* all-electron calculations of the dipole moment functions using substantially different approximations for electronic eigenstates and different approaches to dipole moment evaluation.

### A. Expectation-value MRCI calculations

In the first series the dipole moments for the $D\ ^1\Pi$ and $B\ ^1\Pi$ states were computed as expectation values of the electric dipole operator with conventional multireference configuration interaction (MRCI) WF's. The atomic basis sets $(17s12p7d1f)/[12s9p5d1f]$Na and $(17s13p7d1f)/[11s9p5d1f]$K used in the MRCI calculations were taken from Ref. [43] and Ref. [44], respectively. Molecular orbitals (MO's) were obtained from restricted Hartree-Fock (RHF) calculations on the ground state of the $NaK^{2+}$ ion. Eight MO's corresponding to $1s2s$(Na) and $1s2s2p3s$(K) cores were frozen after the RHF step and 14 electrons including the $2p$(Na) and $3p$(K) core were correlated. The reference space was spanned by all possible arrangements of two valence electrons among five $\sigma$ and four $\pi$ active MO's. The CI space has included all the reference space configurations plus all configurations generated by single and double excitations of the reference functions. The dimension of the MRCI problem was about $3\times10^5$. All calculations mentioned above were performed using the GAMESS program package [32]. The resulting MRCI $d(R)$ functions are presented in Fig. 8 for the $D\ ^1\Pi$ state and in Fig. 10 for the $B\ ^1\Pi$ state. The respective MRCI $d(v)=\langle v|d(R)|v\rangle$ values are presented in Fig. 6 for $D\ ^1\Pi$ $v=0$–22 and in Fig. 9 for $B\ ^1\Pi$ $v=0$–14 states.

### B. Finite-field MPPT calculations

The finite-field method derives the PEDM estimates from the variation of electronic state energy $E$ under a perturbation by a small finite electric field $\mathcal{E}$ [45–47]:

$$d=\left.\frac{dE(\mathcal{E})}{d\mathcal{E}}\right|_{\mathcal{E}=0}=\frac{E(-\Delta\mathcal{E}/2)-E(\Delta\mathcal{E}/2)}{\Delta\mathcal{E}}, \tag{15}$$

where $\Delta\mathcal{E}$ is the step size of the finite difference scheme. The diagonal Hellmann-Feynman theorem ensures equivalence between the derivatives in Eq. (15) and the corresponding expectation value of the electric dipole operator for the exact electronic WF. For approximate solutions of the electronic problem appearing in practical *ab initio* calculations such equivalence usually does not hold, and the finite-field estimates are, as a rule, believed to be less sensitive to the quality of approximation [46].

The necessary $E(\mathcal{E})$ values were calculated by the state-selective multipartitioning perturbation theory (MPPT) [48], using the recently developed program [49] interfaced to the MOLCAS suite of electronic structure codes [50]. Two differently constructed Gaussian basis sets were employed. The smallest basis set $(14s10p4d1f)/[7s5p3d1f]$Na, $(15s13p4d1f)/[9s7p3d1f]$K (hereafter referred to as B-I) was obtained from the standard basis for finite-field electric property calculations [51] by decontracting the outermost $d$ functions and adding the $f$ functions with exponential parameters 0.06(Na) and 0.04(K). Basis II (B-II) comprised additional single sets of diffuse $s$, $p$, $d$, and $f$ functions on each center. Orthogonal one-particle functions were generated by solving the state-average SCF problem for two lowest states of $NaK^+$. The configuration subspace spanned by all the configurations with doubly occupied core MO's (i.e., the two-valence electron CI subspace) was considered as a model space for MPPT calculations with the basis B-I. In passing to the basis B-II we restricted the model space size to ~500 by omitting valence configurations with negligible contributions to the target WF's. Within the model space we have constructed a state-selective Hermitian effective Hamiltonian [48], which incorporated the core-valence correlation and the remaining core polarization effects at second order in MPPT. At the perturbation step the innermost core orbitals $1s$(Na) and $1s2s2p$(K) were kept frozen, i.e., 18 electrons were correlated explicitly.

The diagonalization of the effective Hamiltonian yielded the energy values of both states under study simultaneously. It should be emphasized that this "diagonalization-after-perturbation" strategy is essential for reproducing the effect of core-valence correlations on the composition of the valence part of WF's and therefore on the diffuse part of the charge-density distribution. In contradiction to the effective potential method used in [4–6], our approach takes properly into account the effective two-particle interactions of valence electrons arising from core-valence correlations. Let us finally mention that the present MPPT scheme ensures exact (for complete model spaces, basis B-I) or at least very good approximate (for restricted model spaces used with basis B-II) size consistency of the results [48]. This feature is particularly important because of the relatively large number of correlated electrons.

Let us now consider the results. The dipole moment function $d(R)$ values calculated by the finite-field MPPT with different basis sets (B-I and B-II) are presented in Table III. It may be seen that extension of the basis set from B-I to B-II almost does not affect the results in both $D\ ^1\Pi$ and $B\ ^1\Pi$

TABLE III. Finite-field MPPT results of *ab initio* dipole moment ($d$) calculations (in a.u.) for $B\ ^1\Pi$ and $D\ ^1\Pi$ states obtained with two atomic basis sets (B-I and B-II). Positive $d$ value indicates Na$^+$K$^-$ polarity.

| | $d(B\ ^1\Pi)$ | | $d(D\ ^1\Pi)$ | |
|---|---|---|---|---|
| $R$ (bohr) | B-I | B-II | B-I | B-II |
| 6.0 | −0.392 | 0.391 | 1.075 | 1.104 |
| 7.0 | −0.842 | −0.831 | 1.944 | 1.929 |
| 8.0 | −1.241 | −1.183 | 2.616 | 2.636 |
| 9.0 | −1.187 | −1.164 | 2.731 | 2.787 |
| 10.0 | 0.922 | 0.894 | 2.246 | 2.339 |
| 11.0 | 0.632 | 0.608 | 1.558 | 1.655 |
| 12.0 | −0.402 | −0.387 | 0.958 | 1.097 |

states within the $R$ range exploited. Resulting finite-field MPPT $d(v)$ functions and $d(R)$ values, along with effective potential data [4], are presented in Figs. 6 and 8 for the $D\ ^1\Pi$ state and in Figs. 9 and 10 for the $B\ ^1\Pi$ state, respectively.

Although we had no intention to study the potential curves, we found it interesting to see how the methods used here are able to reproduce the difference potential between the $D\ ^1\Pi$ and $B\ ^1\Pi$ states where the PEDM's have been calculated. The results presented in Fig. 11 show that the present MPPT calculations agree markedly better with experimental RKR values than MRCI and Ref. [4] results, thus demonstrating the correlation between the accuracy of the methods in reproducing energetic and electric properties.

## VII. THE EFFECT OF $^1\Pi$ $^3\Pi$ SPIN-ORBIT INTERACTION

As it is well known, the singlet $D\ ^1\Pi$ and the closely lying triplet $d\ ^3\Pi$ states perturb each other owing to the spin-orbit interaction. In spite of the fact that both states are in the same energy range, their interaction is of a purely local nature, since only levels with certain $v$ and $J$ exhibit considerable interaction, namely the ones with sufficiently close energies and appreciable overlap integral $\langle v_s^J(D\ ^1\Pi)|v_t^J(d\ ^1\Pi)\rangle$ values [52]. If we neglect mixing between different $d\ ^3\Pi$ state $\Omega$ components $^3\Pi_{\Omega,t}$, the spin-orbit interaction operator $\hat{\mathbf{H}}_{so}$ produces the only nonzero matrix elements $\langle D\ ^1\Pi|\hat{\mathbf{H}}_{so}|d\ ^3\Pi_1\rangle$. Then, vibronic WF's for perturbed levels will be expressed by a linear combination of unperturbed WF's $\Psi^0(d\ ^1\Pi_1)$ and $\Psi^0(D\ ^1\Pi)$ as $\Psi^{pert}(D\ ^1\Pi,d\ ^1\Pi_1)=C_s\Psi^0(D\ ^1\Pi)+C_t\Psi^0(d\ ^1\Pi_1)$, where $\Psi^0(d\ ^1\Pi_1)=\Psi^{el}(d\ ^1\Pi_1)|v_t^J\rangle$, $\Psi^0(D\ ^1\Pi)=\Psi^{el}(D\ ^1\Pi)|v_s^J\rangle$, and mixing coefficients $C_s$ and $C_t$ are normalized to unity: $C_s^2+C_t^2=1$. Vibrational WF's $|v_s^J\rangle$ and $|v_t^J\rangle$, as well as adiabatic electronic WF's $\Psi^{el}(d\ ^1\Pi_1)$ and $\Psi^{el}(D\ ^1\Pi)$, are dependent on the internuclear distance $R$. Since $L$ uncoupling and PEDM operators do not mix states with different multiplicity, the perturbed $q$ factors ($q^{pert}$) and dipole moments ($d^{pert}$) can be written as a combination $q^{pert}(v,J)=q^0_{v_sJ}+C_t^2(q^0_{v_tJ}-q^0_{v_sJ})$ and $d^{pert}(v,J)=d^0_{v_sJ}+C_t^2(d^0_{v_tJ}-d^0_{v_sJ})$, where $q^0_{v_sJ}(D\ ^1\Pi),d^0_{v_sJ}(D\ ^1\Pi)$ and $q^0_{v_tJ}(d\ ^1\Pi_1),d^0_{v_tJ}(d\ ^1\Pi_1)$ are the respective values for deperturbed singlet and triplet states.

To analyze the perturbation strength for $D\ ^1\Pi$ rovibronic states involved in $q$ and $d$ measurements, see Table I, we have calculated the mixing coefficients $C_s$ and $C_t$ using deperturbed $d\ ^1\Pi$ state molecular constants, which were determined from the level shifts experimentally measured in Ref. [52] using the nondiagonal electronic spin-orbit matrix element value $\xi_{so}^{el}=4.2\pm0.2$ cm$^{-1}$ [52]. The overlap integrals needed to evaluate the vibronic spin-orbit matrix elements entering in $H_{so}=\xi_{so}^{el}\langle v_s|v_t\rangle$ have been calculated numerically on the basis of vibrational WF's obtained from the solution of Eq. (9) with IPA [34] and RKR [52] $D\ ^1\Pi$ and $d\ ^1\Pi$ potentials, respectively. It turned out that only two levels from Table I, namely $v_s=11,J=46$ and $v_s=12,J=7$, possess, although not very large, a considerable triplet state admixture: $C_t^2(v_t=12,J_t=46)\approx0.12$ and $C_t^2(v_t=13,J_t=7)\approx0.13$. Now, since the mixing coefficients $C_t^2$ along with the singlet-state experimental $q$ and $d$ values are known, and supposing that their fitting values can be taken as the deperturbed ones, we estimated the deperturbed $d_t^0$ and $q_t^0$ values: $d^0_{v_t=12,J=46}\approx(-2.0\pm1.1)$ D, $d^0_{v_t=13,J=7}\approx(-3.1\pm1.9)$ D, $q^0_{v_t=12,J=46}\approx(-1.5\pm0.4)\times10^{-5}$ cm$^{-1}$, and $q^0_{v_t=13,J=7}\approx(-1.6\pm0.5)\times10^{-5}$ cm$^{-1}$. Taking into account large relative errors in small mixing coefficients, our $d_t^0$ and $q_t^0$ estimation is by no means an accurate one. We can, however, advocate the fact that the dipole moments of the singlet and the triplet have opposite signs. Indeed, this result is in perfect agreement with the findings of *ab initio* studies. In particular, the pseudopotential calculations [4] yielded the $d\ ^3\Pi$ dipole moment value $d_t^0=-2.3$ D for $R=8$ a.u., the latter being close to $R_e$ for this state. Besides, the all-electron MPPT (B-II) scheme described in Sec. VI yields the $d\ ^3\Pi$ state equilibrium dipole moment estimate $d_t^0=-2.2$ D. It is interesting to note that the signs of the $d\ ^3\Pi$ and $D\ ^1\Pi$ state dipole moment functions coincide for $R>9.4$ a.u. The negative sign of the $d\ ^3\Pi$ state $q$ factors (the $f$ component lies higher than the $e$ component), see Fig. 1, shows unambiguously that the $q$ values are mainly determined by interaction with the lower $c\ ^3\Sigma^+$ state. Λ doubling of the triplet $\Omega$ component $^3\Pi_1$ is caused by the interaction between $f$ components of $^3\Pi_1$ and $^3\Sigma^+$ states [14], unlike the $e$-component interaction of singlet states. Now, assuming that the interacting $d\ ^1\Pi$ and $c\ ^3\Sigma^+$ states at small $R$ can be related to the

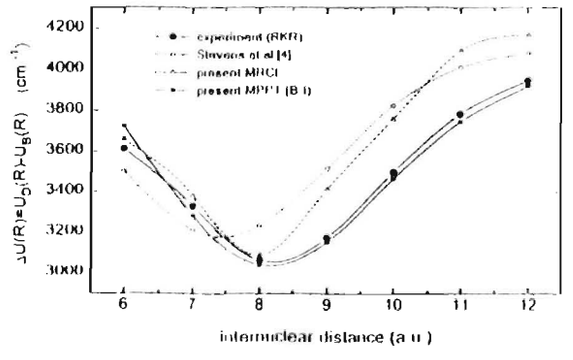


FIG. 11. Difference potential $\Delta U(R)$ between $D\ ^1\Pi$ and $B\ ^1\Pi$ states.

same $3d$-Rydberg complex [4], we arrive at the following estimate:

$$q_v^0(d\,^3\Pi_1) \approx -\frac{2J(J+1)B_v^2(d\,^3\Pi_1)}{T_e(d\,^3\Pi_1) - T_e(c\,^3\Sigma^+)} \approx -1.2\times 10^{-5}\ \text{cm}^{-1}, \tag{16}$$

where $J=2$ for the $d$ complex.

## VIII. CONCLUDING REMARKS

(i) To make definite conclusions on the behavior of $\Lambda$-doubling constants $q(v,J)$ and PEDM's $d(v,J)$ in excited states, it is necessary to perform reliable measurements in as wide as possible a $v,J$ (or, consequently, $R$) range. A combination of dc Stark and RF-ODR methods in laser induced fluorescence turned out to be adequate to achieve this aim.

(ii) The measured $\Lambda$ doubling factors $q(v,J)$ allow one to describe the specific electronic structure of a $^1\Pi$ state. In particular, it appeared to be possible to understand the principal difference between the electronic structure of the first two excited singlet $^1\Pi$ states in the NaK molecule, namely that, while the $B\,^1\Pi$ state is essentially $np$, the $D\,^1\Pi$ one contains a considerable ($\sim 44\%$) $nd$ admixture. By analyzing $^1\Pi$ - $^1\Sigma^+$ interactions, it was possible to show that $\Lambda$ doubling is caused by a single $C\,^1\Sigma^+$ perturber in the $D\,^1\Pi$ state, and by two competing perturbers ($A\,^1\Sigma^+$ and $C\,^1\Sigma^+$) in the $B\,^1\Pi$ state.

(iii) Systematic $q(v,J)$ and $d(v,J)$ measurements make it possible to single out, by means of $d$ and $q$ values dropping out from a smooth variation, the local singlet-triplet interaction and, what is more, to evaluate the respective $q_t$ and $d_t$ values for the perturbing (dark) $d\,^3\Pi$ state, which has not been studied directly.

(iv) The suggested inversion procedure allows us to determine reliable $d(R)$ functions from the measured $d(v,J)$ values.

(v) It was confirmed that, in order to obtain highly accurate calculated PEDM's for excited electronic states (as distinct from the ground states), one has, first, to account correctly for effective interactions of valence electrons arising from core-valence correlations. Apparently, this cannot be done properly by means of pseudopotential technique. Second, for the approximate WF's that do not strictly obey the Hellmann-Feynman theorem, it is preferable to use the finite-field strategy. The latter inclines one to think that it does make sense to apply an external electric field both in measurements and calculations.

## ACKNOWLEDGMENTS

This work was supported by the European Commission in the framework of PECO Human Capital and Mobility (Network) LAMBDA Programme under Contract No. ERB-CIPDCT940033, and we are especially indebted to Dr. Henrik Rudolph and Dr. Henk Dijkerman for their constant efforts in helping us to carry out the project. The Riga group participants have been supported by the Latvian Science Council (Grant No. 96.0323). Financial support of this work by the Russian Fund of Fundamental Research under Grant Nos. 96-03-32331a and 97-03-33714a is gratefully acknowledged by three of us (E.P., A.S., and A.Z.). The authors are heartily indebted to Dr. A. Shcherbinin and A. Granovskii for their help in using the GAMESS package, as well as to the investment company TERM Ltd. for granting CPU time for the MRCI calculations. A.Z. thanks Professor Björn O. Ross for supplying him with the MOLCAS 3 software. Support by the research group "Interaction of Oriented Molecules" of the Center for Interdisciplinary Research (ZiF) at the University of Bielefeld is gratefully acknowledged by one of us (M.A.). We are grateful to Dr. Klaus Stark for providing us with his unpublished results of NaK *ab initio* CI calculations using the MOLPRO program package. We are especially grateful to Janis Alnis for participation in the measurements. We are indebted to Dr. Jazep Eidus for his assistance in the preparation of the paper.

[1] K. P. Huber and G. Herzberg, *Molecular Spectra and Molecular Structure. IV. Constants of Diatomic Molecules* (Van Nostrand, New York, 1979).

[2] J. Derouard, H. Debontride, T. D. Nguyen, and N. Sadeghi, J. Chem. Phys. **90**, 5936 (1989).

[3] M. Tamanis, M. Auzinsh, I. Klincare, O. Nikolayeva, A. V. Stolyarov, and R. Ferber, J. Chem. Phys. **106**, 2195 (1997).

[4] W. J. Stevens, D. D. Konowalow, and L. B. Ratcliff, J. Chem. Phys. **80**, 1215 (1984).

[5] W. Müller and W. Meyer, J. Chem. Phys. **80**, 3311 (1984).

[6] S. Magnier and Ph. Millie, Phys. Rev. A **54**, 204 (1996).

[7] R. F. Wormsbecher, M. M. Hessel, and F. J. Lovas, J. Chem. Phys. **74**, 6983 (1981).

[8] K. Stark (unpublished).

[9] H.-J. Werner and P. J. Knowles, *User's Manual for* MOLPRO (University of Sussex, Brighton, 1995).

[10] H. Lefebvre-Brion and R. W. Field, *Perturbations in the Spectra of Diatomic Molecules* (Academic, New York, 1986).

[11] M. Mizushima, *Theory of Rotating Diatomic Molecules* (Wiley, New York, 1975).

[12] M. M. Hessel and S. Girand-Cotton (unpublished).

[13] R. E. Drullinger, M. M. Hessel, and E. W. Smith, in *Laser Spectroscopy*, edited by S. Haroche *et al.* (Springer, Berlin, 1975), p. 91.

[14] H. Katô, M. Sakano, N. Yoshie, M. Baba, and K. Ishikawa, J. Chem. Phys. **93**, 2228 (1990).

[15] M. Baba, S. Tanaka, and H. Katô, J. Chem. Phys. **89**, 7049 (1989).

[16] C. A. Moore, G. P. Davis, and R. A. Gottscho, Phys. Rev. Lett. **52**, 538 (1984).

[17] R. A. Gottscho, Phys. Rev. A **36**, 2233 (1987).

[18] J. Derouard and N. Sadeghi, Opt. Commun. **57**, 239 (1986).

[19] K. Blum, *Density Matrix Theory and Application* (Plenum, New York, 1996).

[20] R. N. Zare, *Angular Momentum* (Wiley, New York, 1988).

[21] G. Herzberg, *Molecular Spectra and Molecular Structure* (Van

Nostrand, Princeton, NJ, 1957).

[22] S. J. Silvers, T. H. Bergeman, and W. Klemperer, J. Chem. Phys. **52**, 4385 (1970).

[23] J. Pfaff, M. Stock, and D. Zevgolis, Chem. Phys. Lett. **65**, 310 (1979).

[24] M. Tamanis, M. Auzinsh, I. Klincare, O. Nikolayeva, R. Ferber, A. Zaitsevskii, E. A. Pazyuk, and A. V. Stolyarov, J. Chem. Phys. (to be published).

[25] M. Auzinsh and R. Ferber, *Optical Polarization of Molecules* (Cambridge University Press, Cambridge, 1995).

[26] C. H. Townes and A. L. Shawlow, *Microwave Spectroscopy* (McGraw-Hill, New York, 1955).

[27] M. H. Alexander, P. Andresen, R. Bacis, R. Bersohn, F. J. Comes, P. J. Dagdigian, R. N. Dixon, R. W. Field, G. W. Flynn, K.-H. Gericke, E. R. Grant, B. J. Howard, J. R. Huber, D. S. King, J. L. Kinsey, K. Kleinermanns, K. Kuchitsu, A. C. Luntz, A. J. McCaffery, B. Pouilly, H. Reisler, S. Rosenwaks, E. W. Rothe, M. Shapiro, J. P. Simons, R. Vasudev, J. R. Wiesenfeld, C. Wittig, and R. N. Zare, J. Chem. Phys. **89**, 1749 (1988).

[28] K. F. Freed, J. Chem. Phys. **45**, 4214 (1966).

[29] I. I. Sobelman, *Atomic Spectra and Radiative Transitions* (Springer, Berlin, 1992).

[30] J. Bulthuis, J. M. Milan, H. M. Jassen, and S. Stolte, J. Chem. Phys. **94**, 7181 (1991).

[31] W. Gordy and R. Cooks, *Microwave Molecular Spectra* (Interscience, New York, 1979).

[32] M. W. Schmidt, K. K. Baldrige, J. A. Boatz, J. H. Jensen, S. Koseki, M. S. Gordon, K. A. Nguyen, T. L. Windus, S. J. Su, N. Matsunaga, and S. T. Elbert, J. Comput. Chem. **14**, 1347 (1993).

[33] W. M. Kosman and J. Hinze, J. Mol. Spectrosc. **56**, 93 (1975).

[34] C. R. Vidal and H. Scheingraber, J. Mol. Spectrosc. **65**, 46 (1977).

[35] R. F. Barrow, R. M. Clements, J. Deronard, N. Sadeghi, C. Effantin, J. d'Incan, and A. J. Ross, Can. J. Phys. **65**, 1154 (1987).

[36] B. R. Johnson, J. Chem. Phys. **67**, 4086 (1977).

[37] L. F. Richardson, Philos. Trans. R. Soc. London, Ser. A **226**, 299 (1927).

[38] A. V. Abarenov and A. V. Stolyarov, J. Phys. B **23**, 2419 (1990).

[39] J. H. van Vleck, Phys. Rev. **33**, 467 (1929).

[40] E. A. Colbourn and F. D. Wayne, Mol. Phys. **37**, 1755 (1979).

[41] L. B. Ratcliff, D. D. Konowalow, and W. J. Stevens, J. Mol. Spectrosc. **110**, 242 (1985).

[42] C. Lawson and R. J. Hanson, *Solving Least Squares Problems* (Prentice-Hall, Englewood Cliffs, NJ, 1974).

[43] Y. Liu, J. Li, M. Xue, D. Chen, J. Li, and G.-H. Jeng, J. Chem. Phys. **103**, 7213 (1995).

[44] A. Yiannopoulou, T. Leininger, A. M. Lyyra, and G.-H. Jeng, Int. J. Quantum Chem. **57**, 575 (1996).

[45] J. A. Pople, J. W. McIver, and N. S. Ostlund, J. Chem. Phys. **49**, 2965 (1968).

[46] A. J. Sadlej, J. Chem. Phys. **75**, 320 (1981); G. H. F. Diercksen and A. J. Sadlej, *ibid.* **75**, 1253 (1981), and references therein.

[47] P. M. Kozlowski and E. R. Davidson, Int. J. Quantum Chem. **53**, 149 (1995).

[48] A. Zaitsevskii and J. P. Malrieu, Theor. Chim. Acta **96**, 269 (1997), and references therein.

[49] R. Cimiraglia and A. Zaitsevskii (unpublished).

[50] K. Andersson, M. R. A. Blomberg, M. P. Fülscher, G. Karlström, V. Kellö, R. Lindh, P. Å. Malmquist, J. Noga, J. Olsen, B. O. Roos, A. J. Sadlej, P. E. M. Siegbahn, M. Urban, and P. O. Wildmark, MOLCAS 3 (University of Lund, Sweden, 1995).

[51] A. J. Sadlej and M. Urban, J. Mol. Struct.: THEOCHEM **234**, 147 (1991).

[52] P. Kowalczyk, J. Mol. Spectrosc. **136**, 1 (1989).

# NaK $D^1\Pi$ electric dipole moment measurement by Stark level crossing and $e$–$f$ mixing spectroscopy

M. Tamanis, M. Auzinsh, I. Klincare, O. Nikolayeva, A. V. Stolyarov,[a] and R. Ferber
*Department of Physics, University of Latvia, Riga LV-1586, Latvia*

(Received 15 April 1996; accepted 7 November 1996)

The paper presents the first permanent electric dipole moment $d_p$ measurements for NaK $D^1\Pi$ state rovibronic levels. Two different methods were applied to obtain $d_p$ values. Stark effect induced level crossing registered as the changes of fluorescence linear polarization $P(\mathcal{E})$ with external electric field $\mathcal{E}$ yielded from one fit both the electric dipole moment value and the $\Lambda$-doubling splitting between $e$,$f$ substates of an individual rotational state. Another method consisted of obtaining the ratio $\Delta^J_{ef}/d_p$ from $\mathcal{E}$-dependence of the forbidden line appearing in fluorescence as a result of $e$–$f$ Stark mixing, along with direct $\Delta^J_{ef}$ measurement by RF – optical double resonance. The respective dipole moment values obtained are 5.9 – 6.4 D for the state $v'=7$, $J'=23$, as well as 4.5 – 4.8 D for $v'=12$, $J'=7$, the typical errors being ca. 12%–20%. The $d_p$ value for the latter state reflects $d_p$ diminution expected due to the admixture of the $d^3\Pi$ state caused by intramolecular interaction. Signal simulation and data fitting have been accomplished using direct Hamiltonian diagonalization accounting for Stark interaction within rotational states $J \pm \Delta J$, $\Delta J = 0, 1$ and 2 in the initial, excited and final state. © *1997 American Institute of Physics*. [S0021-9606(97)02106-5]

## I. INTRODUCTION

There is interest in determining the permanent electric dipole moment of a molecule since this quantity reflects very sensitively the details of electronic structure. At the same time there is still a lack of information about electric dipole moments for short-lived excited states of diatomic molecules. One of the methods to determine electric dipole moments consists of applying the electric-field-induced analog to the Hanle effect. The electric-field-caused changes in atomic fluorescence polarization were first revealed by Hanle[1] as early as in 1926, very soon after his discovery of magnetic-field-induced fluorescence depolarization, or the "Hanle effect."[2] These two phenomena are caused by Stark and Zeeman effects respectively, having their physical origin in removing the degeneracy between coherently excited magnetic sublevels $M$, being thus called "zero field electric/magnetic field level crossing," see monographs.[3–5] The application of external-field-caused level crossing methods to molecules was proposed by Zare.[6] However, as distinct from widely applied magnetic-field-induced level crossings,[1–5] the pure electric-field level crossing signals in resonance fluorescence, first applied to atoms,[7,8] for molecules have been observed in relatively few works, see Refs. 9–11. For the states with closed electronic shells, such as $A^1\Sigma$ in BaO (Ref. 11) and $B^3\Pi_{0^+_u}$ in $I_2$,[10] the monotonic "Stark–Hanle" (Stark analog of Hanle effect) curves were observed in laser-induced fluorescence (LIF). In these cases it is the second-order Stark effect[12,13] which determines the Stark splitting manifold. This follows directly from the selection rules for the electric-dipole allowed interaction, which connects only the states with different, even or odd, total parity, labelled as + or −, respectively. Hence, the first-order perturbation terms are absent in the non-degenerated perturbation approach for the Stark operator

$$\hat{H}_{St} = -\mathbf{d}_p \cdot \mathcal{E} \tag{1}$$

This means that the terms linear over electric field strength $\mathcal{E}$ equal zero for a rovibronic level with fixed rotational quantum number $J$. The appearance of linear over $\mathcal{E}$ terms is possible only in the case when the states, which are interacting due to $\hat{H}_{St}$, are so close in energy that it is impossible to use the non-degenerate perturbation theory. This is the case for quasi-degenerate electronic states with $\Lambda \neq 0$. In particular, the $^1\Pi$-state possesses two $\Lambda$-doublet components of different total parity, + or −, within a rotational state $J$, see Fig. 1(a). The total parity alternates with $J$, and another type of label, named the $e/f$ symmetry, is often used, which factors out the $(-1)^J$ $J$-dependence, thus being a rotation-independent label,[14,15] see Fig. 1(a). The $\Lambda$-doublet splitting $\Delta^J_{ef}$ caused by electron-rotation interaction, is regularly given by $\Delta^J_{ef} = q[J(J+1) - \Lambda^2]$, where $q$ is the $\Lambda$-doubling constant. This leads, as distinct from the $^1\Sigma$ state, to the "quasi-linear" Stark effect[15] in the $^1\Pi$ state (see Fig. 1(b)).

A deeper insight into the $^1\Pi$ state Stark effect, including Stark zero-field level crossing, was first given by Klemperer and co authors[9] and applied to the $(A^1\Pi)$ CS molecule. Further, in a number of works,[16–21] the main attention was paid to the changes in the $^1\Sigma \rightarrow {}^1\Pi \rightarrow {}^1\Sigma$ LIF spectra induced by dc Stark effect mixing of $e/f$ levels. Indeed, due to $\Delta J = 0, \pm 1$ and $+ \leftrightarrow -$ selection rules,[14,15] see Fig. 1(a), only the $(P,R)$-doublet emission is allowed at $P$- or $R$-type excitation, whereas only $Q$-singlet emission is allowed at $Q$-type excitation. If, however, an external electric field is applied, the $+ \leftrightarrow -$, or $e/f$ Stark effect mixing in a $^1\Pi$ state with fixed $J$ gives rise to the appearance of a "forbidden"

[a]Department of Chemistry, Moscow M. Lomonosov State University, Moscow W-234, 119899, Russia

 0021-9606/97/106(6)/2195/10/$10.00  

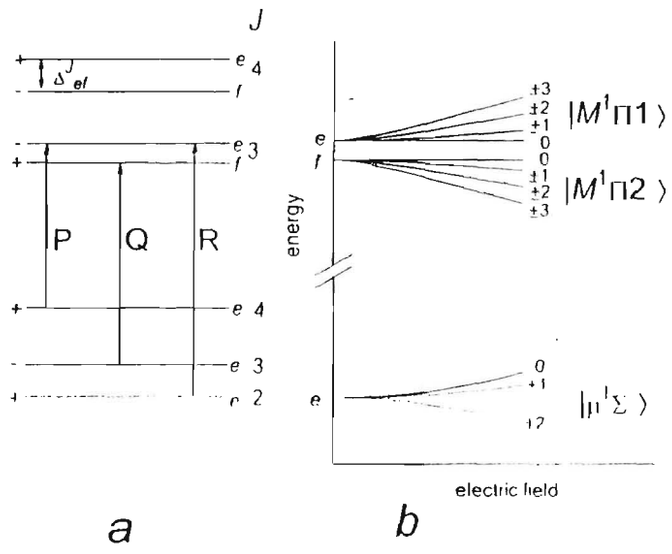


FIG. 1. Selection rules (a) and Stark effect energy shifts (b) for $^1\Sigma - {}^1\Pi$ transition. Notations for (b) refer to Eqs. (4) and (5).

line. Therefore, one can observe in the LIF progression the whole $(P,Q,R)$-triplet, instead of either doublets or singlets. The relative intensity of a forbidden line, in the case when $\Delta^J_{ef}$ is much larger than the natural width of each $\Lambda$-doubling component, is mainly governed by the $|(d_p\mathcal{E})/\Delta^J_{ef}|$ parameter, allowing one to obtain the absolute value of $d_p$, provided additional information on $q$ values can be obtained.

Concerning electronically excited alkali dimers, there have been, according to our knowledge, two attempts to determine $d_p$, both for NaK $^1\Pi$ states. Drullinger and co-workers[16] have recorded Stark induced "forbidden" lines in LIF from NaK $(D^1\Pi)$, and have also demonstrated the RF-optical double resonance signal on the $v'=7, J'=5$ level. However, they present only qualitative information without mentioning any $d_p$ values. Later, Derouard and co-workers[24] made an attempt to determine NaK $(B^1\Pi)$ dipole moments by applying Stark $e$–$f$ mixing. They present dipole moment values for several vibrational states. These are ca. two times smaller than the values obtained from *ab initio* calculations by Stevens, Konowalow and Ratcliff.[25] In this sense, the predicted[25] large permanent electric dipole moment values, reaching 4.5 D for NaK $(B^1\Pi)$ and 7.8 D for NaK $(D^1\Pi)$ have still not been proved experimentally. It seems, however, that there could be some contradictions within the results given in Ref. 24, manifested in the large discrepancy of $q$ values obtained. Thus, there is still a lack of reliable information about excited state dipole moments even for such a "test" alkali dimer as NaK. We also are not aware of such data pertaining to any other alkali dimer. It is important to mention that in Refs. 9,16–24 the description was restricted by the first-order Stark effect, without accounting for Stark mixing of different rotational states, thus the approach used in data processing has to be improved.

The main goals of the present paper are as follows. First, we intend to determine the NaK permanent electric dipole moment values in its $D^1\Pi$ state, for which there exists developed spectroscopic information,[26–32] including lifetime measurements.[33] We have applied two methods: (i) Stark-induced changes in LIF polarization; (ii) Stark induced "forbidden" line relative intensity ratio measurements in combination with the direct $\Delta^J_{ef}$ measurement by RF-optical double resonance method.[9,34,35] Secondly, we developed further the description of $^1\Pi$-state dc Stark effect, allowing one to calculate the $\mathcal{E}$ dependence of fluorescence intensity for any geometry and polarization type. We used different order perturbation theory, as well as the direct numerical diagonalization of the Hamiltonian matrix accounting for the interaction of rotational states with different $J$, both in the excited $^1\Pi$ state and in the ground $^1\Sigma$ state. At this point we have not considered the influence of hyperfine effects. In the situation under discussion, the Stark energy remains small with respect to the rotational energy, $d_p\mathcal{E} \ll BJ(J+1)$, which means that the main rotational-vibrational pattern is conserved, as distinct from the "pendular states" situation,[36] which takes place for extremely strong electric fields, destroying the rotational motion of a molecule.

The paper starts from the theoretical description of the Stark effect manifestation in $^1\Pi - {}^1\Sigma$ fluorescence (Section II). After a quick description of the experiment (Section III), the simulation of expected signals in LIF polarization is given (Section IV), followed by the presentation of experimental results (Section V) and discussion (Section VI).

## II. THEORETICAL DESCRIPTION

Let us consider the interaction of cw broad band radiation with diatomic molecules causing a $^1\Pi(v',J') - {}^1\Sigma(v'',J'')$ rovibronic transition in the presence of an external static electric field. Using the general density matrix approach,[5,37–39] one may write the density matrix element ${}^{kl}f_{MM'}$ of the excited state as

$$ {}^{kl}f_{MM'} = \frac{\Gamma_p}{\Gamma + i^{kl}\Delta\omega_{MM'}} \sum_{\mu} \langle M'^1\Pi k|\hat{\mathbf{E}}^*\hat{\mathbf{D}}|\mu^1\Sigma\rangle \times \langle M'^1\Pi l|\hat{\mathbf{E}}^*\hat{\mathbf{D}}|\mu^1\Sigma\rangle^*. \tag{2} $$

Here $\mu$ are magnetic sublevels of the ground state $^1\Sigma$ with rotational quantum number $J''$, whilst $M,M'$ are magnetic sublevels of the excited state with rotational quantum number $J'$, belonging to $\Lambda$-doublet components $k,l$. The unit vector $\hat{\mathbf{E}}$ describes the exciting light polarization, $\hat{\mathbf{D}}$ is the transition dipole moment unit vector, $\Gamma_p$ is the reduced absorption rate, $\Gamma$ is the effective excited state relaxation rate, ${}^{kl}\Delta\omega_{MM'}$ is the energy splitting between $M,M'$ sublevels, belonging either to the same $(l=k)$ or to the different $(l \neq k)$ $\Lambda$-doublet components, accounting both for $\Lambda$-doubling and Stark effect level shifts. The excited state density matrix ${}^{kl}f_{MM'}$ allows one to calculate the intensity of fluorescence $I_f(\hat{\mathbf{E}}_f)$ with polarization vector $\hat{\mathbf{E}}_f$, originating from this state in the transition $J' \to J''_1$, as

$$I_f(\hat{\mathbf{E}}_f) = I_0 \sum_{MM'\mu} \sum_{kl} \langle M'^1\Pi k|\hat{\mathbf{E}}_f^*\hat{\mathbf{D}}|\mu^1\Sigma\rangle \times \langle M'^1\Pi l|\hat{\mathbf{E}}_f^*\hat{\mathbf{D}}|\mu^1\Sigma\rangle^{*kl} f_{MM'}. \quad (3)$$

Here $I_0$ is proportionality coefficient. The structure of Eq. (3) allows one to notice that the terms entering the sums are formed as excited state matrix elements ${}^{kl}f_{MM'}$ multiplied by observation matrix elements.

The next step is to represent the molecular wave functions in Eqs. (2), (3) accounting for static external electric field effects. Since the external electric field destroys the spherical symmetry, the rotational quantum number $J$ does not remain a good quantum number any more. At the same time the external electric field does not change the axial symmetry, therefore the projection quantum number $M$ (or $\mu$) is still conserved.

The wave functions included in Eqs. (2) and (3) are obtained in a coupled-basis set as expansions over nonperturbed states with different $J_i'(i=e,f)$ and $J''$ values fixed by the static external electric field. For a $^1\Pi$ excited state we have

$$|M^1\Pi k\rangle = \sum_{J'=1}^{\infty} \sum_{i=e,f} C_{\Pi i}^k(J',M)|J'Mi\rangle, \quad (4)$$

thus obtaining, as it is usually done, a new wave function for each $k=1,2$, found as the linear combination of $e$ and $f$ substates, with mixing coefficients $C_{\Pi e}^k(J',M)$ and $C_{\Pi f}^k(J',M)$.

For the ground electronic state $^1\Sigma$, one can represent the wavefunction $|\mu^1\Sigma\rangle$, by accounting for $J''$-mixing, as

$$|\mu^1\Sigma\rangle = \sum_{J''=0}^{\infty} C_\Sigma(J'',\mu)|J''\mu\rangle. \quad (5)$$

Coefficients $C_{\Pi i}$ and $C_\Sigma$ have to be found from diagonalization of the Hamiltonian accounting for molecular rotation and the Stark effect (Eq. (1)).

It is easy to see that the respective matrix elements, both absorption and fluorescence, are proportional to the multiplication of the correspondent mixing coefficients $C_{\Pi i}^k(J',M)$, and $C_\Sigma(J'',\mu)$ or $C_\Sigma(J_1'',\mu)$. For the absorption, one obtains

$$\langle M^1\Pi k|\hat{\mathbf{E}}^*\hat{\mathbf{D}}|\mu^1\Sigma\rangle = \sum_{J'J''_i} C_{\Pi i}^k(J',M)C_\Sigma(J'',\mu) \times \langle J'Mi|\hat{\mathbf{E}}^*\hat{\mathbf{D}}|J''\mu\rangle. \quad (6)$$

And the same for the fluorescence, if one replaces $J''$ by $J_1''$ and $\hat{\mathbf{E}}$ by $\hat{\mathbf{E}}_f$. Eq. (6) allows one to apply the Wigner–Eckart theorem:[5,39–42]

$$\langle J'Mi|\hat{\mathbf{E}}''\hat{\mathbf{D}}|J''\mu\rangle = \sum_q (E^q)^* \frac{1}{\sqrt{2J'+1}} C_{J''\mu 1q}^{J'M}\langle J'i\|D\|J''\rangle. \quad (7)$$

in which, due to the selection rules propagation into the reduced matrix element,[41,42] we have

$$\langle J'ei\|D\|J''\rangle = \begin{cases} \sqrt{G(J',J'')}, & J'-J''=\pm 1 \\ 0, & J'-J''=0,\pm 2,\pm 3,\ldots \end{cases} \quad (8)$$

$$\langle J'fi\|D\|J''\rangle = \begin{cases} \sqrt{G(J',J'')}, & J'-J''=0, \\ 0, & J'-J''=\pm 1,\pm 2,\ldots \end{cases} \quad (9)$$

The $E^q$ in Eq. (7) are cyclic components of unit vector $\hat{\mathbf{E}}$ describing light polarization,[5,43] whilst $G(J',J'')$ in Eqs. (8) and (9) is the Hönl–London factor

$$G(J',J'') = (2J''+1)(C_{J''\lambda''1\lambda'-\lambda''}^{J'\lambda'})^2, \quad (10)$$

$C_{\alpha\beta b\beta}^{\gamma}$ being Clebsch–Gordan coefficients.

To determine ${}^{kl}\Delta\omega_{MM'}$, one needs Stark energy expressions $E_M^{ef}$. In the first approximation one can obtain first order Stark energies ${}^{(1)}E_M^{ef}$ in a simple analytical form (the energy of $^1\Pi$ state $f$-sublevel is considered to be zero):

$${}^{(1)}E_M^{ef} = \frac{1}{2}\Delta_{ef}^J \mp \sqrt{\frac{(\Delta_{ef}^J)^2}{4} + \frac{d_p^2\mathscr{E}^2M^2}{|J(J+1)|}} \quad (11)$$

It is easy to see that, as $\mathscr{E}$ increases, leading to $d_p\mathscr{E}M/|J(J+1)| \gg \Delta_{ef}^J/2$, Stark energy shifts have linear asymptotic behaviour with respect to $|\mathscr{E}M|$, see Fig. 1(b). A second order approximation in the ${}^{kl}\Delta\omega_{MM'}$ calculation takes place if one is accounting for the interaction between $J'$ and adjacent $J'\pm 1$ excited state levels. The Stark-effect-induced energy second order correction for a $^1\Pi$ state can be also written in analytical form, see Ref. 13. However, with $\mathscr{E}$ increasing, the second-order perturbation treatment becomes incorrect as well, and one has to solve the secular equation system[11] for the relevant Hamiltonian matrix. The analysis of such a treatment, accounting for $J\pm\Delta J$ mixing within a given vibrational state centered at the initial $(J'')$, excited $(J')$ and final $(J_1'')$ rotational state of a $J''\to J'\to J_1''$ transition, will be given in Section IV.

## III. EXPERIMENT

$^{23}Na^{39}K$ molecules were formed thermally in a glass cell joined to the vacuum system by means of a dry valve. The cylindrical head of the cell was made from a special alkali-resistant glass tube. An electric field was produced by applying a static voltage across a pair of round polished stainless steel parallel Stark plates located inside the cell. Altogether three cells were used, differing in diameter $(d)$ and spacing $(l)$ of the electrodes, namely: (1) $d=25$ mm, $l=2.9\pm0.1$ mm; (2) $d=7$ mm, $l=1.8\pm0.1$ mm; (3) $d=7$ mm, $l=1.2\pm0.1$ mm. The spacing between the electrodes was measured by means of a measuring microscope. The cells were filled with metallic potassium and sodium, via a repeated distillation process, in a weight ratio of approximately 7:3, respectively. The metal-containing reservoir was kept at stabilised temperatures between 270 °C and 320 °C. The dc voltage was kept below the threshold for electrical breakdown in the cell, which did not exceed 6 kV/cm at any of the temperatures employed.

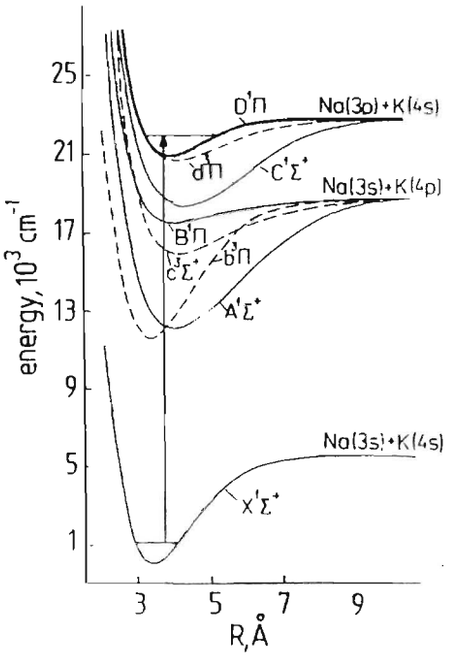


FIG. 2. Low-lying bonded terms of the NaK molecule (Ref. 25).

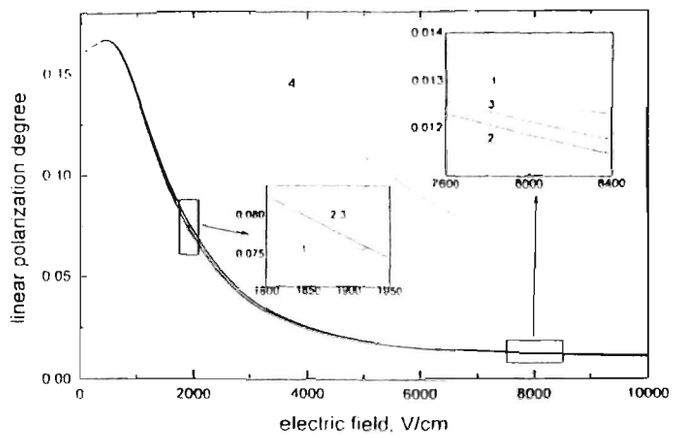


FIG. 3. Stark zero-field level-crossing signals calculated in a wide range of electric field $\mathcal{E}$ for degree of linear polarization $P(\mathcal{E}) = (I_\parallel - I_\perp)/(I_\parallel + I_\perp)$ in "traditional" Stark–Hanle effect geometry ($\hat{E} \perp \mathcal{E}$, observation along $\mathcal{E}$) at a transition $(J'' = 22) \rightarrow (J' = 23) \rightarrow (J_1'' = 22)$. 1 — first order, 2 — Hamiltonian diagonalization, $\Delta J' = \Delta J'' = \Delta J_1'' = 1$, 3 — $\Delta J' = \Delta J'' = \Delta J_1'' = 2$. The parameters characteristic for NaK($D\,^1\Pi$) state were used for simulation: $\Gamma = 5 \times 10^7$ s$^{-1}$ (Ref. 33), $B_v' = 0.0643$ cm$^{-1}$, $B_v'' = 0.0945$ cm$^{-1}$, $q = 1.2 \times 10^{-5}$ cm$^{-1}$ (Ref. 26), $d_p = 7$ D (Ref. 25). Curve 4 (dashed line) refers to pure quadratic Stark effect in a hypothetic $^1\Sigma$ excited state with the same $\Gamma$ and $d_p$ values.

The linearly polarized light from a cw $Ar^+$ laser was used to excite $X\,^1\Sigma^+ \rightarrow D\,^1\Pi$ transitions in $^{23}Na^{39}K$ molecules, see Fig. 2. Fluorescence at right angles, both to the laser beam and to the electric field $\mathcal{E}$, originating from the ca. 0.5–1.2 mm diameter laser beam excitation region, was imaged onto the entrance slit of a double monochromator with 5 Å/mm dispersion and resolved by a 1200 lines/mm grating in first diffraction order, providing an overall spectral resolution up to 0.3 Å. We restricted the observation zone to the size of ca. 1.5 mm in height, thus diminishing the possible influence of electric field inhomogeneity. The particular $D\,^1\Pi \rightarrow X\,^1\Sigma^+$ LIF progressions, originating from the definite $D\,^1\Pi$, $v'.J'$ states, were identified from the recorded LIF spectrum by comparison of line positions and relative intensities with the ones calculated by means of spectroscopic constants given by the authors of Ref. 26, for the transitions mentioned by them at excitation by 4765 Å and 4880 Å $Ar^+$-laser lines. The data from Ref. 45, considering optical depopulation of the ground $^1\Sigma^+$ state of NaK, allowed us to suppose that non-linear optical pumping effects[5,46] are negligible at the range of excitation–relaxation parameters employed. The degree of linear polarization was measured by dividing the entrance slit of the monochromator in height into two parts, placing two orthogonal polarizers in front of them. Light guides conducted fluorescence light from the two respective parts of the exit slit to the two photomultipliers, with subsequent counting of one-photon pulses from the two channels. The unpolarized LIF in the absence of an external electric field, excited by the laser light with $\hat{E}$-vector set parallel to the observation direction, was used to calibrate the channels before each experiment.

In the case of optical–electric RF double resonance experiments, we used a 1–300 MHz (0.2 W, 50 Ω) Wavetek RF oscillator supply, which was connected to the same Stark plates instead of a static electric field source. A fast oscilloscope served as a 50 Ω load and as a RF output drift monitor. The resonance was measured by sweeping the frequency of the RF generator.

## IV. SIMULATION OF EXPECTED SIGNALS

We will apply the developed theory to simulate the $^1\Pi$ state Stark signals in the intensity and linear polarization $P(\mathcal{E})$ of $D\,^1\Pi \rightarrow X\,^1\Sigma^+$ fluorescence. We use the dynamical parameters close to the ones which can be found in literature, namely, the dipole moment value $d_p = 7$ D (following theoretical prediction in Ref. 25), the lifetime $\Gamma^{-1} = 20$ ns (as determined in Ref. 33), the $q$-factor $q = 1.2 \times 10^{-5}$ cm$^{-1}$ and the rotational constant $B_v$ values given in Ref. 26. The absolute values of $d_p$ and $q$ will be assumed hereafter, since their sign does not affect the calculation results.

First, we will present zero-field level-crossing signal simulations for the "traditional" geometry ($\hat{E} \perp \mathcal{E}$, observation along $\mathcal{E}$). Figure 3 presents such calculations for the $J' = 23$ level of the $D\,^1\Pi$ state. In the $\mathcal{E}$ range demonstrated in Fig. 3, the signal is determined by the first-order effect, the difference between the first-order approximation (curve 1) and the second-order one (curve 2) being small, yet still distinguishable. Taking into account the Stark mixing between $J \pm \Delta J$ with $\Delta J > 1$ practically does not change the signal, cf. curves 2 and 3 at the insertion in Fig. 3. The monotonous behaviour of pure quadratic Stark-Hanle effect for a hypothetic $^1\Sigma$ state, supposing the same $\Gamma$, $d_p$ and $B_v'$ as for $^1\Pi$ state, is also presented in Fig. 3, see curve 4. A comparison of curves 1–3 and curve 4 demonstrates clearly the peculiarity of $^1\Pi$-state Stark effect, the latter possessing a small additional maximum, which appears mainly due to

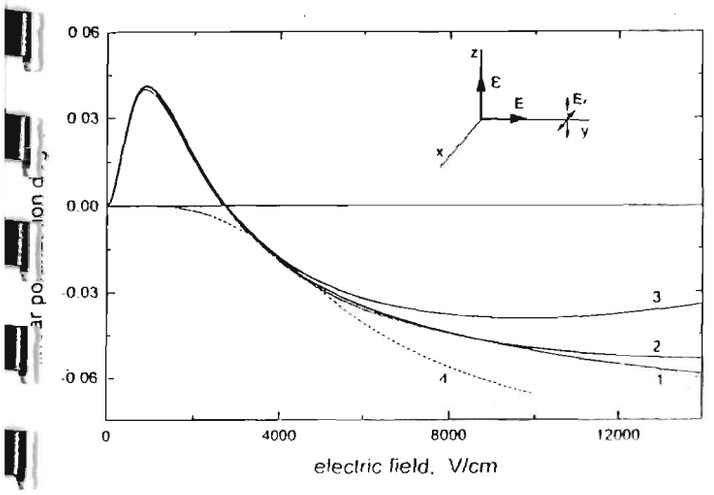


FIG. 4. Calculated $^1\Pi$ ($J'=23$) state Stark level crossing signals in degree of linear polarization $P(\mathscr{E})=(I_{\parallel}-I_{\perp})/(I_{\parallel}+I_{\perp})$ of LIF viewed from the "end" of the exciting light vector $\hat{\mathbf{E}}$ as shown in the setting-in. 1 — $\Delta J=0$ (linear approximation), 2 — $\Delta J=1$, 3 — $\Delta J=2$. Curve 4 represents calculated signal for a hypothetic $^1\Sigma$ state. Parameters are the same as in Fig. 3.

The competition between the $M$-dependent Stark induced $J$ mixing and the destruction of coherence among $M$-sublevels.

This peculiarity in $P(\mathscr{E})$ is more pronounced at another geometry, when fluorescence is observed "from the end" of $\hat{\mathbf{E}}$-vector, $\hat{\mathbf{E}}\perp\mathscr{E}$ (see Fig. 4). Both first-order ($\Delta J=0$, curve 1) and second-order ($\Delta J=1$, curve 2) approximations are sufficient to describe with adequate accuracy the polarization in the coherence destruction region. This can be seen from comparison with curve 3 obtained via Hamiltonian diagonalization accounting for Stark mixing between $J\pm\Delta J$ with $\Delta J=2$; accounting for $\Delta J>2$ practically does not affect the result. We will further exploit the geometry shown in Fig. 4, performing ($\Delta J=2$)-approximation in the calculations of Stark effect signals.

Let us now investigate the sensitivity of the signal presented in Fig. 4 to the variations of the main parameters of the $^1\Pi$ state, namely to the permanent electric dipole moment $d_p$, $\Lambda$-doubling constant $q$ and relaxation rate $\Gamma$ values. The results are presented in Figs. 5 and 6. Figure 5(a) demonstrates a polarization signal simulation at $d_p$ values taken as 3 D, 5 D and 7 D, when all other parameters remained unchanged. In Fig. 5(b), the $d_p$ and $q$ values have been varied simultaneously, whereas their ratio was maintained constant. It can be seen from comparison between Figs. 5(a) and 5(b) that the peak amplitude is uniquely determined by the $q$ value, whilst the position of the peak in $\mathscr{E}$-scale and the slope of the growing part are mainly determined by the $d_p$ value. This allows one to determine simultaneously both $d_p$ and $q$ values from one fit, provided that $\Gamma$ is known. The situation is quite different for the intensity ratios $I_Q/I_{P,R}$ of Stark induced "forbidden" line $I_Q$ to the "parent" line $I_{P,R}$, see Fig. 5(c). Indeed, the respective curves in Fig. 5(c) undergo minor changes at different $d_p$ and $q$ used in calculations presented in Figs. 5(a) and 5(b), if the $q/d_p$ ratio remains unchanged, thus only this ratio can be

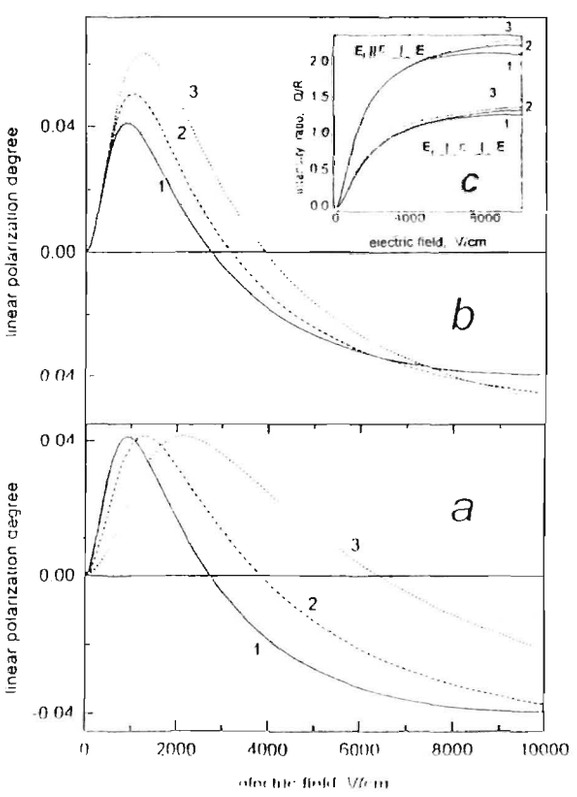


FIG. 5. (a) Simulations of Stark level crossing signals in polarization of LIF from $^1\Pi$ ($J'=23$) assuming the same $q=1.2\times10^{-5}$ cm$^{-1}$ value and different permanent electric dipole moment values: 1 — $d_p=7$ D, 2 — $d_p=5$ D, 3 — $d_p=3$ D. (b) The same signals for different $q$ and $d_p$ values in condition of the constant $q/d_p$ ratio. 1 — $q=1.2\times10^{-5}$ cm$^{-1}$, $d_p=7$ D, 2 — $q=0.857\times10^{-5}$ cm$^{-1}$, $d_p=5$ D, 3 — $q=0.514\times10^{-5}$ cm$^{-1}$, $d_p=3$ D. (c) Correspondent intensity ratios $I_Q/I_{P,R}$ calculated for the same parameters at two orthogonal fluorescence polarization directions. Calculations are performed with fixed relaxation rate $\Gamma=5\times10^7$ s$^{-1}$. Geometry and other parameters are the same as in Fig. 4.

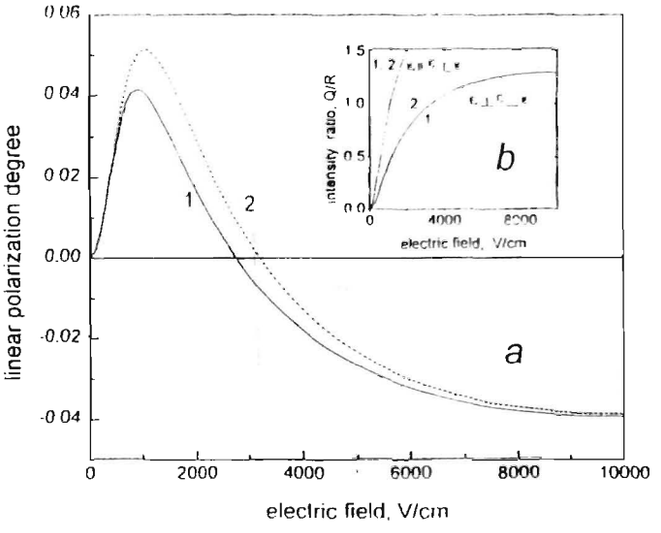


FIG. 6. Simulations of Stark level crossing signals in polarization of LIF from $^1\Pi$ ($J'=23$), and intensity ratio $I_Q/I_R$, assuming different $\Gamma$ values. 1 — $\Gamma=5\times10^7$ s$^{-1}$, 2 — $\Gamma=7\times10^7$ s$^{-1}$. Calculations are performed with $q=1.2\times10^{-5}$ cm$^{-1}$, $d_p=7$ D. (a) — LIF polarization, (b) — Intensity ratios.

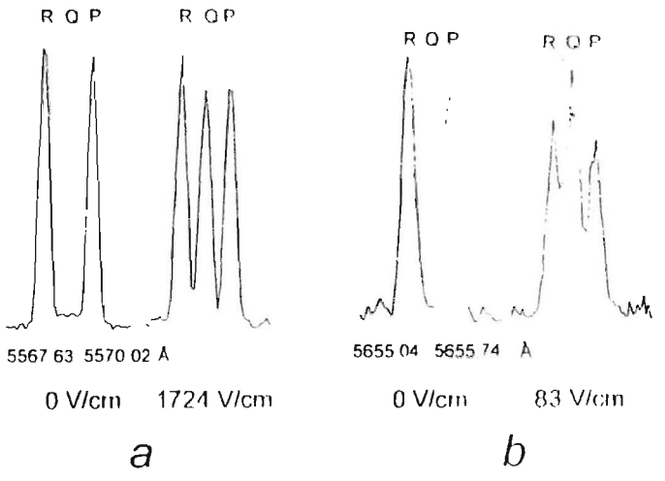


FIG. 7. Effect of electric field on spectrally resolved LIF signal for NaK $D^1\Pi \rightarrow X^1\Sigma^+$ system. (a) transition $(v''=1, J''=22) \rightarrow (v'=7, J'=23) \rightarrow (e''_f = 24, J''_f = 22$ and 24); 4880 Å excitation. (b) transition $(v''=0, J''=8) \rightarrow (v'=12, J'=7) \rightarrow (e''_f = 31, J''_f = 6$ and 8); 4765 Å excitation.

determined from the fitting. Figure 6 demonstrates the sensitivity of the signals under discussion with respect to the variation in the relaxation rate $\Gamma$. As expected, the changes of polarization signal $P(\nearrow)$ with $\Gamma$ are quite similar to respective $P(\nearrow)$ changes with $q$ (cf. Fig. 6(a) and Fig. 5(b)). In contrast, the intensity ratios are almost insensitive to $\Gamma$ variations, especially for the $\mathscr{E} \| \hat{\mathbf{E}}_f$ geometry (see curves 1 and 2 in Fig. 6(b)).

## V. MEASUREMENTS AND RESULTS

NaK $D^1\Pi$ state electric dipole moment and $\Lambda$-splitting measurements have been carried out by the following methods:

(i) by recording spectrally resolved LIF and measuring the intensity ratio between "forbidden" and allowed ("parent") lines as a function of static voltage;

(ii) by measuring the variation of the degree of linear polarization of the "parent" line with variation in the static voltage;

(iii) by measuring the electric RF – optical double resonance $\Lambda$-doublet signal from the "forbidden" line intensity dependence on RF field frequency.

### A. Intensity ratios

Figure 7 demonstrates the effect of static electric field on the spectrally resolved LIF leading to the appearance of forbidden $Q$ line due to $e$–$f$ mixing. Since the effect is mainly governed by the $\mathscr{E} d_p / \Delta^J_{ef}$ ratio, one needs a larger electric field strength to observe the $Q$-lines originating from $v'=7, J'=23$ than from the $v'=12, J'=7$ state. The $(P,Q,R)$-triplet component separation for the latter case, being ca. 0.3 Å, is on the edge of the spectral resolution of the monochromator used.

A fitting procedure employing three Gaussians was used to obtain "forbidden"/"parent" line ratio $I_Q/I_{P,R}$. The intensity ratios $I_Q/I_{P,R}$, obtained in different cells (see Section III) and experimental geometries, are shown as insets in Figs

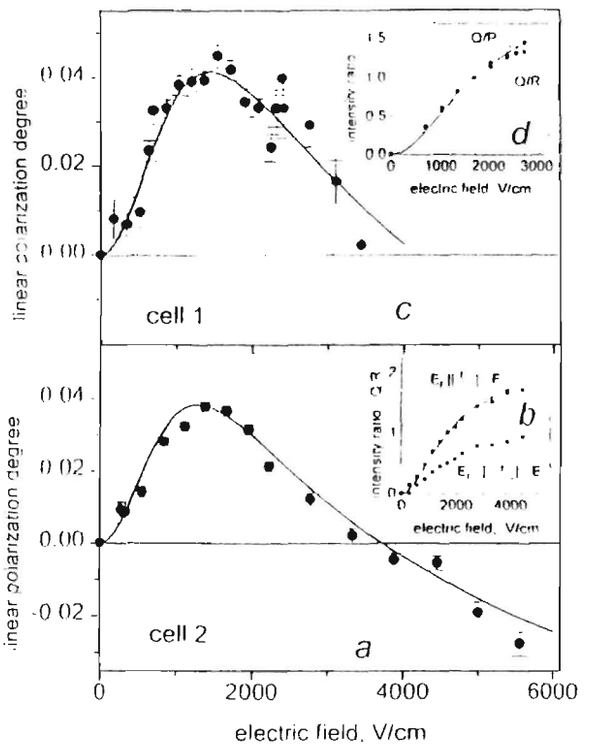


FIG. 8. Linear polarization degree and intensity ratios measured in LIF from NaK $(D^1\Pi)$ state with $v'=7, J'=23$. (a), (c) — electric field dependence of the polarization degree obtained on $R(22)$ component. (b), (d) — electric field dependence of intensity ratios $I_Q/I_P$ or $I_Q/I_R$. Results are obtained in different cells at geometry depicted in Fig. 4, dots are the measured values, the lines refer to the calculations at fitted parameters.

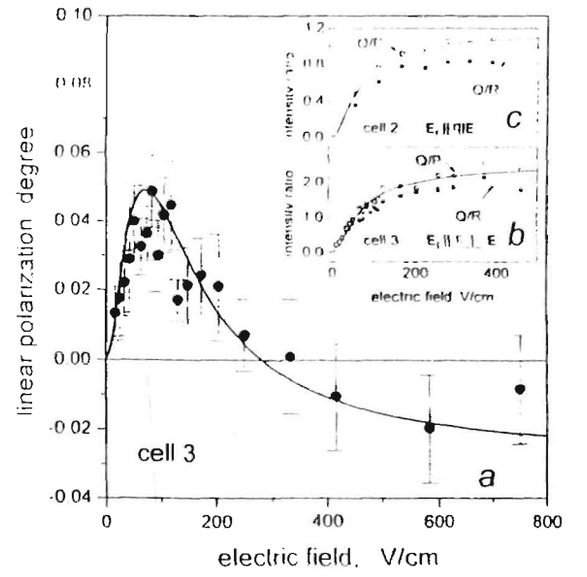


FIG. 9. Linear polarization degree and intensity ratios measured in LIF from NaK $(D^1\Pi)$, $v'=12, J'=7$. (a) — electric field dependence of polarization degree obtained on $P(8)$ component. (b), (c) — electric field dependence of intensity ratios $I_Q/I_P$ and $I_Q/I_R$. Data for (a), (b) are obtained at geometry depicted in Fig. 4, whereas for (c) we used $\hat{\mathbf{E}} \| \nearrow$. Dots are the measured values, full lines refer to the calculations with fitted parameters.

TABLE I. Experimental values of permanent electric dipole moment $d_p$ and $\Lambda$ – doubling constant $q$ for NaK $(D^1\Pi, v', J')$. Values $d_p^{th}$ are *ab initio* calculations (Ref. 25) averaged for a particular $v'$.

| $v'$ | $J'$ | $q$, $10^{-5}$ cm$^{-1}$ | $d_p$, Debye | $d_p^{th}$ Debye |
|---|---|---|---|---|
| 7 | 23 | $1.65\pm0.20$[a] | $6.4\pm0.8$[a] | 7.1 |
| | | $1.42\pm0.07$[b] | $5.9\pm0.9$[c] | |
| 12 | 7 | $1.10\pm0.20$[a] | $4.5\pm0.8$[a] | 6.5 |
| | | $1.03\pm0.08$[b] | $4.8\pm0.9$[c] | |

[a]Values determined from two parameter fitting of LIF polarization $\mathcal{E}$-dependencies.
[b]Values determined directly from RF optical double resonance.
[c]Values determined using $q/d_p$ obtained from the $\mathcal{E}$-dependence of $I_Q/I_{P,R}$ and $q$ obtained from RF optical double resonance.

8 and 9. Least-square data processing yielded $q/d_p$ ratios. The averaged values are $(2.40\pm0.25)\times10^{-6}$ cm$^{-1}/D$ for $v'=7, J'=23$ and $(2.10\pm0.20)\times10^{-6}$ cm$^{-1}/D$ for $v'=12, J'=7$ state. The $q/d_p$ systematic errors are most likely attributable to uncertainties in Stark plate separation. For instance, the curves in Figs. 9(b), 9(c) demonstrate the $\mathcal{E}$-dependences of $I_Q/I_P$ and $I_Q/I_R$, which are registered for two different cells and different exciting light vector directions, $\hat{\mathbf{E}}\|\mathcal{E}$ or $\hat{\mathbf{E}}\|\mathcal{E}$, with fluorescence light vector $\hat{\mathbf{E}}_f\|\mathcal{E}$ in both cases. The one-parameter ($q/d_p$) least-square routine yields the following constant ratios: $q/d_p=1.9\times10^{-6}$ cm$^{-1}/D$ for Fig. 9(b) and $q/d_p=2.3\times10^{-6}$cm$^{-1}/D$ for Fig. 9(c), the discrepancy reflecting both statistical and systematic errors.

## B. Polarization measurements

### 1. Results for the $D^1\Pi(v'=7, J'=23)$ state

Experimentally measured electric field dependencies of the polarization degree are presented in Fig. 8. The results are obtained in two different cells (see Section III), using the most favourable geometry when LIF is viewed from the "end" of exciting light vector $\hat{\mathbf{E}}\|\mathcal{E}$, as depicted in Fig. 4. The data fitting was realized by accounting for Stark interaction among five rotational states $J, J\pm1, J\pm2$ for all $J'', J'$ and $J_1''$ involved in the transition. The best-fit constants $q$ and $d_p$, obtained from a two-parameter weighted least-square routine, yield the values in question. Cell 1 yields $q=1.6\times10^{-5}$ cm$^{-1}$ and $d_p=6.3$ D, whilst cell 2 yields $q=1.7\times10^{-5}$ cm$^{-1}$ and $d_p=6.5$ D. Cell 2 allowed us to achieve higher electric field intensities (up to 5.6 kV/cm) owing to the special working of Stark plates surface and edges in order to avoid sparking; the conditions were more favourable also because of lower cell temperatures (ca. 270 °C). On the other hand, the results for cell 2 may have a larger systematic error because of smaller plate separation. Evaluation of the possible contribution of both statistical and systematic errors for different cells enabled us to take $d_p=(6.4\pm0.8)$ D and $q=(1.65\pm0.2)\times10^{-5}$ cm$^{-1}$ as the averaged permanent electric dipole moment and $q$-factor values, see Table I. As it follows from the simulations presented in Figs. 5 and 6, the $\Lambda$-doubling constant $q$ obtained from the fit seems to be more subject to the systematic error in absolute polarization values, which can arise, say, from even slight inaccuracies in the calibration of channels and in accounting for background signal, as well as any possible uncertainty in the relaxation constant $\Gamma$ value.

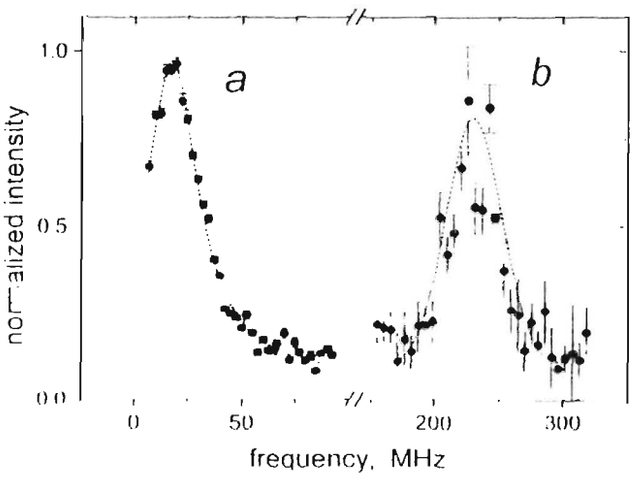


FIG. 10. RF-optical double resonance signals. (a) For NaK $D^1\Pi$ $v'=12, J'=7$ state. (b) For NaK $D^1\Pi$ $v'=7, J'=23$ state.

### 2. Results for the $D^1\Pi(v'=12, J'=7)$ state

Measurements for this state were much more complicated because of the small spectral separation between the triplet components (see Fig. 7(b)), requiring narrow spectrometer slits to maintain necessary resolution. This leads to considerably larger errors, both statistical and systematic, in polarization measurements (see Fig. 9(a)). The most favourable conditions were achieved using cell 3 (see Section III). $P(\mathcal{E})$ was registered in $P$-transitions $(J'=7)\rightarrow(J_1''=8)$ because of better spectral separation. In spite of wide statistical scatter in the results, we have accomplished direct least-square two-parameter fitting, which yielded the values $d_p=4.5\pm0.8$ D and $q=(1.1\pm0.2)\times10^{-5}$ cm$^{-1}$, see Table I. The large inaccuracy in the $q$ value accounts for the uncertainty in relaxation rate $\Gamma$ for this state. We supposed $\Gamma$ to be $5\times10^7$ s$^{-1}$, that is the same as for the $v'=7, J'=23$ state.[31]

## C. Electric RF – optical double resonance

Since the routine based on both $d_p$ and $\Delta_{ef}^J$ variation in the fitting of the measured $P(\mathcal{E})$ signal is very sensitive to inaccuracies in absolute $P(\mathcal{E})$ measurements, as well as to $\Gamma$ values (see Figs. 5 and 6), it seemed important to exploit a method allowing direct $\Delta_{ef}^J$ measurement in some independent experiment. For this purpose we have employed the electric RF – optical double resonance method. In order to increase the RF field amplitude $\mathcal{E}_{RF}^0$, the measurements were carried out at a Stark-plate separation of $0.85\pm0.05$ mm. The RF field voltage enabled us to produce $\mathcal{E}_{RF}^0\leq20$ V/cm. In order to diminish LIF intensity drift during signal accumulation the normalised difference $(I_F-I_{F_0})/I_{F_0}$ was considered to be a result of a single measurement, that is the difference

between intensity at current frequency $F$ and at some reference frequency $F_0$. The signal accumulation time varied from 10 minutes to 1 hour.

### 1. Results for the $D^1\Pi_u, v'=7, J'=23$ state

Figure 10(b) (dots) presents experimental data obtained by registering the intensity of a "forbidden" $Q$-line as dependent on the RF electric field frequency, demonstrating resonance intensity increase, with a maximum near 230 MHz. Although the resonance signal width exceeded the one expected from the natural broadening, probably possessing some structure, we assumed that the signal is reliable enough to determine the $e/f$ separation $\Delta^J_{ef}$, yielding $q=(1.42\pm0.07)\times10^{-5}$ cm$^{-1}$ as an averaged value. This makes it possible to determine the permanent electric dipole moment $d_p$ in question, using $q/d_p$ values presented in Section VA, as $d_p=5.9\pm0.9$ D.

### 2. Results for the $D^1\Pi_u, v'=12, J'=7$ state

Figure 10(a) presents the experimental data (dots) demonstrating the RF field frequency dependence of the "forbidden" $Q$-line intensity in $(J''=8)\rightarrow(J'=7)\rightarrow(J''_1=7)$ transition. The average of $q$ over a number of experiments is $q=(1.03\pm0.08)\times10^{-5}$ cm$^{-1}$. Taken together with $q/d_p$ obtained from intensity ratios, see Section VA, the dipole moment value is $d_p=(4.8\pm0.9)$ D, where the estimated relative error consists of 10% assigned to $q/d$ fitting and 8% assigned to $\Delta^J_{ef}$ uncertainty.

## VI. DISCUSSION AND CONCLUSIONS

### A. Method

Investigation of permanent electric dipole moments is not an easy matter for short-lived excited molecular states with large rotational numbers ($J\gg1$). Let us compare the two more or less independent methods exploited in the present work. Both methods are based on analyzing Stark effect induced changes in fluorescence, which are caused predominately by $e-f$ mixing within the same rotational state, which, in turn, is governed mainly by dipole moments ($d_p$), $\Lambda$-splittings ($\Delta^J_{ef}$ or $q$-factors) and relaxation rates ($\Gamma$).

(i) *$\mathcal{E}$-dependence of linear polarization degree $P(\mathcal{E})$.* In the most favourable experimental geometry the $P(\mathcal{E})$ signal is characteristic enough to obtain both $q$ and $d_p$ from the fitting. This demands high accuracy in measuring $P(\mathcal{E})$ and precise knowledge of the relaxation rate $\Gamma$.

(ii) *RF – optical double resonance along with $\mathcal{E}$-dependence of intensity ratios* of "forbidden" – to – "parents" lines in LIF triplet exhibit an alternative method. In this case the RF resonance yields directly the $\Lambda$ doubling splitting $\Delta^J_{ef}$ whilst the processing of relative intensity data yields $\Delta^J_{ef}/d_p$, the latter procedure being weakly dependent on $\Gamma$. Thus, the accuracy of $d_p$ values in question, obtained by this method is only slightly affected by the accuracy of relaxation rate $\Gamma$. A crude estimate of $\Gamma$ gained from the width of the RF–optical double resonance may even work to obtain reliable $d_p$ values without any previous knowledge of molecular lifetime.

The developed theoretical description (Section II) and simulations of expected signals (Section IV) allowed us to conclude that, even though the main Stark features arise from the 1st order effect, in order to avoid possible inaccuracies in the case when the Stark energy is not too small in comparison with rotational splitting (i.e., in case of not too small $d_p\mathcal{E}/(B'_vJ')$), it is necessary, for both methods (i) and (ii), to consider Stark interaction with no less than four neighbouring rotational levels, both in excited and ground (initial and final) states.

*Dipole moments and $\Lambda$-splittings.* The dipole moments determined seem to be reliable, in particular since there is good agreement between the results gained from two independent methods. As for the absolute $d_p$ values, they can be considered as very large when compared to typical dipole moment values which had been measured for diatomic molecules.[13,47] Let us compare the measured $d_p$ values with theoretical quantities given by Stevens, Konowalow and Ratcliff.[25] In order to pass from *ab initio* $d^{th}_p(R)$ dependence presented in Ref. 25 to the predicted $d_p$ values for particular $v',J'$ states, we have used the averaging routine based on either *ab initio* potentials,[25] or RKR potentials[26] for the NaK $D^1\Pi$ state. The results differ by no more than 1%, yielding the following predicted $d^{th}_p(v',J')$ values for the states under study: $d^{th}_p(7,23)=7.1$ D and $d^{th}_p(12,7)=6.5$ D, see Table I.

As follows from Table I, the measured $d_p$ value for the $v'=12, J'=7$ state is smaller than for the $v'=7, J'=23$, being also markedly smaller than the theoretically predicted value. As is well known,[2,31,32] levels belonging to the NaK $D^1\Pi$ state are perturbed, at least to some extent, by the close lying $d^3\Pi$ state. Basing on Ref. 26, the level $v'=7, J'=23$ can be considered as almost unperturbed, whereas the level $v'=12, J'=7$ is shifted to $\Delta E=0.468$ cm$^{-1}$ with respect to the deperturbed position. Using the calculated difference of deperturbed $D^1\Pi$ ($v'=12$) and $d^3\Pi$ ($v'=13$) terms[31] with $J'=7$, being $E_{^1\Pi}-E_{^3\Pi}=3.87$cm$^{-1}$, one can get the estimation for the squared state mixing coefficient $C^2_{^3\Pi}=\Delta E/(E_{^1\Pi}-E_{^3\Pi})\approx0.13$. This creates a reduction in pure singlet character of the state to $C^2_{^1\Pi}=1-C^2_{^3\Pi}\approx0.87$ and allows one to estimate the relative change in the $D^1\Pi$ ($v'=12, J'=7$) state electric dipole moment, which arises due to singlet–triplet coupling, as $C^2_{^1\Pi}+C^2_{^3\Pi}(d^{^3\Pi}_p/d^{^1\Pi}_p)$, $d^{^3\Pi}_p$ and $d^{^1\Pi}_p$ being unperturbed dipole moments. The averaging of the *ab initio* calculations[25] for the $d^3\Pi, v'=13$ state yields $d^{^3\Pi}_p\approx-0.7$ D, which is opposite in sign from $d^{^1\Pi}_p$. As a result, the experimentally measured $d_p$ value for ($D^1\Pi$, $v'=12, J'=7$) is expected to be ca. 15% smaller than would be anticipated for the unperturbed state. It is thus not excluded that the difference between $d_p$ values obtained for the two states, see Table I, reflects the role of perturbations.

Indeed, the relative difference between the measured $d_p$ values for $v'=7, J'=23$ and $v'=12, J'=7$ is ca. 20% – 25%, which does not contradict the above estimation. Hence, the experimentally measured $d_p$ values do not disprove the *ab initio* calculation in Ref. 25, accounting for the fact that the deperturbed quantities have been calculated.

Regarding the $\Lambda$-doubling factor $q$, it can be noted that its tendency to be smaller for $v'=12, J'=7$ level, corresponds to what can be expected due to the perturbation, allowing one to estimate a ca. 13% diminution from the following considerations. Although the singlet–triplet $D^1\Pi - d^3\Pi$ interaction does not change the $\Lambda$-doubling splitting directly since $e$ and $f$ components of the $D^1\Pi$ state are perturbed by the two $\Lambda$-doublet substates of the $d^3\Pi$ state to about the same amount, this singlet–triplet interaction diminishes the singlet character of the perturbed state as $C^2_{^1\Pi}$. Hence, the matrix element of electronic–rotational interaction with the remote singlet $\Sigma$ states, giving rise to $\Lambda$-doubling in the $D^1\Pi$ state, has to be $C_{^1\Pi}\langle D^1\Pi|L^+|^1\Sigma\rangle$, since the matrix elements between the states having a different multiplicity vanish. The $q$ value for NaK ($D^1\Pi$) presented in Ref. 26 has been obtained from conventional spectroscopic analysis as $q_e = q_0 - q_1(v+1/2) = 1.16\times10^{-5} - 1.5\times10^{-7}(v+1/2)$ cm$^{-1}$. The RF – optical double resonance signal for NaK ($D^1\Pi, v'=7, J'=5$) can be found in Ref. 16, yielding $q = 1.5\times10^{-5}$ cm$^{-1}$. Thus, the $q$-factor values presented in Table I do not disagree much with the previous data. The $\Lambda$-doubling constant for $D^1\Pi$ state can be estimated from the well-known relation: $q \approx 4B_e^2/\nu(\Pi,\Sigma)$, where $\nu(\Pi,\Sigma)$ is the difference between the electronic term values $T_\Pi - T_\Sigma$. Then, assuming that $D^1\Pi$ state $\Lambda$-doubling arises from the interaction with low-lying $C^1\Sigma$ and $A^1\Sigma$ states, one gets $q \approx 1.2\times10^{-5}$ cm$^{-1}$.

As mentioned above, the experimental data on excited-state electric dipole moments of any alkali diatomic are extremely scanty. The authors of Ref. 24 present $d_p$ values varying from 2.4 to 2.1 D for the NaK $B^1\Pi$ state with $v'$ equaling 1, 5, 10 and 14. The $d_p$ values are smaller than the ones predicted from *ab initio* calculations by Stevens and co-authors,[25] which, according to averaging as mentioned above, range from $d_p^{th} = 4.5$ D for $v'=1$ to $d_p^{th} = 2.8$ D for $v'=14$. It can be noted however that there are some contradictions in $q$-factors determined in the measurements,[24] presenting, for instance, the absolute values $q = 0.65\times10^{-6}$ cm$^{-1}$ for $v'=1$ and $q = 1.77\times10^{-6}$ cm$^{-1}$ for $v'=5$. These quantities disagree with the respective values $q = 2.08\times10^{-6}$ cm$^{-1}$ and $q = 2.36\times10^{-6}$ cm$^{-1}$ obtained for corresponding $v'$ by Baba, Tanaka and Kato[18] using Doppler free polarization spectroscopy. In order to obtain the same $q/d_p$ ratio as presented in Ref. 24 with $q$ values from Ref. 18 instead of the ones given in Ref. 24, the $d_p$ for $v'=5$ should be increased from 2.4 D to 3.2 D, the latter being not far from the averaged calculated value $d_p^{th}(v'=5) = 3.9$ D.[25] The results given in Ref. 24 for the $v'=1$ level of NaK $B^1\Pi$ seem strange since it is hard to imagine so dramatic a change in $q$ (being 3 times smaller than for $v'=5$), whilst dipole moments remain unchanged, see Table III in Ref. 24.

In conclusion, the measurements constituted in the present work confirm the existence of a large permanent electric dipole moment in the NaK $D^1\Pi$ state. It is of importance to strive to refine the experimental $d_p$ values. Besides increasing the accuracy of measurements and extending the number of vibrational states involved in the investigation, there is reason to believe that further progress is connected with accounting for intramolecular perturbation, the most important of which might involve the simultaneous effects of hyperfine structure and $d^3\Pi - D^1\Pi$ interaction.

## ACKNOWLEDGMENTS

This work was supported by Long Term Grant LJ7100 (1995) in the frame of the Joint Programme of the Government of Latvia and the International Science Foundation. Four of us (M.T., M.A., I.K., and R.F.) are grateful for the support from the Latvian Science Council (Grant No. 93.256), as well as for the support from the European Commission in the frame of PECO Human Capital & Mobility (Networks) programme, Contract No. ERBCIPDCT940633. One of us (A.V.S.) is grateful for the support from Russian Foundation for Basic Research (Grant No. 93-03-18059). It is our pleasant duty to thank Professor Richard N. Zare for fruitful recommendations. We are also indebted to Dr. Yelena Pazyuk and Professor Pawel Kowalczyk for useful discussions. We are grateful to Vitauts Borerishis for his assistance in experiments, as well as to Dr. Henrik Rudolph and Dr. Henk Dijkerman for granting the RF oscillator.

[1] W. Hanle, Z. Phys. **5**, 246 (1926).
[2] W. Hanle, Z. Phys. **30**, 93 (1924).
[3] E. B. Alexandrov, M. P. Chaika, and G. I. Khvostenko, *Interference of Atomic States* (Springer, New York, 1993).
[4] G. Moruzzi and F. Strumia, *Hanle Effect and Level-Crossing Spectroscopy* (Plenum, New York, 1991).
[5] M. Auzinsh and R. Ferber, *Optical Polarization of Molecules* (Cambridge University Press, Cambridge, 1995).
[6] R. N. Zare, J. Chem. Phys. **45**, 4510 (1966).
[7] A. Khadjavi, A. Lurio, and W. Happer, Phys. Rev. **167**, 128 (1968).
[8] N. D. Bhaskar and A. Lurio, Phys. Rev. A **10**, 1685 (1974).
[9] S. J. Silvers, T. H. Bergeman, and W. Klemperer, J. Chem. Phys. **52**, 4385 (1970).
[10] F. W. Dalby, M. Broyer, and J. C. Lehmann, Colloid Int. CNRS **217**, 227 (1974).
[11] G. Dohmi, A. Hese, A. Renn, and H. S. Schweda, Chem. Phys. **42**, 183 (1979).
[12] C. H. Townes and A. L. Schawlow, *Microwave Spectroscopy* (McGraw-Hill, New York, 1955).
[13] M. Mizushima, *Theory of Rotating Diatomic Molecules* (Wiley, New York, 1975).
[14] G. Herzberg, *Molecular Spectra and Molecular Structure. I. Spectra of Diatomic Molecules* (Van Nostrand, Princeton, 1957).
[15] H. Lefebvre-Brion and R. W. Field, *Perturbations in the Spectra of Diatomic Molecules* (Academic, New York, 1986).
[16] R. E. Drullinger, M. M. Hessel, and E. W. Smith, in *Laser Spectroscopy*, edited by S. Haroche *et al.* (Springer, Berlin, 1975), p. 91.
[17] C. V. Moore, G. P. Davis, and R. A. Gottscho, Phys. Rev. Lett. **52**, 538 (1984).
[18] M. L. Mandich, C. E. Giebe, and R. A. Gottscho, J. Chem. Phys. **83**, 3349 (1985).
[19] R. A. Gottscho, Phys. Rev. A **36**, 2233 (1987).
[20] J. Derouard and N. Sadeghi, Opt. Commun. **57**, 239 (1986).

[21] H. Debontride, J. Derouard, and N. Sadeghi, Ann. Phys. **13**, 97 (1988).
[22] M. H. Alexander, J. Chem. Phys. **83**, 3340 (1985).
[23] J. Derouard and M. H. Alexander, J. Chem. Phys. **85**, 134 (1986).
[24] J. Derouard, H. Debontride, T. D. Nguyen, and N. Sadeghi, J. Chem. Phys. **90**, 5936 (1989).
[25] W. J. Stevens, D. D. Konowalow, and L. B. Ratcliff, J. Chem. Phys. **80**, 1215 (1984).
[26] M. M. Hessel and S. Giraud-Cotton, NaK revisited: The ground $^1\Sigma$ and $D^1\Pi$ states (unpublished, preprint, 1980).
[27] D. Eisel, D. Zevgolis, and W. Demtröder, J. Chem. Phys. **71**, 2005 (1979).
[28] E. J. Breford and F. Engelke, Chem. Phys. Lett. **53**, 282 (1978).
[29] E. J. Breford and F. Engelke, J. Chem. Phys. **71**, 1994 (1979).
[30] H. Katô and C. Noda, J. Chem. Phys. **73**, 4940 (1980).
[31] P. Kowalczyk, J. Mol. Spectrosc. **136**, 1 (1989).
[32] A. J. Ross, C. Effantin, J. d'Incan, and R. F. Barrow, J. Phys. B **19**, 1449 (1986).
[33] J. Pfaff, M. Stock, and D. Zevgolis, Chem. Phys. Lett. **65**, 310 (1979).
[34] R. W. Field and T. H. Bergeman, J. Chem. Phys. **54**, 2936 (1971).
[35] T. J. Scholl, R. Cameron, S. D. Rosner, and R. A. Holt, Can. J. Phys. **73**, 101 (1995).
[36] B. Friedrich and D. R. Herschbach, Nature (London) **353**, 412 (1991).
[37] C. Cohen-Tannoudji, Ann. Phys. **7**, 423 (1962).
[38] C. Cohen-Tannoudji, Ann. Phys. **7**, 469 (1962).
[39] K. Blum, *Density Matrix. Theory and Applications* (Plenum, New York, 1981).
[40] A. R. Edmonds, *Angular Momentum in Quantum Mechanics* (Princeton University Press, Princeton, New Jersey, 1974).
[41] R. N. Zare, *Angular Momentum* (Wiley, New York, 1988).
[42] I. I. Sobelman, *Atomic Spectra and Radiative Transitions* (Springer, Berlin, 1992).
[43] D. A. Varshalovich, A. N. Moskalev, and V. K. Khersonskii, *Quantum Theory of Angular Momentum* (World Scientific, Singapore, 1988).
[44] I. Roegger, J. Phys. B **4**, 168 (1971).
[45] M. P. Auzinsh, R. S. Ferber, Ya. A. Harya, and I. Ya. Pirags, Chem. Phys. Lett. **124**, 116 (1986).
[46] R. E. Druffinger and R. N. Zare, J. Chem. Phys. **51**, 5532 (1969).
[47] K. P. Huber and G. Herzberg, *Molecular Spectra and Molecular Structure IV. Constants of Diatomic Molecules* (Van Nostrand, New York, 1979).
[48] M. Baba, S. Tanaka, and H. Kato, J. Chem. Phys. **89**, 7049 (1989).

Reprinted from

Journal of MOLECULAR STRUCTURE

Journal of Molecular Structure 410–411 (1997) 55–58

# Studies of rotational level Λ-doubling by rf–optical double resonance spectroscopy: application to NaK $D^1\Pi$

M. Auzinsh[a], I. Klincare[a,*], O. Nikolayeva[a], A.V. Stolyarov[b], M. Tamanis[a], R. Ferber[a]

[a]*Department of Physics, University of Latvia, 19 Rainis boulevard, LV-1586 Riga, Latvia*
[b]*Department of Chemistry, Moscow State University, 119899 Moscow, Russia*

ELSEVIER

INFORMATION FOR AUTHORS

# JOURNAL OF MOLECULAR STRUCTURE

## Scope

The *Journal of Molecular Structure* is dedicated to the publication of full-length articles, review articles, and short communications, providing important new structural information on all types of chemical species, including:

- stable and unstable molecules in any environment (vapour, molecular beam, liquid, solution, liquid crystal, solid state, matrix-isolated, surface-adsorbed, etc.)
- chemical intermediates
- molecules in excited states
- biochemicals
- polymers

The methods used may include any combination of spectroscopic and non-spectroscopic techniques, for example:

- infrared spectroscopy (mid, far, near)
- Raman spectroscopy and non-linear Raman methods (CARS, etc.)
- force constant and molecular mechanics calculations
- electronic absorption spectroscopy
- optical rotatory dispersion and circular dichroism
- fluorescence and phosphorescence techniques
- electron spectroscopies (PES, XPS), EXAFS, etc.
- microwave spectroscopy
- electron diffraction
- NMR and ESR spectroscopies
- Mössbauer spectroscopy
- X-ray crystallography

Papers describing routine studies of little structural significance (e.g. straightforward X-ray crystal structure determinations) are not encouraged.

Publications combining experimental and theoretical approaches to a problem are particularly welcomed. However, purely theoretical (semiempirical or ab initio) studies should be submitted to the *Journal of Molecular Structure (Theochem)*.

## Submission of manuscripts

Authors are requested to send three good copies of their manuscript to one of the following editors.

- Dr Austin Barnes, Department of Chemistry and Applied Chemistry, University of Salford, Salford, M5 4WT, UK. Tel: (+44) 161 245 5698, Fax: (+44) 1204 656 958; e-mail: a.j.barnes@chemistry.salford.ac.uk
- Professor Jaan Laane, Department of Chemistry, Texas A&M University, College Station, TX 77843-3255, USA. Tel: (+1) 409 845 3352, Fax: (+1) 409 845 3154; e-mail: laane@chemvx.tamu.edu

Submission of an article is understood to imply that the article is original and is not being considered for publication elsewhere. Those intending to write a review should first contact an Editor. Letters to the Editor, book reviews and meeting/course announcements are also welcome. There are no page charges.

## Language

Please use good, explicit English. Consult a native speaker and/or dictionary where necessary.

## Manuscript preparation

The manuscript should be double spaced with wide margins. The content should be ordered as follows: Title, author(s) name(s), affiliations and addresses, abstract, up to five keywords for indexing. Illustrations must be original drawings or sharp black and white prints. Notations and details must be legible after reduction. Please number consecutively and refer to in the text.

## Electronic manuscripts

Contributions on disk are encouraged. Upon acceptance of the article, the disk and three exactly matching printouts should be submitted together. Instructions for disk preparation are available from the Editors on request.

## Colour

Colour illustrations can be reproduced at the author's expense. The author should contact the Publisher for details (Fax: (+44) 1865 314990).

## Referees

Every paper is subject to peer review. Authors may suggest suitable referees for their paper, although the editors will not necessarily approach them.

## Reprints

50 Reprints will be supplied free of charge.

**Enquiries concerning manuscripts and proofs:** questions arising after the acceptance of the manuscript, especially those relating to proofs should be directed to Elsevier Editorial Services, Mayfield House, 256 Banbury Road, Oxford OX2 7DH, UK; Tel (44) (0) 1865 314900; Fax (44) (0) 1865 314990.

ELSEVIER

Journal of Molecular Structure 410–411 (1997) 55–58

Journal of
MOLECULAR
STRUCTURE

# Studies of rotational level Λ-doubling by rf–optical double resonance spectroscopy: application to NaK $D^1\Pi$

M. Auzinsh[a], I. Klincare[a,*], O. Nikolayeva[a], A.V. Stolyarov[b], M. Tamanis[a], R. Ferber[a]

[a]*Department of Physics, University of Latvia, 19 Rainis boulevard, LV-1586 Riga, Latvia*
[b]*Department of Chemistry, Moscow State University, 119899 Moscow, Russia*

Received 26 August 1996; accepted 6 September 1996

**Abstract**

We report here the application of optical–radio frequency double resonance spectroscopy for individual rotational levels of the NaK $D^1\Pi$ state. Lambda doubling constant $q$ values for five $v'$, $J'$ levels are obtained. These data are combined with measurements of dc $e$–$f$ Stark-mixing-induced changes in optical spectra, and the electric dipole moment $d_p$ in the $D^1\Pi$ state is determined. © 1997 Elsevier Science B.V.

*Keywords:* Optical–rf double resonance; Stark effect; NaK Λ-doubling; Dipole moment

## 1. Introduction

The electronic–rotational interaction of the $^1\Pi$ state with $^1\Sigma$ states induces well known Λ-doubling in $^1\Pi$ with splitting $\Delta_{ef}^J = q[J(J+1) - \Lambda]$, $q$ being the Λ-doubling constant. Only quantitative information for Λ-doubling splitting in the NaK $D^1\Pi$ state is given in [1], where the $q$ value for levels with large rotational quantum number $J$ ($J \geq 100$) has been deduced from level shifts. However, for this state there exists developed spectroscopic information [1–3], including lifetime measurements [4]. Numerous more-or-less pronounced local perturbations caused by the $D^1\Pi$–$d^3\Pi$ interaction have been revealed.

Our interest in $q$ values for particular rotational levels was caused by an investigation of electric dipole moment performed on the NaK $D^1\Pi$ state. The usefulness of rf (or μw) spectroscopy in order to determine Λ-doubling splitting for short-lived electronic states has been demonstrated in [5] for the ($A^1\Pi$) CS molecule. In [6] Stark-effect-induced changes in laser-induced fluorescence (LIF) spectra from NaK $D^1\Pi$ have been recorded, and the optical–rf double resonance signal on the $v' = 7$, $J' = 5$ level has been demonstrated, but only qualitative information without mentioning any $q$ values is presented.

## 2. Method

Fig. 1 explains the methods used in this work. Due to the combination of $\Delta J = 0, \pm 1$ and $+ \leftrightarrow -$ selection rules, only $P$,$R$ doublet emission is allowed at $P$- or $R$-type excitation of the $^1\Sigma \rightarrow {}^1\Pi$ transition, whereas only $Q$ singlet emission is allowed at $Q$-type excitation. If, however, an external electric rf or dc field is applied, the $+ \leftrightarrow -$ or *e*/*f* Stark effect mixing

* Corresponding author.


*PII* S0022-2860(96)09565-8

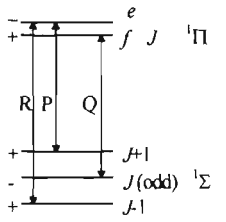


Fig. 1. Selection rules for $^1\Sigma - {}^1\Pi$ transition.

in a $^1\Pi$ state with fixed $J$ gives rise to the appearance of forbidden lines. Therefore, one can observe in the LIF progression $^1\Pi \rightarrow {}^1\Sigma$ the whole $(P,Q,R)$ triplet, instead of either doublets or singlets (see Fig. 2).Two types of experiment can be performed in such a system:

1. recording the 'forbidden' line intensity as a function of rf field frequency gives an optical–rf double resonance signal, from which Λ-splitting $\Delta^J_{ef}$ or the $q$ value for particular $J$ can be deduced.
2. measuring the intensity ratio between 'forbidden' and 'parent' lines as a function of static electric field gives the ratio of Λ-splitting to electric dipole moment $d_p$: $\Delta^J_{ef} / d_p$ or $q/d_p$

## 3. Experimental

The experimental set-up is shown in Fig. 3(a). $^{23}Na^{39}K$ molecules were formed thermally in a glass cell joined to the vacuum system by means of a dry valve. The cylindrical head (Fig. 3(b)) of the cell was made from special alkali-resistant glass tube. The electric field was produced by applying rf or static voltage across a pair of round polished stainless steel Stark plates. A separation of 0.85 ± 0.05 mm between the Stark plates was used for the resonance measurements. For dc Stark mixing altogether three cells were used, differing in diameter and spacing of the electrodes. The metal-containing reservoir was kept at a stabilized temperature between 270°C and 320°C.

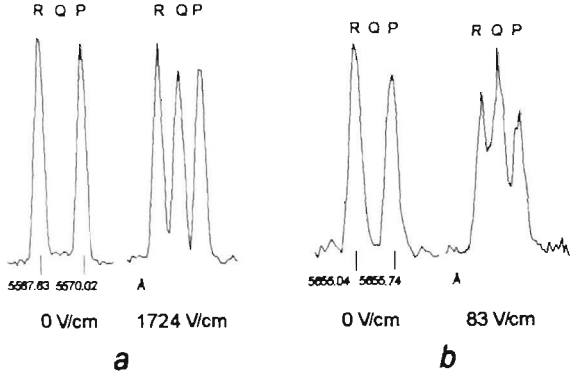


Fig. 2. Effect of static electric field on spectrally resolved LIF for the NaK $D^1\Pi \rightarrow X^1\Sigma^+$ system: (a) transition from $v' = 7$, $J' = 23$; (b) transition from $v' = 12$, $J' = 7$.

Linearly polarized light from a cw $Ar^+$ laser was used to excite $X^1\Sigma^+ \rightarrow D^1\Pi$ transitions in $^{23}Na^{39}K$ molecules. Fluorescence at right angles, both to the laser beam and to the electric field $\epsilon$, was imaged onto the entrance slit of a double monochromator (M) and registered in a photon counting regime. The particular $D^1\Pi \rightarrow X^1\Sigma^+$ LIF progressions were identified from the recorded LIF spectrum by comparison of line positions and relative intensities with the ones calculated by means of a spectroscopic constant set as given in [1], for the transitions mentioned there at excitation by $Ar^+$ laser lines.

In the optical–electric rf double resonance experiments we used a 1–300 MHz (0.2 W, 50 Ω) *Wavetek* rf oscillator (RF) supply, which was connected to the Stark plates (E). The rf field voltage enabled us to produce $\epsilon^0_{rf} \leq 20$ V cm$^{-1}$. A fast oscilloscope (OSC), placed closely across the plates, served as 50 Ω load and as rf output drift monitor. An auxiliary generator output producing a dc voltage proportional to the generated frequency was used to measure the voltage by means of a digital voltmeter. A computer (PC) together with the CAMAC system controlled the driving and data collection of the experiment. In the dc Stark mixing experiments a dc voltage source was connected to the same Stark plates instead of the rf source. Polarizers (P) and the polarization plane rotator (R) fixed the polarization conditions for excitation–registration.

## 4. Signals and results

### *4.1. Optical–rf double resonance signals*

These were obtained by measuring the intensity of 'forbidden' lines as a function of the electric field frequency. Multiple frequency sweeping in a chosen

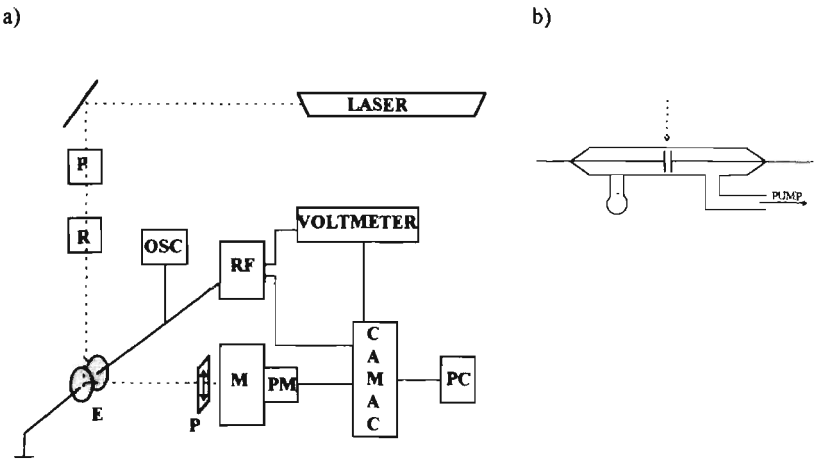


Fig. 3. (a) Experimental set-up: P = polarizers, R = polarization plane rotator, E = Stark plates, OSC = osciloscope, RF = radiofrequency generator, M = spectrometer, PM = photomultiplier, PC = computer; (b) thermal cell.

range and signal accumulation were used. The accumulation time varied from 10 min to 1 h. In order to diminish the influence of LIF intensity drift during signal accumulation the normalized difference $(I_F - I_{F_0})/I_{F_0}$ was considered to be a result of a single measurement, that is the difference between intensity at current frequency $F$ and at some reference frequency $F_0$.

Fig. 4 presents experimental resonance signals for levels $v' = 12$, $J' = 7$ and $v' = 7$, $J' = 23$. Although the resonance signal width exceeded the one expected from the natural broadening, probably with a tendency to exhibit some structure, we assumed that the signal was reliable enough to determine the *e/f* separation, yielding $q$. Resonance signals were registrated for five $v'$, $J'$ levels; corresponding $q$ values are given in Table 1.

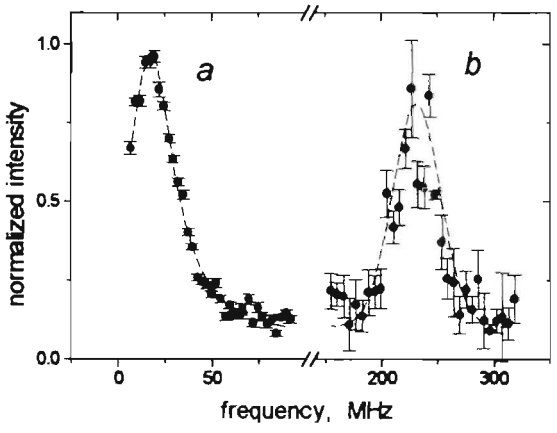


Fig. 4. Optical–rf double resonance signals: (a) – $v' = 12$, $J' = 7$; (b) – $v' = 7$, $J' = 23$.

### 4.2. Intensity ratios

Fig. 2 demonstrates the effect of a static electric field on the spectrally resolved LIF from $v' = 7$, $J' = 23$ and $v' = 12$, $J' = 7$, leading to the appearance of the forbidden $Q$ line due to *e/f* mixing. A fitting procedure using three Gaussians was used to obtain the 'forbidden'/'parent' line ratio $I_Q/I_{P,R}$ dependences on electric field intensity.

Ratio signal simulation and data fitting were accomplished using direct Hamiltonian diagonalization, accounting for Stark interaction within rotational states $J \pm \Delta J$, $\Delta J = 0$, 1 and 2 in initial, excited and final states [7]. Least-square data processing of the intensity ratios, obtained in different cells and geometries, allowed us to get $q/d_p$ ratios. The averaged values are $(2.4 \pm 0.25) \times 10^{-6}$ cm$^{-1}$ D$^{-1}$ for $v' = 7$, $J' = 23$ and $(2.1 \pm 0.2) \times 10^{-6}$ cm$^{-1}$ D$^{-1}$ for $v' = 12$, $J' = 7$. Taken together with $q$ values obtained from

Table 1
Experimantal values of NaK ($D^1\Pi$,$v'$,$J'$) Λ-doubling constant $q$ determined from RF-optical double resonance

| $v'$ | 3 | 4 | 7 | 12 | 14 |
|---|---|---|---|---|---|
| $J'$ | 23 | 19 | 23 | 7 | 19 |
| $q$ ($10^{-5}$ cm$^{-1}$) | 1.39 ± 0.06 | 1.32 ± 0.06 | 1.42 ± 0.07 | 1.03 ± 0.08 | 1.33 ± 0.05 |

double resonance signals, the dipole moment values have been determined: $d_p(v' = 7, J' = 23) = 5.9 \pm 0.9$ D; $d_p(v' = 12, J' = 7) = 4.8 \pm 0.9$ D.

## 5. Discussion

The $q$ values presented in Table 1 lie between those obtained from conventional spectroscopic analysis [1], $q_v = q_0 - q_1(v + 1/2) = 1.16 \times 10^{-5} - 1.5 \times 10^{-7}(v + 1/2)$ cm$^{-1}$, and from the rf–optical double resonance signal [6] for NaK ($D^1\Pi$ $v' = 7$, $J' = 5$), yielding $q = 1.5 \times 10^{-5}$ cm$^{-1}$. Thus the $q$-factor values obtained do not disagree much with the previous data. Regarding the smaller $q$ value for the $v' = 12$, $J' = 7$ level, it corresponds to what can be expected due to the $D^1\Pi$–$d^3\Pi$ perturbation. Although the singlet–triplet interaction does not change $\Delta_{ef}^J$ directly since the $e$ and $f$ components of the $D^1\Pi$ state are perturbed by the two Λ-doublet substates of the $d^3\Pi$ state to about the same amount, this interaction diminishes the singlet character of the perturbed state to $C_{1\Pi}^2$ . The $D^1\Pi$–$d^3\Pi$ mixing coefficient $C_{1\Pi}^2 = 1 - C_{3\Pi}^2$ can be estimated using the calculated difference between the deperturbed $D^1\Pi$ ($v' = 12$) and $d^3\Pi$ ($v' = 13$) terms [3], with $J' = 7$ being $E_{1\Pi} - E_{3\Pi} = -3.87$ cm$^{-1}$ and the level $v' = 12$, $J' = 7$ shift $\Delta E = 0.468$ cm$^{-1}$ with respect to the deperturbed position. The estimated value of $C_{1\Pi}^2$ equals 0.87, thus giving a reduction of the $q$ value since Λ-doubling in the $D^1\Pi$ state has to be $C_{1\Pi}\langle D^1\Pi|L^{\pm}|^1\Sigma\rangle$. As for the absolute dipole moment $d_p$ values obtained here, they can be considered as very large when compared to typical dipole moment values which have been measured for diatomic molecules, but they are consistent with theoretical predictions [8].

## Acknowledgements

This work was supported by Long-term Grant LJ7100 (1995) in the framework of the Joint Program of the Government of Latvia and the International Science Foundation. Four of us (M.T., M.A., I.K. and R.F.) are grateful for support from the Latvian Science Council (Grant 93.256), as well as for support from the European Commission in the framework of the PECO Human Capital and Mobility (Networks) program, contract ERBCIPDCT940633. One of us (A.V.S.) is grateful for support from the Russian Foundation for Basic Research (Grant 93-03-18059).

## References

[1] M.M. Hessel, S. Giraud-Cotton, NaK revisited, unpublished preprint, 1980.
[2] D. Eisel, D. Zevgolis, W. Demtröder, J. Chem. Phys. 71 (1979) 2005.
[3] P. Kowalczyk, J. Mol. Spectrosc. 136 (1989) 1.
[4] J. Pfaff, M. Stock, D. Zevgolis, Chem. Phys. Lett. 65 (1979) 310.
[5] S.J. Silvers, T.H. Bergman, W. Klemperer, J. Chem. Phys. 52 (1970) 4385.
[6] R.F. Drullinger, M.M. Hessel, E.W. Smith, in: Laser Spectroscopy, Springer, Berlin, 1975, p. 91.
[7] M. Tamanis, M. Auzinsh, I. Klincare, O. Nikolayeva, A.V. Stolyarov, R. Ferber, J. Chem. Phys. 106 (1997) 2195.
[8] W.J. Stevens, D.D. Konowalow, L.B. Ratcliff, J. Chem. Phys. 80 (1984) 1215.

# JOURNAL OF MOLECULAR STRUCTURE

The *Journal of Molecular Structure* is dedicated to the publication of full-length articles, review articles, and short communications, providing important new structural information on all types of chemical species, including: stable and unstable molecules in any environment (vapour, molecular beam, liquid, solution, liquid crystal, solid state, matrix-isolated, surface-adsorbed, etc.); chemical intermediates; molecules in excited states; biochemicals; polymers.
The methods used may include any combination of spectroscopic and non-spectroscopic techniques, for example: infrared spectroscopy (mid, far, near); Raman spectroscopy and non-linear Raman methods (CARS, etc.); force constant and molecular mechanics calculations; electronic absorption spectroscopy; optical rotatory dispersion and circular dichroism; fluorescence and phosphorescence techniques; electron spectroscopies (PES, XPS), EXAFS, etc.; microwave spectroscopy; electron diffraction; NMR and ESR spectroscopies; Mössbauer spectroscopy; X-ray crystallography.
Papers describing routine studies of little structural significance (e.g. straightforward X-ray crystal structure determinations) are not encouraged.
Publications combining experimental and theoretical approaches to a problem are particularly welcomed. However, purely theoretical (semiempirical or ab initio) studies should be submitted to the *Journal of Molecular Structure (Theochem)*.

## Editors



**Publication**

The *Journal of Molecular Structure* (ISSN 0022-2860). For 1997 volumes 402–416 are scheduled for publication. (*Journal of Molecular Structure (Theochem)*, for 1997 volumes 386–401 are scheduled for publication)
Subscription prices are available upon request from the Publisher. Subscriptions are accepted on a prepaid basis only and are entered on a calendar year basis. Issues are sent by surface mail except to the following countries where Air delivery via SAL mail is ensured: Argentina, Australia, Brazil, Canada, Hong Kong, India, Israel, Japan, Malaysia, Mexico, New Zealand, Pakistan, PR China, Singapore, South Africa, South Korea, Taiwan, Thailand, USA. For all other countries airmail rates are available on request.
Claims for missing issues must be made within six months of our publication (mailing) date.

**Orders, claims, and product enquiries**: please contact the Customer Support Department at the Regional Sales Office nearest you:
**New York**: Elsevier Science, P.O. Box 945, New York, NY 10159-0945, USA; Tel. (+1)212-633-3730, [Toll free number for North American customers: 1-888-4ES-INFO (437-4636)], Fax (+1)212-633-3680, E-mail usinfo-f@elsevier.com.
**Amsterdam**: Elsevier Science, P.O. Box 211, 1000 AE Amsterdam, The Netherlands; Tel. (+31)20-4853757, Fax (+31)20-4853432, E-mail nlinfo-f@elsevier.nl.
**Tokyo**: Elsevier Science, 9–15 Higashi-Azabu 1 -chome, Minato-ku, Tokyo 106, Japan; Tel. (+81)3-5561-5033, Fax (+81)3-5561-5047, E-mail kyf04035@niftyserve.or.jp.
**Singapore**: Elsevier Science, No. 1 Temasek Avenue, #17-01 Millenia Tower, Singapore 039192; Tel. (+65)434-3727, Fax (+65)337-2230, E-mail asianfo@elsevier.com.sg.

US mailing notice — The *Journal of Molecular Structure* (ISSN 0022-2860) is published semi-monthly by Elsevier Science (Molenwerf 1, Postbus 211, 1000 AE Amsterdam). Annual subscription price in the USA US $4120.00 (valid in North, Central and South America), including air speed delivery. Second class postage is paid at Jamaica, NY 11431.
**USA POSTMASTERS**: Send address changes to the *Journal of Molecular Structure*, Publications Expediting, Inc., 200 Meacham Avenue, Elmont, NY 11003.
**AIRFREIGHT AND MAILING** in the USA by Publication Expediting, Inc., 200 Meacham Avenue, Elmont, NY 11003.

 0022-2860/97/$17.00



⊗ The paper used in this publication meets the requirements of ANSI/NISO Z39.48-1992 (Permanence of Paper).
Printed in The Netherlands

# Stark level crossing and optical–rf double resonance in NaK $D^1\Pi$

M.Auzinsh[1], I.Klincare[1], O.Nikolayeva[1], A.V.Stolyarov[2], M.Tamanis[1], and R.Ferber[1]

[1]Department of Physics, University of Latvia, LV-1586, Riga, Latvia
[2]Department of Chemistry, Moscow State University, 119899 Moscow, Russia

## ABSTRACT

We report here Λ-doubling splitting and permanent electric dipole moment $d_p$ measurements for a number of vibrotational levels of NaK D $^1\Pi$ state. Two different methods, which are not Doppler limited, were used. Stark effect induced level crossing was registered as fluorescence polarization changes with external electric field, which allowed to obtain, from one fit, the values of electric dipole moment and Λ-doubling splitting $\Delta_{ef}$ between $e, f$ substates of an individual rotational state. Another method consisted in obtaining the ratio $\Delta_{ef}/d_p$ from electric field dependence of the intensity of forbidden line appeared in fluorescence as a result of $e$-$f$ Stark mixing, along with direct $\Delta_{ef}$ measurements by optical-rf double resonance. Signal simulations and data fitting were accomplished using direct Hamiltonian diagonalization accounting for Stark interaction within rotational states $J \pm \Delta J$, $\Delta J$ = 0, 1, 2 in initial, excited and final state. Dipole moment values obtained confirm theoretical predictions.

## 1. INTRODUCTION

There is interest in determination of permanent electric dipole moment $d_p$ of a molecule since this quantity reflects very sensitively the details of electronic structure. At the same time there is still a lack of information about electric dipole moments for short-living excited states of diatomic molecules including alkali dimers. We present first $d_p$ measurements for $^{23}Na^{39}K$ $D$ $^1\Pi$ state rovibronic levels by two different methods[1]. (i) Measurements of external electric field $\varepsilon$-dependence of the relative intensity of a forbidden line, which appears in fluorescence as a result of $e$–$f$ Stark mixing[2]. Indeed, due to the combination of ΔJ = 0, ±1 and + ↔ – selection rules, only the ($P$, $R$)-doublet emission is allowed at $P$- or $R$-type excitation, whereas only $Q$-singlet emission is allowed at $Q$-type excitation, see Fig. 1. If, however, external electric field is applied, the + ↔ –, or $e/f$ Stark effect mixing in a $^1\Pi$ state with fixed $J$ gives rise to the appearance of a "forbidden" line. The intensity ratio $I_Q/I_{P,R}$ or *vice versa* of a "forbidden" line to the "parent" one is mainly governed by the $|(d_p\varepsilon)/\Delta_{ef}|$ parameter, allowing to obtain the absolute value $|d_p/q|$, where Λ–doubling splitting $\Delta^J_{ef} = q[J(J+1)-1]$. The $q$ value was measured by us independently by optical–radio frequency (RF) double resonance method. (ii) Stark analogue of Hanle effect, or Stark effect induced level crossing, has been registered via changes of fluorescence linear polarization degree $P(\varepsilon)$ with external electric field $\varepsilon$ and allowed to obtain, from one fit, both $d_p$ value as well as Λ-doubling splitting between $e,f$ substates of an individual rotational state $J$, see Fig. 1.

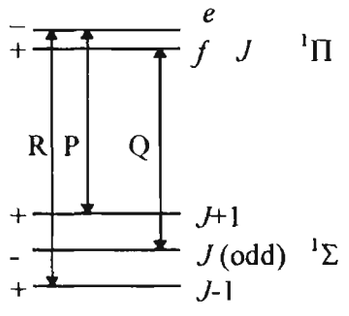


Fig.1. Selection rules for $^1\Sigma$ – $^1\Pi$ transition



SPIE Vol. 3090 • 0277-786X/97/$10.00

## 2. THEORETICAL APPROACH

The general theoretical approach is based on density matrix formalism, allowing to calculate the $^1\Pi$–$^1\Sigma$ fluorescence intensity in the presence of external electric field for any geometry and polarization type, using both analytical expressions in different order perturbation theory, as well as the direct numerical diagonalization of the Hamiltonian matrix, accounting for the interaction within the set $J \pm \Delta J$ of rotational states, both in the excited $^1\Pi$ state and in the ground $^1\Sigma$ state.

## 3. EXPERIMENTAL

$^{23}Na^{39}K$ molecules were formed thermally in a glass cell joined to the vacuum system by means of a dry valve. The cylindrical head of the cell was made from a special alkali-resistant glass tube. Electric field was produced by applying a static voltage across a pair of round polished stainless steel parallel Stark plates located inside the cell. Altogether three cells were used, differing in diameter ($d$) and spacing ($l$) of the electrodes, namely: (1) $d$=25 mm, $l$=2 9 ± 0.1mm; (2) $d$=7 mm, $l$=1.8 ± 0.1 mm; (3) $d$=7 mm, $l$=1.2 ± 0.1 mm. The cells have been filled with metallic potassium and sodium in a weight ratio of approximately 7:3, respectively. The metal-containing reservoir was kept at stabilized temperatures between 270° C and 320° C.

The linearly polarized light from cw $Ar^+$-laser was used to excite $X\,^1\Sigma^+ \rightarrow D\,^1\Pi$ transitions in $^{23}Na$ $^{39}K$ molecules. Laser induced fluorescence (LIF) at right angles, both to the laser beam and to the electric field $\varepsilon$, see Fig. 2, originating from the ca. 0.5 - 1.2 mm diameter laser beam excitation region, has been imaged onto the entrance slit of a double monochromator providing an overall spectral resolution up to 0.3 Å. We restricted the observation zone to the size of ca. 1.5 mm in height, thus diminishing the possible influence of electric field inhomogenity.

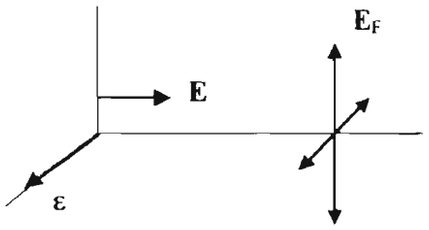


Fig.2. Geometry of the experiment

The particular $D\,^1\Pi \rightarrow X\,^1\Sigma^+$ LIF progressions, originating from the definite $D\,^1\Pi$ $v'$, $J'$ states, were identified from the recorded LIF spectrum by comparison of line positions and relative intensities with the ones calculated by means of spectroscopic constants set[3], for the transitions mentioned[3] at excitation with $Ar^+$-laser lines. The degree of linear polarization was measured by dividing the entrance slit of the monochromator in height in two parts, placing two orthogonal polarizers in front of them. Light guides conducted fluorescence light from the two respective parts of the exit slit to the two photomultipliers, with subsequent counting of one-photon pulses from the two channels. The unpolarized LIF, at absence of external electric field, excited by the laser light with $\hat{\mathbf{E}}$-vector set parallel to the observation direction, was used to calibrate the channels before each experiment.

In the case of optical – electric RF double resonance experiments, we used 1 ÷ 300 MHz (0.2 W, 50 Ω) Wavetek RF oscillator supply, which was connected to the same Stark plates instead of static electric field source. Fast oscilloscope, which was placed closely across the plates, served as 50 Ω load and as RF output drift monitor. The resonance was measured by sweeping the frequency of the RF generator.

## 4. MEASUREMENTS AND RESULTS

*Intensity ratios.* Fig.3 demonstrates the effect of static electric field on the spectrally resolved LIF from $v'=7$, $J'=23$ and $v'=12$, $J'=7$ levels leading to the appearance of forbidden $Q$ line due to $e$–$f$ mixing. Fitting procedure by means of three Gaussians was used to obtain "forbidden"/"parent" line ratio $I_Q/I_{P,R}$. The intensity ratios $I_Q/I_{P,R}$ obtained in different cells and experiment geometry, are shown as settings-in in Figs. 4 and 5. Least-square data processing allowed to get $q/d_p$ ratios. The averaged values are $(2.40\pm0.25)\times10^{-6}$ cm$^{-1}$/D for $v'=7$, $J'=23$ and $(2.10\pm0.20)\times10^{-6}$ cm$^{-1}$/D for $v'=12$, $J'=7$ state.

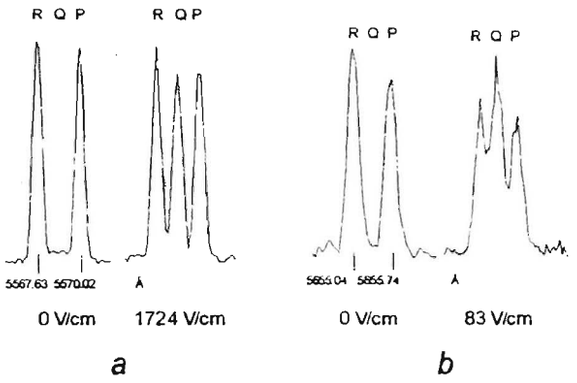


Fig. 3. Effect of electric field on spectrally resolved LIF for NaK $D\,^1\Pi \rightarrow X\,^1\Sigma^+$ system. (a) - transition from $v'=7$, $J'=23$, (b) - from $v'=12$, $J'=7$

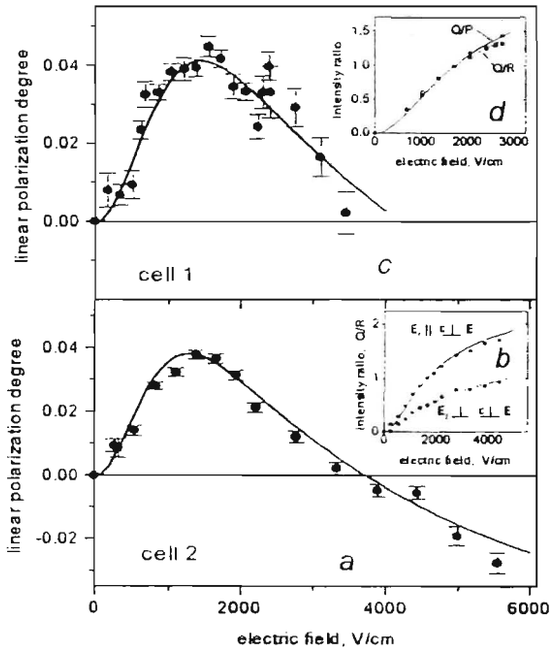


Fig. 4. Linear polarization degree and intensity ratios measured in LIF from $D\,^1\Pi$ state with $v'=7$, $J'=23$. (a),(c)–electric field dependence of the polarization degree obtained on $R(22)$ component; (b), (d)–electric field dependence of intensity ratios $I_Q/I_P$ or $I_Q/I_R$.

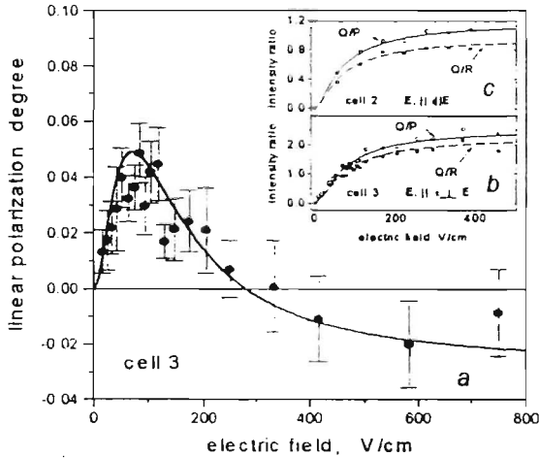


Fig.5. Linear polarization degree and intensity ratios measured in LIF from $D\,^1\Pi$ state with $v'=12$, $J'=7$. (a) - electric field dependence of the polarization degree obtained on $P(8)$ component; (b), (c) - electric field dependence on intensity ratios $I_Q/I_P$ or $I_Q/I_R$.

*Optical-electric RF double resonance.* Fig. 6 (dots) presents experimental data obtained by registering the intensity of a "forbidden" $Q$-line as dependent on the RF electric field frequency, demonstrating resonance intensity increase for $v'=7$, $J'=23$ and $v'=12$, $J'=7$ levels. The signal accumulation time varied from 10 minutes to 1 hour. Optical-RF double resonance signals were obtained for a number of $v'$, $J'$ levels, see Table 1. Although the resonance signal width exceeded the one expected from the natural broadening, probably with a tendency to exhibit some structure, we assumed that the signals are reliable enough to determine the *e/f* separation $\Delta^{J}_{ef}$, yielding $q$. This makes it possible to determine the permanent electric dipole moment $d_p$ in question, using $q/d_p$ values obtained from intensities ratios, see Table 1.

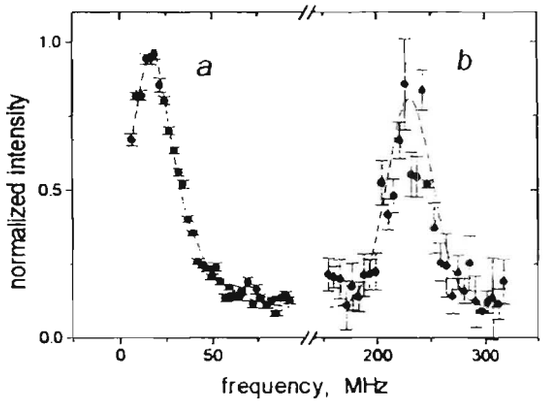


Fig.6. Optical-rf double resonance signals.
(a) - $v'=12$, $J'=7$, (b) - $v'=7$, $J'=23$.

Table 1.

$q$-factors and dipole moments
(superscript P means, that values are obtained from polarization measurements)

| v(J) | q, $10^{-5}$ cm$^{-1}$ | $d_p$, Debye | $d_p^{th}$, Debye |
|---|---|---|---|
| 3(23) | 1.39±0.06 | — | — |
| 4(19) | 1.32±0.06 | — | — |
| 7(23) | 1.42±0.07<br>1.65±0.20$^P$ | 5.9±0.9<br>6.4±0.8$^P$ | 7.1 |
| 12(7) | 1.03±0.08<br>1.10±0.20$^P$ | 4.8±0.9<br>4.5±0.8$^P$ | 6.5 |
| 14(19) | 1.33±0.05 | — | — |

*Polarization measurements.* Experimentally measured for $v'=7$, $J'=23$ and $v'=12$, $J'=7$ levels electric field dependencies of the polarization degree are presented in Figs. 4 and 5. The results are obtained using the most favorable geometry when LIF is viewed from the "end" of exciting light vector $\hat{\mathbf{E}}$ ($\hat{\mathbf{E}} \perp \varepsilon$). The processing of experimental data was realized using theoretical dependencies $P(\varepsilon)$ calculated by accounting for Stark interaction among five rotational states $J$, $J \pm 1$, $J \pm 2$ by Hamiltonian matrices diagonalization for all $J''$, $J'$ and $J''_l$ involved in the transition. The best fitting constants $q$ and $d_p$, obtained from a two-parameter weighted least-square routine, yield the values in question, Table 1.

## 5. DISCUSSION

The dipole moments determined seem to be reliable, in particular since there is good agreement between the results gained from two independent methods. As for the absolute $d_p$ values, they can be considered as very large when compared to typical dipole moment values which had been measured for diatomic molecules. Let us compare the measured $d_p$ values with theoretical quantities[4]. In order to pass from *ab initio* $d_p^{th}(R)$ dependence[4] to the predicted $d_p$ values for particular $v'$, $J'$ states, we have used the averaging routine yielding the following predicted $d_p^{th}(v', J')$ values for the states under study: $d_p^{th}(7, 23) = 7.1$ D and $d_p^{th}(12, 7) = 6.5$ D, see Table 1.

As follows from Table 1, the measured $d_p$ value for the $v'$=12, $J'$=7 state is smaller than for the $v'$=7, $J'$=23, being also markedly smaller than the theoretically predicted value. As it is well known [3,5], levels belonging to the NaK $D\ ^1\Pi$ state are perturbed, at least to some extent, by the close lying $d\ ^3\Pi$ state. The level $v'$=7, $J'$=23 can be considered as almost unperturbed[3], whereas the level $v'$=12, $J'$=7 is shifted to $\Delta E$ = 0.468 $cm^{-1}$ with respect to the deperturbed position. As a result, the experimentally measured $d_p$ value for the level $v'$=12, $J'$=7 is expected to be ca. 15% smaller than could been suspected for unperturbed state. It is thus not excluded that the difference between $d_p$ values obtained for the two states, see Table 1, reflects the role of perturbations. Hence, the experimentally measured $d_p$ values do not disprove the *ab initio* calculation[4], accounting for the fact that the deperturbed quantities have been calculated.

The $q$ values presented in Table 1 lies between ones obtained from conventional spectroscopic analysis[3] as $q_0$= $1.16\times10^{-5}$ $cm^{-1}$ and from the RF – optical double resonance signal[6] for NaK ($D\ ^1\Pi$ $v'$=7, $J'$=5), yielding $q$=$1.5\times10^{-5}$ $cm^{-1}$. Thus, the $q$-factor values obtained do not disagree much with the previous data. Regarding Λ-doubling factor $q$, smaller value for $v'$=12, $J'$=7 level, it corresponds to what can be expected due to the perturbation, allowing to estimate ca. 13% diminution from the following considerations. Although the singlet-triplet $D\ ^1\Pi$ - $d\ ^3\Pi$ interaction does not change Λ-doubling splitting directly since $e$ and $f$ components of the $D\ ^1\Pi$ state are perturbed by the two Λ-doublet substates of the $d\ ^3\Pi$ state to about the same amount, this singlet-triplet interaction diminishes a singlet character of the perturbed state as $C^2_{^1\Pi}$. Hence, the matrix element of electronic–rotational interaction with the remote singlet Σ states has to be $C_{^1\Pi}\left\langle D\ ^1\Pi\middle|L^+\middle|^1\Sigma\right\rangle$, giving rise to diminution of Λ-doubling in $D\ ^1\Pi$ state.

In conclusion, the measurements constituted in the present work confirmed the existence of large permanent electric dipole moment in NaK $D\ ^1\Pi$ state.

## 6. ACKNOWLEDGMENTS

This work was supported by Long Term Grant LJ7100 (1995) in the frame of the Joint Program of the Government of Latvia and the International Science Foundation. Four of us (M.T., M.A., I.K. and R.F.) are grateful for the support from Latvian Science Council (Grant 93.256), as well as for the support from the European Commission in the frame of PECO Human Capital & Mobility (Networks) program, contract ERBCIPDCT940633. One of us (A.V.S.) is grateful for the support from Russian Foundation for Basic Research (Grant 93-03-18059)

## 7. REFERENCES

[1] M.Tamanis, M.Auzinsh, I.Klincare, O.Nikolayeva, A.V.Stolyarov, and R.Ferber, *submitted to J.Chem.Phys.*

[2] J.Derouard, H.Debontride, T.D.Nguyen, and N.Sadeghi, *J.Chem.Phys.*, **90**, 5936 (1989)

[3] M.M.Hessel, and S.Giraud-Cotton, NaK *revisited: The ground* $^1\Sigma$ *and* $D\ ^1\Pi$ *states, unpublished preprint*, (1980).

[4] W.J.Stevens, D.D.Konowalow, and L.B.Ratcliff, *J.Chem.Phys.*, **80**, 1215 (1984)

[5] P.Kowalczyk, *J.Mol.Spectrosc.*, **136**, 1 (1989)

[6] R.E.Drullinger, M.M.Hessel, and E.W.Smith, in *Laser Spectroscopy*, edited by S.Haroche *et al.* (Springer, Berlin, 1975), p. 91

# Revision of $Na_2$ $A^1\Sigma_u^+$ state molecular constants by polarization labeling spectroscopy

**I.Jackowska[†], W.Jastrzębski[†], R.Ferber[††], O.Nikolayeva[††] and P.Kowalczyk[‡]**

[†]Institute of Physics, Polish Academy of Sciences. al.Lotników 32/46, 02-668 Warsaw, Poland.
[‡]Institute of Experimental Physics, Warsaw University, ul. Hoża 69, 00-681 Warsaw, Poland.
[††]Department of Physics, University of Latvia. Riga, Latvia, LV-1586

## ABSTRACT.

This paper contains the analysis of the $A^1\Sigma_u^+$ of $Na_2$ based on the data obtained from the polarization labeling spectroscopy experiment on the $A^1\Sigma_u^+ - X^1\Sigma_g^+$ transition. A set of Dunham coefficients is derived, which describes the A state in the wide range of v ($0 \le v \le 43$) and J ($12 \le J \le 126$) quantum numbers and reproduces the positions of unperturbed rotational lines in the A-X band system to within 0.1 $cm^{-1}$.

## 1. INTRODUCTION.

We report[1] new analysis of the $A^1\Sigma_u^+$ state based on the data obtained from polarization labeling spectroscopy (PLS) experiment[1,2], based on V-type optical–optical double resonance scheme, on the $A^1\Sigma_u^+ - X^1\Sigma_g^+$ band system of sodium dimer. The diatomic alkali molecules, with their simple electronic configuration and main absorption bands conveniently positioned in the visible region, are relatively easy to handle both theoretically and experimentally. Hence they have long been employed for testing quantum chemistry calculations. Modern theoretical methods have a potentiality to predict potential curves and spectroscopic constants with high accuracy[3]. On the experimental side a huge amount of data have been gathered on the $A^1\Sigma_u^+$ state of $Na_2$, but its investigation is still far from complete. The first reliable molecular constants describing the $A^1\Sigma_u^+$ state for $v \le 20$ were obtained from classical absorption spectroscopy by Kusch and Hessel[4]. Subsequently their data set was incorporated to results of the modulated population spectroscopy experiment[5] by Kaminsky, who determined Dunham coefficients[6] applicable to the A state levels in the range $0 \le v \le 44$, $0 \le J \le 44$. In spite if this precise examination of the $A^1\Sigma_u^+ - X^1\Sigma_g^+$ band system has shown[7,8] that the experimentally observed line frequencies still deviate from frequencies calculated using molecular constants[6] much beyond experimental uncertainties. In effort to improve the accuracy, the A state Dunham coefficients were verified and extended up to v=70 by Gerber and Möller[9]. However, their experiment, carried out in a molecular beam, could provide reliable information only on low $J<20$ levels. The analysis of the $A^1\Sigma_u^+$ state was further continued by Chawla et al.[10] who reached v=105 vibrational level but only for J=10-12.

Further work on the $A^1\Sigma_u^+$ state of $Na_2$ is warranted by the fact that at typical working temperatures for sodium vapor in resonance cell or heat-pipe oven conditions ($T \approx 700K$) the maximum populated rotational level is $J \approx 40$, well outside the range of validity of the recommended molecular constants. Even for J=80 or 100 rotational level population decreases only to about 43% or 17% of the maximum value, respectively, and we found experimentally that discrepancies between the predicted and measured line positions in the A-X system may exceed 2 $cm^{-1}$ in this range of rotational quantum numbers.



SPIE Vol. 3090 • 0277-786X/97/$10.00

The goal of the present paper was to accomplish new analysis of the $A^1\Sigma_u^+$ state of $Na_2$ based on the data obtained from the PLS experiment on the $A^1\Sigma_u^+ - X^1\Sigma_g^+$ transition in order to derive a set of Dunham coefficients describing the A state in the wide range of v ($0 \le v \le 43$) and J ($12 \le J \le 126$) quantum numbers.

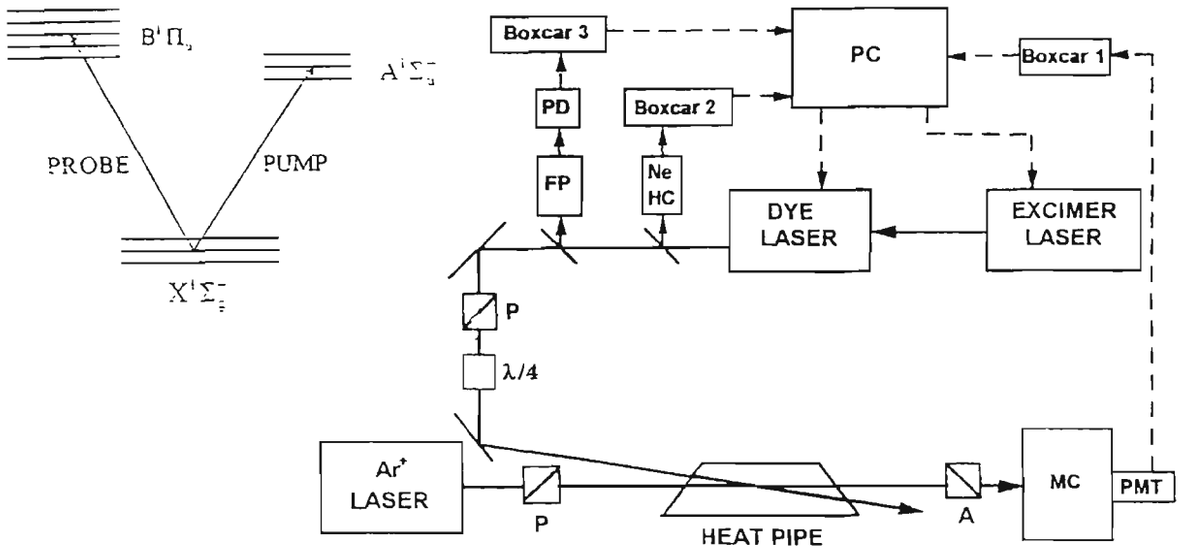


Fig. 1. The excitation scheme and block diagram of the experimental set-up: A-analyser, FP-Fabry-Perot interferometer, HC-hollow-cathode lamp, λ/4 - quarter wave plate, MC-monochromator, P-polarizer, PD-photodiode, PMT-photomultiplier tube.

## 2. EXPERIMENTAL.

The PLS technique is described in works[11,12]. In present work we have exploited the V-type optical-optical double resonance scheme[2,13,14]. The basic principle of the V-type optical double resonance PLS and its experimental realization are schematically depicted in Fig. 1. The two laser beams pass collinearly through the sodium vapor, which is placed between crossed polarizers. Contrary to the classical scheme[12,15] in our experiment the probe laser is of fixed frequency whereas the pump laser is tunable. The frequency of the probe laser accidentally coincides with a set of known transitions $B^1\Pi_u\,(v_1', J_1') \leftarrow X^1\Sigma_g^+\,(v'', J'')$, thus labeling the involved rovibrational levels $(v'', J'')$ in the ground state of sodium dimer. The circularly or linearly polarized pump laser light is tuned across the investigated band system $A^1\Sigma_u^+ \leftarrow X^1\Sigma_g^+$. It orients or aligns the absorbing molecules in the lower (and upper) levels by optical pumping. A linearly polarized weak probe beam is changed in its polarization characteristics whenever the frequency of the pump laser is tuned to a transition originating from the labeled lower level $(v'', J'')$. The photomultiplier placed behind the crossed analyzer therefore receives a signal any time the pump laser frequency coincides with a transition $A^1\Sigma_u^+\,(v', J') \leftarrow X^1\Sigma_g^+\,(v'', J'')$.

In our PLS experiment the pump laser was a pulsed due laser (Lumonics HD500) working on Nile Blue, DCM, Rhodamine B or Rhodamine 6G dyes and pumped with a XeCl excimer laser (Lumonics EX500). The dye laser delivered ca. 1 mJ energy pulses of ca. 10 ns duration and 0.1 $cm^{-1}$ spectral width. The laser wavelength was calibrated against both the optogalvanic spectrum of neon[16] in a hollow cathode discharge tube and the transmission fringes of the six blue-green $Ar^+$ laser lines (Carl Zeiss ILA 120),

λ=514.5, 501.7, 496.3, 488.0, 476.5 and 457.9 nm, with a typical power ranging from 20 to 120 mW. They are known to excite several transitions in the $B^1\Pi_u \leftarrow X^1\Sigma_g^+$ system of sodium dimer, observed in previous experiments[17,18,19]. However, in addition to the resonances reported before, we were able to assign 12 new transitions. Table I presents a summary of all the identified labeling transitions induced by the probe laser lines, which gave rise to the polarization spectra.

**Table I.** Observed transitions in the $B\ ^1\Pi_u \leftarrow X\ ^1\Sigma^+_g$ band system of $Na_2$ excited by six lines of the $Ar^+$ laser used as the probe laser. The transitions marked as 17-19 have been reported previously (in Refs. [17-19]).

| Exciting line (nm) | Excited transition (v',J') ← (v'',J'') | Reference |
|---|---|---|
| 514.5 | (1,48) ← (6,49) | |
| | (1,60) ← (6,59) | 17 |
| | (2,82) ← (6,83) | 17 |
| | (2,36) ← (7,37) | |
| | (3,32) ← (8,31) | 18 |
| | (9,64) ← (12,65) | 17,18 |
| | (11,49) ← (14,49) | 17,18 |
| 501.7 | (0,42) ← (2,43) | 19 |
| | (0,47) ← (2,47) | |
| | (3,97) ← (3,97) | |
| | (5,124) ← (3,125) | 17 |
| | (5,88) ← (5,87) | 17 |
| | (5,37) ← (6,38) | 17 |
| | (5,42) ← (6,42) | 19 |
| 496.5 | (1,99) ← (0,99) | |
| | (0,17) ← (1,17) | |
| | (0,24) ← (1,23) | |
| | (4,30) ← (4,30) | 18 |
| | (7,43) ← (6,44) | 18 |

| Exciting line (nm) | Excited transition (v',J') ← (v'',J'') | Reference |
|---|---|---|
| 488.0 | (2,39) ← (0,40) | |
| | (3,75) ← (0,75) | 18 |
| | (7,98) ← (2,98) | 17,18 |
| | (6,43) ← (3,43) | 17,18 |
| | (7,25) ← (4,25) | 19 |
| | (9,56) ← (5,55) | 17 |
| | (10,42) ← (6,41) | 17,18 |
| 476.5 | (6,27) ← (0,28) | 17,18 |
| | (6,31) ← (0,31) | |
| | (9,98) ← (0,98) | 17,18 |
| | (8,57) ← (1,56) | |
| | (9,75) ← (1,75) | |
| | (9,39) ← (2,39) | |
| | (14,118) ← (2,117) | 17,18 |
| | (10,12) ← (3,13) | 17,18 |
| | (17,124) ← (3,123) | 18 |
| 457.9 | (23,39) ← (5,38) | 17 |
| | (27,31) ← (7,31) | 17,18 |
| | (28,43) ← (7,43) | 17,18 |
| | (29,25) ← (8,24) | 17,18 |

Sodium vapor was generated in a stainless-steel heat-pipe oven operating at T≈750K with 4 Torr of He buffer gas. The pump and probe laser beams were copropagating almost in parallel and passed through the sodium vapor. The pump beam was then removed by a beam stopper whereas the probe beam passed through the crossed analyzer and a 0.3 m monochromator (used to eliminate stray light) onto the photomultiplier connected to the Boxcar 1 averager, see Fig. 1. A computer system, which also controlled the dye laser tuning, stored the polarization spectra together with Ne optogalvanic spectrum (by Boxcar 2) and transmission peaks of the Fabry-Perot interferometer (by Boxcar 3).

## 3. RESULTS AND ANALYSIS.

The polarization spectrum of the $A^1\Sigma_u^+ - X^1\Sigma_g^-$ system of $Na_2$ has been recorded in region from 14200 till 17600 $cm^{-1}$. A typical fragment of the spectrum is shown in Fig. 2. We assigned about 1450 transitions spanning the range $v'=0\div43$ and $J'=12\div126$ in the $A^1\Sigma_u^-$ state. All the lines observed were

processed by means of a global least-squares fit with a Dunham expansion. The ground $X^1\Sigma_g^-$ state constants were taken from the work of Kusch and Hessel[18]. As expected, the initial fit revealed that part of the lines were shifted from the expected positions up to 0.6 $cm^{-1}$ due to perturbation of the $A^1\Sigma_u^-$ state by the $b^3\Pi_u$ state. Since we were interested in the unperturbed constant set, lines for which the difference between the measured and

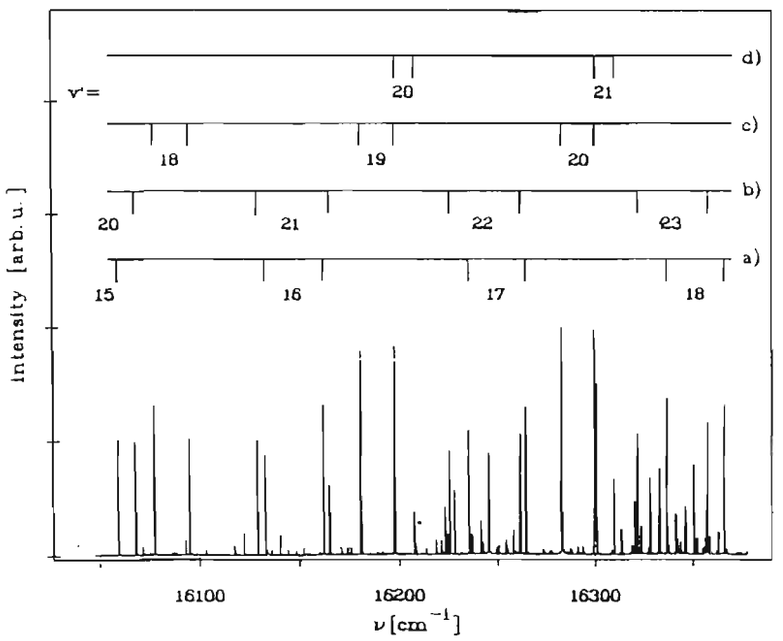


Fig. 2. A portion of the polarization spectrum of $Na_2$ obtained with 488.0 nm line of the $Ar^-$ laser as the probe and linearly polarized pump beam. The assigned progressions (a)-(d) correspond to the transitions $A^1\Sigma_u^- \leftarrow X^1\Sigma_g^+$ from the labeled ground state levels v"= 0, J"= 75 (a), v"= 2, J"= 98 (b), v"= 3, J"= 43 (c) and v"=4, J"=25 (d).

calculated positions exceeded 0.2 $cm^{-1}$ (twice the experimental uncertainty) were excluded from the data field and the fitting procedure has been then repeated until a consistency between the observed and predicted values was achieved. The excluded lines fall in general into the regions of predicted strong perturbations between the A and b states[20]. In this way, 1376 lines of A-X system remained as unperturbed within the 0.1 $cm^{-1}$ accuracy and provided the Dunham coefficients for the $A^1\Sigma_u^+$ state presented in Table II. The root mean square (rms) error of the final fit was 0.052 $cm^{-1}$. For each constant a total of at least six figures is given (more than are statistically significant), as this number is required to reproduce the measured transitions.

The $A^1\Sigma_u^+$ state molecular constants obtained, have been tested against the deperturbed constants presented by Effantin et al[21] and Whang et al[20]. In the common ranges of validity of the constants, the line positions predicted from them for the A-X system agree within 0.1 $cm^{-1}$. Our Dunham coefficients reproduce also correctly excitations by the 647.1 nm line of the $Kr^+$ laser[22] and by the 632.8 nm line of the He-Ne laser[23]. In comparison with the previous Dunham coefficients of Kaminsky[6] and Gerber and Möller[9], the values of constant given in Table II provide a much improved fit to the observed levels particularly for J>50, where the previous values were unreliable.

**Table II.** The Dunham coefficients for the $A\,^1\Sigma_u^+$ state of $Na_2$ obtained in the present work.

| constant | value ($cm^{-1}$) | error (%) |
|---|---|---|
| $T_e$ | 1.468042(+4) | 0.0001 |
| $Y_{10}$ | 1.17406(+2) | 0.003 |
| $Y_{20}$ | -3.69478(-1) | 0.082 |
| $Y_{30}$ | 0.693070(-3) | 1.5 |
| $Y_{40}$ | -0.786759(-5) | 1.5 |
| $Y_{01}$ | 0.110777(+0) | 0.004 |
| $Y_{11}$ | -0.558396(-3) | 0.08 |
| $Y_{21}$ | 0.115972(-5) | 2.2 |
| $Y_{31}$ | -0,202903(-7) | 2.1 |
| $Y_{02}$ | -0.386424(-6) | 0.16 |
| $Y_{12}$ | 0.269103(-9) | 5.9 |
| $Y_{03}$ | 0.112252(-11) | 2.0 |

## 4. ACKNOWLEDGEMENTS.

This work has been supported by a grant from the Polish Committee for Scientific Research (No. 2 P03B 058 10). Two of us (R.F. and O.N.) are grateful for the additional support from the Latvian Science Council (Grant 93.256) and from the European Commission PECO HCM Programme, contract ERBCIPDCT940633.

## 5. REFERENCES.

[1] I.Jackowska, W.Jastrzębski, R.Ferber, O.Nikolayeva and P.Kowalczyk, *Mol.Phys.*, accepted
[2] W.Jastrzębsky and P.Kowalczyk, *Phys.Rev.A*, **51**, 1046 (1995)
[3] S.Magnier, Ph.Millié, O.Dulieu and F.Masnou-Seeuws, *J.Chem.Phys.*, **98**, 7113 (1993) and references therein
[4] P.Kusch, and M.M.Hessel, *J.Chem.Phys.*, **63**, 4087 (1975)
[5] M.E.Kaminsky, R.T.Hawkins, F.V.Kowalski, and A.L.Schawlow, *Phys.Rev.Lett.*, **36**, 671 (1976)
[6] M.E.Kaminsky, *J.Chem.Phys.*, **66**, 4951 (1977)
[7] H.S.Schweda, G.K.Chawla, and R.W.Field, *Opt.Commun.*, **42**, 165 (1982)
[8] R.N.Ahmad-Bitar, and A.S.Al-Ayash, *J.Mol.Spectrosc.*, **106**, 299 (1984)
[9] G.Gerber, and R.Möller, *Chem.Phys.Lett.*, **113**, 546 (1985)
[10] G.Chawla, H.S.Schweda, H.J.Vedder, R.W.Field, S.Churassy, A.M.Lyyra, W.T.Luh, and W.C.Stwalley, *AIP Conf.Proc. (USA)*, **146**, 466 (1986)
[11] W.Demtröder, *Laser Spectroscopy*, (Springer, 1996)
[12] Z.G.Wang, and H.R.Xia, *Molecular and Laser Spectroscopy*, (Springer, 1996)
[13] W.Jastrzębsky, and P.Kowalczyk, *Chem.Phys.Lett.*, **206**, 69 (1993)
[14] W.Jastrzębsky, and P.Kowalczyk, *Chem.Phys.Lett.*, **227**, 283 (1994)
[15] N.W.Carlson, A.J.Taylor, K.M.Jones, and A.L.Schawlow, *Phys.Rev.A.*, **24**, 822 (1981)
[16] A.R.Striganov, and G.A.Odincova, *Tablicy Spectralnych Linii Atomov I Ionov* (Energoizdat, Moscow, 1982)
[17] W.Demtröder, and M.Stock, *J.Mol.Spectrosc.*, **55**, 476 (1975)
[18] P.Kusch, and M.M.Hessel, *J.Chem.Phys.*, **68**, 2591 (1978)
[19] M.M.Hessel, and S.Giraud-Cotton, *NaK Revisited: The Groung $^1\Sigma$ and D $^1\Pi$ States* (unpublished preprint, 1980)
[20] T.J.Whang, W.C.Stwalley, L.Li, and A.M.Lyyra, *J.Chem.Phys.*, **97**, 7211 (1992)
[21] C.Effantin, O.Babaky, K.Hussein, J.d'Incan, and R.F.Barrow, *J.Phys.B.*, **18**, 4077 (1985)
[22] O.Babaky, and K.Hussein, *Can.J.Phys.*, **67**, 912 (1989)
[23] K.K.Verma, T.H.Vu, and W.C.Stwalley, *J.Mol.Spectrosc.*, **85**, 131 (1981)

MOLECULAR PHYSICS, 1996, VOL. 89, NO. 6, 1719–1724

# Reanalysis of the A $^1\Sigma_u^+$ state of $Na_2$ by polarization labelling spectroscopy

By I. JACKOWSKA, W. JASTRZĘBSKI, R. FEBER†, O. NIKOLAYEVA†
Institute of Physics, Polish Academy of Sciences, Al. Lotników 32/46, 02-668 Warsaw, Poland

and P. KOWALCZYK‡
Institute of Experimental Physics, Warsaw University, ul. Hoża 69, 00-681 Warsaw, Poland

(*Received 24 April 1996; accepted 7 May 1996*)

The polarization labelling spectroscopy technique is applied to study the A $^1\Sigma_u^+$–X $^1\Sigma_g^+$ band system of sodium dimer. Six visible lines of an argon ion laser are used to label rovibronic levels in the ground state of $Na_2$. Rotationally resolved polarization spectra are observed in the range 14200–17600 $cm^{-1}$. A set of Dunham coefficients is deduced to fit all unperturbed levels of the A $^1\Sigma_u^+$ state with $0 \leqslant v \leqslant 43$ and $12 \leqslant J \leqslant 126$.

## 1. Introduction

A vast amount of experimental work has been done on the A $^1\Sigma_u^+$ state of $Na_2$, some very precise and elaborate, but its investigation is still far from complete. The first reliable molecular constants describing this state for $v \leqslant 20$ were obtained from classical absorption spectroscopy by Kusch and Hessel [1]. Subsequently their data set was incorporated to results of the modulated population spectroscopy experiment [2] by Kaminsky [3], who determined Dunham coefficients applicable to the A-state levels in the range $0 \leqslant v \leqslant 44$, $0 \leqslant J \leqslant 44$. However, precise examination of the A $^1\Sigma_u^+$–X $^1\Sigma_g^+$ band system has shown [4, 5] that the experimentally observed line frequencies still deviate from frequencies calculated using molecular constants of [3] much beyond experimental uncertainties. In an effort to improve the accuracy, the A-state Dunham coefficients were verified and extended up to $v = 70$ by Gerber and Möller [6]. However, their experiment, carried out in a molecular beam, could provide reliable information only on low $J < 20$ levels. The analysis of the A $^1\Sigma_u^+$ state was further continued by Chawla *et al.* [7] who reached $v = 105$ vibrational level but only for $J = 10$–12.

Particular interest has been paid in the past to understanding perturbation between the A $^1\Sigma_u^+$ and b $^3\Pi_u$ states. After pioneering research by Kusch and Hessel [1], detailed analysis of this perturbation was performed by Effantin *et al.* [8] and later by Whang *et al.* [9]. In both studies a deperturbation procedure was applied to the observed spectral line positions and highly precise molecular constants derived, describing the A state in a level-by-level manner (i.e. the term energy and rotational constants were

† On leave from Department of Physics, University of Latvia, LV-1586 Riga, Latvia.
‡ Author for correspondence.

0026-8976/96 $12.00 

given separately for each vibrational level). However, these constants apply either to low vibrational levels $v \leqslant 10$ [8] or to low rotational levels $J \leqslant 18$ [9] only.

Further work on the A $^1\Sigma_u^+$ state of $Na_2$ is warranted by the fact that at typical working temperatures for sodium vapour in resonance cell or heat-pipe oven conditions ($T \approx 700$ K) the maximum populated rotational level is $J \approx 40$, well outside the range of validity of the recommended molecular constants. Even for $J = 80$ or 100 the rotational level population decreases only to about 43% or 17% of the maximum value, respectively, and we found experimentally that discrepancies between the predicted and measured line positions in the A–X system may exceed 2 $cm^{-1}$ in this range of rotational quantum numbers. This paper presents a new analysis of the A $^1\Sigma_u^+$ state based on the data obtained from the polarization labelling spectroscopy experiment on the A $^1\Sigma_u^+$–X $^1\Sigma_g^+$ transition. We derive a set of Dunham coefficients describing the A state in the wide range of $v$ ($0 \leqslant v \leqslant 43$) and $J$ ($12 \leqslant J \leqslant 126$) quantum numbers and reproducing the positions of unperturbed rotational lines in the A–X band system to within 0·1 $cm^{-1}$.

## 2. Experimental details

The polarization labelling technique has been extensively described in the literature [10, 11]. Our version of the method is based on the V-type optical–optical double-resonance scheme [12–14]. We use a linearly polarized probe laser, the fixed frequency of which is in accidental resonance with a few known transitions in the investigated molecule, thus labelling the involved rovibrational levels in the ground molecular state. A linearly or circularly polarized beam from a pump laser is tuned across the investigated spectrum. At resonance with any molecular transition it produces optical anisotropy in the lower and upper molecular levels involved. However, the polarization of the probe beam will be altered only at those frequencies of the pump laser light, when lower levels for both the pump and the probe transitions coincide. Therefore tuning the pump laser over the spectral range studied and monitoring light passing through the crossed analyser, we obtain excitation spectrum of the molecule starting only from the ground-state levels labelled by the probe light.

In our experiment the pump laser was a pulsed dye laser (Lumonics HD500) working on Nile Blue, DCM, Rhodamine B or Rhodamine 6G dyes and pumped with a XeCl excimer laser (Lumonics EX500). The dye laser delivered 2 mJ energy pulses of 8 ns duration and 0·1 $cm^{-1}$ spectral width. The laser wavelength was calibrated against both the optogalvanic spectrum of neon [15] in a hollow cathode discharge tube and the transmission fringes of a Fabry–Pérot interferometer 0·5 cm long. As a probe light we used one of the six blue-green $Ar^+$ laser lines (Carl Zeiss ILA. 120), $\lambda$ = 514·5, 501·7, 496·5, 488·0, 476·5 and 457·9 nm, with a typical power ranging from 20 to 120 mW. They are known to excite several transitions in the B $^1\Pi_u \leftarrow$ X $^1\Sigma_g^+$ system of sodium dimer, observed in previous experiments [16–18]. However, in addition to the resonances reported before, we were able to assign 12 new transitions. Table 1 presents a summary of all the identified labelling transitions induced by the probe laser lines, which gave rise to the polarization spectra.

Sodium vapour was generated in a stainless steel heat-pipe oven operating at $T \approx 750$ K with helium buffer gas at 4 Torr. The pump and probe beams were axially mixed to copropagate nearly in parallel and passed through the sodium vapour. The

Table 1. Observed transitions in the B $^1\Pi_u \leftarrow$ X $^1\Sigma_g^+$ band system of $Na_2$ excited by six lines of the $Ar^+$ laser used as the probe laser. The transitions that have been reported previously are indicated.

| Exciting line/nm | Excited transition $(v', J') \leftarrow (v'', J'')$ | Reference |
|---|---|---|
| 514·5 | (1, 48) ← (6, 49) | |
| | (1, 60) ← (6, 59) | [16] |
| | (2, 82) ← (6, 83) | [16] |
| | (2, 36) ← (7, 37) | |
| | (3, 20) ← (8, 21) | [17] |
| | (3, 32) ← (8, 31) | [17] |
| | (9, 64) ← (12, 65) | [16, 17] |
| | (11, 49) ← (14, 49) | [16, 17] |
| 501·7 | (0, 42) ← (2, 43) | [18] |
| | (0, 47) ← (2, 47) | |
| | (3, 97) ← (3, 97) | |
| | (5, 124) ← (3, 125) | [16] |
| | (5, 88) ← (5, 87) | [16] |
| | (5, 37) ← (6, 38) | [16] |
| | (5, 42) ← (6, 42) | [18] |
| 496·5 | (1, 99) ← (0, 99) | |
| | (0, 17) ← (1, 17) | |
| | (0, 24) ← (1, 23) | |
| | (4, 30) ← (4, 30) | [17] |
| | (7, 43) ← (6, 44) | [17] |
| 488·0 | (2, 39) ← (0, 40) | |
| | (3, 75) ← (0, 75) | [17] |
| | (7, 98) ← (2, 98) | [16, 17] |
| | (6, 43) ← (3, 43) | [16, 17] |
| | (7, 25) ← (4, 25) | [18] |
| | (9, 56) ← (5, 55) | [16] |
| | (10, 42) ← (6, 41) | [16, 17] |
| 476·5 | (6, 27) ← (0, 28) | [16, 17] |
| | (6, 31) ← (0, 31) | |
| | (9, 98) ← (0, 98) | [16, 17] |
| | (8, 57) ← (1, 56) | |
| | (9, 75) ← (1, 75) | |
| | (9, 39) ← (2, 39) | |
| | (14, 118) ← (2, 117) | [16, 17] |
| | (10, 12) ← (3, 13) | [16, 17] |
| | (17, 124) ← (3, 123) | [17] |
| 457·9 | (23, 39) ← (5, 38) | [16] |
| | (27, 31) ← (7, 31) | [16, 17] |
| | (28, 43) ← (7, 43) | [16, 17] |
| | (29, 25) ← (8, 24) | [16, 17] |

pump beam was then removed by a beam stopper and the probe beam directed through the crossed analyser and a 0·3 m monochromator (used to eliminate stray light) onto the photomultiplier tube coupled to the boxcar averager. A computer system, which also controlled the dye laser tuning, stored the polarization spectra together with neon optogalvanic spectrum and transmission peaks of the Fabry–Pérot interferometer.

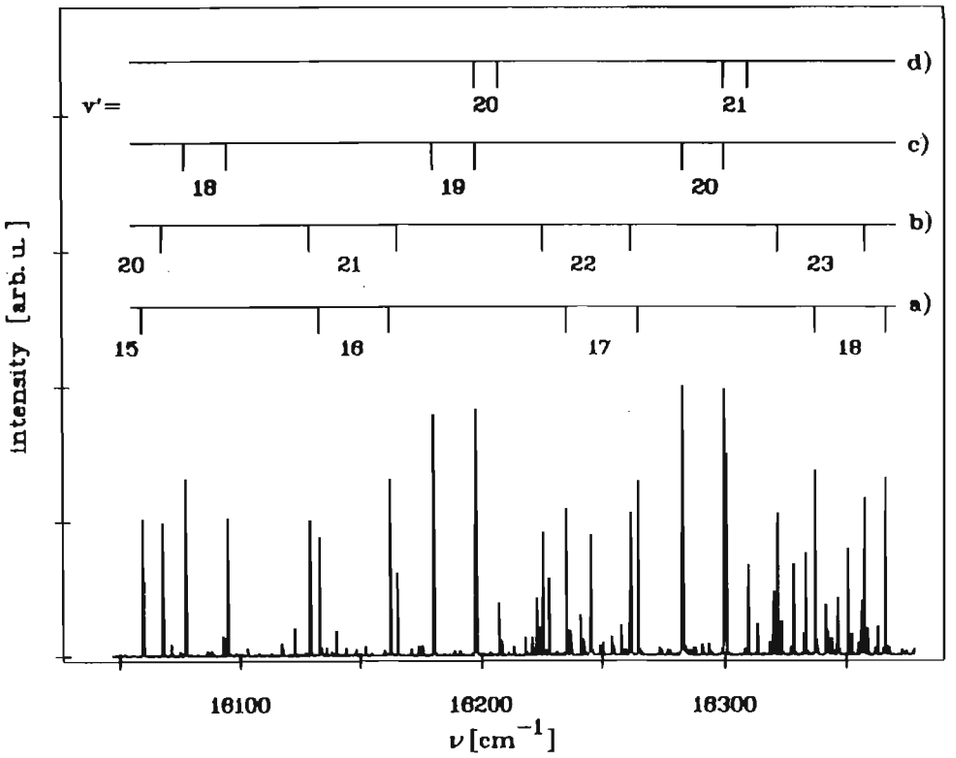


Figure 1. A portion of the polarization spectrum of $Na_2$ obtained with 488·0 nm line of the $Ar^+$ laser as the probe and linearly polarized pump beam. The assigned progressions (*a*)–(*d*) correspond to the transitions $A\ ^1\Sigma_u^+ \leftarrow X\ ^1\Sigma_g^+$ from the labelled ground-state levels (*a*) $v'' = 0$, $J'' = 75$, (*b*) $v'' = 2$, $J'' = 98$, (*c*) $v'' = 3$, $J'' = 43$, and (*d*) $v'' = 4$, $J'' = 25$.

## 3. Results and analysis

We recorded the polarization spectrum of the $A\ ^1\Sigma_u^+$–$X\ ^1\Sigma_g^+$ system of $Na_2$ in the region between 14200 and 17600 $cm^{-1}$. A typical fragment of the spectrum is shown in figure 1. We assigned a total of about 1450 transitions spanning the range $v' = 0$–43 and $J' = 12$–126 in the A state. Originally all observed lines were subjected to a global least-squares fit with a Dunham expansion. Constants of the ground state were fixed at the values given by Kusch and Hessel [17]. As expected, the initial fit revealed that part of the lines displayed shifts from the expected positions reaching up to 0·6 $cm^{-1}$, due to perturbation of the $A\ ^1\Sigma_u^+$ state by the $b\ ^3\Pi_u$ state. Lines for which the difference between the measured and calculated positions exceeded 0·2 $cm^{-1}$ (twice the experimental uncertainty) were subsequently excluded from the data field and the fitting procedure repeated iteratively until a consistency between the observed and predicted values has been achieved. The excluded lines fall in general into the regions of predicted strong perturbations between the A and b states [9]. In this way, 1376 lines of the A–X system remained as unperturbed (taking our wavenumber accuracy of 0·1 cm $^{-1}$) and provided the Dunham coefficients for the $A\ ^1\Sigma_u^+$ state listed in table 2. Figure 2 displays the range of vibrational and rotational levels covered in the final fit. The error of this fit was 0·052 $cm^{-1}$. For each constant a total of at least six figures is given (more than are statistically significant), as this number is required to reproduce the measured transitions.

Once we derived the molecular constants for the A state, we first tested them against the precise, deperturbed constants given by Effantin *et al.* [8] and Whang *et al.*

Table 2. The Dunham coefficients for the A $^1\Sigma_u^+$ state of $Na_2$ obtained in the present work. The quoted uncertainty of a constant is one standard deviation.

| Constant | Value/cm$^{-1}$ | Uncertainty/% |
|---|---|---|
| $T_e$ | 14680·42 | 0·0001 |
| $Y_{10}$ | $0{\cdot}117406 \times 10^{3}$ | 0·003 |
| $Y_{20}$ | $-0{\cdot}369478$ | 0·082 |
| $Y_{30}$ | $0{\cdot}693070 \times 10^{-3}$ | 1·5 |
| $Y_{40}$ | $-0{\cdot}786759 \times 10^{-5}$ | 1·5 |
| $Y_{01}$ | 0·110777 | 0·004 |
| $Y_{11}$ | $-0{\cdot}558396 \times 10^{-3}$ | 0·080 |
| $Y_{21}$ | $0{\cdot}115972 \times 10^{-5}$ | 2·2 |
| $Y_{31}$ | $-0{\cdot}202903 \times 10^{-7}$ | 2·1 |
| $Y_{02}$ | $-0{\cdot}386424 \times 10^{-6}$ | 0·16 |
| $Y_{12}$ | $0{\cdot}269103 \times 10^{-9}$ | 5·9 |
| $Y_{03}$ | $0{\cdot}112252 \times 10^{-11}$ | 2·0 |

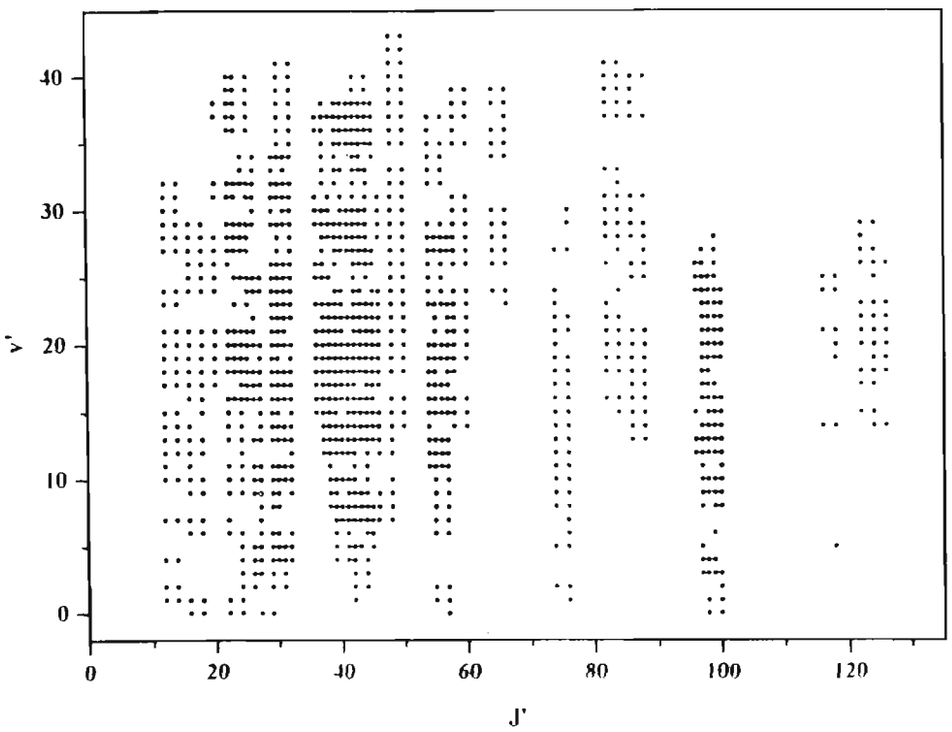


Figure 2. Distribution of the data used to fit the Dunham coefficients in the field of vibrational and rotational quantum numbers of the A $^1\Sigma_u^+$ state in $Na_2$.

[9]. In the common ranges of validity of the constants, the line positions predicted from them for the A–X system agree within 0·1 cm$^{-1}$. Our Dunham coefficients reproduce also correctly excitations by the 647·1 nm line of the $Kr^+$ laser [19] and by the 632·8 nm line of the He–Ne laser [20]. In comparison with the previous Dunham coefficients of Kaminsky [3] and Gerber and Möller [6], the values of constants given in table 2 provide a much improved fit to the observed levels, particularly for $J > 50$, where the previous values were unreliable.

This work has been partially supported by a grant (No. 2 P03B 058 10) from the Polish Committee for Scientific Research. Two of us (R. F. and O. N.) are grateful for

the additional support from the Latvian Science Council (grant No. 93.256) and from the European Commission PECO HCM Programme.

## References

[1] Kusch, P., and Hessel, M. M., 1975, *J. chem. Phys.*, **63**, 4087.
[2] Kaminsky, M. E., Hawkins, R. T., Kowalski, F. V., and Schawlow, A. L., 1976, *Phys. Rev. Lett.*, **36**, 671.
[3] Kaminsky, M. E., 1977, *J. chem. Phys.*, **66**, 4951.
[4] Schweda, H. S., Chawla, G. K., and Field, R. W., 1982, *Optics Commun.*, **42**, 165.
[5] Ahmad-Bitar, R. N., and Al-Ayash, A. S., 1984, *J. molec. Spectrosc.*, **106**, 299.
[6] Gerber, G., and Möller, R., 1985, *Chem. Phys. Lett.*, **113**, 546.
[7] Chawla, G., Schweda, H. S., Vedder, H. J., Field, R. W., Churassy, S., Lyyra, A. M., Luh, W. T., and Stwalley, W. C., 1986, *AIP Conf. Proc.*, **146**, 466.
[8] Effantin, C., Babaky, O., Hussein, K., d'Incan, J., and Barrow, R. F., 1985, *J. Phys.* B, **18**, 4077.
[9] Wang, T. J., Stwalley, W. C., Li, L., and Lyyra, A. M., 1992, *J. chem. Phys.*, **97**, 7211.
[10] Demtröder, W., 1996, *Laser Spectroscopy* (Berlin: Springer).
[11] Wang, Z. G., and Xia, H. R., 1991, *Molecular and Laser Spectroscopy* (Berlin: Springer).
[12] Jastrzębski, W., and Kowalczyk, P., 1993, *Chem. Phys. Lett.*, **206**, 69.
[13] Jastrzębski, W., and Kowalczyk, P., 1994, *Chem. Phys. Lett.*, **227**, 283.
[14] Jastrzębski, W., and Kowalczyk, P., 1995, *Phys. Rev.* A, **51**, 1046.
[15] Striganov, A. R., and Odincova, G. A., 1982, *Tablicy Spektralnych Linii Atomov i Ionov* (Moscow: Energoizdat).
[16] Demtröder, W., and Stock, M., 1975, *J. molec. Spectrosc.*, **55**, 476.
[17] Kusch, P., and Hessel, M. M., 1978, *J. chem. Phys.*, **68**, 2591.
[18] Hessel, M. M., and Giraud-Cotton, S., 1980, NaK revisited: the ground $^1\Sigma$ and D $^1\Pi$ states, unpublished.
[19] Babaky, O., and Hussein, K., 1989, *Can. J. Phys.*, **67**, 912.
[20] Verma, K. K., Vu, T. H., and Stwalley, W. C., 1981, *J. molec. Spectrosc.*, **85**, 131.